11-22-2019

Content Release and Fusion of Quinone-Based Liposomes: Lipid Distribution and Cleavage Symmetry of the Quinone Headgroup at the Bilayer

Huy Huu Nguyen

CONTENT RELEASE AND FUSION OF QUINONE-BASED LIPOSOMES: LIPID DISTRIBUTION AND CLEAVAGE SYMMETRY OF THE QUINONE HEADGROUP AT THE BILAYER

A Dissertation

Submitted to the Graduate Faculty of the
Louisiana State University and
Agricultural and Mechanical College
in partial fulfillment of the
requirements for the degree of
Doctor of Philosophy

in

The Department of Chemistry

by
Huy Huu Nguyen
B.S, Hanoi University of Science, Vietnam, 2013
May 2020

This dissertation is dedicated to the memory of both my grandfathers

Nam Nguyenhuu and Anh Nhu Tran,

Who introduced me to the world

with tremendous inspiration and are heart-warming examples of humanity,

And with love to

My wife, Ngan Doanh Mac Do,

My Dad, Manh Nguyenhuu

My Mom, Huong Thi Nguyen,

My brother, Ha Nguyenhuu,

My parents-in-law, Hong Thanh Do and Le Thanh Tran,

and my baby boy, Mol Nguyen.

ACKNOWLEDGMENTS

I have been fortunate to learn science from many great teachers since middle school, who turn me into a nerd who was curious about the science around me. The most influential mentor to me so far has been my research advisor, Prof. Robin McCarley. I would like to express my deepest appreciation to him as he has given me profound lessons not only about chemistry but also about humanity. I am very honored and proud to be part of his multidisciplinary research group, which cultivated my experience in many different areas of chemistry, from organic synthesis, and instrumental analysis, to biochemistry and physical chemistry. During my Ph.D., he has always provided the best working conditions, persistent help, and extraordinary guidance to help me grow and develop as a professional.

I also would like to thank Prof. Doug Gilman and Prof. Louis Haber, who served on my advisory committee and helped me go through the final stage of my Ph.D. It is my immense pleasure to offer my heartfelt gratitude to Prof. Haber, who allowed me to conduct collaborative research with his research group, and I am fortunate to contribute to the development of this promising collaboration. I would like to thank Dr. Fengli Zhang and Dr. Thomas Weldeghiorghis for training me a lot about NMR instrumentation during my time working in the NMR facility, Dr. Rafael Cueto for helping me with the liposome characterization, and Prof. Isiah Warner, Prof. Megan Macnaughtan, and Prof. Vincent Licata for their permission to use their instruments for my research. I would like to especially thank Prof. Kuroda for his mentorship about a Ph.D.'s life, teaching me how to be an optimistic researcher.

I would like to thank a group of professors from the UIUC, including Prof. Gruebele, Prof. Scheeline, and Prof. James Lisy, who enthusiastically came to Vietnam to develop the chemistry education of Vietnam. Thanks to their inspiration, many Vietnamese students, including myself, have the opportunity to do research abroad. I would like to particularly thank

Prof. Martin Gruebele, who opened the door for me to practice doing research in his lab under the instruction of Dr. Hannah Gelman, where I learned quite a bit of biophysics. As a result, I acquired valuable experience in a professional research environment, which has allowed me to continue pursuing research at LSU. Without those respected professors, my name would not be in LSU Chemistry.

Also, a special thanks goes to my colleagues both past and present in the McCarley group: Dr. James Winter for getting me familiar with my research project, and the current group members for helping me correct my dissertation. The McGroup is my second family, where everyone is so supportive and willing to help each other. I will never forget the great and fun moments that we have shared together during the time we are working in the lab as well as when we are hanging out and playing games.

Last but not least, I would like to send my words of love and gratitude to my beloved wife, who has always accompanied me during this meaningful period in my life. I owe my parents and my entire family for their unconditional love and sacrifices, for giving me the freedom to follow my dreams. Thank you to all my friends in Vietnam and at LSU who have always been sharing and motivating me with great stories.

We meet each other because of predestined relationships in life. Each of you with your unique personality and story has done a part in making me the person I am today.

Thank you.

TABLE OF CONTENTS

LIST OF TABLES

LIST OF FIGURES

LIST OF ABBREVIATIONS AND SYMBOLS

$\chi^{(2)}$	Second-order susceptibility
$\chi^{(3)}$	Third-order susceptibility
^{13}C NMR	Carbon 13 nuclear magnetic resonance
^{1}H NMR	Proton nuclear magnetic resonance
ANTS	8-Aminonapthalene-1,3,6-trisulfonic acid
BG	Brilliant green
d	doublet
DOPC	1,2-Dioleoyl-*sn*-glycero-3-phosphatidylcholine
DOPE	1,2-Dioleoyl-*sn*-glycero-3-phosphatidylethanolamine
DOPG	1,2-Dioleoyl-*sn*-glycero-3-phosphatidylglycerol
DOSY	Diffusion-ordered NMR spectroscopy
DPA	Dipicolinic acid, pyridine-2,6-dicarboxylic acid
DPX	p-xylene-bis-pyridinium bromide
DSC	Differential scanning calorimetry
EDTA	Ethylenediaminetetraacetic acid
EPR	Enhanced permeability and retention
GUV	Giant unilamellar vesicle
H_{II}	Inverted micelle hexagonal phase
HMBQDOPE	Hydroxymethyl benzoquinone-functionalized DOPE lipid
hNQO1	Human NAD(P)H:quinone oxidoreductase-1
IMI	Intermembrane intermediate
I_{SHG}	Intensity of SHG signal

J	Coupling constant
LED	Light-emitting diode
LUV	Large unilamellar vesicle
L_{α}	Lamellar liquid-crystal phase
L_{β}	Lamellar gel phase
m/z	Mass-to-charge ratio
MeOH	Methanol
$MeSQ_3DOPE$	Methyl mercaptan trimethyl-quinone propionic acid-functionalized DOPE lipid
MGD	Malachite green derivative
MGITC	Malachite green isothiocyanate
NBS	*N*-Bromosuccinimide
NHS	*N*-Hydroxysuccinimide
PBS	Phosphate-buffered saline
PC	Phosphatidylcholine
PDI	Polydispersion index
PE	Phosphatidylethanolamine
PEG	Poly-ethylene glycol
PG	Phosphatidylglycerol
POPE	1-Palmitoyl-2-dioleoyl-*sn*-glycero-3-phosphatidylethanolamine
ppm	Parts per million
PS	Phosphatidylserine
q	Quartet
Q_1DOPE	Methyl-quinone propionic acid-functionalized DOPE lipid

Q_3DOPE	Trimethyl-quinone propionic acid-functionalized DOPE lipid
Q_3POPE	Trimethyl-quinone propionic acid-functionalized POPE lipid
R.T.	Room temperature
ROS	Reactive-oxygen species
SFG	Sum frequency generation
SHE	Standard hydrogen electrode
SHG	Second harmonic generation
SUV	Small unilamellar vesicle
t	Triplet
t_{50}	Time required for 50% release of the encapsulated contents
TEA	Trimethylamine
T_H	Lamellar-liquid crystal to inverted hexagonal phase transition temperature
THF	Tetrahydrofuran
T_M	Lamellar-gel to lamellar-liquid transition temperature

ABSTRACT

Delivery of most conventional nanomedicines for tumor treatment is through exploiting the enhanced permeability and retention effect with limited targeting potency. Furthermore, the inability of some nanocarriers to enter the cells via endocytosis, or their limited endocytic escape restrict their applications for intracellular delivery. Liposomal carrier systems offer a solution as they are capable of precisely spatiotemporal releasing the payloads upon sensing specifically targeted environments.

In 2008, the McCarley group demonstrated an example of redox-responsive triggered release of the liposomes, named Q_3DOPE, which can potentially take advantage of elevated quinone reductase activities of $hNOQ_1$ in several cancers. The subsequent research projects focus on elaborating the mechanism of content release of Q_3DOPE-based liposomes, whose fusion property is not clearly understood. To that end, the research here involved (1) study of membrane asymmetry caused by asymmetrical cleavage of the Q_3 group from the outer leaflet of Q_3PE-based liposomes determining the liposomal bilayer stability and their fusion properties (2) investigation of symmetrical cleavage of the Q_3 group from both leaflets of the liposomes, and its effect on the leakage and fusion of the resulted vesicles. The observations lead to the hypothesis that the membrane asymmetry caused by asymmetrical cleavage of the Q_3 group at the outer leaflet of the Q_3PE-based liposomes destabilizes their bilayers, which is the key factor dictating the bilayer contact and phase transition with the inclusion of PE lipids in the liposomal composition resulting in a rapid content release. In addition, the fusion of Q_3PE-based liposomes is facilitated when their inner leaflet is enriched by POPE lipid but not by DOPE, which emphasizes the importance of the lipids' lamellar to hexagonal phase transition temperatures to the fusion. The observed fusion in this research is relevant to the fusion of cellular membranes whose bilayers exhibit an uneven distribution of lipids between the two leaflets.

CHAPTER 1
INTRODUCTION

1.1. Research Goals and Aims

Therapeutic delivery through liposomes has shown a significant impact on many biomedical areas, with an expanding number of products in clinical development and on the market.[1-2] These vesicles made from phospholipids, major components of the cell membrane, can carry a variety of compounds and protect them from early inactivation, degradation, and dilution in the circulation, as well as assisting their encapsulated contents in overcoming biological barriers and remaining in the bloodstream longer.[3-4] In addition, the diversity of phospholipid structures allows for ease of their chemical modification, and a simple variation in liposome formulation composition enables tuning of their biophysical properties, resulting in diverse applications.[5-7] Recent strategies to improve the efficacy of liposomes involve active targeting of and triggered content release from liposomes.[8-9]

In 2008, the McCarley group demonstrated the potential application of targeting property and the internal-stimulus triggered release of liposomes named Q_3DOPE, which exploit the cancer-associated enzyme human NAD(P)H:quinoneoxidoreductase type 1 (hNQO1) that is overexpressed in many cancers. At the physiological conditions, zwitterionic DOPE lipids favor the formation of hexagonal phase, due to their small headgroup/lipid ratio. Chemical modification of DOPE lipids' headgroup with an hNQO1 quinone substrate, Q_3, to form Q_3DOPE lipid increases the headgroup size and its charge density, which sustains the formation of liposomes. When the liposomes are exposed to active enzyme, it is anticipated that cleavage of the Q_3 group from Q_3DOPE lipids will occur, as is the case for those liposomes in the presence of solution-phase reducing agents, producing 1,2-dioleoyl-*sn*-glycero-3-phosphoethanolamine (DOPE) lipids only in the outer leaflet of the liposomes, while the Q_3DOPE lipids in the inner leaflet remain intact.[10]

As a result, the asymmetrical cleavage transforms a symmetric bilayer to an asymmetric bilayer of the liposomes, inducing stress on the membrane due to the difference in hydration and curvature between the two leaflets. Subsequently, the tendency of DOPE to form the H_{II} phase drives the liposomes to aggregate and undergo an $L_{\alpha} \rightarrow H_{II}$ phase transition and release their contents to the surroundings.

Since the first publication of Q_3DOPE liposomes in the McCarley group, this liposomal system has been extensively characterized to elucidate the elementary steps of the release pathway. Martin Loew et alia studied the lipid nature and its influence on the opening of Q_3DOPE-based liposomes. In that work, the inclusion of poly(ethylene glycol)-modified DOPE (PEG-DOPE) to the Q_3DOPE liposomes stabilizes lipid bilayers, causing minimal leakage, while the incorporation of DOPE results in a faster content release.[11]

Forsythe and colleagues showed that content release of Q_3DOPE liposomes is anion-specific, which is slower when weakly hydrated chaotropic anions are added to the liposomal solution compared to the similar addition of highly hydrated kosmotropic anions. This trend in release rates is attributed to hydration alternation at the outer surface of liposomes associated with different amounts of ion accumulation near the zwitterionic DOPE headgroups, as indicated by the specific lamellar to hexagonal phase transition ($L_{\alpha} \rightarrow H_{II}$) temperatures of the generated DOPE lipid in the presence of different salts. Also, liposomal contents release was revealed to be initiated by the contact of apposed deformed liposomes.[12] James Winter developed NMR techniques to monitor phase transitions, and observed the lamellar to hexagonal phase change in reduced Q_3DOPE-based liposomes.[13] All of the mentioned work relies on the asymmetrical reduction and subsequent cleavage of the quinone headgroup from the outer leaflet of the liposomes caused by a reducing agent, sodium dithionite (SDT).

My work adds a unique perspective to previous studies through the achievement of the following goals. The first goal is presented in Chapter 2, which addresses how the asymmetrical cleavage of the quinone headgroup from the outer leaflet of Q_3PE-based liposomes determines the membrane stability and fusion of the subsequent liposomes. The first aim is to examine the membrane-permeability of dithionite anion with the expectation that the cleavage occurs only at the outer leaflet of the quinone-based liposome. The second aim is to investigate how the membrane asymmetry determines the stability of different Q_3PE-based liposomes in related to their release kinetics and phase transitions after adding dithionite. The third aim is to study how the lipid distribution at the bilayer of Q_3PE-based liposomes controls their fusion. Three enzyme-triggerable lipids were synthesized: Q_3DOPE, Q_1DOPE, and Q_3POPE. Commercially available lipids were included in the liposomal compositions: DOPE, POPE, DOPC, and DOPG. The release kinetics and fusion of liposomes made from different liposomal compositions were monitored by fluorescence-based techniques under in vitro conditions.

Within this context, the second goal presented in Chapter 3 proposes that symmetrical cleavage of the quinone group at both layers of the Q_3PE-based liposomes can result in a different manner of leakage/release and fusion of subsequent liposomes. The first aim of this chapter is to achieve the symmetrical cleavage through photochemistry. A modified version of Q_3PE lipid named MeSQ_3PE was synthesized by introducing a thiomethoxide substitution group to the quinone ring, which minimizes the chemical modification while obtaining a blue-light responsibility from the quinone group. Under blue LED irradiation, liposomes made of MeSQ_3PE lipid are expected to undergo a photocleavage of the MeSQ_3 quinone group to produce PE at both leaflets of the bilayer. The formation of new PE lipids at both leaflets of liposomes can alter the release kinetics and fusion properties of the quinone-based liposomes. Noticeably, the release of

Q_3PE-based liposomes caused by SDT has shown to be concentration dependent, which requires the bilayer contact of vesicles for an $L_\alpha \rightarrow H_{II}$ phase transition to occur followed by the subsequent content release. On the other hand, theoretically, the symmetrical photoinduced cleavage of MeSQ_3PE liposomes can produce PE lipid at a much higher proportion of PE (100 % maximum) compared to the SDT-induced asymmetrical cleavage of Q_3PE liposomes (50 % maximum). Therefore, at this high extreme proportion of PE present in both leaflets of liposomes, the release of MeSQ_3PE liposomes are expected to possess a very low concentration dependent, or even non-concentration dependent because of their self-bursting capability. Due to the photobleaching effect of the blue LED towards liposomal encapsulated fluorescence dyes, the second aim of this chapter is to adapt and develop diffusion NMR and capillary electrophoresis to interrogate the content leakage of the MeSQ_3PE liposomes under blue LED irradiation.

In Figure 1.1 are summarized the two main goals of this research, which describes different possible pathways of quinone-based liposomes (made from 100 % Q_3DOPE as the typical example) after the reduction and cleavage of quinone headgroups. This research is significant when considering a more realistic fusion model of lipid bilayers, which is related to membrane asymmetry caused by uneven distribution of lipids at the bilayer as found in the cellular membranes. In addition, the findings in this research can potentially offer a new formulation of liposomes that are able to deliver therapeutics intracellularly into the cytoplasm or other subcellular compartments of cancer cells via fusion of liposomes with the cellular membrane, as well as to exhibit a minimal concentration dependent of liposomes for their release and fusion with the cellular membrane instead of liposome-liposome bilayer contact.

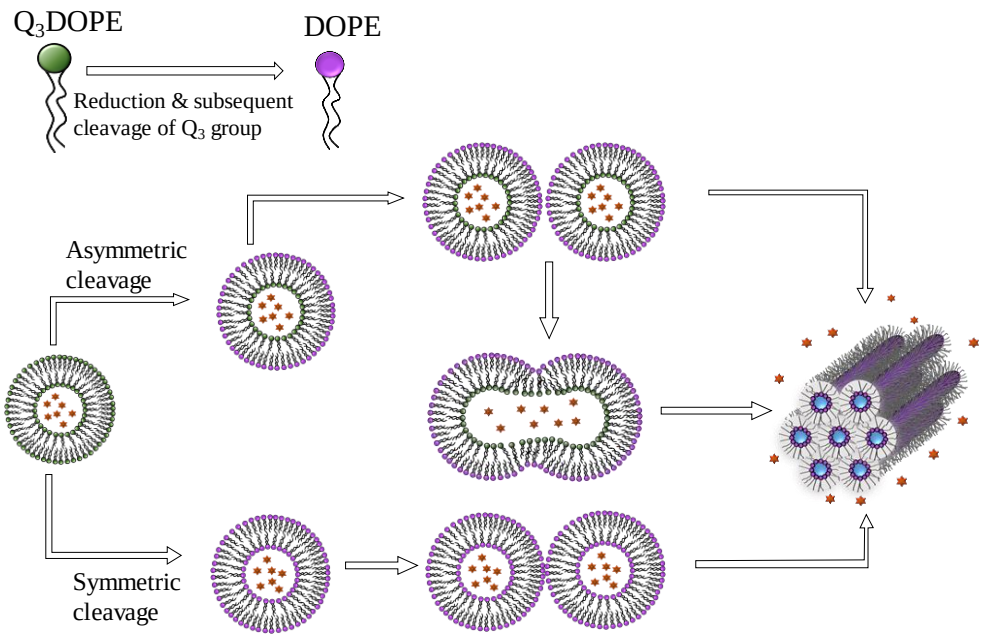

Figure 1.1. Q_3DOPE lipids (green) form lamellar liquid crystal phase (L_α) liposomes, encapsulating payloads (brown). Reduction of quinone to hydroquinone, followed by a lactonization triggers the cleavage of Q_3 headgroups to form DOPE lipids (purple). Asymmetrically or symmetrically cleaved bilayers experiencing possible leakage undergo aggregation with or without fusion before a transformation to hexagonal phase H_{II} that results in the release of the encapsulated contents into their surroundings.

1.2. Cancer Hallmarks

Cancer remains one of the most challenging global healthcare problems, causing about 1 in 6 deaths globally.[14] Based on data from 185 countries, the International Agency for Research on Cancer predicted that the number of new cancer cases would be about 18.1 million, and the mortality count was approximately 9.6 million worldwide in 2018. Lung cancer is not only the most commonly diagnosed cancer, accounting for 11.6% of the total cases, but is also responsible for 18.4% of cancer-related deaths in both males and females. Following lung cancer, breast cancer and prostate cancer account for 11.6% and 7.1% of deaths in women and men, respectively. In addition, there has been a total of 43.8 million people diagnosed with cancer within the past five years.[15]

Based on the remarkable publications of Hanahan and Weinberg in 2000 and 2011 about the hallmarks of cancer, Fouad and Aanei proposed a revision of cancer hallmarks commonly shared by most types of neoplastic diseases, which helps to promote better diagnosis and treatment of cancers.[16-18] Despite the complex and dynamic nature of cancer, identification of cancer can be simplified to several representative principles. Cancer hallmarks are a group of evolutionary-advantageous traits acquired as the result of a succession of changes from normal cells into malignant cells. Typically, genetic mutations in cells are caused by continuous stress from various negative factors, such as replication errors, toxic environmental exposure, and viruses. The oncogene-carrying cells undergo a succession of genetic changes via clonal selection, resulting in a change of phenotype with some growth advantage, and progressive evolution to a neoplastic state, leading to tumor formation and malignancy. From this approach, seven hallmarks of cancer are presented, as shown in Figure 1.2.

The first and most fundamental trait of cancer cells is their capability of sustaining proliferation via self-sufficiency in growth and proliferative signals. Rigorous regulation of cell growth signaling and homeostasis tissue architecture is disrupted in cancer. Cancer cells can produce mitogenic growth factors, known as autocrine signaling, or activate corresponding permanent signaling pathways, allowing them to multiply without external stimulation from their normal tissue microenvironment.[19-20]

The second hallmark of cancer involves cancer's altered stress response favoring overall survival and limitless replicative potential. Tumor development is governed not only by expanding its cell populations but also by the rate of cell loss. In a normal cell, programmed cell death, known as apoptosis, is the key to eliminating abnormal or unwanted cells. When exposed to stress, healthy cells initiate a repair mechanism targeting infected cells or trigger cell suicide in order to avoid

transmission of genetic defects. The stressors include but are not limited to excessive signaling, DNA damage, hypoxia, nutrient scarcity, and even anticancer therapy. Cells encompassing damaged chromosomes can adapt to the tress and evolve a variety of strategies imparting resistance to apoptosis.[21] For example, tumor suppressors of proliferation, such as pRB and p53 proteins, are prohibited or altered, causing an ineffective constraint of inappropriate replication of cells to maintain cellular quiescence and tissue homeostasis, even when they have severe abnormalities.[22-23] On the other hand, most cells are only able to go through a limited number of growth and division cycles because telomeres, the DNA at the end of chromosomes, shorten with every cell division until cells die or become unable to divide. Cancer cells can manipulate enzymes that increase the length of telomeres, and become immortalized.[24-25]

Figure 1.2. Seven hallmarks of cancer.[18]

The third hallmark of cancer denotes aggressive tumor vascularization. Cancer cells promote angiogenesis, forming new blood vessels to support tumor growth due to oxygen and nutrient deficiencies. A transformation of angiogenic phenotype occurs by several mechanisms

including intussusceptive angiogenesis, the recruitment of endothelial progenitor cells, vessel cooption, vasculogenic mimicry, and lymphangiogenesis.[26-27]

The fourth common feature of tumor cells is their metabolic rewiring capability. Most cancer cells use abnormal metabolic pathways to provide energy to fuel their growth. There are six characteristics of this metabolic alteration, including escalating glucose and amino acid uptake, accelerated nutrient acquisition, utilizing glycolysis and tricarboxylic acid cycle intermediates for biosynthesis and cell division support, increasing nitrogen demand, revising metabolite-driven gene regulation, and interplaying metabolism with the microenvironment.[28-29]

The fifth hallmark of cancer addresses the evolved microenvironment of cancer. The microenvironment of the tumor surrounded by extracellular matrix and stromal cells, supported by the blood and lymphatic vascular networks. The physical properties of the tumor microenvironment are closely connected to every step of tumorigenesis, which is the result of bidirectional interaction of tumor cells and their surroundings.[30] Typically, tumor cells can alter gene expression and exert selective pressures on their neighboring cells while the microenvironment can affect evolution pathways of the tumor. Cancer therapeutics in vivo frequently fail to correlate the response of cells derived from these tumors in-vitro, suggesting that tumor microenvironments can protect tumors from the consequences of drug action.[31-32]

The sixth hallmark of cancer describes the mechanisms of the tumor to evade and suppress immune activity. Despite cancer cells causing increased inflammation and angiogenesis, they continue developing under the surveillance of the immune systems. Cancer immune resistance is adapted through a cross-interaction between immune cells, cancer cells, and the microenvironment.[33] Cancer immune modulation undergoes three consecutive steps, elimination, equilibrium and escape. Cancer cells are eradicated under the synchronized interaction of both

innate and adaptive immune responses during the elimination. The equilibrium phase occurs when tumor cell removal and selection of those with reduced immunogenicity are at balance, followed by increasing the production of resistant variants. The immune escape of cancer is achieved when some clones bypass immune surveillance and continue developing without immune detection and elimination as a consequence of its genetic and epigenetic alterations.[34-35]

The critical feature distinguishing cancer cells from all other cells is their migratory ability throughout the body by two related mechanisms, invasion and metastasis. These mechanisms dictate its malignancy compared to other hallmarks also present in the benign tumor, accounting for a majority of cancer-related deaths.[36] Metastasis is the most challenging aspect of cancer treatment. Metastasis begins with the proliferation and invasion of the primary tumor through surrounding tissues until finally reaching blood vessels or lymphatic channels, where tumor cells detach from the tumor mass and migrate to a distant target organ. After invading into the new tissue, cancer cells develop into a new colony as a consequence of the growth of those lesions.[37-38] In summary, understanding the principles of cancer hallmarks, as well as discovering more biomarkers help to develop methods to prevent, diagnose, treat, and, ultimately, cure this fatal disease.

1.3. Nanomedicines for Therapeutic Delivery

1.3.1. Conventional Chemotherapy Issues

After a patient is diagnosed with cancer, the three most common treatments are chemotherapy, radiation, and surgery. Surgery and radiation remove and damage cancer cells, respectively. However, each of those methods works best when tumors are localized whereas chemotherapy is a better option for metastasized cancers. Chemotherapy helps to shrink a tumor before surgery and radiation are conducted, or it can be used after those treatments to kill any remaining cancer cells, or if the patient relapses. Nevertheless, conventional chemotherapy has a

few issues. Firstly, although there are many possible drugs, drugs with poor water-solubility are excluded from the bloodstream significantly due to a rapid drug clearance caused by some biological barriers, such as the renal, hepatic, or immune systems.[39-40] The limited aqueous solubility has been considered the main obstacle in the development and clinical use of new anticancer compounds.

The next obstacle is that even when drugs are able to remain in the bloodstream for enough time, they are diluted and nonspecific, thus leading to them having less of an effect on the target tissues. Historically, chemotherapeutic agents target rapidly dividing cancer cells, however, highly proliferative noncancerous cells, such as those in bone marrow, the digestive tract and hair follicles, are sensitive to this type of treatment. Therefore, the lack of specificity in conventional chemotherapy causes many common side effects, including immunosuppression and myelosuppression, gastrointestinal distress, anemia, nausea and vomiting, and hair loss, to name a few.[41-42]

1.3.2. Advantages of Nanomedicines

Nanomedicines use nanoparticles as a nanocarrier to transport therapeutics through the body to improve their efficacy. Many materials have been investigated for fabrication of nanocarriers, such as lipids, protein, polymers, inorganic materials, and viruses, as presented in Figure 1.3.[43-44] Recently, a number of these platforms have been approved for use in clinical settings by the FDA.[45-49] Oral delivery of GastroMARK by iron oxide nanoparticles for MRI,[50] local delivery of cytarabine by liposomes (DepoCyt) for acute myeloid leukemia treatment,[51] topical delivery of steroid hormone estradiol by liposomes,[52] intravenous delivery of doxorubicin by liposomes (Doxil®) for cancer treatment,[53] and intravenous delivery of small interfering RNA by polymer[54] are a few well-known examples.

Nanomedicines overcome the drawbacks of conventional chemotherapy by several mechanisms. With regard to limited solubility and short circulation time of chemotherapeutics in the bloodstream, nanoparticles are small with high surface-to-volume ratios, that can be used to carry hydrophobic drugs while protecting and preventing them from rapid clearance from the body.[39, 55] For example, polymers such as polysialic acid (PSA),[56-57] and polyethylene glycol (PEG),[58-59] or phospholipids in the form of liposomes[5-6] have been used to carry therapeutic agents to reduce clearance and improve stability. PSA and phospholipids are naturally occurring compounds that can be easily metabolized and ultimately degraded. They form a hydrophilic shield around the therapeutic agents, protecting them against proteolysis, as well as, reducing immune response, therefore, prolonging their circulation to allow adequate time to reach tumor tissue.

To overcome the drawbacks of non-specificity of chemotherapeutics, nanoparticles have been developed for targetted and controlled release of drugs at specific tissue sites. Therefore, high portions of chemotherapeutics are delivered to the tumor by using nanocarriers, thus, reducing the side effects caused by undesirable toxicity of chemotherapeutics to the rest of the body, and lower doses of drugs in undesired targets are achieved.[60-64] The path of nanoparticles traveling from injection site to tumor includes transport through blood, extravasation from tumor vasculature, interstitial transport, and binding to cell membranes.[65]

Nanoparticles without any surface modifications passively concentrate within the tumor tissues through the enhanced permeability and retention effect, which is the result of leaky vasculature and poor lymphatic drainage of the tumor, as shown in Figure 1.4.[66-67] However, nanoparticles exhibiting passive targeting also tend to build up in tissues that generally have fenestrated blood vessels, as found in the liver or the spleen.[67-68] Furthermore, heterogeneity in the tumor microenvironments may possess barriers for nanomedicines to take action.[69-70] Thus,

passive targeting still faces the inherent limitations of cancer specificity in conventional chemotherapy.

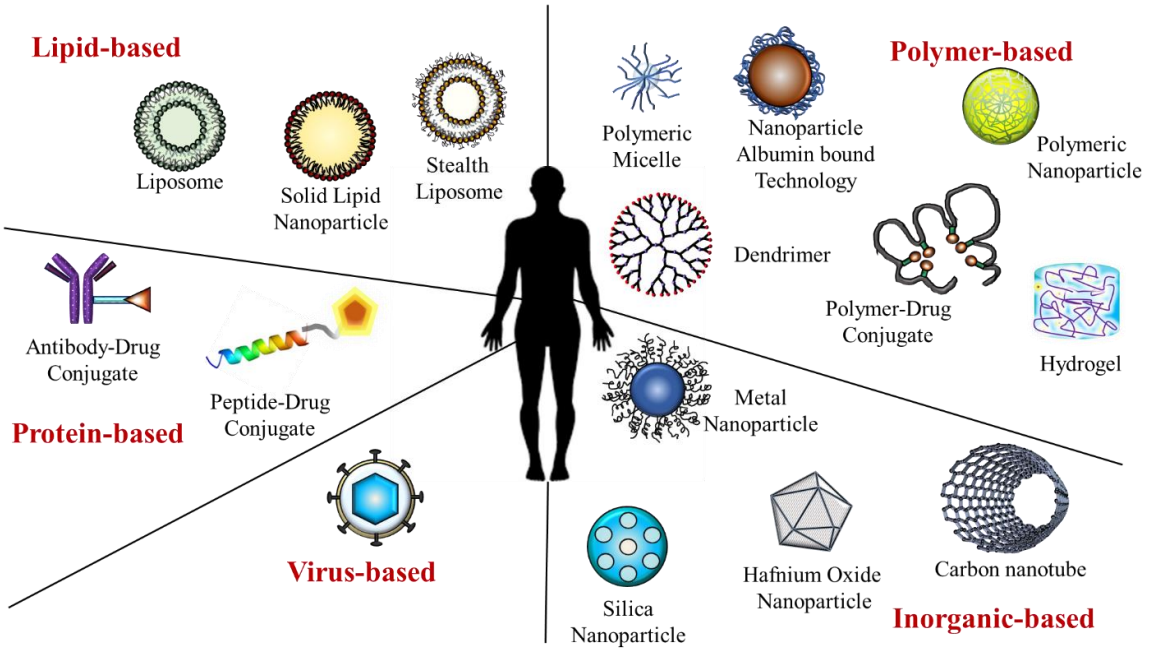

Figure 1.3. Different categories of nanocarrier materials: lipid-based, polymer-based, inorganic-based, virus-based, protein-based.(Modified from Wicki, et al. 2015).[43]

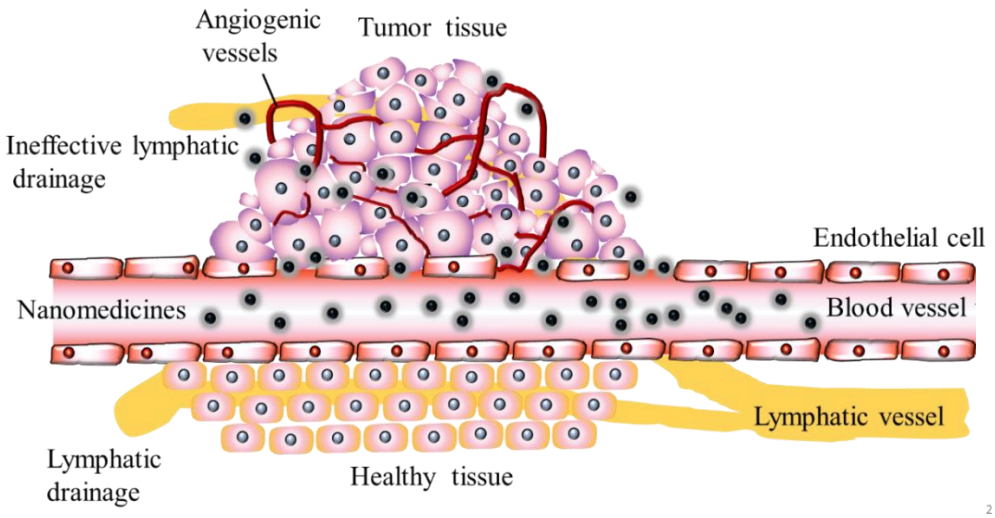

Figure 1.4. Nanoparticles (black) are concentrated passively within the tumor tissues through the enhanced permeability and retention (EPR) effect.

One way to overcoming the limitations of passive delivery of nanoparticles is active targeting, which exploits associated cancer hallmarks or its biomarkers to probe cancer cells and promote a significant accumulation of nanoparticles at tumor tissues during blood circulation and extravasation.[60-61, 71] There are many potential target sites, including tumor vasculature, tumor interstitium, cell membrane, and intracellular compartments, such as the cytosol, nucleus, mitochondria, Golgi apparatus, and endoplasmic reticulum.[65] Nanocarriers modified with ligands showing high specificity to receptors or other cancer-specific targets overexpressed in tumor cells limit nonspecific uptake and modulation of nanocarriers by healthy tissues. Many substances can be used as targeting moieties, including antibodies and their fragments,[72-73] lectins,[74-75] peptides,[76-77] lipoproteins,[78-79] charged molecules,[80-81] saccharides,[82] or some low molecular-weight ligands, such as folate,[83-84] and transferrin.[84-85] In short, targeting nanoparticles carrying drugs improves their efficacy by enhancing their biocompatibility and increasing their proportion of drugs at the targets, requiring a much lower dose of chemotherapeutics.

1.3.3. Controlled Release of Nanomedicines

After nanomedicines accumulate and bind to the surface of target cells, they are internalized into the cells by endocytosis. Internal cellular transport of nanoparticles continue via several processes, such as entrapment of nanoparticles in endosomes, expelling of nanoparticles from these structures, transport of nanoparticles in cytoplasm into the nucleus or uptake by other intracellular organelles, as shown in Figure 1.5.[65]

Therapeutic agents can slowly leak over time from the carriers, causing an incomplete and insufficiently controlled release.[86] Thus, it is necessary to achieve an appropriate spatiotemporal controlled release of the nanomedicines. Optimization of the nanomedicine template allows a controlled release of the encapsulated payloads, which is known as a stimuli-responsive system.[87] In general, these nanoparticles are designed to recognize subtle environmental changes from

external stimuli, or from tumor environment in order to evoke the release of their payloads. External stimuli inducing a remote-controlled release include temperature,[88-89] light,[90-91] ultrasound,[92-93] magnetic force,[94-95] and electric fields,[96-97] while changes in pH,[98-99] redox,[100-101] ionic strength,[102-103] or enzyme activity[104-105] in target tissues are examples of internal stimuli for a local-triggered release.

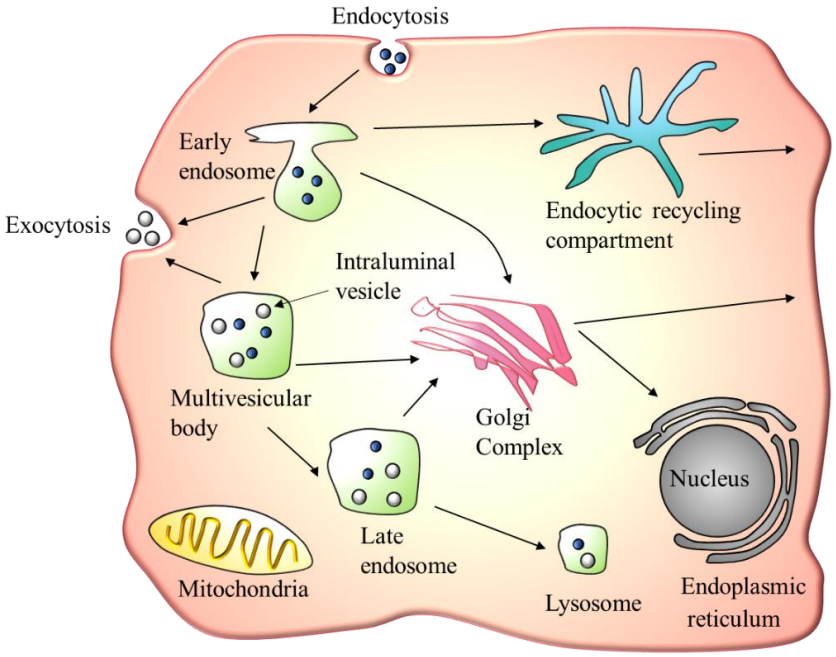

Figure 1.5. Nanomedicines internalization and its intracellular trafficking to subcellular organelles.

In terms of spatial release, if nanoparticles release the chemotherapeutics outside of the cells, followed by diffusion of chemotherapeutics into the cells, it is called extracellular delivery. If the nanoparticles internalize into the cells and release their contents, it is called intracellular delivery. Cellular membranes present a barrier for delivery of biological macromolecules to the cell interior, for example, many anticancer drugs, such as proapoptotic drugs whose primary target is the mitochondrial membrane, and gene therapy whose targets are the nucleus or mitochondrial genomes, which limits the applicability of extracellular delivery.[106-108] Intracellular delivery results in higher portions of drugs delivered into the cancer cells, and it diminishes the degradation of

encapsulated payloads protected by nanoparticles before reaching specific subcellular targets. Therefore, intracellular delivery is necessary for certain therapeutics and more effective for cancer treatment.

Endocytosis is the natural process for cells to internalize essential biomolecules, and is often exploited for intracellular delivery of nanomedicines.[109-110] In endocytosis, the plasma membrane engulfs matter in an intracellular membrane-bound vesicle, and after uncoating, fuses with early endosomes.[111] Different pathways of sorting the internalized materials involve three types of endosomes, which are early, recycling, and late endosomes, characterized by their distinct markers. Early endosomes losing the proteins subjected for recycling become multivesicular bodies before transforming to late endosomes with a more acidic environment, whose pH is decreased from 6.2–6.3 in early endosomes to 5.0–5.5 in late endosomes. The late endosomes can fuse with lysosomes that exhibit high degradative enzyme activity with pH of about 4.8–5.4.[112] Budding of the endosomal membrane producing intraluminal vesicles discharge the materials to the cellular exterior via exosomes when multivesicular bodies fuse with the plasma membrane.[113-115] Intracellular delivery of nanomedicines is effective when nanomedicines are intended to end up at endosomes or lysosomes, where the metabolic potential of endosomes and lysosomes is utilized to trigger the release.[116-121] However, for other targets located inside cytoplasm, such as lysosomes, mitochondria, endoplasmic reticulum, or nucleus, chemotherapeutics may not be able to escape endosomes/lysosomes, and they experience a degradation caused by the detrimental environment inside these vacuoles.[108] In addition, because endocytosis depends on size, shape, surface charge density, surface modification, and the identity of nanoparticles, not all types of nanoparticles can enter the cells through this mechanism of uptake.[122-124] Therefore, nanomedicines that transport drugs directly through the plasma membrane

or escape from endocytic pathway are needed for more diverse applications of intracellular delivery. Because the plasma membrane and membrane of organelles within the cell are made of a lipid bilayer, understanding their structures and properties are critical for a possible solution to overcoming the issues of the endocytic pathway of intracellular drug delivery.

1.4. Lipid Bilayer Structure

1.4.1. Phospholipids, the Main Building Blocks of the Cell Membrane

The plasma membrane of a cell is a selectively permeable lipid bilayer that separates its cytoplasm from its surroundings. This boundary not only impedes foreign materials from entering the cell but also inhibits the cellular contents from leaking out. Lipid membranes also define the boundaries of the cell's organelles, such as the nucleus, mitochondria, lysosomes, peroxisomes, Golgi apparatus, and endoplasmic reticulum. Although those membranes differ by functions, their basic structure is similar, which is mainly composed of membrane lipids, proteins and cholesterol.[125-126]

Three major classes of membrane lipids include phospholipids which are the fundamental building blocks of cellular membranes, glycolipids, and cholesterol, whose structures are shown in Figure 1.6. Depending on the glycerol sphingosine backbone, phospholipids can fall under two groups, phosphoglycerides and sphingomyelin. A phospholipid molecule is amphiphilic, possessing a hydrophilic head (water-loving, polar) and two hydrophobic tails (fat-loving, non-polar). Different structures of the headgroups and tails of the phospholipids determine their diversity. The phospholipid fatty acid components usually contain an even number of carbon atoms, saturated or unsaturated, with the cis-configuration of 16- and 18-carbons being the most common.[127-128]

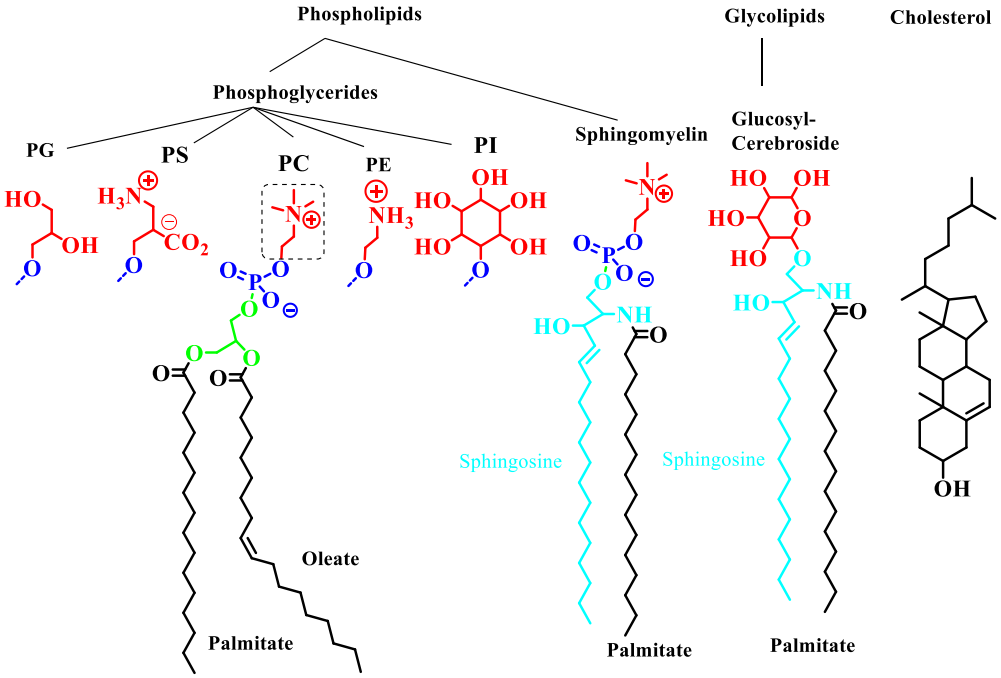

PC: Phosphatidylcholine

PE: Phosphatidylethanolamine

PS: Phosphatidylserine

PG: Phosphatidylglycerol

PI: Phosphatidylinositol

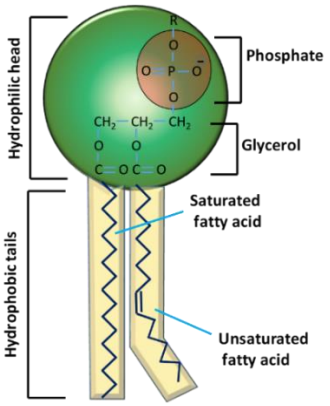

Figure 1.6. The basic structure of some lipids. Substitution of choline in the dotted box with other functional groups results in other phospholipid structures. Typically, if a full notation of a phospholipid is 18:1 *Δ*9-*cis* 1,2-dioleoyl-*sn*-glycerol-3-phosphoethanolamine, it means this phospholipid has a PE headgroup, with two 18-carbon fatty acid chains, each chain has one double bond at the ninth carbon with a *cis* configuration; which is abbreviated DOPE.

In aqueous medium, the hydrocarbon domains of the lipids' tails assemble to minimize the total surface area in contact with water while the polar domains of the headgroups are hydrated by forming hydrogen bonding or charge-charge interaction with water from their charged sites, making them energetically stable.[129-131] These interactions drive the formation of the bilayer. The bilayer nature of phospholipids can be demonstrated in vitro when a dry, thin layer of long-chain

phospholipids is hydrated, leading to the spontaneous formation of multilamellar bilayer structures.[132]

The fluid mosaic of the membrane allows constant rotational or lateral movement of lipids. While phospholipids construct a membrane structure, sterols regulate membrane rigidity. Membrane proteins can move freely in the lipid matrix and function as receptors and channel pores to control the exchange of molecules and ions between the intracellular and extracellular environment, which is vital in the cell's metabolism and regulation of signaling pathways.[125-126, 133]

1.4.2. Phospholipid Diversity and their Physical Properties

Phospholipids were once thought to play only structural roles as a permeability barrier of cells and organelles. However, despite their simple bilayer nature, hundreds of different lipid species are found in membranes with the variation in headgroups and aliphatic chains,[134] and the necessity for their diversity is not completely understood.[135-137] The basic structure of the cell membrane is similar in all tissue cells, but its actual composition of lipids and proteins species differs drastically depending on the specific function of the membrane, which further differentiates cell types.[138-139] In eukaryotic cell membranes, the predominant lipid species are phospholipids, including phosphatidylcholine (PC), phosphatidylethanolamine (PE), phosphatidylserine (PS) phosphatidylglycerol (PG), phosphatidylinositol (PI).[135, 140] The lipid composition of various biological membranes is shown in Table 1.1.

Phospholipids can exist in many structures, which is known as lipid polymorphism, depending on the nature of their headgroups and acyl chains, and solvent conditions, such as ion content, pH, and temperature.[141-143] For example, cylindrical shaped lipids, in which the headgroup occupies a volume comparable to its hydrophobic acyl chains, such as PC and PG, favor the bilayer or lamellar phase. Cone-shaped lipids, such as PE, which have small headgroups relative to their

large hydrophobic domain, favor hexagonal phase. Inverted cone-shaped lipids, such as lysophospholipid or phosphatidylinositol-4-phosphate prefer micellar phase.

Table 1.1. Approximate lipid compositions of different cell membranes.[144]

Lipid	Percentage of total lipid by weight				
	Liver cell plasma membrane	Red Blood cell plasma membrane	Myelin	Mitochondrion membrane	Endoplasmic reticulum
Cholesterol	17	23	22	3	6
PE	7	18	15	25	17
PS	4	7	9	2	5
PC	24	17	10	39	40
Sphingomyelin	19	18	8	0	40
Glycolipids	7	3	28	trace	trace
Others	22	13	8	21	27

Lipid geometrical shapes also dictate the membrane curvature. When a portion of the membrane monolayer contains lipids with similar shape, that segment will adopt the spontaneous curvature of the local lipids. For example, PC and PS form a flat monolayer, PE imposes a negative curvature, and PI adapts a positive curvature.[145] The presence of non-bilayer favoring lipids in the bilayer causes stress or strain in the bilayer by influencing membrane curvature.[146-147] The presence of PE in PC bilayers introduces curvature stress onto the membrane, which plays a role in budding, fission, and fusion of cells.[148-149] The molecular geometry of phospholipids related to their phase of existence and their physical properties are demonstrated in Figure 1.7.

The phase transition temperature for the lamellar to hexagonal phase is called T_H. In the bilayer form, lipids organize in either ordered gel (L_β) or liquid crystalline (L_α) phases, which have different fluidity (i.e., the inverse of viscosity) in the hydrophobic domains of the lipids. The temperature inducing a phase transition from L_β to L_α is named T_M. The hydrocarbon chains are fully extended and tightly packed in L_β while they randomly arrange and are fluidic in L_α. The T_M and T_H of different PC and PE lipids are summarized in Table 1.2.[150-151]

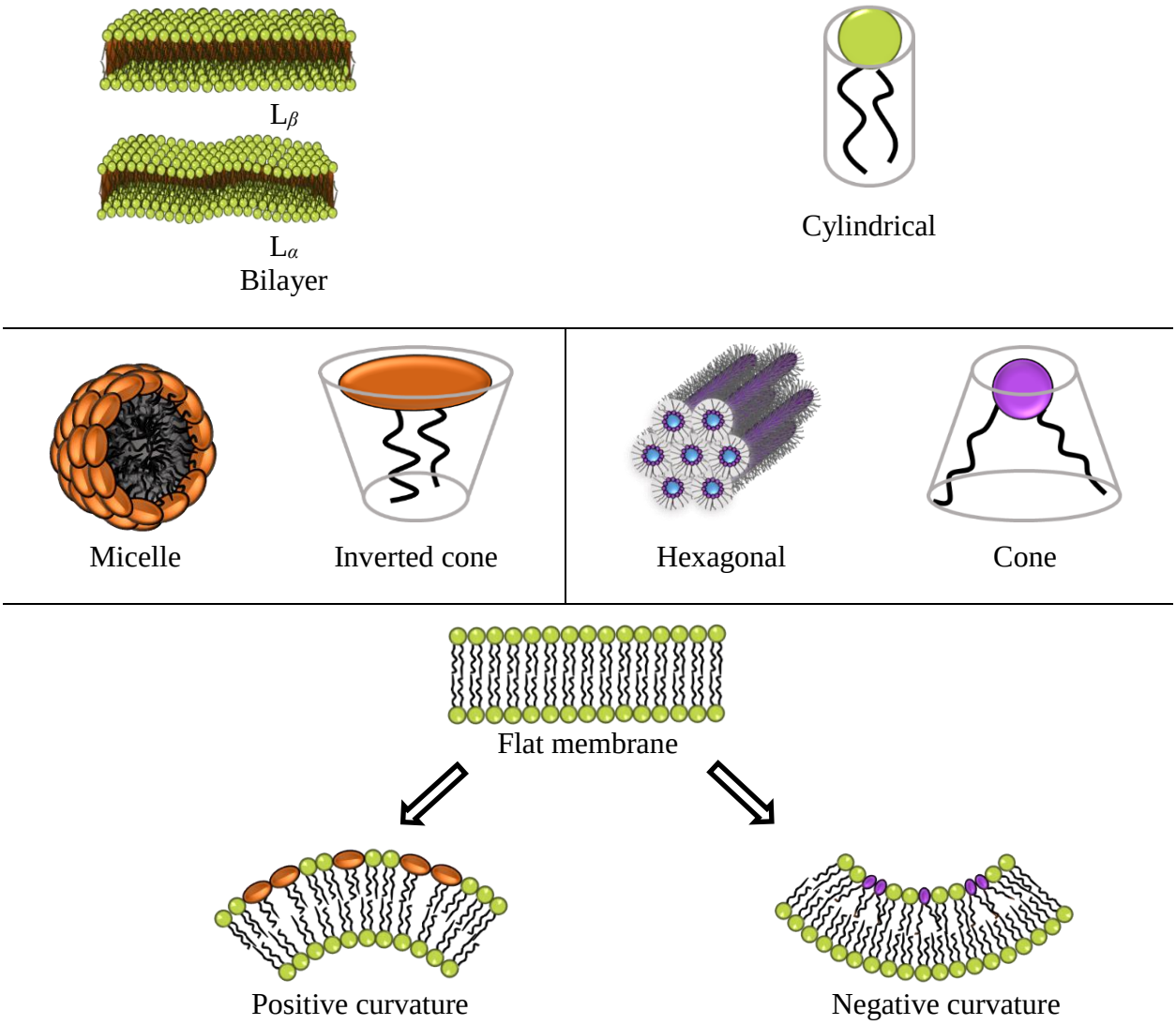

Figure 1.7. Molecular geometry of lipids determines their polymorphic phases and membrane curvature. Cylindrical, cone and inverted cone-shaped adapt bilayer, hexagonal, and micelle phase, respectively. The L_{β} (ordered gel) and L_{α} (liquid crystalline) bilayer phases have different fluidity, dependent on the degree of order within the hydrophobic domain and the mobility of the individual molecules. Introduction of non-bilayer lipid cause stress on the membrane by changing its curvature.[149]

In both lipids, as the hydrocarbon chains get longer, van der Waals interactions of the lipids become stronger, requiring more thermal energy to disrupt the ordered packing, increasing T_M. Likewise, introducing a *cis* double bond into the acyl group puts a kink in the chain, which induces an ordered packing arrangement at much lower temperatures. Because PC lipids have a large headgroup and are more hydrated, they favor a bilayer phase at a wide range of temperatures. On

the other hand, PE lipids at a certain length and unsaturation degree of the tail will experience a phase transition from a lamellar phase to a hexagonal phase. Thus, in general, the fluidity of the bilayer increases with an increasing degree of unsaturation or with decreasing alkyl chain length.[152] When the temperature is increased, the fluidity of the membrane also increases due to the enhanced thermal mobility of the chains, thereby occupying more space volume.[153-155] Therefore, the leakage and phase transition of the bilayer are influenced by the lipid composition. Typically, the bilayer containing lipids with lower T_M experience more leakage, and the bilayer consisting of a high portion of PE lipids tend to transform to the hexagonal phase.

Table 1.2. Phase transition temperature of some PC, PG, and PE lipids.[150-151]

Lipid	T_M (°C)	Lipid	T_M (°C)	T_H (°C)
18:1c9 (DOPC)	-17	18:1c9 (DOPE)	-16	10
12:0 (DLPC)	-2	12:0 (DLPE)	29	
14:0 (DMPC)	24	14:0 (DMPE)	50	
16:0 (DPPC)	41	16:0 (DPPE)	63	118
18:0 (DSPC)	55	18:0 (DSPE)	74	100

1.4.3. Membrane Asymmetry and its Importance

In addition to the diversity of phospholipids in different organelle membranes, the two leaflets of the lipid bilayer have distinct phospholipid contents. The endoplasmic reticulum (ER) membrane bilayer displays a symmetric lipid distribution between its two leaflets, whereas the Golgi apparatus, plasma and endosomal membranes have an asymmetric lipid distribution, with PC enriched in the outer or exoplasmic leaflet and PS and PE enriched in the cytoplasmic leaflet.[135, 156-159] The qualitative and quantitative difference in the lipid content located in the two monolayers are known as membrane asymmetry. This construction reflects the different functions of the two faces of the membrane to regulate cellular homeostasis and activities, and the lack of this maintenance of correct lipid asymmetry causes several diseases.[160-161] Most phospholipids are neutral at physiological pH, while PS, PG, and PI have a net negative charge. Two layers with

unequal charged lipid distribution generate a membrane potential, which controls the flux of molecules in and out of the cell. In addition, changes in expression levels of individual lipids are associated with many diseases, such as cancers, diabetes, Alzheimer's disease, HIV, and atherosclerosis.[162] For example, changing the PC/PE ratio appears to be associated with heart myocytes in mammalian cells[163] or liver failure[164] due to a subsequent change in membrane fluidity causing variations in membrane integrity and functions of membrane proteins.

PC is a major constituent of cell membranes and pulmonary surfactant. PC favors a bilayer formation, and it mainly functions as the bulk structural element of biological membranes. PC is involved in membrane-mediated cell signaling and activation of other enzymes. PC is also an important substrate in the synthesis of the neurotransmitter acetylcholine and has the function of nourishing the brain.[165-166] On the other hand, the non-bilayer propensity of PE plays an important role in membrane-embedded proteins' functions and processes such as membrane fusion and fission.[142, 167] PE metabolism in the heart is vital because the PE distribution in sarcolemmal membranes is altered during ischemia, causing sarcolemmal disruption.[168]

Cells exploit an alteration of lipid asymmetry of their plasma membranes to discriminate between live and dead cells. When cells undergo apoptosis, PS is rapidly translocated to the extracellular monolayer, which is commonly used as a marker for apoptosis. Some viruses express PS in the outer surface of the membrane to be incorporated more easily by phagocytosis or macropinocytosis. In addition, exposure of PS on blood cells or platelets produce signals for blood coagulation. Moreover, during sperm maturation, PS becomes exposed on the outer layer.[169]

Another example showing the importance of membrane asymmetry can be seen in human red blood cells, which have no nucleus or organelles but consist primarily of the plasma membrane and hemoglobin to maximize oxygen-carrying capacity. The outer monolayer of the plasma

membrane contains PC and sphingomyelin, the inner monolayer contains PS, PE, and PI while cholesterol is distributed evenly throughout the two monolayers.[156] Although these examples are just a few of the many biologically relevant processes, they do highlight the importance of understanding the function of membrane asymmetry in cells.

1.4.4. Membrane Fusion, a Unique Property of Lipid Bilayers

In biology, membrane fusion occurs when two distinct lipid bilayers merge their hydrophobic cores to form a unified lipid bilayer. There are two types of fusion, complete fusion and hemifusion. Complete fusion proceeds via a mix of both leaflets of both bilayers, resulting in content mixing between the two internal aqueous portions. Hemifusion involves only mixing of the outer leaflet from each bilayer, while the aqueous contents enclosed by each bilayer remain unmixed.[170-171]

Fusion plays a vital role in many cellular events, typically for cells or bio-structures coated by lipid bilayers, such as fertilization of an egg by a sperm[172], and even the entry of pathogens with coated bilayer into the host cell.[173] In addition, fusion is related to membrane trafficking, including endocytosis and exocytosis, which regulate transport and delivery of cargo to the correct location either inside the cell at different organelles or across the cell plasma membrane using membrane-bound transport vesicles.[174-176] Therefore, fusion can be exploited as an entryway for intracellular delivery of therapeutics in addition to the standard endocytic pathway. Moreover, fusion provides an escape possibility for materials from endosomes/lysosome membranes.

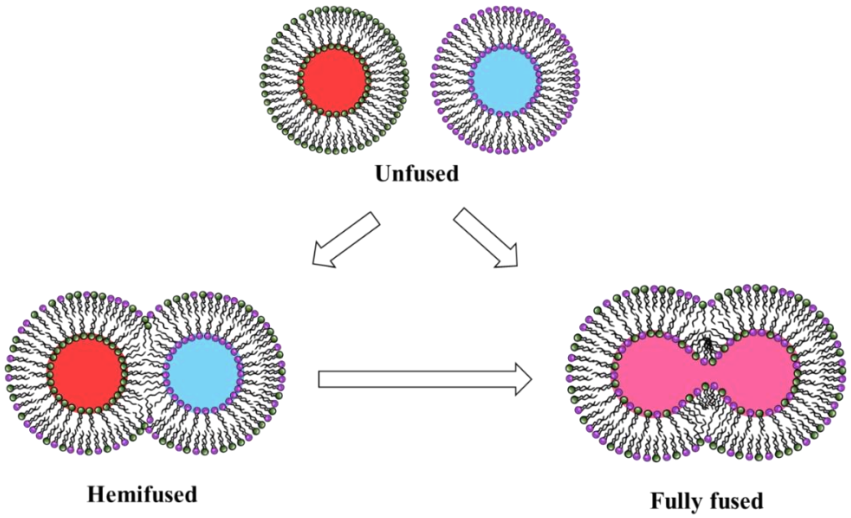

Figure 1.8.Illustration of membrane fusion. Fusion of two lipid bilayers exhibits two possible outcomes. Hemifusion involves mixing of the outer bilayer leaflets only. Complete fusion requires mixing of both leaflets and the internal contents.

1.5. Liposomes for Drug Delivery

1.5.1. Liposomes Structures

Nanocarriers must possess certain requirements for drug delivery: the capability of loading adequate amount of active drug, easy modification of the nanocarrier surface, non-toxicity or nonimmunogenicity, biodegradability or biocompatibility, the ability to retain drugs until the biological target is reached, and the ability to release drugs under control. Phospholipids are highly attractive materials to meet these requirements because they are the natural building blocks for cell membranes, which exhibit a low immune response, are nontoxic, and are highly biocompatible and biodegradable as they can be metabolized similarly to endogenous phospholipids. In addition, due to the ability to form enclosed bilayer structures of phospholipids, they are used to produce liposomes. These spherical vesicles with specifically controlled sizes, ranging from 30 nanometers to a few micrometers in diameter[132] serve as a convenient vehicle to encapsulate and deliver a variety of both hydrophilic and hydrophobic compounds, including nutrients and therapeutics drugs, such as cancer chemotherapeutics, proteins, and genes.[177] The headgroup diversity of

phospholipids allows versatile chemical surface modification to achieve active targeting ability, and simple formulation by changing lipid compositions results in convenient physical modulation of the liposomes.[4] These advantages improve drug potency, minimize side effects, and allow for dosage reduction.

Diverse applications of liposomes are demonstrated in Figure 1.9, with many of them being utilized for human use and clinical tests currently.[1, 6] For instance, the first class of therapeutic-liposome nanomedicine platform was liposomal doxorubicin (Doxil and Myocet) that was received clinical approval for cancer treatment. Other lipid-based nanoparticles also add to a large proportion of clinical-stage nanotherapeutics.

1.5.2. Fusion Delivery of Liposomes

As discussed before, to date, efficient intracellular delivery of therapeutics to cells remains a significant challenge. For example, most delivery approaches are based on the endocytic pathway, which presents a low delivery efficiency because of the limited endosomal escape and degradation of drugs in lysosomes.[178-179] Therefore, the development of a new alternative delivery method that bypasses the endocytosis pathway is essential. Thus, current efforts involve developing more advanced pathways of enhancing endosomal escape. Three mechanisms are exploited to promote endosomal escape.[180-181] First, pore formation on the endosomal membrane is facilitated when cationic amphiphilic peptides are inserted into the endosomal membrane, leading to the internal membrane. Second, the proton sponge effect ruptures the endosomal membrane. Typically, the acidic environment in the endosome protonates the entrapped agents possessing a high buffering capacity. This chemical potential drop leads to an inflow of protons and chloride, as well as water, into the endosomes, causing osmotic swelling and endosome rupture. Third, some agents, such as fusogenic lipids or peptides, can disrupt the endosomal

membrane, or enhance the fusion of the carrier with the endosomal membrane to induce the payload release into the cytoplasm.

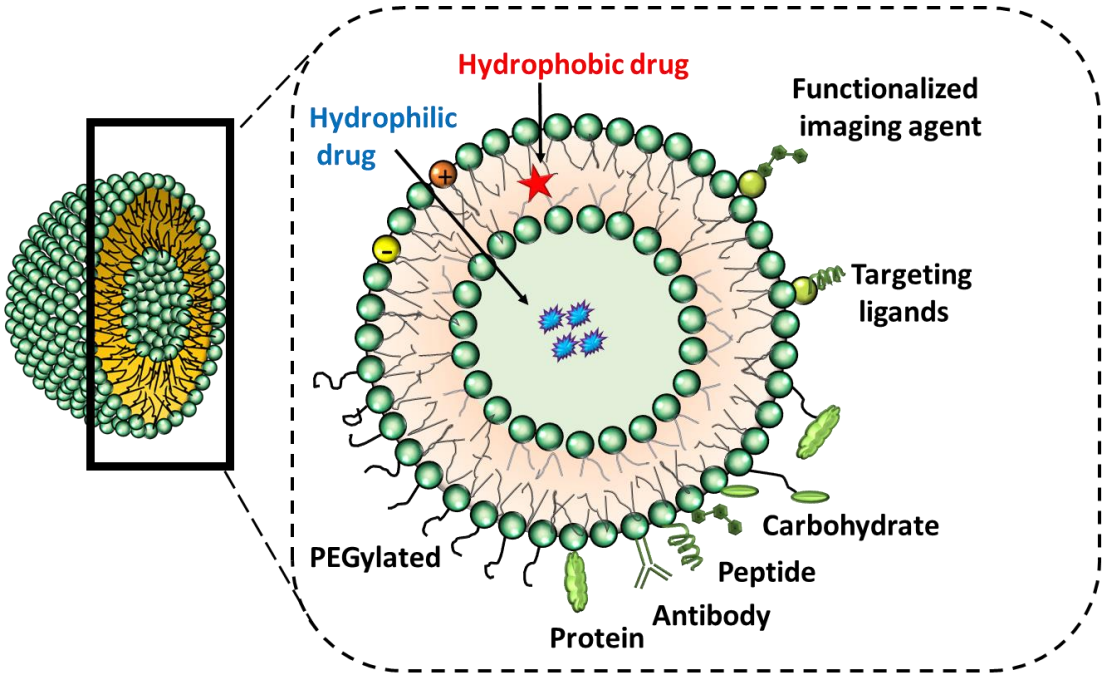

Figure 1.9. Different types of liposomal drug delivery systems. (Adapted from Sercombe, 2015)[3]

Due to the similarity in structure of the lipid bilayer, liposomes can merge with the lipid bilayer structure components of the cell, including the plasma membrane, endosomes/exosomes, and nuclear membranes, resulting in content mixing by fusion. Different possible fusion delivery pathways of liposomes can be seen in Figure 1.10. Fusion delivery of liposomes has been demonstrated to deliver molecules into the cell cytoplasm or escape the endocytic pathway. However, they all need the aid of cell penetrating peptides,[182-183] coiled-coil peptides,[184-186] or viruses.[187-189] These techniques may lead to unfavorable interactions with blood components[190] or safety issues.[184] In addition, mechanistic studies to understand the underlying fusion processes are challenging in vivo because of the complex nature of the imaging of rapid processes inside the endosome.[191] For this reason, the intracellular conditions are mimicked in vitro, using a liposome-liposome fusion as a representative model. However, because of the nature of lipid bilayer

formation, the liposomes membrane is symmetrical. Therefore, the simplicity of those systems does not correctly represent the basic characteristics of native membrane fusion regarding the asymmetric nature of the fusion system in the cell. In addition, the relationships of lipids and their asymmetrical distribution in the bilayer with fusion are still not clear. As a result, understanding the role of membrane asymmetry in the leakage/release and fusion in lipid bilayers is important and helpful for a possible formulation of fusion delivery of liposomes.

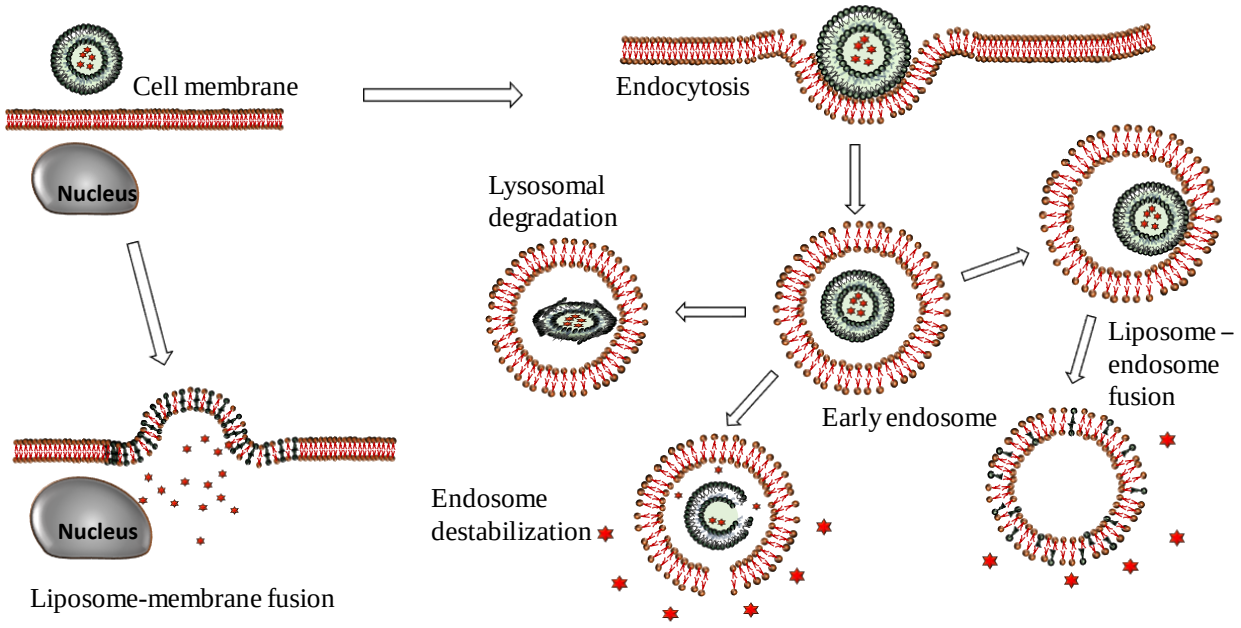

Figure 1.10. Possible pathways of intracellular delivery through liposomes.

1.6. References

1. Bulbake, U., et al., Liposomal Formulations in Clinical Use: An Updated Review. *Pharmaceutics* **2017,** *9* (2), 12.

2. Laouini, A., et al., Preparation, Characterization and Applications of Liposomes: State of the Art. *Journal of Colloid Science and Biotechnology* **2012,** *1* (2), 147-168.

3. Sercombe, L., et al., Advances and Challenges of Liposome Assisted Drug Delivery. *Frontiers in Pharmacology* **2015,** *6*, 286.

4. Riaz, M., et al., Surface Functionalization and Targeting Strategies of Liposomes in Solid Tumor Therapy: A Review. *International Journal of Molecular Sciences* **2018,** *19* (1), 195.

5. Alavi, M., et al., Application of Various Types of Liposomes in Drug Delivery Systems. *Advanced Pharmaceutical bBulletin* **2017,** *7* (1), 3.

6. Daraee, H., et al., Application of Liposomes in Medicine and Drug Delivery. *Artificial Cells, Nanomedicine, and Biotechnology* **2016,** *44* (1), 381-391.

7. Bozzuto, G.; Molinari, A., Liposomes as Nanomedical Devices. *International Journal of Nanomedicine* **2015,** *10*, 975.

8. Wang, Y.; Kohane, D. S., External Triggering and Triggered Targeting Strategies for Drug Delivery. *Nature Reviews Materials* **2017,** *2* (6), 17020.

9. Nogueira, E., et al., Design of Liposomal Formulations for Cell Targeting. *Colloids and Surfaces B: Biointerfaces* **2015,** *136*, 514-526.

10. Ong, W., et al., Redox-Triggered Contents Release from Liposomes. *Journal of the American Chemical Society* **2008,** *130* (44), 14739-14744.

11. Loew, M., et al., Lipid Nature and Their Influence on Opening of Redox-Active Liposomes. *Langmuir : the ACS Journal of Surfaces and Colloids* **2013,** *29* (22), 6615-6623.

12. McCarley, R. L., et al., Release Rates of Liposomal Contents Are Controlled by Kosmotropes and Chaotropes. *Langmuir : the ACS Journal of Surfaces and Colloids* **2013,** *29* (46), 13991-13995.

13. Winter, J. E., On the Development of Analytical Methodologies to Interrogate the Lipid Dynamics and Phase Transition Resulting from the Reduction of Stimuli-Responsive Vesicles. Ph.D Dissertation, Louisiana State University, Baton Rouge, LA, 2015.

14. Https://Www.Who.Int/News-Room/Fact-Sheets/Detail/Cancer (Accessed 5/1/2019).

15. Bray, F., et al., Global Cancer Statistics 2018: Globocan Estimates of Incidence and Mortality Worldwide for 36 Cancers in 185 Countries. *CA: a Cancer Journal for Clinicians* **2018,** *68* (6), 394-424.

16. Hanahan, D.; Weinberg, R. A., The Hallmarks of Cancer. *Cell* **2000,** *100* (1), 57-70.

17. Hanahan, D.; Weinberg, R. A., Hallmarks of Cancer: The Next Generation. *Cell* **2011,** *144* (5), 646-674.

18. Fouad, Y. A.; Aanei, C., Revisiting the Hallmarks of Cancer. *American Journal of Cancer Research* **2017,** *7* (5), 1016.

19. Witsch, E., et al., Roles for Growth Factors in Cancer Progression. *Physiology* **2010,** *25* (2), 85-101.

20. Duronio, R. J.; Xiong, Y., Signaling Pathways That Control Cell Proliferation. *Cold Spring Harbor Perspectives in Biology* **2013,** *5* (3), a008904.

21. Fulda, S., Tumor Resistance to Apoptosis. *International Journal of Cancer* **2009,** *124* (3), 511-515.

22. Marshall, C. J., Tumor Suppressor Genes. *Cell* **1991,** *64* (2), 313-326.

23. Sherr, C. J., Principles of Tumor Suppression. *Cell* **2004,** *116* (2), 235-246.

24. Ouyang, L., et al., Programmed Cell Death Pathways in Cancer: A Review of Apoptosis, Autophagy and Programmed Necrosis. *Cell Proliferation* **2012,** *45* (6), 487-498.

25. Günes, C.; Rudolph, K. L., The Role of Telomeres in Stem Cells and Cancer. *Cell* **2013,** *152* (3), 390-393.

26. Hillen, F.; Griffioen, A. W., Tumour Vascularization: Sprouting Angiogenesis and Beyond. *Cancer and Metastasis Reviews* **2007,** *26* (3-4), 489-502.

27. Forster, J. C., et al., A Review of the Development of Tumor Vasculature and Its Effects on the Tumor Microenvironment. *Hypoxia* **2017,** *5*, 21.

28. Pavlova, N. N.; Thompson, C. B., The Emerging Hallmarks of Cancer Metabolism. *Cell Metabolism* **2016,** *23* (1), 27-47.

29. Dang, C. V., Links between Metabolism and Cancer. *Genes & Development* **2012,** *26* (9), 877-890.

30. Witz, I. P., Tumor–Microenvironment Interactions: Dangerous Liaisons. *Advances in Cancer Research* **2008,** *100*, 203-229.

31. Fiedler, E. C.; Hemann, M. T., Aiding and Abetting: How the Tumor Microenvironment Protects Cancer from Chemotherapy. *Annual Review of Cancer Biology* **2019**.

32. Sun, Y., Tumor Microenvironment and Cancer Therapy Resistance. *Cancer Letters* **2016,** *380* (1), 205-215.

33. Sharma, P., et al., Primary, Adaptive, and Acquired Resistance to Cancer Immunotherapy. *Cell* **2017,** *168* (4), 707-723.

34. Dunn, G. P., et al., Cancer Immunoediting: From Immunosurveillance to Tumor Escape. *Nature Immunology* **2002,** *3* (11), 991.

35. Ribas, A., Adaptive Immune Resistance: How Cancer Protects from Immune Attack. *Cancer Discovery* **2015,** *5* (9), 915-919.

36. Guan, X., Cancer Metastases: Challenges and Opportunities. *Acta Pharmaceutica Sinica B* **2015,** *5* (5), 402-418.

37. Hunter, K. W., et al., Mechanisms of Metastasis. *Breast Cancer Research* **2008,** *10* (1), S2.

38. Riggi, N., et al., Cancer Metastasis: A Reappraisal of Its Underlying Mechanisms and Their Relevance to Treatment. *Annual Review of Pathology: Mechanisms of Disease* **2018,** *13*, 117-140.

39. Merisko-Liversidge, E. M.; Liversidge, G. G., Drug Nanoparticles: Formulating Poorly Water-Soluble Compounds. *Toxicologic Pathology* **2008,** *36* (1), 43-48.

40. Lipinski, C. A., Drug-Like Properties and the Causes of Poor Solubility and Poor Permeability. *Journal of Pharmacological and Toxicological Methods* **2000,** *44* (1), 235-249.

41. Airley, R., *Cancer Chemotherapy: Basic Science to the Clinic*. John Wiley & Sons: 2009.

42. Lake, R. A.; Robinson, B. W., Immunotherapy and Chemotherapy—a Practical Partnership. *Nature Reviews Cancer* **2005,** *5* (5), 397.

43. Wicki, A., et al., Nanomedicine in Cancer Therapy: Challenges, Opportunities, and Clinical Applications. *Journal of Controlled Release* **2015,** *200*, 138-157.

44. Shahriari, M., et al., Enzyme Responsive Drug Delivery Systems in Cancer Treatment. *Journal of Controlled Release* **2019**.

45. Tran, S., et al., Cancer Nanomedicine: A Review of Recent Success in Drug Delivery. *Clin Transl Med* **2017,** *6* (1), 44.

46. Duncan, R.; Gaspar, R., Nanomedicine (S) under the Microscope. *Molecular Pharmaceutics* **2011,** *8* (6), 2101-2141.

47. Liu, H.; Webster, T. J., Nanomedicine for Implants: A Review of Studies and Necessary Experimental Tools. *Biomaterials* **2007,** *28* (2), 354-369.

48. LaVan, D. A., et al., Moving Smaller in Drug Discovery and Delivery. *Nature Reviews Drug Discovery* **2002,** *1* (1), 77.

49. Anselmo, A. C.; Mitragotri, S., Nanoparticles in the Clinic. *Bioengineering & Translational Medicine* **2016,** *1* (1), 10-29.

50. Cortajarena, A. L., et al., Engineering Iron Oxide Nanoparticles for Clinical Settings. *Nanobiomedicine* **2014,** *1* (Godište 2014), 1-2.

51. Min, Y., et al., Clinical Translation of Nanomedicine. *Chemical Reviews* **2015,** *115* (19), 11147-11190.

52. Weissig, V., et al., Nanopharmaceuticals (Part 1): Products on the Market. *International Journal of Nanomedicine* **2014,** *9*, 4357.

53. Barenholz, Y. C., Doxil®—the First Fda-Approved Nano-Drug: Lessons Learned. *Journal of Controlled Release* **2012,** *160* (2), 117-134.

54. Davis, M. E., The First Targeted Delivery of Sirna in Humans Via a Self-Assembling, Cyclodextrin Polymer-Based Nanoparticle: From Concept to Clinic. *Molecular Pharmaceutics* **2009,** *6* (3), 659-668.

55. Narvekar, M., et al., Nanocarrier for Poorly Water-Soluble Anticancer Drugs—Barriers of Translation and Solutions. *Aaps Pharmscitech* **2014,** *15* (4), 822-833.

56. Zhang, T., et al., Application of Sialic Acid/Polysialic Acid in the Drug Delivery Systems. *Asian Journal of Pharmaceutical Sciences* **2014,** *9* (2), 75-81.

57. Bader, R. A.; Wardwell, P. R., Polysialic Acid: Overcoming the Hurdles of Drug Delivery. *Therapeutic Delivery* **2014,** *5* (3), 235-237.

58. Otsuka, H., et al., Pegylated Nanoparticles for Biological and Pharmaceutical Applications. *Advanced Drug Delivery Reviews* **2012,** *64*, 246-255.

59. Milton, H. J., et al., Pegylation: A Novel Process for Modifying Pharmacokinetics. *Clin Pharmacokinet* **2001,** *40* (7), 539-551.

60. Wang, M.; Thanou, M., Targeting Nanoparticles to Cancer. *Pharmacological Research* **2010,** *62* (2), 90-99.

61. Brannon-Peppas, L.; Blanchette, J. O., Nanoparticle and Targeted Systems for Cancer Therapy. *Advanced Drug Delivery Reviews* **2012,** *64*, 206-212.

62. Du, J., et al., Stimuli-Responsive Nanoparticles for Targeting the Tumor Microenvironment. *Journal of Controlled Release* **2015,** *219*, 205-214.

63. Ganta, S., et al., A Review of Stimuli-Responsive Nanocarriers for Drug and Gene Delivery. *Journal of Controlled Release* **2008,** *126* (3), 187-204.

64. Hossen, S., et al., Smart Nanocarrier-Based Drug Delivery Systems for Cancer Therapy and Toxicity Studies: A Review. *J Adv Res* **2019,** *15*, 1-18.

65. Li, Y., et al., Delivery of Nanomedicines to Extracellular and Intracellular Compartments of a Solid Tumor. *Advanced Drug Delivery Reviews* **2012,** *64* (1), 29-39.

66. Maeda, H., et al., The Epr Effect for Macromolecular Drug Delivery to Solid Tumors: Improvement of Tumor Uptake, Lowering of Systemic Toxicity, and Distinct Tumor Imaging in Vivo. *Advanced Drug Delivery Reviews* **2013,** *65* (1), 71-79.

67. Balasubramanian, S. K., et al., Biodistribution of Gold Nanoparticles and Gene Expression Changes in the Liver and Spleen after Intravenous Administration in Rats. *Biomaterials* **2010,** *31* (8), 2034-2042.

68. Peracchia, M., et al., Stealth® Pegylated Polycyanoacrylate Nanoparticles for Intravenous Administration and Splenic Targeting. *Journal of Controlled Release* **1999,** *60* (1), 121-128.

69. Yoo, J.-W., et al., Factors That Control the Circulation Time of Nanoparticles in Blood: Challenges, Solutions and Future Prospects. *Current Pharmaceutical Design* **2010,** *16* (21), 2298-2307.

70. Sanhai, W. R., et al., Seven Challenges for Nanomedicine. *Nature Nanotechnology* **2008,** *3* (5), 242.

71. Bazak, R., et al., Cancer Active Targeting by Nanoparticles: A Comprehensive Review of Literature. *Journal of Cancer Research and Clinical Oncology* **2015,** *141* (5), 769-784.

72. Yang, L., et al., Single Chain Epidermal Growth Factor Receptor Antibody Conjugated Nanoparticles for in Vivo Tumor Targeting and Imaging. *Small* **2009,** *5* (2), 235-243.

73. El-Sayed, I. H., et al., Surface Plasmon Resonance Scattering and Absorption of Anti-Egfr Antibody Conjugated Gold Nanoparticles in Cancer Diagnostics: Applications in Oral Cancer. *Nano Letters* **2005,** *5* (5), 829-834.

74. Gao, X., et al., Lectin-Conjugated Peg–Pla Nanoparticles: Preparation and Brain Delivery after Intranasal Administration. *Biomaterials* **2006,** *27* (18), 3482-3490.

75. Obaid, G., et al., Cancer Targeting with Biomolecules: A Comparative Study of Photodynamic Therapy Efficacy Using Antibody or Lectin Conjugated Phthalocyanine-Peg Gold Nanoparticles. *Photochemical & Photobiological Sciences* **2015,** *14* (4), 737-747.

76. Pan, L., et al., Nuclear-Targeted Drug Delivery of Tat Peptide-Conjugated Monodisperse Mesoporous Silica Nanoparticles. *Journal of the American Chemical Society* **2012,** *134* (13), 5722-5725.

77. Ruan, G., et al., Imaging and Tracking of Tat Peptide-Conjugated Quantum Dots in Living Cells: New Insights into Nanoparticle Uptake, Intracellular Transport, and Vesicle Shedding. *Journal of the American Chemical Society* **2007,** *129* (47), 14759-14766.

78. Zheng, G., et al., Rerouting Lipoprotein Nanoparticles to Selected Alternate Receptors for the Targeted Delivery of Cancer Diagnostic and Therapeutic Agents. *Proceedings of the National Academy of Sciences* **2005,** *102* (49), 17757-17762.

79. Ng, K. K., et al., Lipoprotein-Inspired Nanoparticles for Cancer Theranostics. *Accounts of Chemical Research* **2011,** *44* (10), 1105-1113.

80. Nigam, S., et al., Development of Citrate-Stabilized Fe3o4 Nanoparticles: Conjugation and Release of Doxorubicin for Therapeutic Applications. *Journal of Magnetism and Magnetic Materials* **2011,** *323* (2), 237-243.

81. Mout, R., et al., Surface Functionalization of Nanoparticles for Nanomedicine. *Chemical Society Reviews* **2012,** *41* (7), 2539-2544.

82. Seidi, F., et al., Saccharides, Oligosaccharides, and Polysaccharides Nanoparticles for Biomedical Applications. *Journal of Controlled Release* **2018**.

83. Stella, B., et al., Design of Folic Acid-Conjugated Nanoparticles for Drug Targeting. *Journal of Pharmaceutical Sciences* **2000,** *89* (11), 1452-1464.

84. Liu, Y., et al., Folic Acid Conjugated Nanoparticles of Mixed Lipid Monolayer Shell and Biodegradable Polymer Core for Targeted Delivery of Docetaxel. *Biomaterials* **2010,** *31* (2), 330-338.

85. Sahoo, S. K.; Labhasetwar, V., Enhanced Antiproliferative Activity of Transferrin-Conjugated Paclitaxel-Loaded Nanoparticles Is Mediated Via Sustained Intracellular Drug Retention. *Molecular Pharmaceutics* **2005,** *2* (5), 373-383.

86. Wang, Y., et al., Nanomedicine: Swarming Towards the Target. *Nature Materials* **2011,** *10* (7), 482.

87. Li, H.-J., et al., Stimuli-Responsive Clustered Nanoparticles for Improved Tumor Penetration and Therapeutic Efficacy. *Proceedings of the National Academy of Sciences* **2016,** *113* (15), 4164-4169.

88. Kim, Y. J., et al., A Smart Hyperthermia Nanofiber with Switchable Drug Release for Inducing Cancer Apoptosis. *Advanced Functional Materials* **2013,** *23* (46), 5753-5761.

89. May, J. P.; Li, S.-D., Hyperthermia-Induced Drug Targeting. *Expert Opinion on Drug Delivery* **2013,** *10* (4), 511-527.

90. Vivero-Escoto, J. L., et al., Photoinduced Intracellular Controlled Release Drug Delivery in Human Cells by Gold-Capped Mesoporous Silica Nanosphere. *Journal of the American Chemical Society* **2009,** *131* (10), 3462-3463.

91. An, X., et al., Photoinduced Drug Release from Thermosensitive Aunps-Liposome Using a Aunps-Switch. *Chemical Communications* **2010,** *46* (38), 7202-7204.

92. Hernot, S.; Klibanov, A. L., Microbubbles in Ultrasound-Triggered Drug and Gene Delivery. *Advanced Drug Delivery Reviews* **2008,** *60* (10), 1153-1166.

93. Kim, H. J., et al., Ultrasound-Triggered Smart Drug Release from a Poly (Dimethylsiloxane)–Mesoporous Silica Composite. *Advanced Materials* **2006,** *18* (23), 3083-3088.

94. Derfus, A. M., et al., Remotely Triggered Release from Magnetic Nanoparticles. *Advanced Materials* **2007,** *19* (22), 3932-3936.

95. Satarkar, N. S.; Hilt, J. Z., Magnetic Hydrogel Nanocomposites for Remote Controlled Pulsatile Drug Release. *Journal of Controlled Release* **2008,** *130* (3), 246-251.

96. Ge, J., et al., Drug Release from Electric-Field-Responsive Nanoparticles. *ACS nano* **2011,** *6* (1), 227-233.

97. Abidian, M. R., et al., Conducting-Polymer Nanotubes for Controlled Drug Release. *Advanced Materials* **2006,** *18* (4), 405-409.

98. Ahmed, F., et al., Shrinkage of a Rapidly Growing Tumor by Drug-Loaded Polymersomes: Ph-Triggered Release through Copolymer Degradation. *Molecular Pharmaceutics* **2006,** *3* (3), 340-350.

99. Muhammad, F., et al., Ph-Triggered Controlled Drug Release from Mesoporous Silica Nanoparticles Via Intracelluar Dissolution of Zno Nanolids. *Journal of the American Chemical Society* **2011,** *133* (23), 8778-8781.

100. Ma, N., et al., Dual Redox Responsive Assemblies Formed from Diselenide Block Copolymers. *Journal of the American Chemical Society* **2009,** *132* (2), 442-443.

101. Ma, X., et al., Functional Silica Nanoparticles for Redox-Triggered Drug/Ssdna Co-Delivery. *Advanced Healthcare Materials* **2012,** *1* (6), 690-697.

102. Manocha, B.; Margaritis, A., Controlled Release of Doxorubicin from Doxorubicin/Γ-Polyglutamic Acid Ionic Complex. *Journal of Nanomaterials* **2010,** *2010*, 12.

103. Park, M.-R., et al., Dual Ionic Interaction System Based on Polyelectrolyte Complex and Ionic, Injectable, and Thermosensitive Hydrogel for Sustained Release of Human Growth Hormone. *Biomaterials* **2013,** *34* (4), 1327-1336.

104. Azagarsamy, M. A., et al., Enzyme-Triggered Disassembly of Dendrimer-Based Amphiphilic Nanocontainers. *Journal of the American Chemical Society* **2009,** *131* (40), 14184-14185.

105. Andresen, T. L., et al., Enzyme-Triggered Nanomedicine: Drug Release Strategies in Cancer Therapy (Invited Review). *Molecular Membrane Biology* **2010,** *27* (7), 353-363.

106. Chou, L. Y., et al., Strategies for the Intracellular Delivery of Nanoparticles. *Chemical Society Reviews* **2011,** *40* (1), 233-245.

107. Torchilin, V. P., Recent Approaches to Intracellular Delivery of Drugs and DNA and Organelle Targeting. *Annu. Rev. Biomed. Eng.* **2006,** *8*, 343-375.

108. Stewart, M. P., et al., In Vitro and Ex Vivo Strategies for Intracellular Delivery. *Nature* **2016,** *538* (7624), 183.

109. Besterman, J. M.; Low, R. B., Endocytosis: A Review of Mechanisms and Plasma Membrane Dynamics. *Biochemical Journal* **1983,** *210* (1), 1.

110. Iversen, T.-G., et al., Endocytosis and Intracellular Transport of Nanoparticles: Present Knowledge and Need for Future Studies. *Nano Today* **2011,** *6* (2), 176-185.

111. Helenius, A., et al., Endosomes. *Trends in Biochemical Sciences* **1983,** *8* (7), 245-250.

112. Aubry, L., et al., Kinetics of Endosomal Ph Evolution in Dictyostelium Discoideum Amoebae. Study by Fluorescence Spectroscopy. *Journal of cell science* **1993,** *105* (3), 861-866.

113. Seaman, M.; Luzio, J., Lysosomes and Other Late Compartments of the Endocytic Pathway. *Endocytosis (Marsh, M., ed.)* **2001**, 111-148.

114. Piper, R. C.; Luzio, J. P., Late Endosomes: Sorting and Partitioning in Multivesicular Bodies. *Traffic* **2001,** *2* (9), 612-621.

115. Luzio, J. P., et al., Lysosomes: Fusion and Function. *Nature Reviews Molecular Cell Biology* **2007,** *8* (8), 622.

116. Sabella, S., et al., A General Mechanism for Intracellular Toxicity of Metal-Containing Nanoparticles. *Nanoscale* **2014,** *6* (12), 7052-7061.

117. Panyam, J., et al., Rapid Endo-Lysosomal Escape of Poly (Dl-Lactide-Co-Glycolide) Nanoparticles: Implications for Drug and Gene Delivery. *The FASEB journal* **2002,** *16* (10), 1217-1226.

118. Gilleron, J., et al., Image-Based Analysis of Lipid Nanoparticle–Mediated Sirna Delivery, Intracellular Trafficking and Endosomal Escape. *Nature Biotechnology* **2013,** *31* (7), 638.

119. Murthy, N., et al., A Macromolecular Delivery Vehicle for Protein-Based Vaccines: Acid-Degradable Protein-Loaded Microgels. *Proceedings of the National Academy of Sciences* **2003,** *100* (9), 4995-5000.

120. Du, J.-Z., et al., Tailor-Made Dual Ph-Sensitive Polymer–Doxorubicin Nanoparticles for Efficient Anticancer Drug Delivery. *Journal of the American Chemical Society* **2011,** *133* (44), 17560-17563.

121. Bae, Y., et al., Design of Environment-Sensitive Supramolecular Assemblies for Intracellular Drug Delivery: Polymeric Micelles That Are Responsive to Intracellular Ph Change. *Angewandte Chemie International Edition* **2003,** *42* (38), 4640-4643.

122. Toy, R., et al., Shaping Cancer Nanomedicine: The Effect of Particle Shape on the in Vivo Journey of Nanoparticles. *Nanomedicine* **2014,** *9* (1), 121-134.

123. Lammers, T., et al., Drug Targeting to Tumors: Principles, Pitfalls and (Pre-) Clinical Progress. *Journal of Controlled Release* **2012,** *161* (2), 175-187.

124. Azevedo, C., et al., Strategies for the Enhanced Intracellular Delivery of Nanomaterials. *Drug Discovery Today* **2018,** *23* (5), 944-959.

125. Singer, S. J.; Nicolson, G. L., The Fluid Mosaic Model of the Structure of Cell Membranes. *Science* **1972,** *175* (4023), 720-731.

126. Yeagle, P. L., *The Structure of Biological Membranes*. CRC press: 2011.

127. Fenton, W. S., et al., Essential Fatty Acids, Lipid Membrane Abnormalities, and the Diagnosis and Treatment of Schizophrenia. *Biological Psychiatry* **2000,** *47* (1), 8-21.

128. Söderberg, M., et al., Fatty Acid Composition of Brain Phospholipids in Aging and in Alzheimer's Disease. *Lipids* **1991,** *26* (6), 421.

129. Lis, L., et al., Interactions between Neutral Phospholipid Bilayer Membranes. *Biophysical Journal* **1982,** *37* (3), 657.

130. Israelachvili, J.; Wennerström, H., Role of Hydration and Water Structure in Biological and Colloidal Interactions. *Nature* **1996,** *379* (6562), 219.

131. Feller, S. E., Molecular Dynamics Simulations of Lipid Bilayers. *Current Opinion in Colloid & Interface Science* **2000,** *5* (3-4), 217-223.

132. Akbarzadeh, A., et al., Liposome: Classification, Preparation, and Applications. *Nanoscale Research Letters* **2013,** *8* (1), 102.

133. Ingólfsson, H. I., et al., Lipid Organization of the Plasma Membrane. *Journal of the American Chemical Society* **2014,** *136* (41), 14554-14559.

134. Sud, M., et al., Lmsd: Lipid Maps Structure Database. *Nucleic acids research* **2006,** *35* (suppl_1), D527-D532.

135. Van Meer, G., et al., Membrane Lipids: Where They Are and How They Behave. *Nature Reviews Molecular Cell Biology* **2008,** *9* (2), 112.

136. Harayama, T.; Riezman, H., Understanding the Diversity of Membrane Lipid Composition. *Nature reviews Molecular cell biology* **2018**.

137. Zinser, E., et al., Phospholipid Synthesis and Lipid Composition of Subcellular Membranes in the Unicellular Eukaryote Saccharomyces Cerevisiae. *Journal of Bacteriology* **1991,** *173* (6), 2026-2034.

138. Antonny, B., et al., From Zero to Six Double Bonds: Phospholipid Unsaturation and Organelle Function. *Trends in Cell Biology* **2015,** *25* (7), 427-436.

139. Hicks, A. M., et al., Unique Molecular Signatures of Glycerophospholipid Species in Different Rat Tissues Analyzed by Tandem Mass Spectrometry. *Biochimica et Biophysica Acta (BBA)-Molecular and Cell Biology of Lipids* **2006,** *1761* (9), 1022-1029.

140. Sezgin, E., et al., The Mystery of Membrane Organization: Composition, Regulation and Roles of Lipid Rafts. *Nature reviews Molecular Cell Biology* **2017,** *18* (6), 361.

141. Veatch, S. L.; Keller, S. L., Seeing Spots: Complex Phase Behavior in Simple Membranes. *Biochimica et Biophysica Acta (BBA)-Molecular Cell Research* **2005,** *1746* (3), 172-185.

142. Cullis, P. R., et al., Lipid Polymorphism and the Roles of Lipids in Membranes. *Chemistry and Physics of Lipids* **1986,** *40* (2-4), 127-144.

143. Casal, H. L.; Mantsch, H. H., Polymorphic Phase Behaviour of Phospholipid Membranes Studied by Infrared Spectroscopy. *Biochimica et Biophysica Acta (BBA)-Reviews on Biomembranes* **1984,** *779* (4), 381-401.

144. Raff, M., et al., Molecular Biology of the Cell 4th Edition. National Center for Biotechnology InformationÕs Bookshelf: 2002.

145. McMahon, H. T.; Boucrot, E., Membrane Curvature at a Glance. *J Cell Sci* **2015,** *128* (6), 1065-1070.

146. Cooke, I. R.; Deserno, M., Coupling between Lipid Shape and Membrane Curvature. *Biophysical Journal* **2006,** *91* (2), 487-495.

147. Frolov, V. A., et al., Lipid Polymorphisms and Membrane Shape. *Cold Spring Harbor Perspectives in Biology* **2011,** *3* (11), a004747.

148. Marsh, D., Lateral Pressure Profile, Spontaneous Curvature Frustration, and the Incorporation and Conformation of Proteins in Membranes. *Biophysical Journal* **2007,** *93* (11), 3884-3899.

149. Pinot, M., et al., Polyunsaturated Phospholipids Facilitate Membrane Deformation and Fission by Endocytic Proteins. *Science* **2014,** *345* (6197), 693-697.

150. Silvius, J. R., Thermotropic Phase Transitions of Pure Lipids in Model Membranes and Their Modifications by Membrane Proteins. *Lipid-protein Interactions* **1982,** *2*, 239-281.

151. Caffrey, M., et al., A Database of Lipid-Phase Transition Temperatures and Enthalpy Changes. *Journal of Chemical Information and Computer Sciences* **1991,** *31* (2), 275-284.

152. Mannock, D. A., et al., An Analysis of the Relationship between Fatty Acid Composition and the Lamellar Gel to Liquid-Crystalline and the Lamellar to Inverted Nonlamellar Phase Transition Temperatures of Phosphatidylethanolamines and Diacyl-A-D-Glucosyl Glycerols. *European Biophysics Journal* **2001,** *30* (7), 537-554.

153. Murata, N.; Los, D. A., Membrane Fluidity and Temperature Perception. *Plant physiology* **1997,** *115* (3), 875.

154. Harlos, K.; Eibl, H., Hexagonal Phases in Phospholipids with Saturated Chains: Phosphatidylethanolamines and Phosphatidic Acids. *Biochemistry* **1981,** *20* (10), 2888-2892.

155. Seelig, A.; Seelig, J., Dynamic Structure of Fatty Acyl Chains in a Phospholipid Bilayer Measured by Deuterium Magnetic Resonance. *Biochemistry* **1974,** *13* (23), 4839-4845.

156. Devaux, P. F., Static and Dynamic Lipid Asymmetry in Cell Membranes. *Biochemistry* **1991,** *30* (5), 1163-1173.

157. Kiessling, V., et al., Domain Coupling in Asymmetric Lipid Bilayers. *Biochimica et Biophysica Acta (BBA)-Biomembranes* **2009,** *1788* (1), 64-71.

158. Daleke, D. L., Phospholipid Flippases. *Journal of Biological Chemistry* **2007,** *282* (2), 821-825.

159. Devaux, P. F.; Morris, R., Transmembrane Asymmetry and Lateral Domains in Biological Membranes. *Traffic* **2004,** *5* (4), 241-246.

160. Yesylevskyy, S. O., et al., The Influence of Curvature on the Properties of the Plasma Membrane. Insights from Atomistic Molecular Dynamics Simulations. *Scientific Reports* **2017,** *7* (1), 16078.

161. Fadeel, B.; Xue, D., The Ins and Outs of Phospholipid Asymmetry in the Plasma Membrane: Roles in Health and Disease. *Critical Reviews in Biochemistry and Molecular Biology* **2009,** *44* (5), 264-277.

162. Holthuis, J. C.; Menon, A. K., Lipid Landscapes and Pipelines in Membrane Homeostasis. *Nature* **2014,** *510* (7503), 48.

163. Kučerka, N., et al., Structural Significance of Lipid Diversity as Studied by Small Angle Neutron and X-Ray Scattering. *Membranes* **2015,** *5* (3), 454-472.

164. Li, Z., et al., The Ratio of Phosphatidylcholine to Phosphatidylethanolamine Influences Membrane Integrity and Steatohepatitis. *Cell Metabolism* **2006,** *3* (5), 321-331.

165. Little, A., et al., A Double-Blind, Placebo Controlled Trial of High-Dose Lecithin in Alzheimer's Disease. *Journal of Neurology, Neurosurgery & Psychiatry* **1985,** *48* (8), 736-742.

166. Li, J., et al., A Review on Phospholipids and Their Main Applications in Drug Delivery Systems. *Asian Journal of Pharmaceutical Sciences* **2015,** *10* (2), 81-98.

167. Verkleij, A., et al. In *Non-Bilayer Structures in Membrane Fusion*, Ciba Foundation Symposium, 1984; pp 45-59.

168. Post, J., et al., Phosphatidylethanolamine and Sarcolemmal Damage During Ischemia or Metabolic Inhibition of Heart Myocytes. *American Journal of Physiology-Heart and Circulatory Physiology* **1995,** *268* (2), H773-H780.

169. Gadella, B.; Harrison, R., The Capacitating Agent Bicarbonate Induces Protein Kinase a-Dependent Changes in Phospholipid Transbilayer Behavior in the Sperm Plasma Membrane. *Development* **2000,** *127* (11), 2407-2420.

170. Jahn, R., et al., Membrane Fusion. *Cell* **2003,** *112* (4), 519-533.

171. Giraudo, C. G., et al., Snares Can Promote Complete Fusion and Hemifusion as Alternative Outcomes. *The Journal of Cell Biology* **2005,** *170* (2), 249-260.

172. Primakoff, P.; Myles, D. G., Penetration, Adhesion, and Fusion in Mammalian Sperm-Egg Interaction. *Science* **2002,** *296* (5576), 2183-2185.

173. Cossart, P.; Helenius, A., Endocytosis of Viruses and Bacteria. *Cold Spring Harbor Perspectives in Biology* **2014,** *6* (8), a016972.

174. Burgoyne, R. D.; Morgan, A., Membrane Trafficking: Three Steps to Fusion. *Current Biology* **2007,** *17* (7), R255-R258.

175. Finger, F. P.; White, J. G., Fusion and Fission: Membrane Trafficking in Animal Cytokinesis. *Cell* **2002,** *108* (6), 727-730.

176. Wu, L.-G., et al., Exocytosis and Endocytosis: Modes, Functions, and Coupling Mechanisms. *Annual Review of Physiology* **2014,** *76*, 301-331.

177. Hofheinz, R.-D., et al., Liposomal Encapsulated Anti-Cancer Drugs. *Anti-cancer Drugs* **2005,** *16* (7), 691-707.

178. Yang, J., et al., Drug Delivery Via Cell Membrane Fusion Using Lipopeptide Modified Liposomes. *Acs Central Science* **2016,** *2* (9), 621-630.

179. Sharei, A., et al., A Vector-Free Microfluidic Platform for Intracellular Delivery. *Proceedings of the National Academy of Sciences* **2013,** *110* (6), 2082-2087.

180. Varkouhi, A. K., et al., Endosomal Escape Pathways for Delivery of Biologicals. *Journal of Controlled Release* **2011,** *151* (3), 220-228.

181. Au, J. L., et al., Delivery of Cancer Therapeutics to Extracellular and Intracellular Targets: Determinants, Barriers, Challenges and Opportunities. *Adv Drug Deliv Rev* **2016,** *97*, 280-301.

182. Karagiannis, E. D., et al., Rational Design of a Biomimetic Cell Penetrating Peptide Library. *ACS nano* **2013,** *7* (10), 8616-8626.

183. Brock, R., The Uptake of Arginine-Rich Cell-Penetrating Peptides: Putting the Puzzle Together. *Bioconjugate Chemistry* **2014,** *25* (5), 863-868.

184. Yang, J., et al., Drug Delivery Via Cell Membrane Fusion Using Lipopeptide Modified Liposomes. *ACS Central Science* **2016,** *2* (9), 621-630.

185. Jahn, R.; Scheller, R. H., Snares—Engines for Membrane Fusion. *Nature Reviews Molecular Cell Biology* **2006,** *7* (9), 631.

186. Zope, H. R., et al., In Vitro and in Vivo Supramolecular Modification of Biomembranes Using a Lipidated Coiled-Coil Motif. *Angewandte Chemie International Edition* **2013,** *52* (52), 14247-14251.

187. Kunisawa, J., et al., Pharmacotherapy by Intracellular Delivery of Drugs Using Fusogenic Liposomes: Application to Vaccine Development. *Advanced Drug Delivery Reviews* **2001,** *52* (3), 177-186.

188. Voskuhl, J.; Ravoo, B. J., Molecular Recognition of Bilayer Vesicles. *Chemical Society Reviews* **2009,** *38* (2), 495-505.

189. Harrison, S. C., Viral Membrane Fusion. *Nature Structural & Molecular Biology* **2008,** *15* (7), 690.

190. Torchilin, V. P., et al., Tat Peptide on the Surface of Liposomes Affords Their Efficient Intracellular Delivery Even at Low Temperature and in the Presence of Metabolic Inhibitors. *Proceedings of the National Academy of Sciences* **2001,** *98* (15), 8786-8791.

191. Kuhn, P., et al., A Microfluidic Device for the Delivery of Enzymes into Cells by Liposome Fusion. *Engineering in Life Sciences* **2018,** *18* (2), 149-156.

CHAPTER 2
RELEASE AND FUSION OF Q_3PE-BASED LIPOSOMES RESULTING FROM AN ASYMMETRICAL CLEAVAGE OF THE Q_3 GROUP AT THE LIPOSOMAL OUTER LEAFLET

2.1. Introduction

Conventional delivery of most nanomedicines for tumor treatment is fundamentally assisted by passive accumulation at bodily target sites having leaky vasculature and poor lymphatic drainage via the enhanced permeability and retention (EPR) effect, which requires a high dose and long treatment time.[1-2] In addition, some nanocarriers might not be able to enter cells via endocytosis, or they possibly suffer from limited endocytic escape or perhaps release their payloads extracellularly; such limitations restrict their application in intracellular delivery.[3-4]

Liposomal delivery agents offer excellent advantages to overcome these obstacles. The chemical structural diversity of lipid head groups allows versatility of liposomal surface modification so as to actively target certain biomarkers. As a result, a high portion of nanomedicines can accumulate at the target sites, resulting in a lower dose of chemotherapeutics and minimal toxicity to healthy tissues when compared to the non-targeted nanomedicines. Furthermore, simple variations in lipid composition can tune the physical and chemical properties of liposomes, allowing for control of encapsulated drug release rates (kinetics) and their pathways for delivery. Finally, because liposomes are made of a lipid bilayer, they can fuse with plasma membranes or the membranes of organelles after entering cells, resulting in direct delivery of contents to the cytosol or providing an endocytic escape and entry to other subcellular compartments.[5-9]

Research of liposomal carrier systems capable of precise spatiotemporal release of payloads upon sensing specific target environments has been expanded remarkably.[10-12] Several endogenous triggers correlated to a number of cancers have been exploited for liposomal delivery

such as low pH,[13-15] high redox potential,[16-17] and enzymatic action.[18-19] Regarding internal stimulus triggered release, the McCarley group presented investigations of redox-responsive trigger release liposomes named Q_3DOPE, which take advantage of the high quinone reductase activities of $hNQO_1$ in several cancers.[20-22] The liposomes are composed of trimethyl-locked, quinone-capped phospholipids that require a two-electron reductive activation by hNQO1 to release the encapsulated payloads. Previous work in the group demonstrated that the content release kinetics of Q_3DOPE liposomes are regulated by manipulating lipid compositions of liposomes. The regulation is aimed to achieve a fast content release triggered by the enzyme, whose potency is simplified by in-vitro chemical reduction of a reducing reagent, sodium dithionite. The significance of rapid content release by the liposomal system is to enable liposomes, after accumulating at the targets, to deliver their payloads in an off-on switch scenario. Moreover, the short activation time results in limited clearance of liposomes by the reticuloendothelial system (RES) during blood circulation.[23-24] In addition, during delivery of chemotherapeutic drugs, expulsion from cancer cells by efflux pumps in the cell's plasma membrane has been reported. Indeed, cancer stem cells exhibiting drug resistance overexpress these transporter-based efflux pumps.[25] Thus, nanomedicines slowly releasing their payloads suffer cellular excretion more severely before reaching the cellular interior targets. Therefore, it is important to acquire a burst content release so that significant concentrations of drugs can bind to their targets before being excreted out of the cells.

In addition to increasing drug delivery efficiency, controlling release kinetics can shed light on the mechanism and pathways of the release of Q_3PE-based liposomes whose fusion property is not clearly understood. It is possible that membrane stress caused by hydration and curvature differences between the inner and outer leaflets of Q_3PE-based liposomes after the asymmetric

cleavage of the Q_3 group can provoke the resulting deformed vesicles to undergo bilayer contact accompanied with fusion before transforming to the hexagonal phase. In Figure 2.1 is shown a proposal outlining the content release and fusion pathways of representative liposomes made from pure Q_3DOPE lipid after the SDT-based reduction and cleavage of the Q_3 group.[26] Because the fusion of liposomes is lipid nature sensitive,[27-28] manipulating the lipid compositions of Q_3PE-based vesicles can be used to examine the fusion behavior of those vesicles.

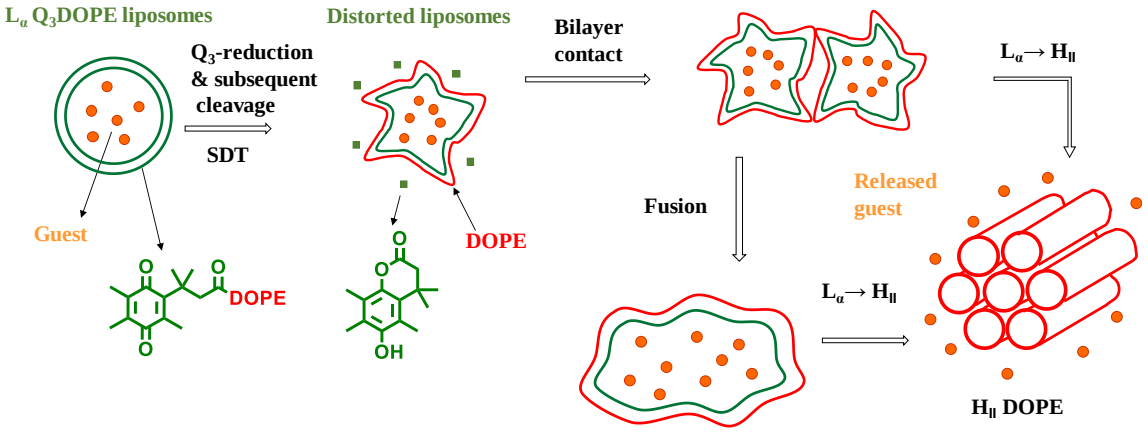

Figure 2.1. Q_3DOPE lipids (green) form lamellar liquid crystal phase (L_α) liposomes, encapsulating guest molecules (brown). Reduction of the capping quinone to hydroquinone, followed by lactonization to triggers the cleavage of Q_3 headgroups, forming DOPE lipids (red) at the outer leaflet of the liposomes. The asymmetrical distribution of lipids, with Q_3DOPE lipids remaining intact in the inner leaflet and DOPE at the outer leaflet, causes stress on the membrane due to the hydration and curvature difference between the two leaflets. Vesicles with protrusions/asperities in the membrane aggregate with or without fusion before undergoing the phase conversion to the non-lamellar inverted hexagonal phase (H_{II}), resulting in the release of the encapsulated contents into their surroundings.

The goal of this chapter is to investigate how compositions and distributions of lipids determine the fusion behavior of Q_3PE-based liposomes in correlation with their content release kinetics as a result of the asymmetrical cleavage of the Q_3 group from the outer leaflet of liposomes upon reduced by SDT. Both commercially available lipids and synthesized lipids were used for liposomal formulations. Understanding the fusion behavior of liposomes can offer a feasible

delivery method based on liposome-cell fusion that delivers the therapeutics directly into the cytosol or provides an endocytic escape to deliver the cargo to other subcellular compartments.

2.2. Experimental

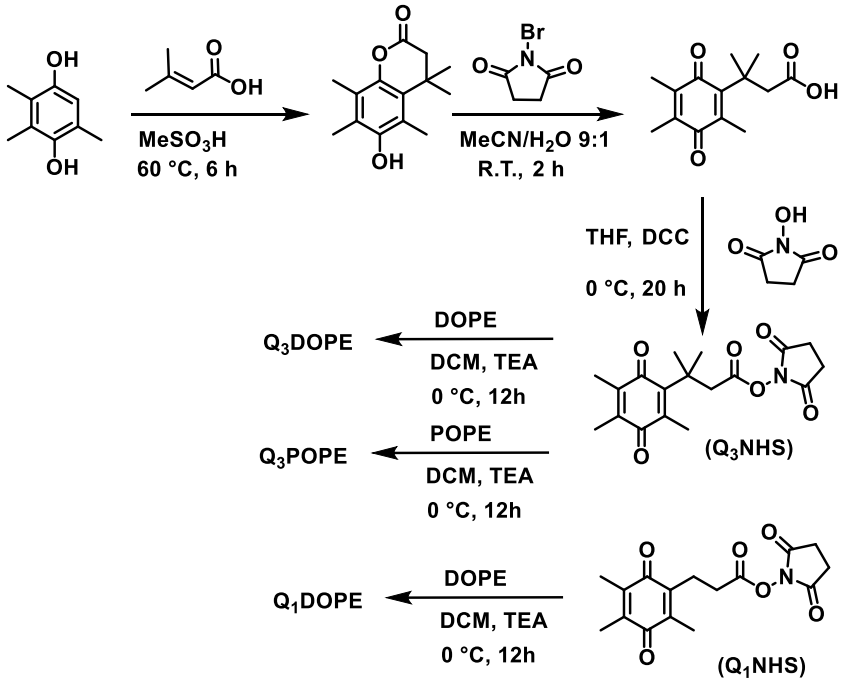

Figure 2.2. The synthesis scheme of Q_3DOPE, Q_3POPE, and Q_1DOPE.

Q_3DOPE was synthesized and purified as reported in Ong et al.,[26] whose synthesis pathway is shown in Figure 2.2. Q_3POPE and Q_1DOPE lipids were synthesized in a similar manner, using POPE lipids or Q_1NHS groups for the final coupling step, respectively. The structures of different lipids used for liposomal formulations are shown in Table 2.1. Large unilamellar vesicles (LUVs) were prepared by hydration of a lipid thin film, followed by freeze-thaw and extrusion procedures as presented before,[29] all of which are summarized in Figure 2.3. The total lipid concentration of the resulting LUVs containing encapsulates was determined by a Stewart assay or Barlette assay, depending on the buffers used; these protocols were validated, as shown in the Appendix E.[30] Dynamic light scattering (DLS) measurements demonstrate that the LUVs have a mean diameter of 100–120 nm and have a low polydispersity index (PDI < 0.2).

Table 2.1. Structures of the lipids used for Q_xPE-based liposomes formulations.

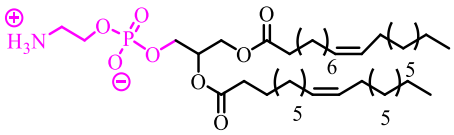 DOPE	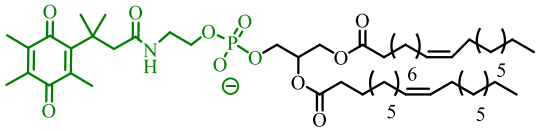 Q_3DOPE
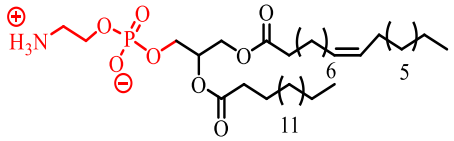 POPE	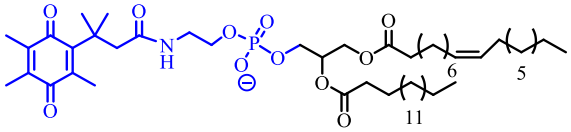 Q_3POPE
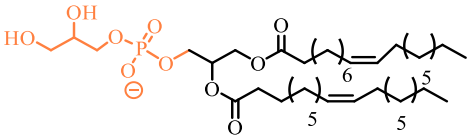 DOPG	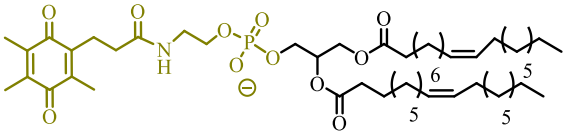 Q_1DOPE
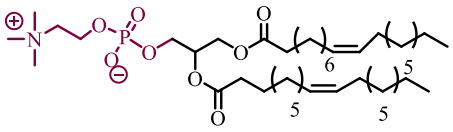 DOPC	

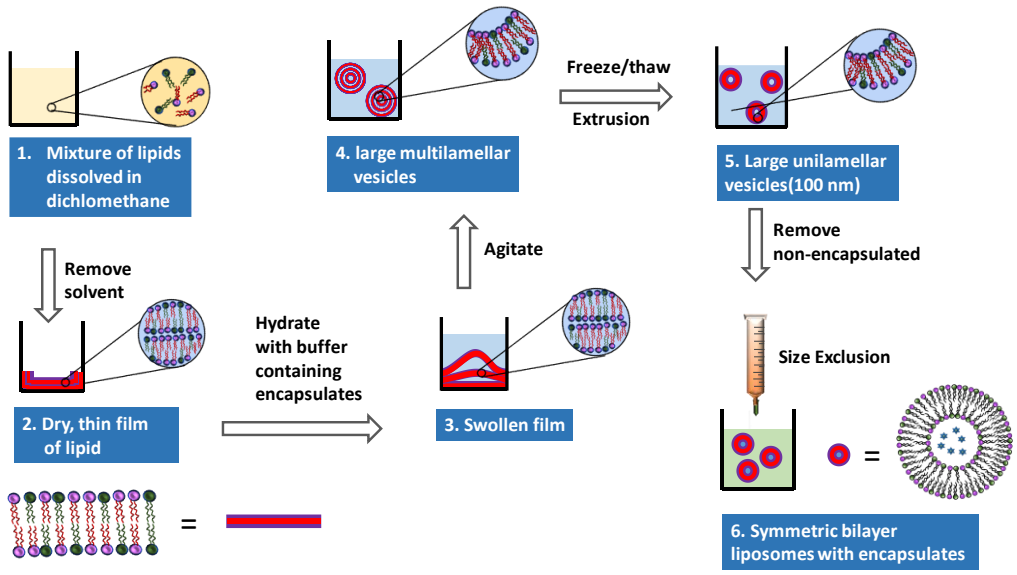

Figure 2.3. Liposomes produced by lipid hydration, freeze/thaw, and extrusion procedures have a symmetric bilayer, in which lipid composition in the outer leaflet and the inner leaflet is the same. (Adapted from Rudd, 2019).[31]

All fluorescence measurements were performed with a Perkin-Elmer LS-55 fluorometer to monitor the fluorescence signal of calcein whose excitation wavelength is at 491 nm and emission wavelength is at 515 nm. The slit widths and neutral filters were adjusted to achieve a proper baseline signal (about 200 counts/second). Liposome samples containing 1.0×10^{-4} M of lipids were added SDT stock solution of 5.0×10^{-4} M final concentration to reduce quinone headgroups, whose time at the addition is marked as $t_0 = 0$ min.

To measure content release, 0.040 M of calcein in phosphate buffer, a concentration that leads to self-quenching of its fluorescence, was encapsulated inside liposomes and any nonencapsulated calcein was removed by size-exclusion chromatography. Liposomes were then suspended in, 0.050 M phosphate buffer at a pH of 7.4 containing 0.10 M KCl and 1.0×10^{-4} M EDTA. Any possible release of calcein results in an immediate increase in fluorescence signal due to decreased self-quenching upon its release into the surroundings. All release curves are normalized so as to provide content release in comparison to the total maximum content release, as per Equation 2.1; F_0 represents the fluorescence baseline before adding SDT, F_t represents the fluorescence intensity after introduction of SDT at time *t*, and F_{100} is the maximum fluorescence intensity as determined after TritonX-100 addition (0.1 % v/v). Light-scattering was also measured and normalized in a similar manner, except the excitation and emission wavelengths were set at 600/610 nm, respectively, with 10 nm slit width each.

$$\%\ Content\ release = \frac{F_t - F_0}{F_{100} - F_0} \times 100\ \% \qquad \text{Equation 2.1}$$

For fusion measurements, the cobalt-calcein/EDTA leakage and content-mixing fusion assay was used, which involves encapsulating the quenched fluorescent complex of calcein and Co^{2+} in one set of vesicles (vesicle A) and EDTA in the second set (vesicle B). If fusion occurs, EDTA chelates Co^{2+}, releasing free calcein that may be assayed through the significant increase

of calcein's fluorescence.[32] Four buffers were prepared. Buffer A contains 0.010 M TES, 0.10 M KCl, 1.0×10^{-3} M $CoCl_2$ and 8.0×10^{-4} M calcein. Buffer B contains 0.010 M TES, 0.10 M KCl, and 2.0×10^{-4} M EDTA. Buffer C contains 0.010 M TES, 0.10 M KCl, and 5.0×10^{-3} M EDTA. Buffer D contains 0.010 M TES, 0.10 M KCl, and 4.0×10^{-4} M $CoCl_2$. All buffers were adjusted to have a pH of 7.4 and the same osmolality, about 190 mosmol/kg (determined with a vapor pressure Osmometer, Wescom Instrument), by adding a proper amount of saturated KCl solution. Vesicles A and B were prepared by using buffer A and B, respectively. For leakage measurements, vesicle A solution, after removal of unencapsulated contents, was suspended in buffer C. Any leakage of Co-calcein complexes encapsulated inside vesicles A to the surroundings results in an increase of calcein fluorescence signal due to the higher affinity chelating of EDTA to Co^{2+}. The vesicles were then lysed with Triton X-100 (0.1 % v/v) to obtain a 100 % leakage reference. For the fusion evaluation, vesicles A and vesicles B were resuspended in buffer D after the size exclusion chromatography. If fusion occurs, there will be an increase in the fluorescence signal. The vesicles were then lysed with TritonX-100 (0.1 % v/v) followed by adding EDTA with a final concentration of 5.0×10^{-3} M to obtain a 100 % fusion reference. The total lipid concentration for each experiment is 100 μM. Differential Scanning Calorimetry (DSC) and ^{31}PNMR spectrometry were conducted as previously reported.[33]

2.3. Results and Discussion

Because dithionite ($S_2O_4^{2-}$) is a highly charged anion and strongly hydrated, our prior work has presumed that the anion does not passively cross the lipid bilayer.[34-35] As a result, when dithionite is added to Q_xPE-based liposome solutions, it reduces quinone to hydroquinone at the outer leaflet of the liposomes only, which subsequently results in an asymmetrical cleavage of the quinone headgroup.[33] To examine the impermeability of dithionite through the lipid bilayer, two different liposomes made from negatively charged lipid DOPG and zwitterionic lipid DOPC

encapsulating resorufin were prepared. If dithionite crosses the bilayer, reduction of fluorescent resorufin to its colorless dihydroquinoneimine form, dihydroresorufin, occurs.[36] Figure 2.4 shows that dithionite in the solution does not diffuse into either DOPG or DOPC liposomes' interior during the time scale of the experiments. Thus, it is reasonable to use dithionite as a reagent to evaluate the asymmetrical cleavage of quinone at the outer layer of the Q_xPE-based liposomes.

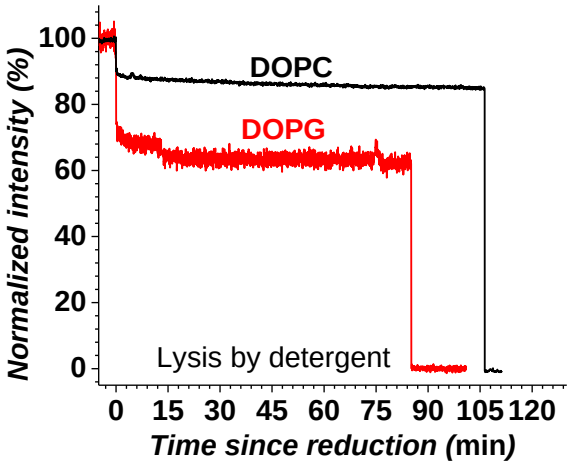

Figure 2.4. Fluorescence response of DOPG and DOPC LUVs (1.0×10^{-4} M total lipid concentration) containing 5.0×10^{-3} M resorufin upon addition of 1.0×10^{-3} M $Na_2S_2O_4$ at $t = 0$. Solution conditions: 0.050 M phosphate, 0.100 M KCl, and 1.0×10^{-4} M EDTA, pH 7.7. T = 41 °C. Excitation at 550 nm, emission at 585 nm, with both slit widths at 5.0 nm. At $t = 0$, the immediate decrease in fluorescence upon addition of $Na_2S_2O_4$ is due to a reduction of free resorufin in solution to dihydroresorufin, which is fluorescently silent. After the vesicles were lysed with 0.1 % (v/v) Triton X-100 detergent, the resorufin encapsulated within the liposomes was released into the bulk solution where it was reduced.

It is well known that inter-bilayer contact between apposed bilayers is a prerequisite for liposomal content release based on $L_\alpha \rightarrow H_{II}$ phase transition of PE lipids.[37-38] The aggregation of vesicles in the suspension is controlled by the interplay of the van der Waal's attractive force and repulsive forces from hydration, electrostatics, and the steric effect.[39-40] Previously, research in the McCarley group showed the inclusion of POPE to the Q_3DOPE liposomal composition leads to a faster content release, and the content release is much less dependent on the concentration of the

liposomes in solution compared to that of vesicles made from 100 % Q_3DOPE.[21, 33] Thus, the original postulation is that at a higher portion of POPE in Q_3DOPE liposomes, the reduction of quinone to hydroquinone is sufficient to decrease the hydration at the outer layer of the liposomes, which leads to the aggregation and content release of Q_3DOPE:POPE vesicles, while the cleavage of the Q_3 head group is not necessary. To verify this idea, Q_1DOPE lipids, which were reported to undergo a quinone reduction with no cleavage of the Q_1 head group due to the lack of the trimethyl lock moiety,[26] was used to prepare Q_1DOPE:POPE 20:80 vesicles with the lipid composition of 20% Q_1DOPE and 80% POPE molar percentage. Throughout this document, the number ratio denotes the molar percentage of each lipid in the liposomal composition. Figure 2.5 shows that Q_1DOPE:POPE 20:80 vesicles exhibit no observable release of any contents over the measured time scale. This experiment proves that asymmetrical reduction does not produce enough dehydration at the outer leaflet of the liposomes, which would lead to a curvature difference between the two leaflets, thereby destabilizing the liposomal membrane so as to trigger the aggregation and content release of Q_1DOPE:POPE liposomes. As a result, the cleavage of the Q_3 group is indispensable for membrane destabilization and subsequent content release.

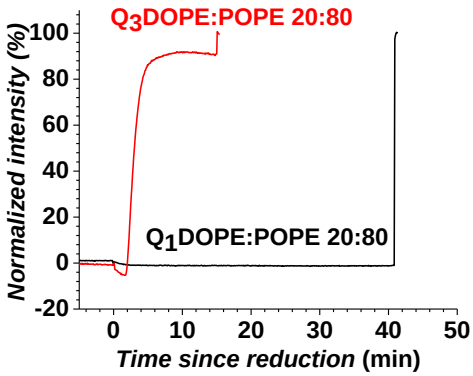

Figure 2.5. Content release from LUVs composed of: 20% Q_3DOPE:80% POPE (Q_3DOPE:POPE 20:80) and 20% Q_1DOPE:80% POPE (Q_1DOPE:POPE 20:80; unable to cyclize and release Q head group). Conditions: 0.040 M calcein encapsulated in LUVs with 0.10 M KCl and 1.0×10^{-4} M EDTA buffered with 0.050 M phosphate, pH = 7.4; T = 41 °C; lipid concentration = 1.0×10^{-4} M.

The second hypothesis is that the inclusion of POPE lipids, which are zwitterionic and less hydrated due to the small headgroup size and the hydrogen bonding of the amine hydrogen with phosphate group,[41-42] produces vesicles with less charge density and hydration repulsion. An increasing portion of POPE in Q_3DOPE:POPE vesicles decreases their charge density, as indicated by zeta potential measurements in Figure 2.6. As a result, after the asymmetrical reduction and removal of the headgroup, increasing portions of PE in the liposomal composition leads to the deformed vesicles that aggregate more easily, with faster subsequent $L_\alpha \rightarrow H_{II}$ transition when compared to the vesicles made from 100% Q_3DOPE.

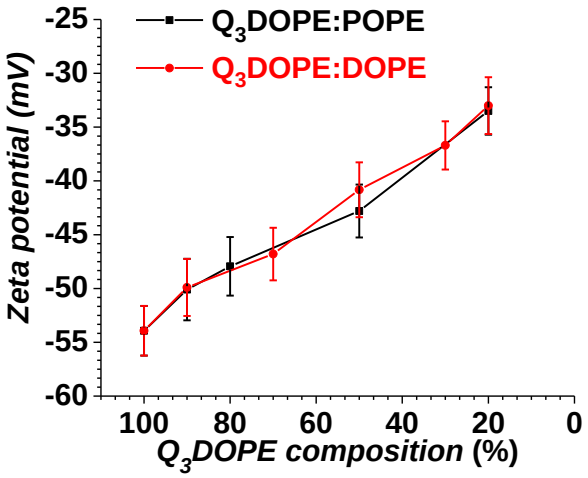

Figure 2.6. Zeta-potential measurements of Q_3DOPE:PE LUVs at various Q_3DOPE portions.

The influence of charge density and hydration is examined by preparation of Q_3DOPE:DOPG, Q_3DOPE:DOPC, and Q_3DOPE:DOPE liposomes with various lipid ratios. PG is negatively charged, while PC is zwitterionic, but both are more hydrated than PE.[43-44] DOPE has a similar PE headgroup to POPE but differs in one hydrocarbon chain. Figure 2.7 shows that the inclusion of DOPC and DOPG, starting at 20% total lipid concentration, inhibits the content release of Q_3DOPE liposomes. However, inclusion of DOPE to Q_3DOPE liposomes results in a similar trend of the release rate to Q_3DOPE:POPE vesicles. In particular, the content release of

Q_3DOPE:DOPE 20:80 vesicles also shows less concentration dependence, which is similar to that reported for Q_3DOPE:POPE 20:80 vesicles (Figure SI2.1 in the supporting information).[33] Thus, lipid hydration level has a more pronounced effect on vesicle aggregation and content release than does lipid/liposome charge.

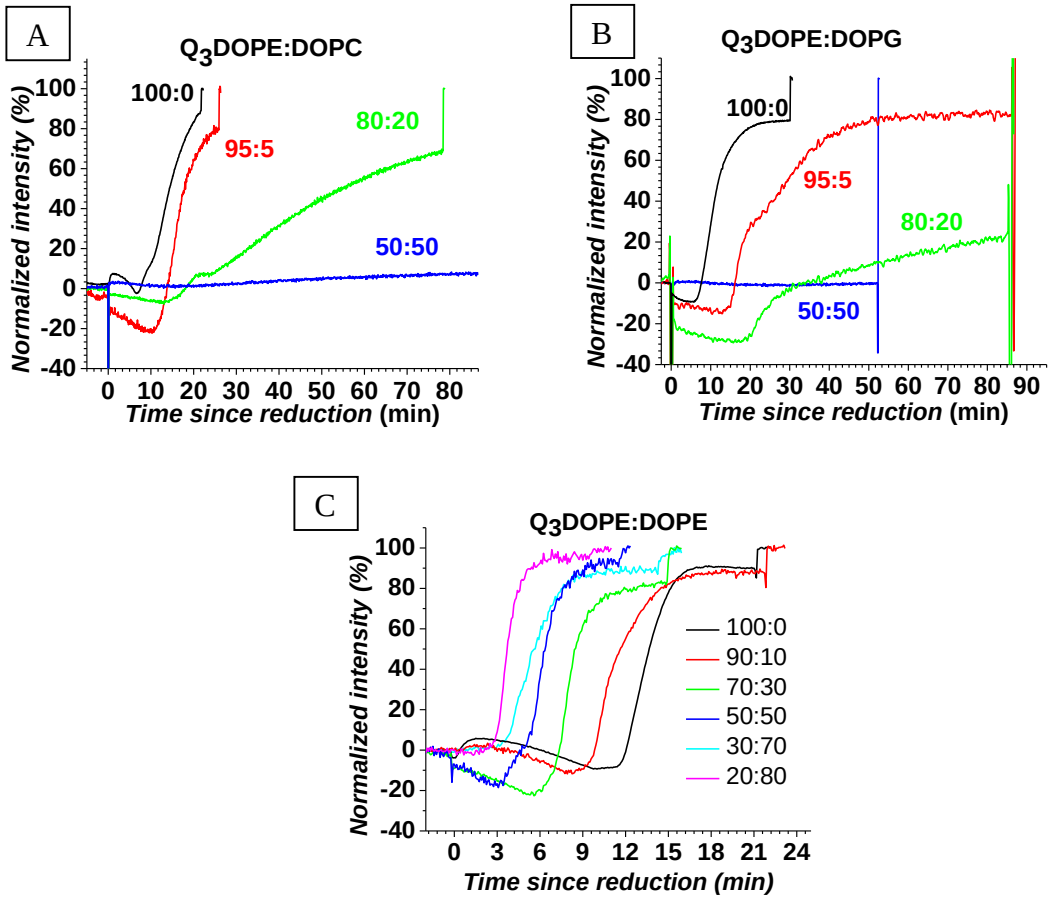

Figure 2.7. Content release from LUVs composed of: Q_3DOPE mixed with **A**. DOPC, **B**. DOPG, and **C**. DOPE. Conditions: 0.040 M calcein encapsulated in LUVs with 0.10 M KCl and 1.0 × 10^{-4} M EDTA buffered with 0.050 M phosphate, pH = 7.4; *T* = 37 °C; lipid concentration = 1.0 × 10^{-4} M.

It is important to note that even when the whole outer leaflet of vesicles made from 100% Q_3DOPE undergoes Q_3 headgroup cleavage, the outer leaflet will have 100% DOPE, while the inner leaflet remains 100% Q_3DOPE. This results in the membrane being assigned 100% membrane asymmetry, with DOPE accounting for 50% of the total lipid in the liposomes.

However, Q_3DOPE:DOPE 50:50 and Q_3DOPE:DOPE 20:80 vesicles with a symmetric bilayer are able to be prepared, and they are stable in solution, which is confirmed by DLS measurements, as shown in Figure 2.8. Liposomes with high portions of PE lipid, up to 90% of liposomal compositions, have been produced before, but content encapsulation in the liposomes is inefficient at such high portions of PE lipid.[37, 45-49] Although DOPE adopts the inverted hexagonal phase at room temperature, stable vesicles that do not aggregate can be prepared, as long as the vesicles possess a sufficient amount of the lamellar phase-adopting lipid Q_3DOPE (~20%); symmetrical distribution of lipid at both liposomal leaflets prevents the aggregation of liposomes. Remarkably, in the case of Q_3DOPE:POPE 20:80 and Q_3DOPE:DOPE 20:80 LUVs, only 20% of the membrane asymmetry generated upon the cleavage of Q_3 head group is needed to trigger the release of the membranes.

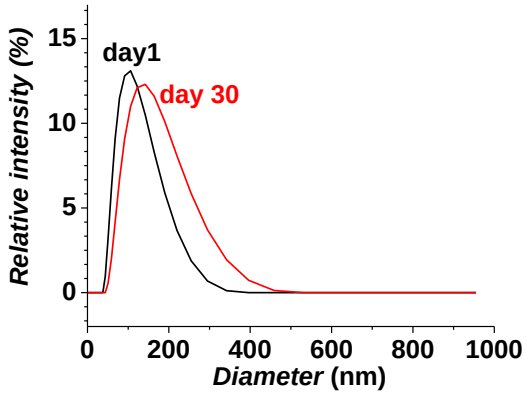

Figure 2.8. Q_3DOPE:DOPE 20:80 LUVs stability in 0.10 M KCl and 1.0×10^{-4} M EDTA buffered with 0.050 M phosphate, pH = 7.4. The liposomes are stable with a small increase in the mean size and PDI after 30 days.

It was previously reported that liposomes made from 100% Q_3POPE do not experience a content release, though the vesicles are expected to experience stress on the membrane that is similar to that for vesicles made from 100% Q_3DOPE, upon the asymmetric cleavage of the Q_3 group.[33] To further evaluate the influence of PE lipids present in the liposome compositions,

DOPE, POPE, and Q_3DOPE lipids were incorporated in Q_3POPE liposomal compositions. In Figure 2.9 is shown that the inclusion of the three lipids in the liposomal formulation can restore content release of Q_3POPE liposomes. Interestingly, when DOPE is included either initially in the Q_3POPE liposome composition or produced by the cleavage of Q_3DOPE, even at a small portion (about 20 % of total lipid concentration), the release of Q_3POPE is faster when compared to that portion of POPE lipid included. These experiments emphasize the pronounced impact of DOPE presence at the outer leaflet of Q_3POPE liposomes has on triggering content release. Importantly, the ability of Q_3POPE:POPE 50:50 liposomes to provide content release upon quinone group reduction points to the key role and importance of sufficient amounts of POPE in the inner leaflet of liposomes for successful content release. Overall, the content release profiles of Q_3PE-based liposomes highlight the fact that a tiny change in lipid structure (DOPE vs POPE) can result in significantly different liposomal release behavior. Further investigation to rationalize the difference between DOPE and POPE will be achieved by studying the fusion properties of Q_3PE-based liposomes.

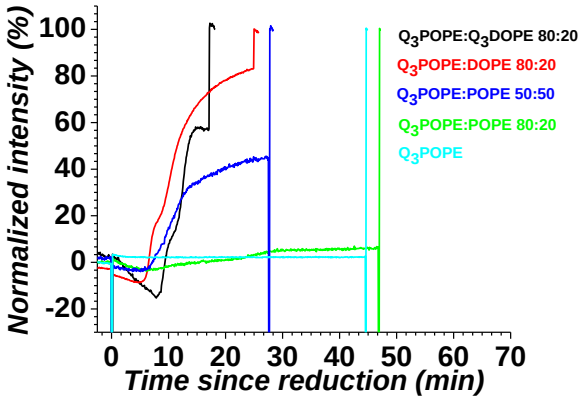

Figure 2.9. The inclusion of Q_3DOPE, DOPE, and POPE in Q_3POPE liposomal compositions enables content release from Q_3POPE LUVs. Conditions: 0.040 M calcein encapsulated in LUVs with 0.10 M KCl and 1.0×10^{-4} M EDTA buffered with 0.050 M phosphate, pH = 7.4; T = 37 °C; lipid concentration = 1.0×10^{-4} M.

Because content release from Q_3PE-based liposomes requires bilayer contact of the vesicles, intermembrane fusion might take place before the $L_\alpha \rightarrow H_{II}$ phase transition occurs. The overlaid profiles of leakage, light scattering, and content-mixing (fusion) of different liposomes presented in Figure 2.10 show that Q_3DOPE, Q_3DOPE:DOPE 20:80, and Q_3POPE:DOPE 20:80 vesicles experience content release without any fusion. On the contrary, Q_3DOPE:POPE 20:80 and Q_3POPE:POPE 20:80 vesicles undergo a massive amount of fusion accompanied by a rapid and significant release, while Q_3POPE vesicles do not exhibit fusion or release. When fusion occurs, the light scattering signal exhibits a small initial increase with a subsequent drop followed by a sharp increase, especially in PBS buffer (Figure SI2.2). It has been observed that 200–300 nm (diameter) liposomes, when fusing for a period of time, also exhibit a similar pattern.[50-51] Light scattering intensity is proportional to the size, shape, and number density of particles in the solution, which determines the scattering volume and refractivity.[52-54] There is no simple and rigorous explanation for the light scattering observation found here. However, the initial increase in light scattering might be attributed to the aggregation and fusion of liposomes to yield a "dimer structure." The subsequent drop in the light scattering profile is assigned to the aggregates of fused liposomes, whose formation significantly diminishes the number of liposomes in the solution. Also, the aggregates of fused liposomes may exhibit less spherical shapes, which lead to weaker light scattering. The final observed increase in the light scattering is attributed to the formation of giant structures of hexagonal phase material, which results in cloudy solutions. Interestingly, when liposomes have high portions of DOPE, the ultimate increase in light scattering will be followed immediately by a decrease in light scattering that is caused by precipitation of the hexagonal phase structures, as shown in Figure SI2.3.

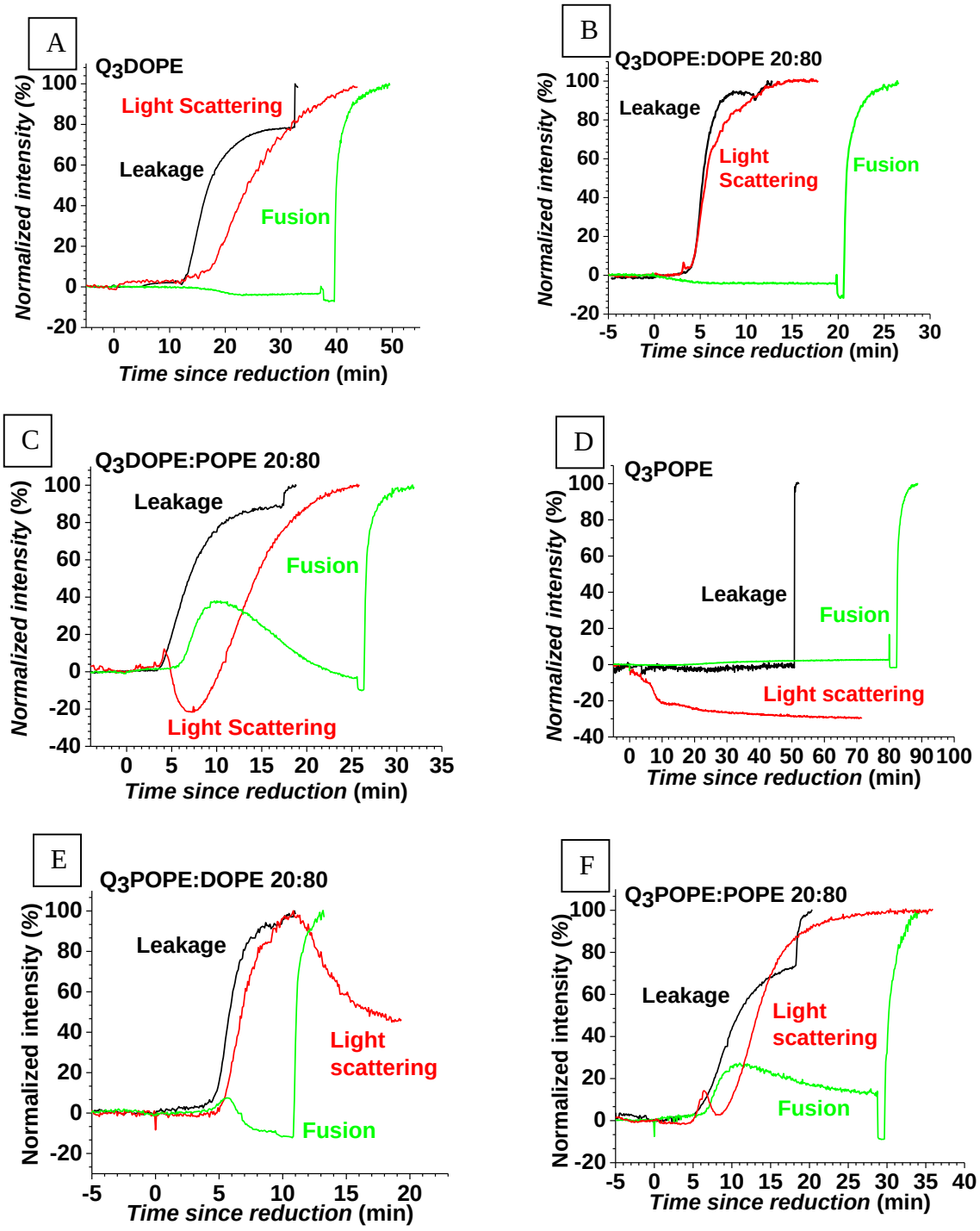

Figure 2.10. Leakage, light scattering, and content-mixing fusion of 100-nm LUVs composed of **A.** 100% Q_3DOPE, **B.** 20% Q_3DOPE:80% DOPE, **C.** 20% Q_3DOPE:80% POPE, **D**. 100% Q_3POPE, **E**. 20% Q_3POPE:80% DOPE, **F**. 20% Q_3POPE:80% POPE. Condition: 0.10M KCl buffered with 0.01 M TES, pH = 7.4; T = 37 °C. Total lipid concentration is 1.0×10^{-4} M.

In Figure 2.11 are summarized the proposed elementary steps in the fusion mechanism of Q_3PE-based liposomes, which facilitates understanding the above observations.[55-57] Fusion begins with bilayer contact (due to formation of point-like membrane protrusions on each apposing bilayer, caused by lipid fluctuations), which is followed by formation of a semi-toroidal lipidic structure (the stalk) between the two apposing membranes. The hemifusion stalk then elongates laterally to form the hemifusion diaphragm, an event which results in either hemifusion, or stalk expansion and pore formation as the membranes fully fuse.

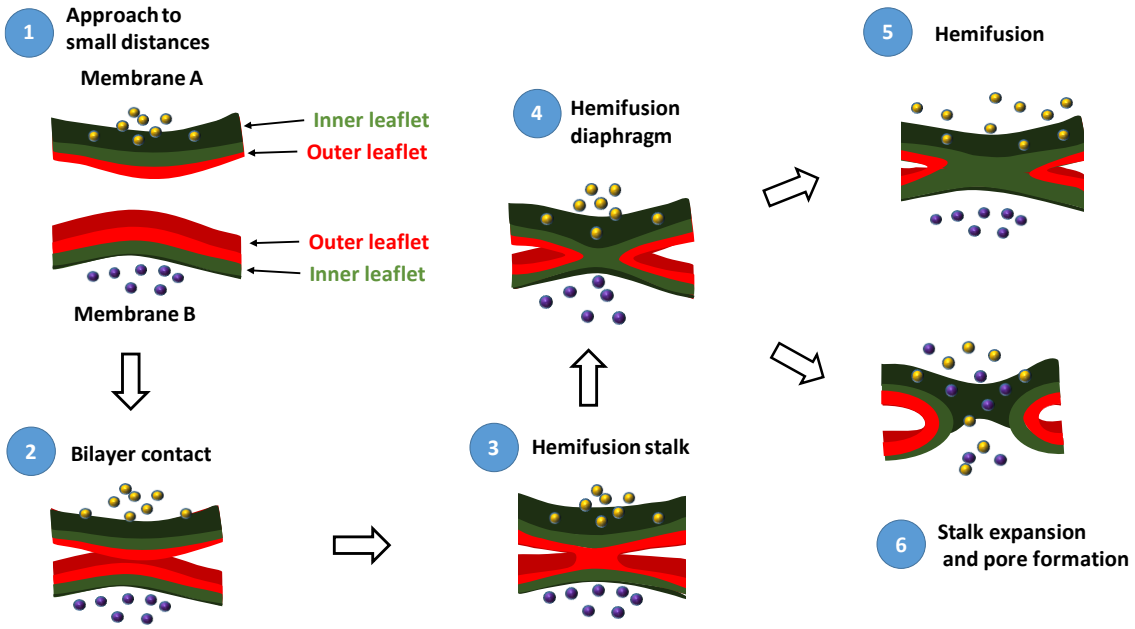

Figure 2.11. Proposed mechanism of fusion for Q_3PE-based liposomes: **1**) A point-like membrane protrusion reduces hydration repulsion between membranes during liposomes collision. **2**) Close approach of the membranes establishes a zone of bilayer contact at the proximal leaflets. **3**) Destabilization of the membrane in the zone of contact promotes a hemifusion stalk with proximal leaflets fused and distal leaflets unfused. **4**) Stalk evolves to hemifusion diaphragm. **5**) Hemifusion diaphragm develops to hemifusion without any content-mixing. **6**) Hemifusion diaphragm develops to pore opening, which results in content-mixing. Red denotes the outer leaflets while the green denotes the inner leaflets of the liposomal membranes. (Adapted from Jahn, 2002).[57]

Contact between lipids in apposed bilayers is the first crucial step in the $L_\alpha \rightarrow H_{II}$ phase transition and fusion of PE-based liposomes in general.[33, 38] Bilayer contact requires sufficient

energy from both membranes to overcome the hydration and charge-charge repulsion between them, which could be provided by select reagents or conditions, such as ions, peptides, or osmotic pressure.[58] In the case of Q_3PE-based liposomes, after asymmetric cleavage of the Q_3 headgroups, curvature stress on the membrane (caused by an uneven distribution of lipids at both leaflets) generates many protrusions/asperities in the membrane, which drives the bilayer contact at those points. Poorly hydrated PE lipids that are located at a protrusion/asperity might serve as a point of initiation for membrane adhesion.[59] Therefore, it is reasonable that Q_3PE:PE liposomes possessing both low charge density and low hydration level experience efficient aggregation after the asymmetric cleavage of the Q_3 group, which accounts for their rapid content release that exhibits a low concentration dependence.

After contact of the two approaching Q_3PE-based liposomes, merging of the outer membrane leaflets at the contact surface might occur to reduce the curvature strain, the latter achieved by formation of bigger vesicles.[60] Small liposomes (~45 nm diameter) of practically any composition are able to fuse extensively due to their high curvature strain.[61-62] Extended space within the bilayer at the bilayer contact region facilitates temporary disorder of the lipids in this area, thereby increasing their mobility. It has been proposed that formation of a spatiotemporal nonlamellar phase by PE lipids is essential for membrane fusion.[63-65] Nevertheless, PEs with different $L_\alpha \rightarrow H_{II}$ transition temperatures (T_H) may influence the elementary steps of fusion differently, due to intrinsic differences in their headgroup hydration, mobility, packing parameter, and lipid volume. The observation of fusion for different Q_3PE-based liposomes suggests that only when POPE, but not DOPE, is present in the inner leaflet of the liposomal bilayer does the content-mixing fusion occur, which implies a crucial role of the inner leaflet for completion of bilayer

mixing. This is in agreement with Step 5 in Figure 2.11, where evolution of the inner monolayers can determine whether content-mixing occurs or if the process stops at the hemifusion structure.

Ellens et al. observed essentially the same phenomena when inducing the fusion of several PE-based liposomes by low pH. They found that liposome fusion occurred when the experimental temperature (T_{exp}) was below T_H of the lipids, while above T_H, the fusion was abolished, and contact-mediated lysis occurred with massive leakage and lipid mixing.[50] The authors proposed a simple model explaining the behaviors of PE-containing membranes with respect to liposome fusion and/or lysis, as shown in Figure 2.12.[50-51]

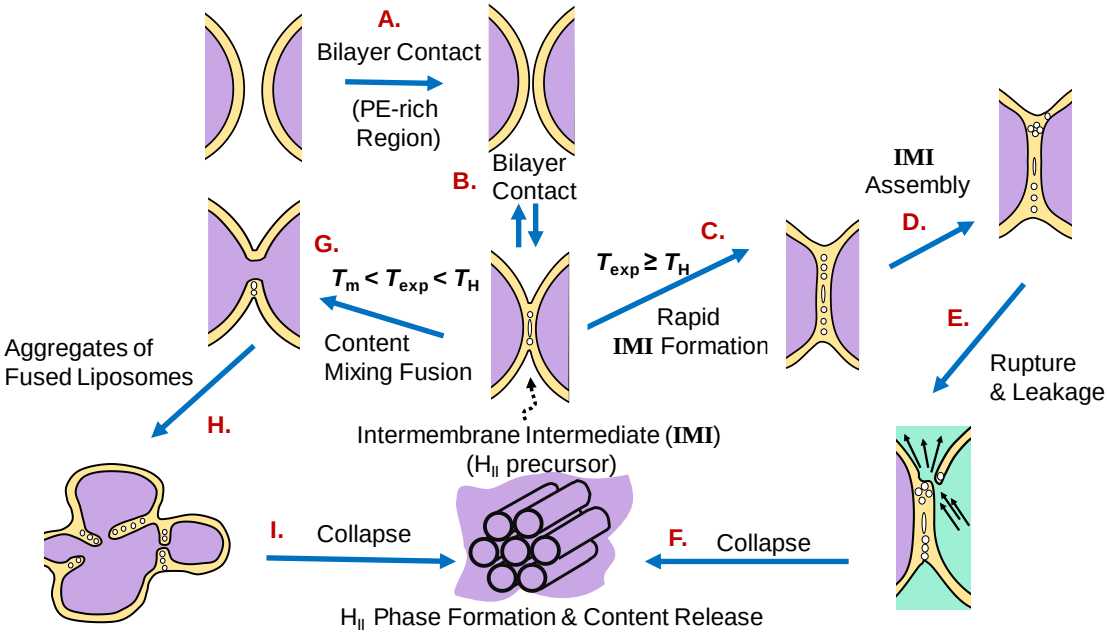

Figure 2.12. Diagram and pathways for liposome fusion and destabilization for liposomes composed of polymorphic lipids. Adapted from Bentz (1988)[50] and Ellens (1986)[51]. Step **A**: bilayers are in contact at the PE-rich region. Step **B:** reversible formation of a few intermembrane intermediates (IMI) at the contact area, which are also the precursor for the $L_\alpha \rightarrow H_{II}$ phase transition. If the temperature of the experiment (T_{exp}) is above T_H, more IMI are rapidly formed (step **C**) and assemble into the localized temporal non-lamellar structure (step **D**) which leads to a facile rupture and content leakage (step **E**). Step **F**: the destabilized bilayer collapses and induces the H_{II} phase formation. This pathway is called contact-mediated lysis. If $T_m < T_{exp} < T_H$, the IMIs drive a pore formation, followed by the mixing of aqueous contents (step **G**). After that, fused liposomes aggregate (step **H**) and undergo a precipitous collapse leading to immediate H_{II} phase formation and subsequent content release (step **I**). This pathway of release is called fusion-mediated lysis.

Step A above represents the close apposition of the liposomes, displaying just the apposed sections of the bilayers. It is noticed that for Q_3PE-based liposomes after cleavage of the Q_3 headgroups, the apposition may occur at multiple points, depending on the protrusion/asperity density in the membrane. A few nonbilayer intermembrane intermediates (IMI), such as inverted micelles or other molecular architectures whose precise structure is not crucial to the establishment of the model, could be generated at the contact area (step B). The initial formation of IMI is expected to be reversible, allowing reversion of apposed bilayers back to their non-contacted states. When $T_{exp} > T_H$, the number of IMI is presumed to rapidly increase, as shown in step C. The assembly of these IMI at the triangle intersection of the membrane (step D) leads to rapid rupture and leakage (step E), followed by a fast collapse of the apposed bilayers and formation of H_{II} phase structures (step F), accompanied by the lack of aqueous contents mixing. This pathway of release is called the lytic pathway. If $T_{exp} < T_H$, IMI have sufficiently long lifetimes to develop the stalk into an open structure (pore), given that the IMI remain isolated (step G). After that, more liposomes aggregate in "trimer" or higher forms, with such aggregates then coalescing until enough IMI are generated and assemble to catalyze a rapid H_{II} phase formation. Thus, the IMI within the area of contact can promote fusion or lysis, depending on the kinetics of IMI formation and assembly, as well as the structural evolution of IMI.

The above model relates the T_H with the pathway of release when considering membranes with a symmetrical bilayer, though the detailed molecular mechanism is not known. The question is, how can this model help to explain the release and fusion difference among Q_3PE-based liposomes caused by DOPE and POPE? The two PE lipids differ from each other by only a single hydrocarbon chain, which is a 16:0 acyl tail in POPE versus an 18:1 unsaturated chain in DOPE. Generally, PE lipids with shorter hydrocarbon chain length or a higher degree of unsaturation

exhibit a marked propensity to adopt inverted hexagonal phases due to the higher volume of the lipid tails and less headgroup hydration, indicated by their lower T_H.[45-47] For example, DOPE possesses a higher average head group area compared to POPE, with the values of 63.5 Å^2 and 56.4 Å^2.[66-68] DOPE has a T_H near 5 °C, while that of POPE is higher, near 72 °C.[33, 44]

Thus, regarding content release, after completion of the asymmetric Q_3 headgroup removal/cleavage in DOPE-enriched liposomes, due to T_{exp} (37 °C) > T_H of DOPE, those liposomes will undergo bilayer contact and $L_\alpha \rightarrow H_{II}$ transition accompanied by content release. For POPE-enriched liposomes, due to T_{exp} (37 °C) < T_H of POPE, liposomes made from 100% Q_3POPE should not experience the phase transition, although leakage may occur. Only when DOPE is included, or the T_{exp} is increased to 70 °C, was the phase transition and release of Q_3POPE achieved (Figure SI 2.4). However, after Q_3 headgroup cleavage, Q_3POPE:POPE LUVs with POPE portions > 50 % experience significant content release. It might be that the release from Q_3POPE:POPE LUVs (with POPE > 50 %) results from the rupture of fused aggregates rather than from $L_\alpha \rightarrow H_{II}$ transitions. The leakage, fusion, and light scattering of Q_3POPE:POPE 50:50 likely support this argument, as seen in Figure 2.13

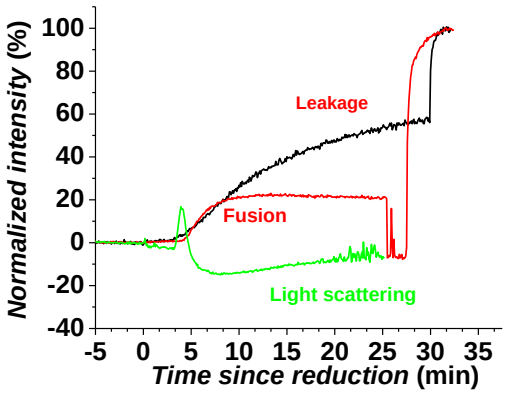

Figure 2.13. Leakage, light scattering, and content-mixing fusion of 100-nm LUVs composed of 50% Q_3POPE:50% POPE.Conditions: 0.10 M KCl buffered with 0.01 M TES, pH = 7.4; T = 37 °C. Total lipid concentration is 1.0×10^{-4} M.

The fusion assay signal of Q_3POPE:POPE 50:50 LUVs is steady for quite a long time, suggesting fusion structures are stable without committing a phase transformation, in accordance with the lack of increase in the light scattering signal, while the leakage still happens. Leakage, fusion and light scattering of Q_3POPE:POPE 20:80 suggest that at these high portions of POPE, other isotropic states of fused vesicles with a large size, such as cubic phase, might be formed. For liposomes made from 100 % Q_3POPE or Q_3POPE:POPE 80:20 LUVs, probably because there is not enough POPE in the inner leaflet, the vesicles have not reached the critical point of POPE portions to overcome the significant higher hydration level of POPE compared to DOPE in order to trigger the aggregation. Furthermore, it also possible that the time scale for aggregation of those vesicles is so slow and reversible that only a small fraction of liposomes is actually in an aggregated state.

Regarding the difference in fusion behavior of Q_3DOPE:DOPE 20:80 and Q_3POPE:POPE 20:80 LUVs, as the result of the different properties of DOPE and POPE, the model by Ellens can be applied to explain the observations; at this high portion of PE, the liposomal bilayers are nearly symmetrical after headgroup cleavage. The enhanced packing of the POPE saturated chain, as well its more hydrated headgroup compared to DOPE, initiates the formation of IMI slowly, which provides enough time for IMI to assemble and allow pore formation and completion of fusion of the inner leaflets before the aggregated liposomes undergo the $L_\alpha \rightarrow H_{II}$ phase transition. On the other hand, because DOPE is more curved and less hydrated than POPE, the DOPE-enriched liposomes should have more protrusions/asperities forming per unit time than the POPE-enriched liposomes with the same portion of POPE, leading to more IMI formation between apposed bilayers, which is highly important for formation of the H_{II} phase. In addition, because of the wide splay of the tails, DOPE has less hydrocarbon packing constraints causing IMI to be able to form

and aggregate in the membrane at a rate sufficiently fast so as to promote the bilayer collapse faster than pore formation; that is, the rupture is kinetically favored over pore formation.

Interestingly, the important role of POPE in fusion events observed here is in agreement with the reported fusion study of plasma membrane SNARE-containing, planar-supported bilayers and purified neuroendocrine dense core vesicles regarding how different distributions of PE lipids between the two leaflets of the supported bilayers affected SNARE-mediated fusion. In that work, porcine brain L-*α*-phosphatidylethanolamine (18:1, 18:0), which is more similar to POPE than DOPE, was selected for fusion investigation. It was shown that the highest efficiency fusion was achieved with the PE lipid exclusively present in the distal (cytoplasmic face-mimicking) leaflet of the target membrane, while fusion was strongly inhibited and content-mixing was lost with PE exclusively in the opposite leaflet (extracellular face-mimicking leaflet).[69]

In addition, research from the McCarley group has shown that liposomes made from pure Q_3DOPE after the asymmetric cleavage experience a hemifusion whose structure appeared to be sufficiently long-lived to be observed under fluorescence microscopy.[70] Because the Q_3DOPE headgroup exhibits extremely pronounced hydrophobicity compared to that of the PE lipid due to the quinone group, Q_3DOPE presence in the inner leaflets of the bilayers led to long-lived hemifusion structures due to strong hydrophobic-hydrophobic interaction among quinone groups. This also explains the non-fusion property of Q_3POPE LUVs. It is noticed that asymmetric unsaturated lipids are more common in natural membranes, whereas lipids with both unsaturated acyl chains are present in much lower proportions.[71] Eukaryotic and prokaryotic membranes possess POPE as the major PE lipids enriched in the inner leaflet of the plasma membrane, suggesting that POPE in the inner lipid membrane may play an important role in their cellular fusion.[67, 72-73] Thus, the observation of POPE in the inner leaflet determining successful fusion of

Q_3PE-based liposomes emphasizes the role of lipid composition in the inner leaflet to fusion of cellular membranes whose bilayer is asymmetric.

2.4. Conclusion

In this chapter, the effect of membrane asymmetry on the stability of the liposomes and lipid distribution at the bilayer on the release kinetics and fusion of Q_3PE-based liposomes were presented, with focus being placed on the uneven lipid distribution in the inner and outer membrane leaflets caused by the asymmetric cleavage of the quinone headgroup. Inclusion of PE lipids in Q_3PE-based liposomes leads to rapid content release in an off-on switch scenario after the symmetric bilayer of the liposomes transforms to an unsymmetric bilayer, with the content release exhibiting a low concentration dependence, which suggests possible use of such liposomes at low concentration with maintained high release efficiency. Furthermore, the seemingly *slight* difference in the structure of POPE and DOPE resulting in their different of $L_\alpha \rightarrow H_{II}$ phase transition temperatures can produce a *pronounced* difference in the fusion behavior of Q_3PE-based liposomes, because POPE drastically facilitates the content-mixing fusion when POPE is present in the inner leaflet of liposomes, while the presence of DOPE does not.

The findings of how POPE lipids and their distribution play a significant role in the fusion of Q_3PE-based liposomes in this work are important when relating it to cellular fusion, as POPE is found to be a major component of PE lipids in eukaryotic and prokaryotic membranes. In addition, the inner leaflet of the cellular membrane is enriched by PE lipids which have been proposed to promote membrane deformation and stabilize fusion pores during exocytotic events. However, understanding of interleaflet PE distributions has not been studied well because of the challenge in producing liposomes with an asymmetric bilayer. The findings in this research emphasize the structural importance of intermembrane intermediates for the Q_3PE-based

liposomal fusion, which could be crucial for elucidating the molecular mechanisms of biological membrane fusion. Furthermore, the fusion control capability of the Q_3PE-based liposomes allows a potential design that vesicles can deliver drugs intracellularly via liposome-cellular membrane fusion.

2.5. References

1. Maeda, H., et al., A Retrospective 30 Years after Discovery of the Enhanced Permeability and Retention Effect of Solid Tumors: Next-Generation Chemotherapeutics and Photodynamic Therapy—Problems, Solutions, and Prospects. *Microcirculation* **2016,** *23* (3), 173-182.

2. Zhang, L., et al., Nanoparticles in Medicine: Therapeutic Applications and Developments. *Clinical Pharmacology & Therapeutics* **2008,** *83* (5), 761-769.

3. Torchilin, V. P., Recent Advances with Liposomes as Pharmaceutical Carriers. *Nature Reviews Drug Discovery* **2005,** *4* (2), 145.

4. Varkouhi, A. K., et al., Endosomal Escape Pathways for Delivery of Biologicals. *Journal of Controlled Release* **2011,** *151* (3), 220-228.

5. Kunisawa, J., et al., Pharmacotherapy by Intracellular Delivery of Drugs Using Fusogenic Liposomes: Application to Vaccine Development. *Advanced Drug Delivery Reviews* **2001,** *52* (3), 177-186.

6. Yang, J., et al., Drug Delivery Via Cell Membrane Fusion Using Lipopeptide Modified Liposomes. *ACS Central Science* **2016,** *2* (9), 621-630.

7. Nogueira, E., et al., Design of Liposomal Formulations for Cell Targeting. *Colloids and Surfaces B: Biointerfaces* **2015,** *136*, 514-526.

8. Azevedo, C., et al., Strategies for the Enhanced Intracellular Delivery of Nanomaterials. *Drug discovery today* **2018,** *23* (5), 944-959.

9. Kuhn, P., et al., A Microfluidic Device for the Delivery of Enzymes into Cells by Liposome Fusion. *Engineering in Life Sciences* **2018,** *18* (2), 149-156.

10. Bibi, S., et al., Trigger Release Liposome Systems: Local and Remote Controlled Delivery? *Journal of Microencapsulation* **2012,** *29* (3), 262-276.

11. Gomez-Hens, A.; Fernandez-Romero, J., Analytical Methods for the Control of Liposomal Delivery Systems. *TrAC Trends in Analytical Chemistry* **2006,** *25* (2), 167-178.

12. Ta, T.; Porter, T. M., Thermosensitive Liposomes for Localized Delivery and Triggered Release of Chemotherapy. *Journal of Controlled Release* **2013,** *169* (1-2), 112-125.

13. Auguste, D. T., et al., Triggered Release of Sirna from Poly (Ethylene Glycol)-Protected, Ph-Dependent Liposomes. *Journal of Controlled Release* **2008,** *130* (3), 266-274.

14. Drummond, D. C., et al., Current Status of Ph-Sensitive Liposomes in Drug Delivery. *Progress in Lipid Research* **2000,** *39* (5), 409-460.

15. Fattal, E., et al., "Smart" Delivery of Antisense Oligonucleotides by Anionic Ph-Sensitive Liposomes. *Advanced Drug Delivery Reviews* **2004,** *56* (7), 931-946.

16. Kuai, R., et al., Efficient Delivery of Payload into Tumor Cells in a Controlled Manner by Tat and Thiolytic Cleavable Peg Co-Modified Liposomes. *Molecular Pharmaceutics* **2010,** *7* (5), 1816-1826.

17. Zalipsky, S., et al., New Detachable Poly (Ethylene Glycol) Conjugates: Cysteine-Cleavable Lipopolymers Regenerating Natural Phospholipid, Diacyl Phosphatidylethanolamine. *Bioconjugate Chemistry* **1999,** *10* (5), 703-707.

18. Andresen, T. L., et al., Enzymatic Release of Antitumor Ether Lipids by Specific Phospholipase A2 Activation of Liposome-Forming Prodrugs. *Journal of Medicinal Chemistry* **2004,** *47* (7), 1694-1703.

19. Hu, Q., et al., Enzyme-Responsive Nanomaterials for Controlled Drug Delivery. *Nanoscale* **2014,** *6* (21), 12273-12286.

20. McCarley, R. L., Redox-Responsive Delivery Systems. *Annual Review of Analytical Chemistry* **2012,** *5*, 391-411.

21. Loew, M., et al., Lipid Nature and Their Influence on Opening of Redox-Active Liposomes. *Langmuir : the ACS Journal of Surfaces and Colloids* **2013,** *29* (22), 6615-23.

22. McCarley, R. L., et al., Release Rates of Liposomal Contents Are Controlled by Kosmotropes and Chaotropes. *Langmuir: the ACS Journal of Surfaces and Colloids* **2013,** *29* (46), 13991.

23. Kao, Y.; Juliano, R. L., Interactions of Liposomes with the Reticuloendothelial System Effects of Reticuloendothelial Blockade on the Clearance of Large Unilamellar Vesicles. *Biochimica et Biophysica Acta (BBA)-General Subjects* **1981,** *677* (3-4), 453-461.

24. Gabizon, A.; Papahadjopoulos, D., Liposome Formulations with Prolonged Circulation Time in Blood and Enhanced Uptake by Tumors. *Proceedings of the National Academy of Sciences* **1988,** *85* (18), 6949-6953.

25. Wang, H., et al., Overcoming Ovarian Cancer Drug Resistance with a Cold Responsive Nanomaterial. *ACS Central Science* **2018,** *4* (5), 567-581.

26. Ong, W., et al., Redox-Triggered Contents Release from Liposomes. *Journal of the American Chemical Society* **2008,** *130* (44), 14739.

27. Kasson, P. M.; Pande, V. S., Control of Membrane Fusion Mechanism by Lipid Composition: Predictions from Ensemble Molecular Dynamics. *PLoS Computational Biology* **2007,** *3* (11), e220.

28. Aeffner, S., et al., Energetics of Stalk Intermediates in Membrane Fusion Are Controlled by Lipid Composition. *Proceedings of the National Academy of Sciences* **2012,** *109* (25), E1609-E1618.

29. Mayer, L. D., et al., Vesicles of Variable Sizes Produced by a Rapid Extrusion Procedure. *Biochimica et Biophysica Acta* **1986,** *858* (1), 161-8.

30. Stewart, J. C., Colorimetric Determination of Phospholipids with Ammonium Ferrothiocyanate. *Analytical Biochemistry* **1980,** *104* (1), 10-4.

31. Https://Ucsd-Ceng-176.Fandom.Com/Wiki/Liposome_Nanoparticles (Access 07.02.2019).

32. Kendall, D. A.; MacDonald, R. C., A Fluorescence Assay to Monitor Vesicle Fusion and Lysis. *Journal of Biological Chemistry* **1982,** *257* (23), 13892-13895.

33. Winter, J. E., On the Development of Analytical Methodologies to Interrogate the Lipid Dynamics and Phase Transition Resulting from the Reduction of Stimuli-Responsive Vesicles. Ph.D Dissertation, Louisiana State University, Baton Rouge, LA, 2015.

34. Gouaux, E.; MacKinnon, R., Principles of Selective Ion Transport in Channels and Pumps. *science* **2005,** *310* (5753), 1461-1465.

35. Marsden, H. R., et al., Model Systems for Membrane Fusion. *Chemical Society Reviews* **2011,** *40* (3), 1572-1585.

36. Zhao, B., et al., Studies on the Photosensitized Reduction of Resorufin and Implications for the Detection of Oxidative Stress with Amplex Red. *Free Radical Biology and Medicine* **2011,** *51* (1), 153-159.

37. Guo, X., et al., Mechanism of Ph-Triggered Collapse of Phosphatidylethanolamine Liposomes Stabilized by an Ortho Ester Polyethyleneglycol Lipid. *Biophysical Journal* **2003,** *84* (3), 1784-1795.

38. Stevens, M. J., et al., Insights into the Molecular Mechanism of Membrane Fusion from Simulation: Evidence for the Association of Splayed Tails. *Physical Review Letters* **2003,** *91* (18), 188102.

39. Mondal Roy, S.; Sarkar, M., Membrane Fusion Induced by Small Molecules and Ions. *Journal of Lipids* **2011,** *2011*.

40. Rand, R.; Parsegian, V., Hydration Forces between Phospholipid Bilayers. *Biochimica et Biophysica Acta (BBA)-Reviews on Biomembranes* **1989,** *988* (3), 351-376.

41. Orsi, M.; Essex, J. W., Physical Properties of Mixed Bilayers Containing Lamellar and Nonlamellar Lipids: Insights from Coarse-Grain Molecular Dynamics Simulations. *Faraday Discussions* **2013,** *161*, 249-272.

42. Cullis, P.; De Kruijff, B., The Polymorphic Phase Behaviour of Phosphatidylethanolamines of Natural and Synthetic Origin. A 31p Nmr Study. *Biochimica et Biophysica Acta (BBA)-Biomembranes* **1978,** *513* (1), 31-42.

43. Marsh, D., Water Adsorption Isotherms and Hydration Forces for Lysolipids and Diacyl Phospholipids. *Biophysical Journal* **1989,** *55* (6), 1093-1100.

44. Koynova, R.; Caffrey, M., Phases and Phase Transitions of the Hydrated Phosphatidylethanolamines. *Chemistry and Physics of Lipids* **1994,** *69* (1), 1-34.

45. Muñoz-Úbeda, M., et al., Gene Vectors Based on Doepc/Dope Mixed Cationic Liposomes: A Physicochemical Study. *Soft Matter* **2011,** *7* (13), 5991-6004.

46. Chu, C.-J., et al., Efficiency of Cytoplasmic Delivery by Ph-Sensitive Liposomes to Cells in Culture. *Pharmaceutical Research* **1990,** *7* (8), 824-834.

47. Miller, C. R., et al., Visible Light-Induced Destabilization of Endocytosed Liposomes. *FEBS Letters* **2000,** *467* (1), 52-56.

48. Farhood, H., et al., The Role of Dioleoyl Phosphatidylethanolamine in Cationic Liposome Mediated Gene Transfer. *Biochimica et Biophysica Acta (BBA)-Biomembranes* **1995,** *1235* (2), 289-295.

49. Tilcock, C., et al., Influence of Cholesterol on the Structural Preferences of Dioleoylphosphatidylethanolamine-Dioleoylphosphatidylcholine Systems: A Phosphorus-31 and Deuterium Nuclear Magnetic Resonance Study. *Biochemistry* **1982,** *21* (19), 4596-4601.

50. Bentz, J.; Ellens, H., Membrane Fusion: Kinetics and Mechanisms. *Colloids and Surfaces* **1987,** *30* (1), 65-112.

51. Ellens, H., et al., Fusion of Phosphatidylethanolamine-Containing Liposomes and Mechanism of L. Alpha.-Hii Phase Transition. *Biochemistry* **1986,** *25* (14), 4141-4147.

52. Brocca, P., et al., Shape Fluctuations of Large Unilamellar Lipid Vesicles Observed by Laser Light Scattering: Influence of the Small-Scale Structure. *Langmuir : the ACS Journal of Surfaces and Colloids* **2004,** *20* (6), 2141-2148.

53. Matsuzaki, K., et al., Optical Characterization of Liposomes by Right Angle Light Scattering and Turbidity Measurement. *Biochimica et Biophysica Acta (BBA)-Biomembranes* **2000,** *1467* (1), 219-226.

54. White, G. F., et al., Physical Properties of Liposomes and Proteoliposomes Prepared from Escherichia Coli Polar Lipids. *Biochimica et Biophysica Acta (BBA)-Biomembranes* **2000,** *1468* (1), 175-186.

55. Kozlov, M. M.; Markin, V. S., [Possible Mechanism of Membrane Fusion]. *Biofizika* **1983,** *28* (2), 242-7.

56. Ellens, H., et al., Fusion of Phosphatidylethanolamine-Containing Liposomes and Mechanism of the L Alpha-Hii Phase Transition. *Biochemistry* **1986,** *25* (14), 4141-4147.

57. Jahn, R.; Grubmüller, H., Membrane Fusion. *Current Opinion in Cell Biology* **2002,** *14* (4), 488-495.

58. Wickner, W.; Schekman, R., Membrane Fusion. *Nature structural & Molecular Biology* **2008,** *15* (7), 658.

59. Kuzmin, P. I., et al., A Quantitative Model for Membrane Fusion Based on Low-Energy Intermediates. *Proceedings of the National Academy of Sciences* **2001,** *98* (13), 7235-7240.

60. Durell, S. R., et al., What Studies of Fusion Peptides Tell Us About Viral Envelope Glycoprotein-Mediated Membrane Fusion. *Molecular Membrane Biology* **1997,** *14* (3), 97-112.

61. Parente, R. A.; Lentz, B. R., Fusion and Phase Separation Monitored by Lifetime Changes of a Fluorescent Phospholipid Probe. *Biochemistry* **1986,** *25* (5), 1021-1026.

62. Li, L.; Hui, S., The Effect of Lipid Molecular Packing Stress on Cationic Liposome-Induced Rabbit Erythrocyte Fusion. *Biochimica et Biophysica Acta (BBA)-Biomembranes* **1997,** *1323* (1), 105-116.

63. Kinnunen, P. K., On the Mechanism of the Lamellar→ Hexagonal H H Phase Transition and the Biological Significance of the H H Propensity. *Handbook of Nonmedical Applications of Liposomes. Vol* **1996,** *1*, 153-171.

64. Deeba, F., et al., Phospholipid Diversity: Correlation with Membrane–Membrane Fusion Events. *Biochimica et Biophysica Acta (BBA)-Biomembranes* **2005,** *1669* (2), 170-181.

65. Kinnunen, P. K., On the Molecular-Level Mechanisms of Peripheral Protein-Membrane Interactions Induced by Lipids Forming Inverted Non-Lamellar Phases. *Chemistry and Physics of Lipids* **1996,** *81* (2), 151-166.

66. Seddon, J. M., Structure of the Inverted Hexagonal (Hii) Phase, and Non-Lamellar Phase Transitions of Lipids. *Biochimica et Biophysica Acta (BBA)-Reviews on Biomembranes* **1990,** *1031* (1), 1-69.

67. Hills Jr, R. D.; McGlinchey, N., Model Parameters for Simulation of Physiological Lipids. *Journal of Computational Chemistry* **2016,** *37* (12), 1112-1118.

68. Venable, R. M., et al., Mechanical Properties of Lipid Bilayers from Molecular Dynamics Simulation. *Chemistry and Physics of Lipids* **2015,** *192*, 60-74.

69. Kreutzberger, A. J., et al., Asymmetric Phosphatidylethanolamine Distribution Controls Fusion Pore Lifetime and Probability. *Biophysical Journal* **2017,** *113* (9), 1912-1915.

70. Martin Loew, R. M., unpublished results.

71. Stillwell, W.; Wassall, S. R., Docosahexaenoic Acid: Membrane Properties of a Unique Fatty Acid. *Chemistry and Physics of Lipids* **2003,** *126* (1), 1-27.

72. Strandberg, E., et al., Lipid Shape Is a Key Factor for Membrane Interactions of Amphipathic Helical Peptides. *Biochimica et Biophysica Acta (BBA)-Biomembranes* **2012,** *1818* (7), 1764-1776.

73. Vanni, S., et al., A Sub-Nanometre View of How Membrane Curvature and Composition Modulate Lipid Packing and Protein Recruitment. *Nature Communications* **2014,** *5*, 4916.

CHAPTER 3
BLUE LIGHT-PHOTORESPONSIVE LIPOSOMES DELIVERY AGENTS BASED ON SYMMETRICAL CLEAVAGE OF THE QUINONE PROPIONIC ACID GROUP

3.1. Introduction

Development of practical methods for triggered release of payloads with precise spatiotemporal capability is crucial for liposomal drug delivery to achieve a higher local concentration of therapeutics. In addition, when encapsulates are toxic, the triggered release of liposomes enables a reduction of the overall injected dose as well as systemic toxicity. Tremendous efforts have been made to achieve different triggered release modalities capable of unloading therapeutics after liposomes sense a significant change in microenvironment resulting from the action of internal factors, such as pH, enzymes, oxidative stress, or external factors, such as light, magnetic field, ultrasound, or temperature.[1-3] However, when internal triggers are not expressed at the target delivery site, a more general triggered release methodology must be developed. Of the mentioned external triggers, photoirradiation is a viable candidate, because it is easy to access and has a broad range of adjustable parameters (e.g., wavelength, duration, intensity). In addition, it can be patient-friendly, and remote initiation of release with high spatial and temporal resolution can be achieved. As a result, photoresponsive liposomes have great potential for applications in topical and transdermal drug delivery for a wide variety of tissues, some of which include skin, eyes, and mucosal tissues.[4-7] General payload delivery of photoresponsive liposomes for tumor treatment is summarized in Figure 3.1.

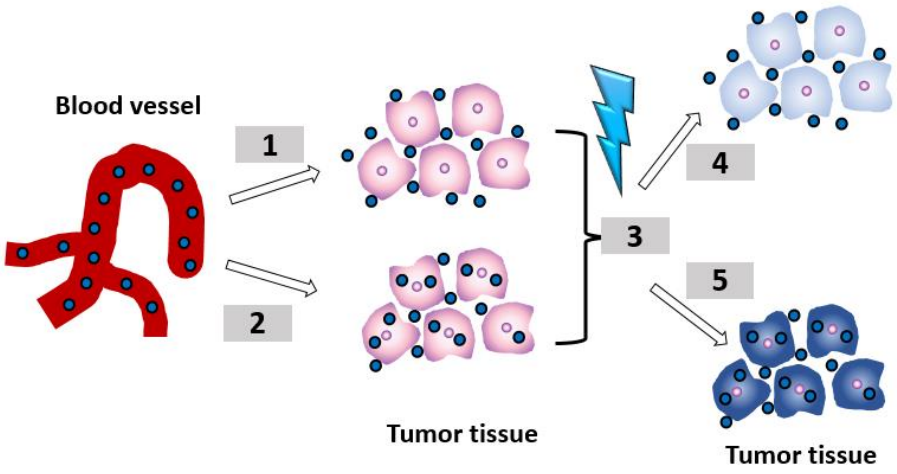

Figure 3.1. Payload release of photoresponsive liposomes. Drug-loaded liposomes (dark blue circles) are transported through blood vessels (red) where they accumulate in the tumor area passively by the enhanced permeability and retention (EPR) effect (**1**) or are taken up by the cells by active targeting (**2**). Upon photoactivation (**3**), liposomes are triggered to release their contents, either extracellularly followed by diffusion of their contents into the cells, shown by the light blue color, indicating low effective concentration of the drug (**4**), or intracellularly, shown by the dark blue color of the cells, showing more efficient drug delivery (**5**). (Adapted from Puri, 2013).[4]

Phototriggered release liposomes can be fabricated by using either non-photoresponsive lipids or photoresponsive lipids, whose release mechanisms are presented in Figure 3.2. The phototriggerred release based on use of non-photoresponsive lipids is achieved through the incorporation of photoresponsive species embedded in the liposome membrane or entrapped in the aqueous core, such as photosensitizers, gold nanostructures, or photoresponsive proteins such as rhodopsin, whose photoactivation induces membrane destabilization and permeabilization.[8-9]

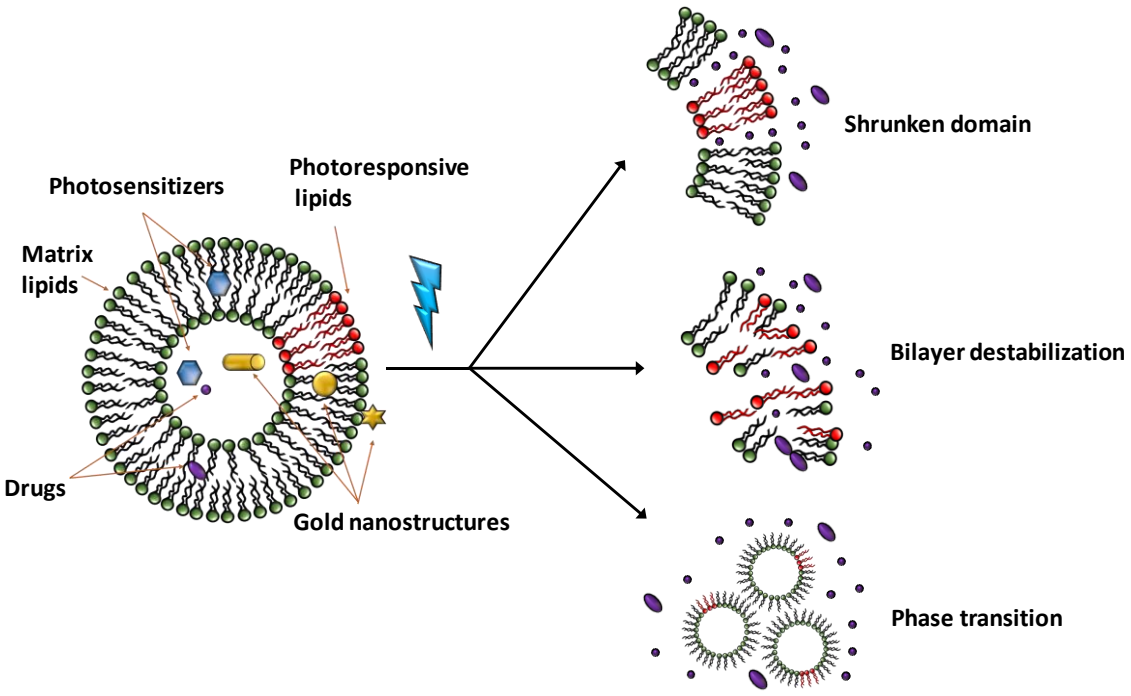

Figure 3.2. Mechanism of phototriggered release of liposomes that encapsulate drugs (purple) via inclusion of photoresponsive lipids (red) or photoresponsive species like gold nanostructures (gold) or photosensitizers (blue) to the matrix lipid (green). Photostimulation results in a shrunken domain, membrane destabilization, or lipid phase transition, leading to the leakage/release of the liposomal contents.

Typically, photosensitizer-assisted release of liposomes exploits photoinduced oxidation of unsaturated lipids that make up the membrane by reactive oxygen species (ROS) generated by the photosensitizers upon photostimulation, which damages the lipid acyl chains and induces the formation of pores in the bilayer, accompanied by cargo leakage.[10-12] For example, when a photosensitizer that can consist of four major groups, such as porphyrin derivatives, chlorins, phthalocyanines, and porphycenes, is exposed to an appropriate wavelength of light, it generates ROS that react with the vinyl ether linkages of plasmalogen or (R)-1,2-di-O-(1′Z,9′Z-octadecadienyl)-glyceryl-3-(*ω*-methoxy-poly(ethyleneglycol)ate (BVEP) lipids. The resulting lysolipid products induce lipid phase transitions, leading to membrane fusion and leakage of the encapsulated contents.[13] Photoinduced oxidation by photosensitizers is also currently applied in photodynamic therapy to kill cancer cells by disrupting their membrane.[12, 14] However, as with

many dyes used in biological applications, the fundamental challenges of this activation method are photobleaching and limited availability of safe photosensitizers with strong molecular absorptivity.

The other photoresponsive species promoting phototriggered release of liposomes are gold nanostructures via a photothermal effect. Gold nanostructures, including shells, particles, rods, and cages, which exhibit rapid and strong absorption in the visible-near IR region four to five times higher than conventional photosensitizers are the most efficient material for photothermal energy conversion. Photoexcitation of these structures results from coherent oscillations of the conduction band electrons, which under photoirradiation produce a heated electron gas that quickly cools down by exchanging energy with the nanoparticle lattice. Rapid heat dissipation to the surrounding medium causes localized heating and imposes membrane stress and rupture, thereby causing cargo leakage and/or release. Photothermal energy conversion also induces the formation and collapse of vapor microbubbles, producing an effect similar to ultrasonication, which disrupts liposomal bilayers. In addition, localized heating can sometimes trigger lipid phase transitions, which increases content release.[5, 15-19] However, the complexity and efficiency of nanostructure-incorporated liposomal formulations result in several challenges as these structures may trigger liposomes to aggregate or disturb the physical and chemical properties of the membrane, which destabilizes the liposomes. Also, nanostructures require a powerful laser for their successful implementation, which can damage tissue.[16] In addition, use of metallic nanostructures raises concerns regarding lack of degradability and possible lack of clearance mechanisms of particles from the body.[9]

To avoid using metallic species, phototriggered liposomes are formulated by employing photoresponsive lipids, which can be considered to be more biocompatible. Typically, three major

parts of phospholipids (i.e., the headgroup, glycerol backbone, and fatty acyl chains) can be chemically modified to become photoactive. Several photoactivation mechanisms of liposomes made of photoresponsive lipids have been proposed to promote cargo release, such as photoisomerization, photopolymerization, and photocleavage.[4-5, 12] In Figure 3.3 are presented examples of some currently available photoactivatable lipids.

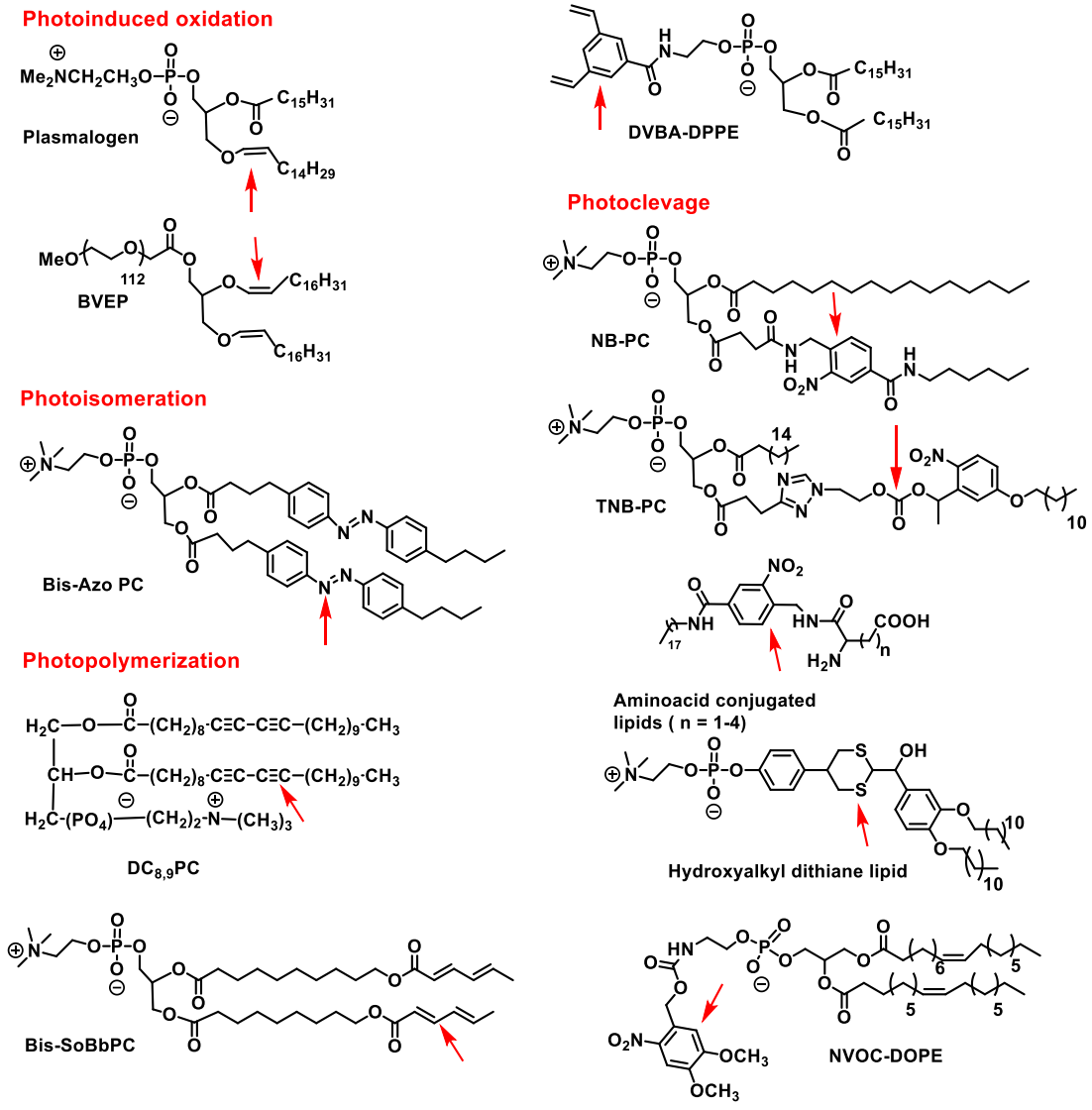

Figure 3.3. Examples of photoresponsive lipids. The photoactivable bonds and their positions in the molecules are indicated by arrows.

Photoisomerization is based on the propensity of lipids to undergo a conformational change upon light stimulation, with azobenzenes being the most commonly used moiety for lipid modification.[20] Upon exposure to UV light in the 300–400 nm range, the double bond between the nitrogen atoms bearing two phenyl rings undergoes a transformation from trans to *cis* conformation. The transition from a polar, linear state to a more polar, twisted state with kinked chains distorts the packing of the bilayer and causes the liposomes to become leaky, allowing the substantial loss of encapsulated materials from liposomes.[21-24] Photoisomerizable liposomes have also been prepared using retinoyl phospholipids or spiropyran.[25-26]

Photopolymerization of unsaturated bonds located in the hydrophobic domain of the bilayer causes parts of the bilayer to shrink, which disrupts the uniform packing of the lipid molecules and produces pores in the bilayer, thereby increasing membrane permeability and content leakage.[5, 27-28] For example, liposomes composed of synthesized $DC_{8,9}PC$ lipid with other matrix lipids are able to release their payloads upon exposure to UV light, as the polymerization of $DC_{8,9}PC$ forms local aggregates in the bilayer.[28-29] The other example is liposomes made of bis-SorbPC, whose photoreaction induced lateral phase separation of PEG-rich and crosslinked polymer-rich domains within the membrane bilayer, breaking the lamellar integrity, which pronounced enhances membrane permeability.[30]

Photocleavage triggering of liposome content release can be achieved by using a photocleavable protecting group, such as those based on dithianes, disulfides, coumarins, diazirines, and the 4-hydroxyphenacyl functionality, as well as the 2-nitrobenzyl group engineered into the lipids. Light stimulation causes cleavage of the moiety, followed by phase separation of fractions possessing lower amphiphilic character, resulting in destabilization of the liposome.[9, 31-32] For example, liposomes made from NB-PC phospholipid generated from the

modification of PC with the photolabile 2-nitrobenzyl group in the acyl chain at the *sn*-2 position release their contents under light irradiation (350 nm), resulting from C-N bond cleavage, to produce aldehyde and amide components.[33] In addition, a photoresponsive TNB-PC lipid-containing triazole and *o*-nitrobenzyl moieties was synthesized by "click" chemistry. Photolysis of TNB-PC liposomes upon exposure to UV light causes cleavage of one nitrobenzyl moiety from one hydrophobic chain, inducing bilayer permeability and eventually causing disruption of the liposome.[34] Another example is based on a photocleavable lipid called NVOC-DOPE. Irradiation of the liposomes at 345 nm produces DOPE, which does not form a bilayer structure, with formation of DOPE inducing calcein release.[35] Chandra et al. also synthesized photocleavable amphiphilic lipids by conjugating a non-polar stearyl amine tail to charged amino acid as polar headgroups via an *o*-nitrobenzyl derivatives spacer; the feasibility of the photocleavage is dictated by pK_a of the amino acids.[31, 36] Linking hydrophilic phosphocholine headgroups to hydrophobic tails via a photolabile, dithiane-based tether has been another approach to synthesize photocleavable lipids. Liposomes formulated by such photolabile lipids mixed with other lipids and cholesterol are capable of unloading their contents upon photoactivation.[37]

However, the mentioned photocleavage moieties often require the use of UV light to activate the chemical bonds of interest, with UV light having limited penetration depth into and potential phototoxicity within biological samples. Thus, strategies to make photoresponsive lipids that are able to be activated at longer wavelengths are necessary. On the other hand, as seen in the previous chapter, the lipid composition in the inner leaflet of the liposomes dictates the fusion of Q_3PE-based liposomes resulting from the asymmetric cleavage of the Q_3 headgroup. *Therefore, it is posited that symmetric cleavage of functional groups of PE lipids at both leaflets of the liposomal bilayer can change the mechanism of release so as to enhance fusion of Q_3PE-based liposomes,*

which would also help to understand to a higher degree the role of membrane asymmetry for liposomal fusion and content release. To achieve a symmetric cleavage of the headgroup, the photocleavage strategy is a feasible option as photons can cross the membrane and induce photoreaction at the two leaflets at the same time. However, Q_3PE lipids are not photoresponsive. In order to create photoresponsive Q_3PE lipids without significantly changing their chemical structures, I propose to exploit modification of the quinone headgroup with methyl sulfide functionalities. Furthermore, it would be beneficial if the lipid is designed to be responsive at a longer wavelength using a low-power source. Recently, Walton and Dougherty demonstrated a unique strategy to form free phenolic oxygen moieties through visible energy photoreduction of quinone derivatives that contain the trimethyl lock motif.[38] This photoreduction route makes use of either sulfides or tertiary amines as electron donors, which promote red-shift absorption and efficient uncaging of different leaving groups. The applicability of this photodecaging method can be extended to the synthesis and preparation of visible light-reactive liposomes, as shown in Figure 3.4. Herein, a blue-light responsive MeSQ_3DOPE lipid is synthesized, and the photoresponsive property of the liposomes constituted by this lipid is examined upon exposure to a light-emitting diode (LED). Due to photobleaching of calcein in the conventional leakage assay used in Chapter 2, diffusion-ordered NMR spectroscopy (DOSY) and capillary electrophoresis (CE) methods are developed to interrogate leakage/release of contents from the new photoresponsive liposome system.

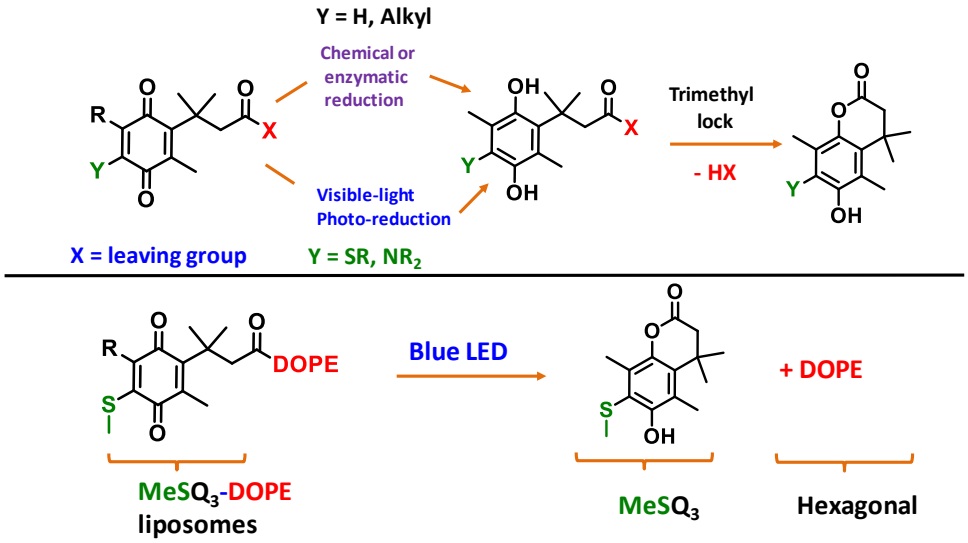

Figure 3.4. General decaging strategies for the quinone trimethyl lock and its adaption for blue-light photoresponsive Q_3DOPE-based liposomes.[38]

3.2. Experimental

3.2.1. Lipid Synthesis

$MeSQ_3$DOPE photoresponsive lipid was synthesized for the first time by coupling $MeSQ_3$NHS to DOPE, using a modified form of the reported protocol, as shown in Figure 3.5.[38] Yield = 90 %; ^{1}H NMR (400 MHz, $CDCl_3$) δ 5.34 (m, 5H), 4.45 (m, 1H) 4.16 (m, 1H), 3.95 (m, 2H), 3.87 (m, 2H), 3.48 (s,1H), 3.38 (m,2H), 2.84 (s, 2H), 2.45 (s,3H), 2.31 (m, 4H), 2.11−1.99 (m, 17H), 1.58 (m, 4H), 1.38−1.26 (m, 46H), 1.26 (m, 40H), 0.88 (t, 6H). HRMS (ESI) calculated for $C_{55}H_{93}NO_{11}PS$ $[M-H]^-$ 1006.6212, found 1006.6218 (0.13 ppm); calculated for $C_{55}H_{94}NO_{11}PS$ $[M+H]^+$ 1008.6358, found 1006.6382 (1.8 ppm). $MeSQ_3$OEt was synthesized as a control (ethanol as the leaving group). Yield = 88 %, ^{1}H NMR (400 MHz, $CDCl_3$) δ 4.04 (q, J = 7.1 Hz, 2H), 2.95 (s, 2H), 2.47 (s, 2H), 2.16 (s, 3H), 2.13 (s, 2H), 1.42 (s, 6H), 1.19 (t, J = 7.1 Hz, 2H); HRMS (ESI) calculated for $C_{16}H_{23}O_4S$ $[M+H]^+$ 311.1312, found 311.1314 (0.67 ppm).

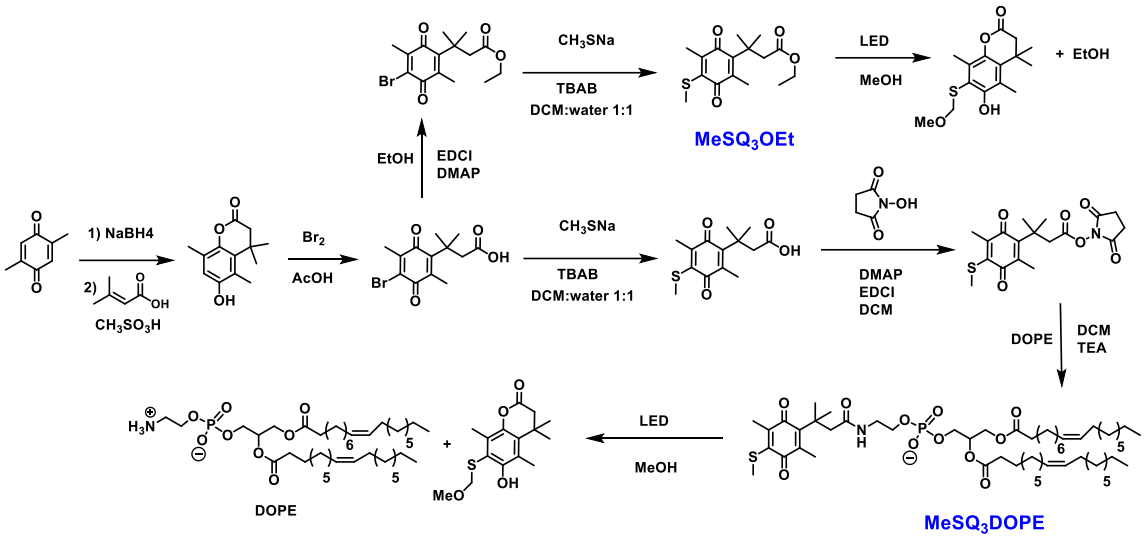

Figure 3.5. The synthesis paths for $MeSQ_3DOPE$ photoresponsive lipid and $MeSQ_3OEt$ with their proposed photoreduction products under blue LED irradiation (440–460 nm) in methanol.

3.2.2. Blue LED Irradiation Setup

A royal-blue LED from Luxeonstar with a typical wavelength of 447.5 nm and wavelength range of 440–460 nm, 520 mW power mounted on a 20-mm Star Cool Base (20×20×5 mm dimension) was used. A 1.0 mL quartz cuvette containing sample was irradiated under the LED for a period of time before being placed in the fluorimeter in order to avoid interfering light from the LED to reach the photomultiplier detector.

3.2.3. Liposomal Leakage Monitoring by Fluorescence Quenching-based Assay

The calcein fluorescence quenching-based assay reported in the previous chapter is not suitable for leakage/release measurements of photoinduced release of contents from $MeSQ_3DOPE$ liposomes due to its photobleaching by the blue LED light (shown later). Sulforhodamine B ("red dye"), which also exhibits a concentration-based fluorescence quenching effect, was exploited because of its far red absorption.[39-40] Red dye stock solutions at a concentration of 0.080 M were prepared using pH 7.4 PBS buffer that contains 0.050 M phosphate, 0.10 M KCl, and 1.0×10^{-4} M EDTA. Liposomes were prepared using the same protocol as in Chapter 2. Fluorescence signals

of red dye-containing samples were measured via excitation at 560 nm and emission intensity recorded at 590 nm via use of an adjustable slit width (1.0−2.5 nm). Triton X-100 (0.1 % final v/v) was used to lyse liposomes, and the subsequent fluorescence signal at the plateau was normalized as being 100% content release.

3.2.4. Liposomal Leakage Monitoring by Capillary Electrophoresis (CE)

CE has been developed for separation and quantification of drug-associated liposomal leakage based on different retention times of probe molecules free in solution and encapsulated in liposomes.[41-42] Herein, CE experiments were performed in a Beckman Coulter instrument. Fused-silica capillaries were cut into effective lengths of 28.6 cm (from the injection end to the detection window). Capillaries were rinsed with 1.0 M NaOH, followed by ultrapure water (18.2 Mohm.cm), and subsequently washed with separation buffer containing 0.020 M phosphate and 0.010 M sucrose at pH 7.4 (CE-PBS buffer) at 20.0 PSI for 10.0 min. After each run, the capillary was rinsed with the CE-PBS buffer at 20.0 PSI for 1.0 min. Red dye was selected for signal detection due to its high molar extinction coefficient (~ 99,000 $cm^{-1}.M^{-1}$),[43] which can enhance the detection capability of conventional CE without increasing the length of the detection window (increasing the thickness of the capillary at the detection area). Liposomes containing 0.080 M red dye were isolated from free red dye by size-exclusion chromatography and resuspended in CE-PBS buffer so as to achieve the total final volume of 200 μL with total lipid concentration of 10 mM. All samples were hydrodynamically injected at 0.5 PSI for 5.0 s, followed by separation at 20.0 kV (~ 500 V/cm), and signal was detected by measuring absorption at 560 nm. All measurements were performed at 25 °C.

3.2.5. Liposomal Leakage Monitoring by Diffusion NMR

While fluorescence-quenching based assays, such as terbium/dipicolinic acid (Tb/DPA), 8-aminonaphthalene-1,3,6-trisulfonic acid/*p*-xylene bispyridinium bromide (ANTS/DPX), and

other fluorescent dyes are simple when liposomal leakage is induced by changes in pH, temperature, and other non-radiative chemical processes, photobleaching of fluorophores and their light absorption interference are big concerns when considering phototriggered release routes. The shortcomings of fluorescence-based leakage assay in liposomal photoinduced release can be overcome by utilizing DOSY.[44-45] The diffusion coefficient of a small probe molecule confined inside vesicles is different from that of the probe free in solution, generally by orders of magnitude. In addition, monitoring liposomal leakage using a fluorine (^{19}F)-containing probe by DOSY is simple, because signal detection is made simple by observing the signal from one nucleus with no interference from multiple proton peaks, and water suppression is not necessary. Therefore, a trifluoromethane sulfonate ion was used as the DOSY probe because of its negative charge. A 0.25 M stock solution of the probe was prepared using 0.15 M phosphate buffer at pH 7.4 containing 10% D_2O (for NMR signal locking purpose). The bulk unencapsulated probe molecules were removed by size-exclusion chromatography (Sephadex G-50) using elution buffer containing 0.40 M phosphate, 10% D_2O at pH 7.4. The liposomes were used freshly right after the column.

The DOSY measurements were carried out with Bruker AVIII 500 MHz spectrometer with liquid-nitrogen-cooled Prodigy TCI (HCN) probe, which is capable of forming pulsed field gradients (PFGs) up to 50 G/cm. The pulse program *ledbpgppr2s* from Bruker was used without modification. The peak area A of the probe follows a Gaussian function of the applied field strength and is related to the diffusion coefficient by the expression

$$A = A_0 e^{-D_s(\gamma\delta G)^2\left(\Delta - \frac{\delta}{3}\right)} \qquad \text{Equation 3.1}$$

where γ is the magnetogyric ratio of fluorine (2.68×10^4 $G^{-1}.s^{-1}$), δ is the length of the pulsed-field gradient (4.4×10^{-3} s), Δ is the diffusion delay time (0.05 s), G is the gradient strength (G/cm),

and D_s is the diffusion coefficient ($cm^2.s^{-1}$). Taking the logarithm of both sides of Equation 3.1 yields

$$lnA = lnA_0 - D_s(\gamma\delta)^2\left(\Delta - \frac{\delta}{3}\right)G^2 \qquad \text{Equation 3.2}$$

Linear fitting of lnA vs G^2 yields probe diffusion coefficient. Theoretically, from Equation 3.1, if two diffusion coefficients are different at about two orders of magnitude, at a certain gradient strength, the signal intensity of the free probe in solution (with bigger D_s) will reduce significantly while the signal intensity of the probe encapsulated in vesicles (with smaller D_s) is barely affected. Monitoring the ratio of the total intensity of the probe at two different gradients enables quantification of the probe in two different environments.

3.3. Results and Discussion

The UV−vis spectra of $MeSQ_3OEt$ and $MeSQ_3DOPE$ in MeOH irradiated under blue LED over time are shown in Figure 3.6. In both compounds, a charge-transfer event results in a broad absorption band in the visible range (λ_{max} ~ 420 nm), so that photoreduction is possible at wavelengths generated by the available blue LED, as indicated by the decrease in intensity of the quinone absorption band (~ 260 nm). Under blue light illumination, the color of solutions of $MeSQ_3DOPE$ in MeOH and the corresponding liposomes in aqueous PBS was observed to gradually change from yellow to colorless. The decrease in intensity of the visible band at λ_{max} was treated as following a pseudo-first-order decay reaction

$$A_t = A_0 e^{-kt} \qquad \text{Equation 3.3}$$

where *k* is the decay constant. The absorbance at time t (A_t) was then normalized to the absorbance at plateau (A_∞) and was fitted with a linear least-squares approach

$$ln\frac{A_t - A_\infty}{A_0 - A_\infty} = -kt \qquad \text{Equation 3.4}$$

In Figure 3.7 is shown that the decay of the visible band at λ_{max} of $MeSQ_3OEt$ is faster than that of $MeSQ_3DOPE$ in MeOH, and both are faster than that of liposomes in PBS.

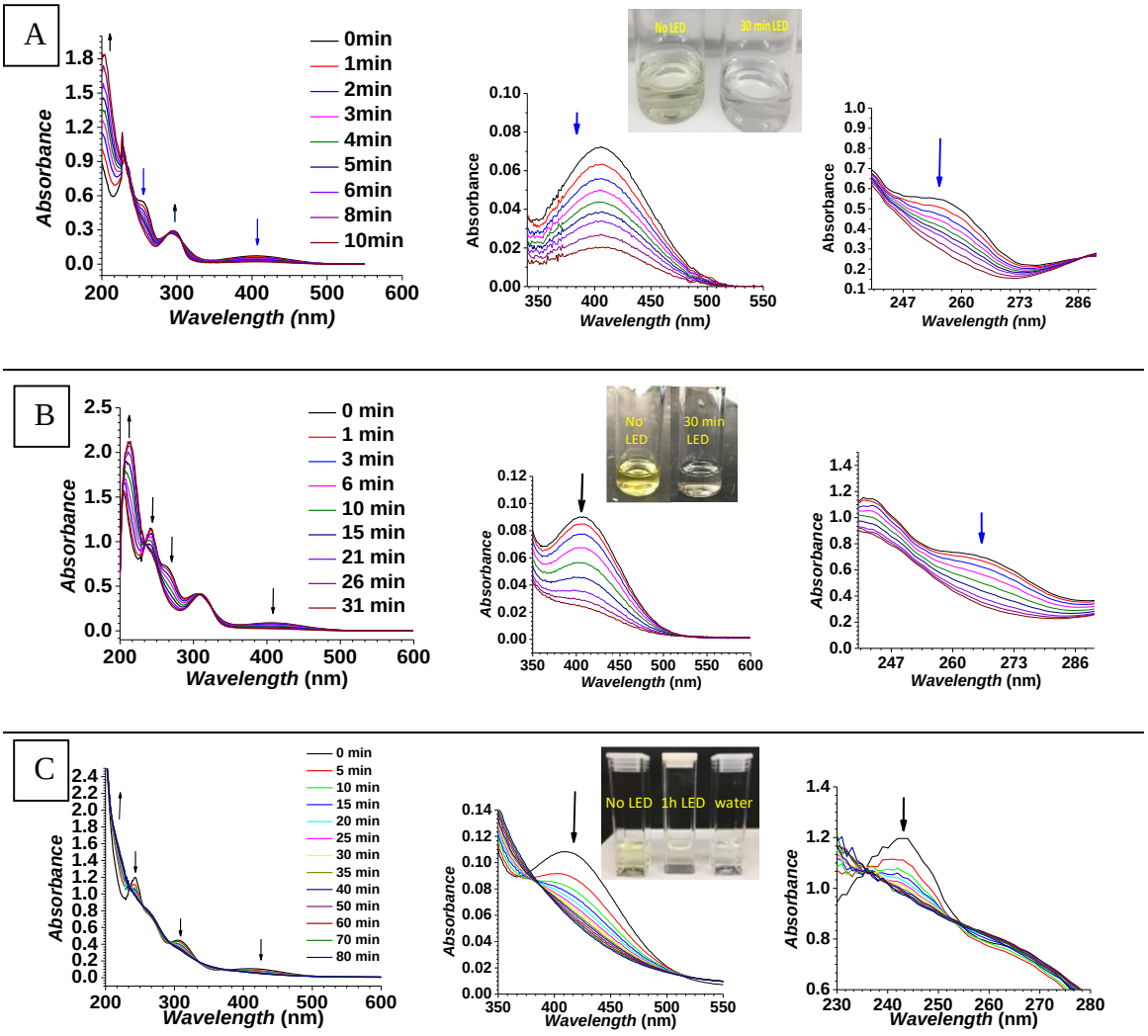

Figure 3.6. Representative time course UV−vis spectra during photolysis by irradiation with a 447.5-nm LED (520 mW). **A**. $MeSQ_3OEt$ in MeOH (λ_{max} = 396 nm), **B**. $MeSQ_3DOPE$ lipid in MeOH (λ_{max} = 407 nm), **C**. $MeSQ_3DOPE$ LUVs in PBS buffer (λ_{max} = 409 nm). Spectra are shown with expansions of the visible (left) and quinone (right) absorption bands. Arrows indicate changes in the spectra over time. Conditions: 100 μM $MeSQ_3OEt$ and $MeSQ_3DOPE$ at T = 25 °C.

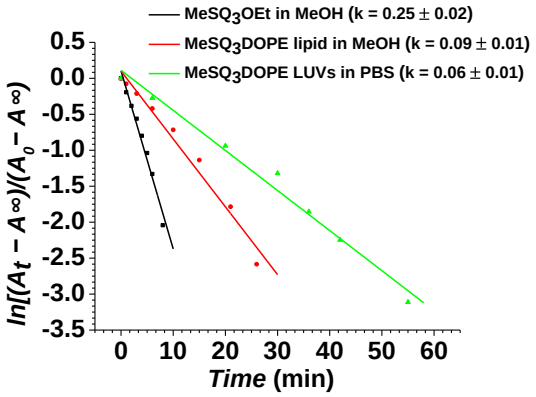

Figure 3.7. Pseudo-first-order fit of the decay of the visible absorption band at λ_{max} under LED irradiation.

To examine the integrity of $MeSQ_3DOPE$ compared to Q_3DOPE, the release of $MeSQ_3DOPE$ LUVs encapsulating calcein was tested with SDT. In Figure 3.8 is shown that $MeSQ_3DOPE$ LUVs exhibit the same behavior as Q_3DOPE LUVs when chemically activated by SDT. Typically, the release of $MeSQ_3DOPE$ LUVs is faster when the temperature is increased, or when POPE or DOPE is included in the liposomal compositions. Their release is also lipid concentration dependent. These observations confirm that adding a photoresponsive moiety to Q_3 group preserves the SDT-induced, release-associated property of Q_3DOPE LUVs.

When $MeSQ_3DOPE$ LUVs containing encapsulated calcein are exposed to the blue LED, calcein experiences photobleaching, which causes to be inaccurate this method of liposomal leakage quantification induced by photoactivation. Thus, the red dye (Sulforhodamine B), which does not display noticeable photobleaching, was selected for this purpose, as shown in Figure 3.9.

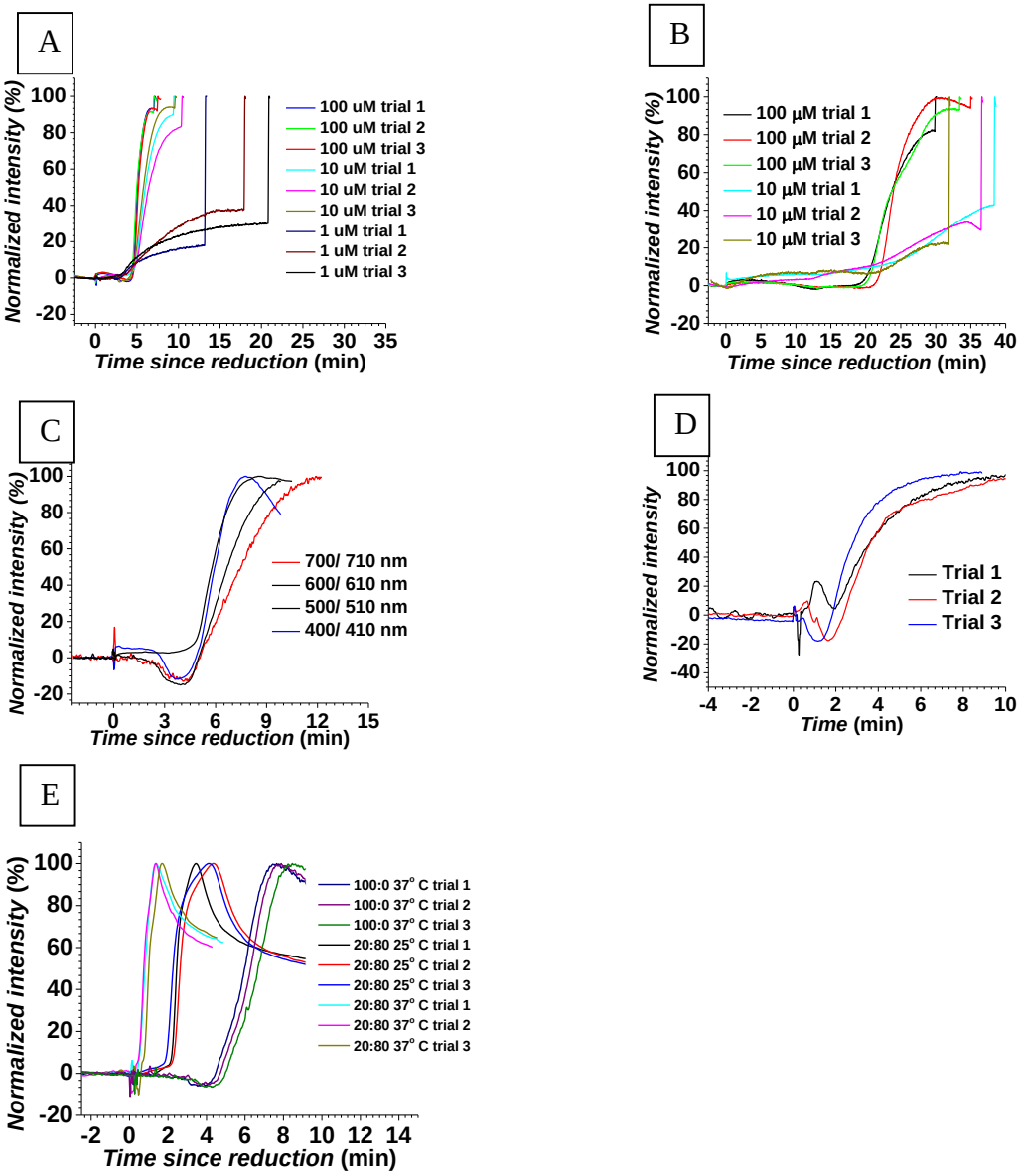

Figure 3.8. The response of $MeSQ_3DOPE$-based LUVs to sodium dithionite. **A**. Release of $MeSQ_3DOPE$ LUVs at 37 °C, **B**. at 25 °C, **C**. Light scattering of $MeSQ_3DOPE$ LUVs at different wavelengths at 37 °C, **D**. Light scattering of $MeSQ_3DOPE$:POPE 20:80 LUVs at 37 °C. **E**. Light scattering of $MeSQ_3DOPE$:DOPE 20:80 LUVs at different temperatures in reference to $MeSQ_3DOPE$ LUVs. Conditions: 0.040 M calcein encapsulated in LUVs with 0.10 M KCl and 1.0×10^{-4} M EDTA buffered with 0.050 M phosphate, pH = 7.4, lipid concentration = 1.0×10^{-4} M.

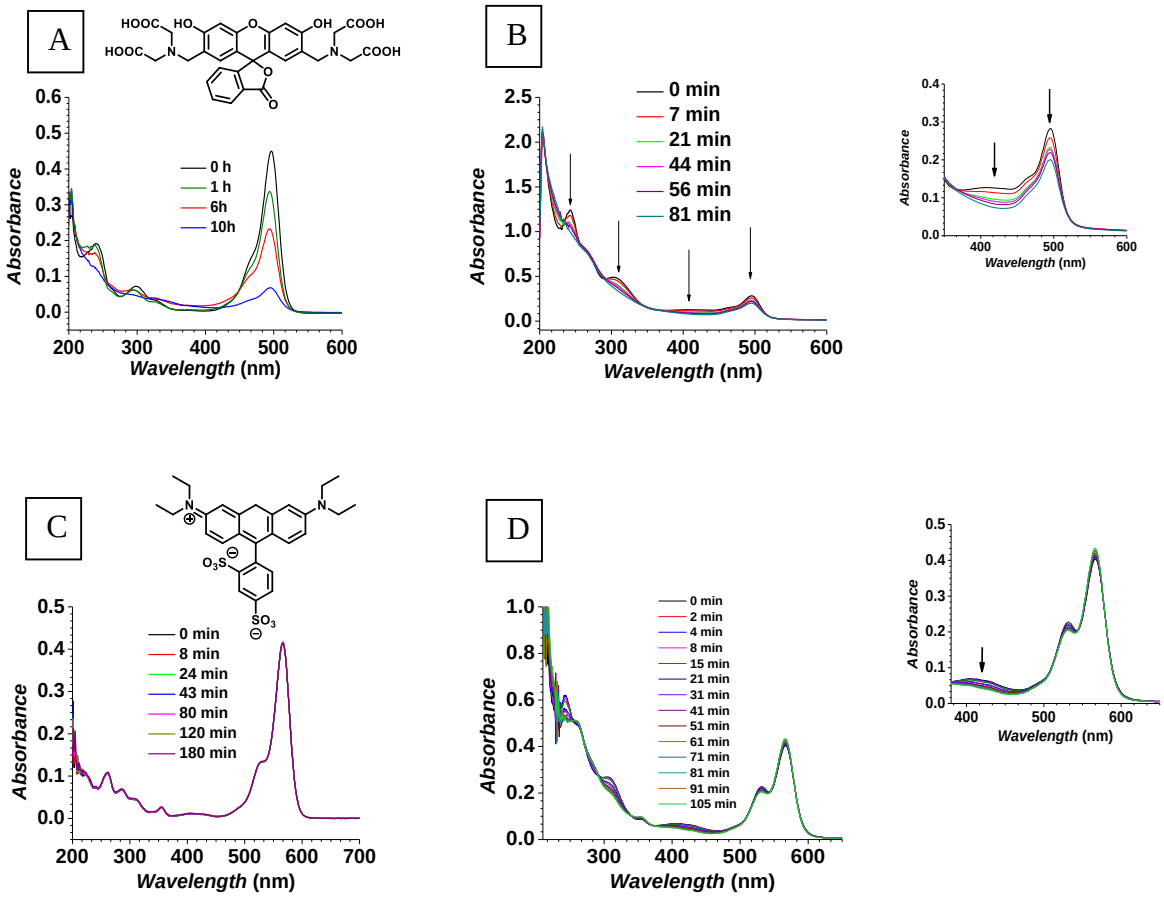

Figure 3.9. Examination of possible photobleaching of calcein and Sulforhodamine B (red dye) under blue LED irradiation. **A**. Free calcein in PBS, **B**. $MeSQ_3DOPE$ LUVs containing encapsulated calcein and its spectral expansion, **C**. Free red dye in PBS, **D**. $MeSQ_3DOPE$ LUVS encapsulating red dye and its expansion. Conditions: PBS buffer at T = 25 °C, free dye concentration = 5.0×10^{-6} M, and lipid concentration = 1.0×10^{-4} M.

Nevertheless, $MeSQ_3DOPE$ LUVs undergo a substantial content leakage without being under blue LED illumination compared to DOPG LUVs, as shown in Figure 3.10. The leakage of red dye in $MeSQ_3DOPE$ LUVs could be associated with increased permeability of red dyes in the hydrophobic $MeSQ_3DOPE$ membrane compared to that of DOPG, as a result of the red dye possessing less negative charge compared to calcein at pH 7.4, which is predicted from the pK_a of calcein. (pK_{a1} = 2.1, pK_{a2} = 2.9, pK_{a3} = 4.2, pK_{a4} = 5.5, pK_{a5} = 10.8 and pK_{a6} =11.7).[46]

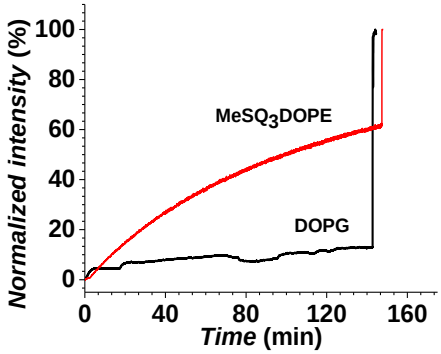

Figure 3.10. Leakage of $MeSQ_3DOPE$ and DOPG LUVs containing red dye (sulforhodamine B) upon storage in the dark at T = 25 °C in PBS buffer.

In addition, when DOPG LUVs containing encapsulated red dye were used for method validation of liposomal leakage quantification, the red dye signals did not behave consistently, as shown in Figure 3.11. Free red dye in CE-PBS buffer has retention time at 4.8 min. When DOPG LUVs encapsulated with red dye were injected into the capillary, a new peak appeared at 3.1 min and was initially assigned to the red dye encapsulated in liposomes. The feasibility of leakage quantification was tested by spiking the liposome samples with red dye stock solution. The data shows that the peak area at 4.8 min increases after the spike. When Triton X-100 was added to lyse the liposomes, the signal at 4.8 min also increased significantly, as a result of the entrapped dyes being released to the surroundings, but the signal at 3.1 min remained unaffected, which contradicts with the prediction that two signals should become one peak after lysis of the liposomes. Thus, using red dye for liposomal leakage quantification by CE needs further investigation in the future.

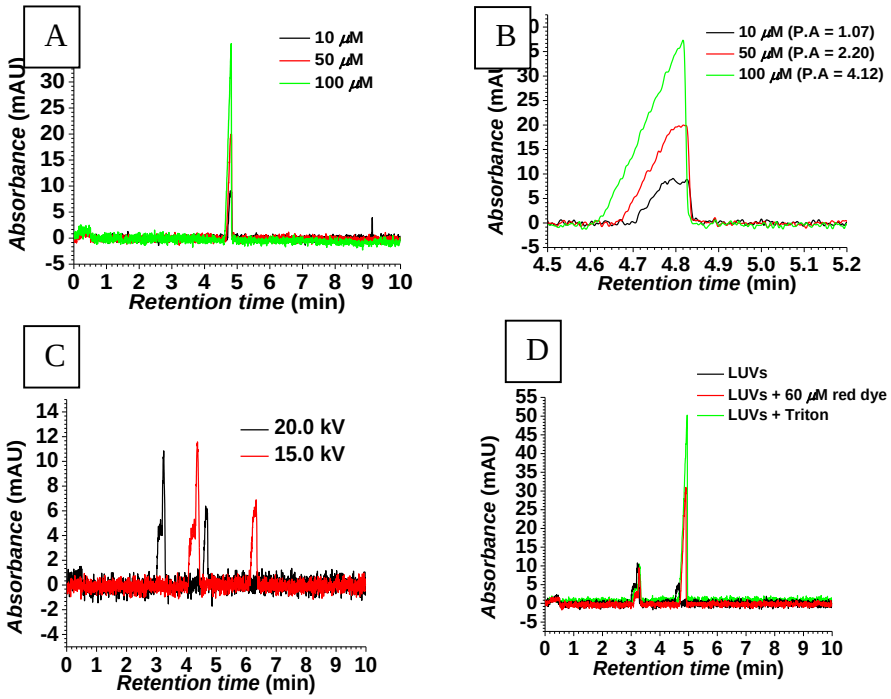

Figure 3.11. Examination of DOPG LUVs with red dye (sulforhodamine B) by CE. **A**. Free red dye standard at different concentrations, **B**. Enlarged view of electropherograms with included peak areas, **C**. DOPG LUVs at different CE separation voltages, **D**. DOPG LUVs containing encapsulated red dye followed by addition of free dye or adding Triton X-100. Conditions: *Voltage* = 20 kV, 0.020 M phosphate-buffered saline (PBS) at pH 7.4 containing 0.010 M sucrose, T = 25 °C.

Additionally, DOSY was validated as another method for obtaining liposomal leakage quantification. Fitting NMR peak areas of the entrapped fluorine probe and the free probe in solution versus the gradient strength through use of Equation 3.4 yields diffusion coefficients of $6.7 \times 10^{-7}\,cm^2.s^{-1}$ and $1.6 \times 10^{-5}\,cm^2.s^{-1}$, as shown in Figure 3.12. The almost 2 order of magnitude difference in diffusion coefficients is sufficient to quantify the probe leakage/release.[44] After inserting the two above measured diffusion coefficient values in the Equation 3.3, it follows that the signal from the free probe should almost disappear (about 5.1% of its initial values) at 16.60 G/cm, while the signal of the probe trapped inside the liposomes is affected less significantly (88.3% of its initial values). At 1.75 G/cm, the signal intensities are only slightly decreased for

both free (96.7 %) and trapped (99.9%) probe. If x is the fraction of trapped (encapsulated) probe, the ratio, R, of peak areas at 16.60 G/cm and 1.75 G/cm is then

$$R = \frac{A_{16.60}}{A_{1.75}} = \frac{88.3x + 5.1(1-x)}{99.9x + 96.7(1-x)} = \frac{83.2x + 5.1}{3.2x + 96.7} \quad \text{Equation 3.5}$$

Conversely, *x* can be expressed in terms of *R* as

$$x = \frac{96.7R - 5.1}{83.2 - 3.2R} \quad \text{Equation 3.6}$$

As following from Equation 3.6, the ratio of the peak areas at the high and the low pulsed-field gradient values is a reasonable measure of the percentage of encapsulated material. However, Figure 3.12 D shows that DOPC LUVs containing encapsulated probe experience an unacceptable high rate of intrinsic leakage in the dark, which is commonly found for small probes.[37] Thus, synthesis of a suitable fluorine-based probe that does not exhibit a significant escape from liposomes is crucial for liposomal leakage quantification using DOSY.

Because the contents leakage measurements from $MeSQ_3$DOPE LUVs via DOSY and CE were unsuccessful, qualitative examination of the leakage was studied by DLS. DLS measurements show that $MeSQ_3$DOPE LUVs do not exhibit any apparent aggregation during LED irradiation, as shown in Figure 3.13. Because stable Q_3DOPE:DOPE 20:80 LUVs can be prepared, as shown in Chapter 2, if $MeSQ_3$DOPE LUVs undergo photocleavage at the headgroup, DOPE must be produced at a sufficient amount (>80%) so as to trigger aggregation of/phase transition of/contents release from the vesicles. Thus, $MeSQ_3$DOPE:DOPE 20:80 LUVs were prepared to see if LED can trigger their aggregation/phase transition.

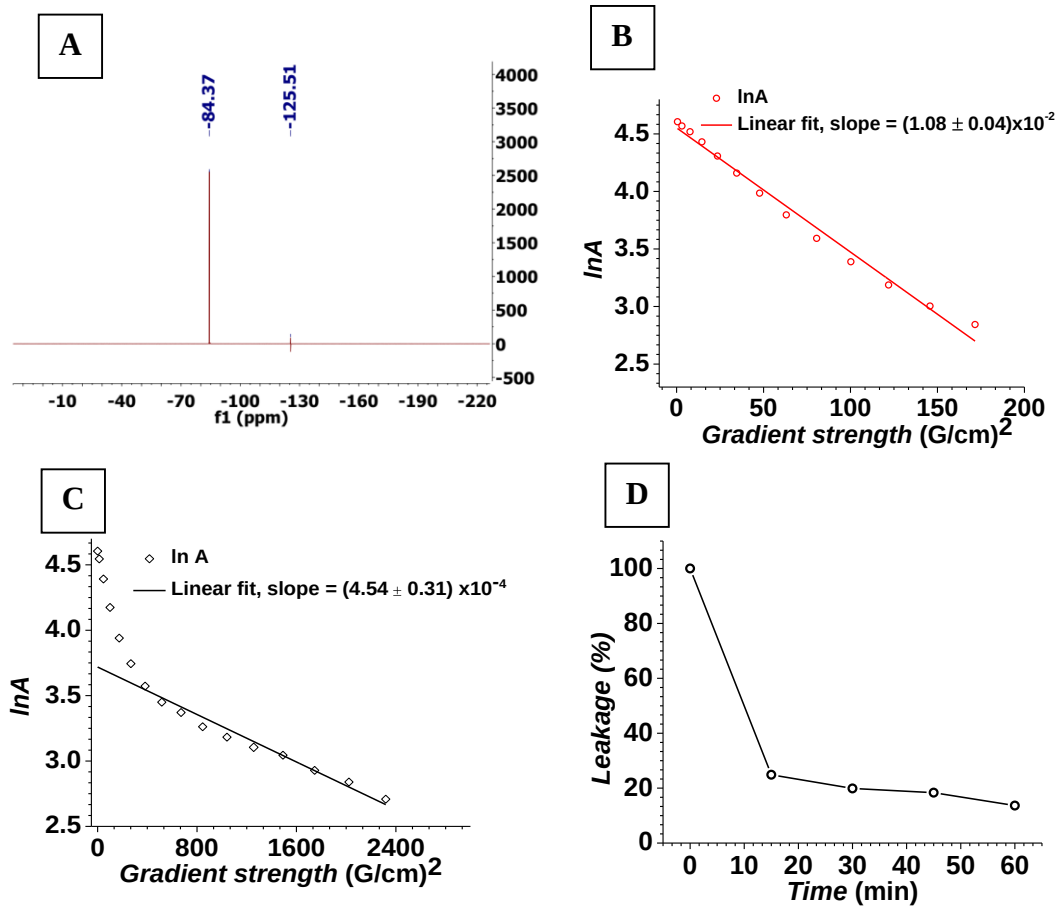

Figure 3.12. DOSY measurements of free probe and DOPC LUVs containing encapsulated trifluoromethanesulfonate anion probe. **A**. ^{19}F-NMR spectrum of the probe with KF as the reference, **B**. DOSY of free probe in solution, **C**. DOSY of encapsulated probe in ~100-nm diameter DOPC LUVs (related to liposome mobility). The initial (steeper) slope in C is due to a small amount of un-encapsulated free probe in the liposome sample. **D**. Probe leakage from of DOPC LUVs containing encapsulated probe in the dark. Conditions: **A**, **B**. 0.25 M probe solution in 0.15 M PBS, pH 7.4 with 10% D_2O, **C**, **D**. Leakage of 10 mM DOPC LUVs encapsulating probe suspended in 0.40 M PBS, pH 7.4, 10% D_2O, T = 25 °C.

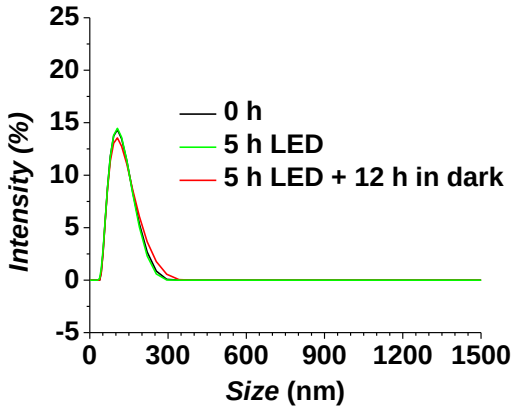

Figure 3.13. DLS measurements of $MeSQ_3$DOPE LUVs in PBS show that the LUVs do not exhibit aggregation under LED irradiation.

In Figure 3.14 is shown that under LED irradiation, $MeSQ_3$DOPE:DOPE 20:80 LUVs experience a slight increase in their size, probably due to a small amount of aggregation.

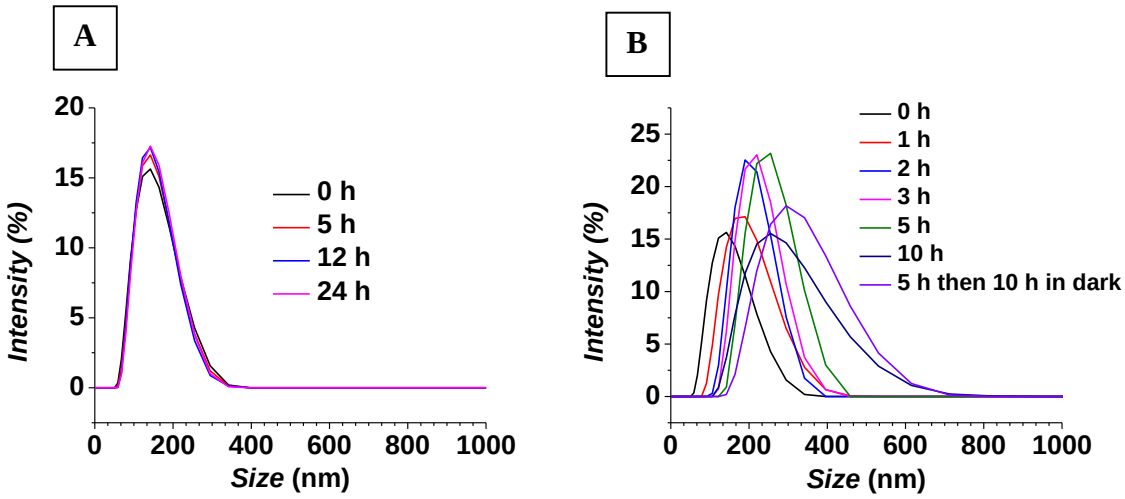

Figure 3.14. DLS measurements of $MeSQ_3$DOPE:DOPE 20:80 LUVs. **A**. in dark, **B**. under various LED irradiation times in PBS buffer, T = 25 °C.

To further evaluate the influence of the LED on the photoreduction of $MeSQ_3$DOPE LUVs, the vesicles were irradiated with the LEDs for different periods of time prior to SDT addition so as to cause reduction-induced release of contents. Light scattering in Figure 3.15 shows that only after about 1 min under LED irradiation, the SDT-induced contents release and PE lipid phase transition of the liposomes starts being inhibited. This trend can be seen in more detail in the

supporting information Figure SI3.1. This observation suggests that there is photochemical reaction changing the chemical properties of the $MeSQ_3DOPE$ lipids, making them so that they are unaffected by SDT presence (reduction by SDT is prevented).

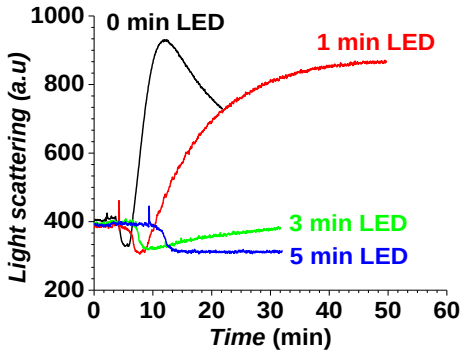

Figure 3.15. Light scattering of ~100-nm diameter $MeSQ_3DOPE$ LUVs as a function of various LED irradiation times prior to addition of SDT reductant. Conditions: PBS buffer at 25 °C, lipid concentration = 1.0×10^{-4} M.

Based on the reported photochemistry of photoresponsive quinone-based compounds,[47] the proposed photochemistry mechanism of $MeSQ_3DOPE$ lipid under LED irradiation in different solvents is shown in Figure 3.16.

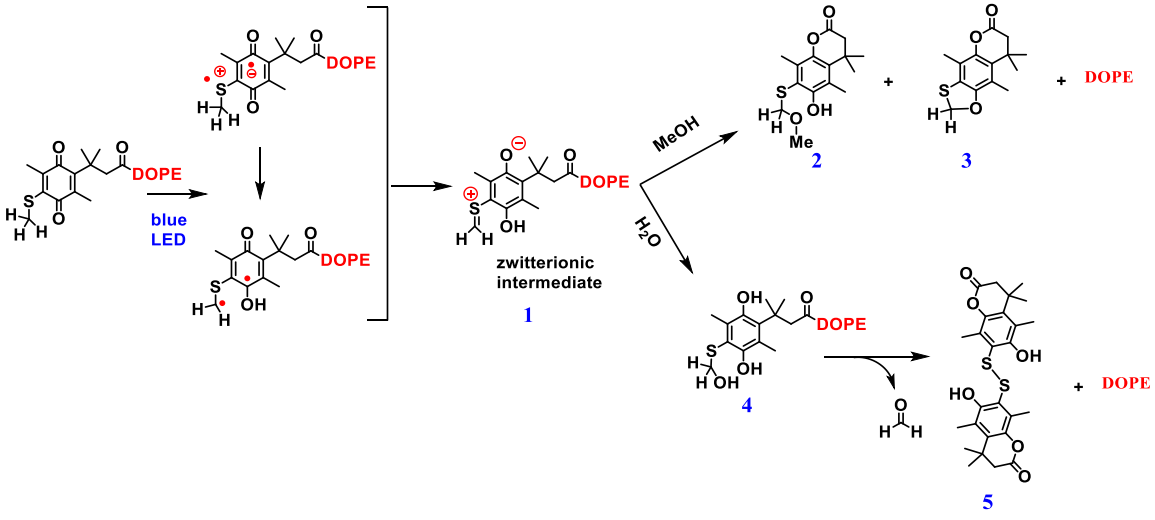

Figure 3.16. Proposed photolysis of $MeSQ_3DOPE$ lipid in different solvents.

The photoreaction begins with an electron transfer from sulfur to the quinone ring, followed by an irreversible β-hydrogen transfer, which leads to a net two-electron intramolecular reduction of quinone to the hydroquinone and formation of a zwitterionic intermediate 1 via both ionic or radical pathways. Capture by solvent or the phenolic oxygen, intermediate 1 undergoes a trimethyl lock ring closure, which completes the decaging of DOPE. Photolysis in water produces the disulfide 5, presumably via a thiohemiacetal intermediate 4. Because water has lower nucleophilicity compared to MeOH, the photolysis rate in aqueous solution is slower than in MeOH, which is in agreement with the data presented in Figure 3.17. Typically, an increasing percentage of water in MeOH slows down the decay rate of the visible absorption band at λ_{max} of $MeSQ_3DOPE$.

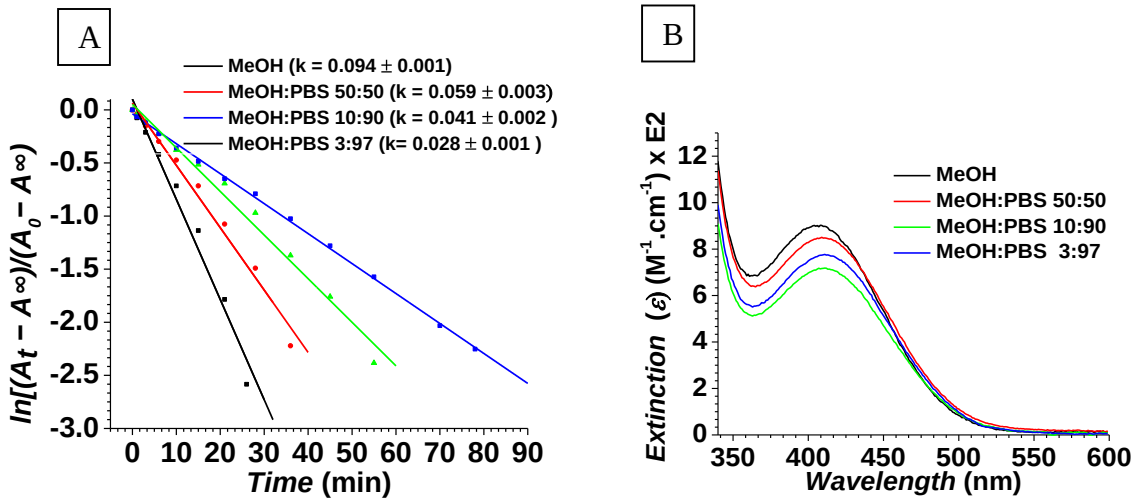

Figure 3.17. **A**. Kinetic plot of $MeSQ_3DOPE$ lipid transformation in MeOH:PBS mixture at different solvent ratios under blue LED irradiation. **B.** Molar extinction coefficient of $MeSQ_3DOPE$ lipid in different solvents. λ_{max} of the visible band is at 397 nm in MeOH, at 409 nm in MeOH:PBS 50:50, at 412 nm in both MeOH:PBS 10:90 and 3:97 (v/v).

To evaluate the influence of MeOH on the photoreaction of $MeSQ_3DOPE$ LUVs, DLS measurements were taken over time and are displayed Figure 3.18. Adding MeOH (at 10% final v/v) to the solution of $MeSQ_3DOPE$:DOPE 20:80 LUVs causes an increase in the average size of liposomes over time, probably due to membrane swelling.[48] However, under LED irradiation, the

vesicles are likely to undergo significant aggregation, which might be resulted from byproducts 2 and 3 are produced in the presence of MeOH at the faster rate than the hydrolysis of intermediate 1 in water, leading to more DOPE lipids being produced.

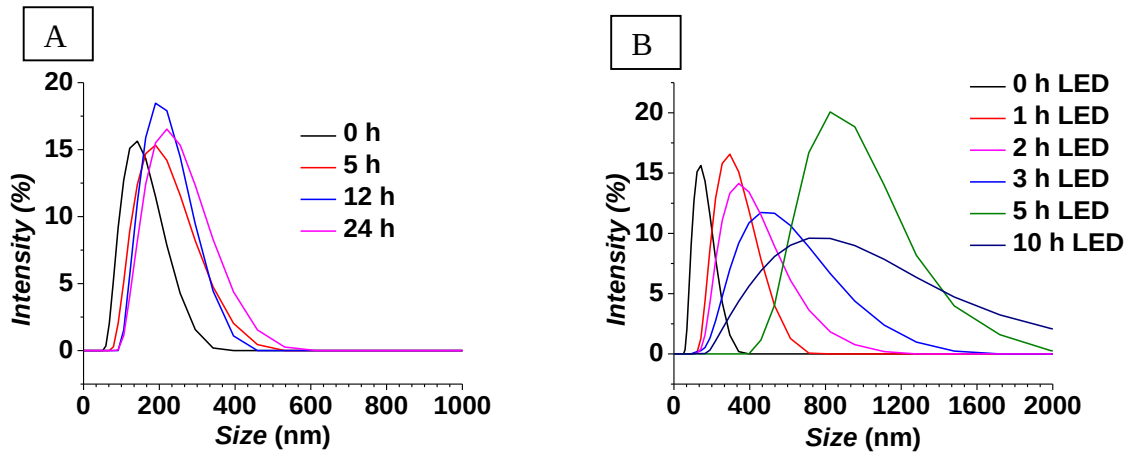

Figure 3.18. DLS measurements of $MeSQ_3DOPE$:DOPE 20:80 LUVs in PBS under the influence of MeOH over time at 25 °C. **A**. without LED irradiation, and **B**. with LED irradiation.

All of the observations above suggest that $MeSQ_3DOPE$-based LUVs do not experience the $L_\alpha \rightarrow H_{II}$ phase transition upon their exposure to blue LED. The first explanation rests on the possibility that the blue LED irradiation is insufficient to induce the reduction and cleavage of the quinone headgroup. However, several examples have demonstrated the photocleavage feasibility of $MeSQ_3DOPE$-like compounds. For example, Walton and Walton reported that decaging of $MeSQ_3GABA$ (compound 6 in Figure 3.19) upon its exposure to 455-nm light from an LED is observed in aqueous conditions with disulfide 5 as the byproduct, and the photoreduction is much faster than trimethyl lock closure.[38]

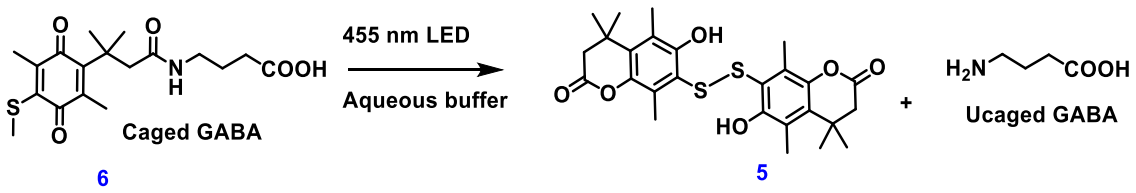

Figure 3.19. Cleavage of the neurotransmitter γ-aminobutyric acid (GABA) to activate GABAA receptors in Xenopus oocytes upon irradiation with a 455-nm LED.[38]

In addition, Truong and Forsythe synthesized photodegradable hydrogels via a thio-bromo click reaction to form a benzoquinone link for 3D cell encapsulation, and release by visible-light unclick chemistry under an aqueous environment was achieved, as shown in Figure 3.20.[49] In these cases, the leaving groups are primary amines and the quinones are alkylated sulfides, with such motifs being quite similar to those of $MeSQ_3$DOPE. Thus, the headgroup photocleavage of $MeSQ_3$DOPE LUVs to produce DOPE and disulfide 5 should happen to some extent, and this event is confirmed by mass spectrometry, as shown in Figure 3.21.

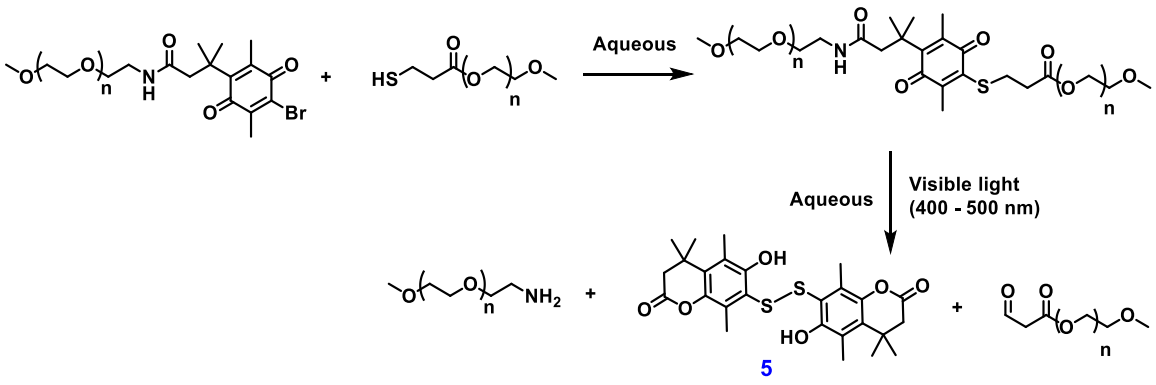

Figure 3.20. Schematic of polymer precursor crosslinking in aqueous via thio-bromo click reaction and its subsequent decomposition under visible light irradiation.[49]

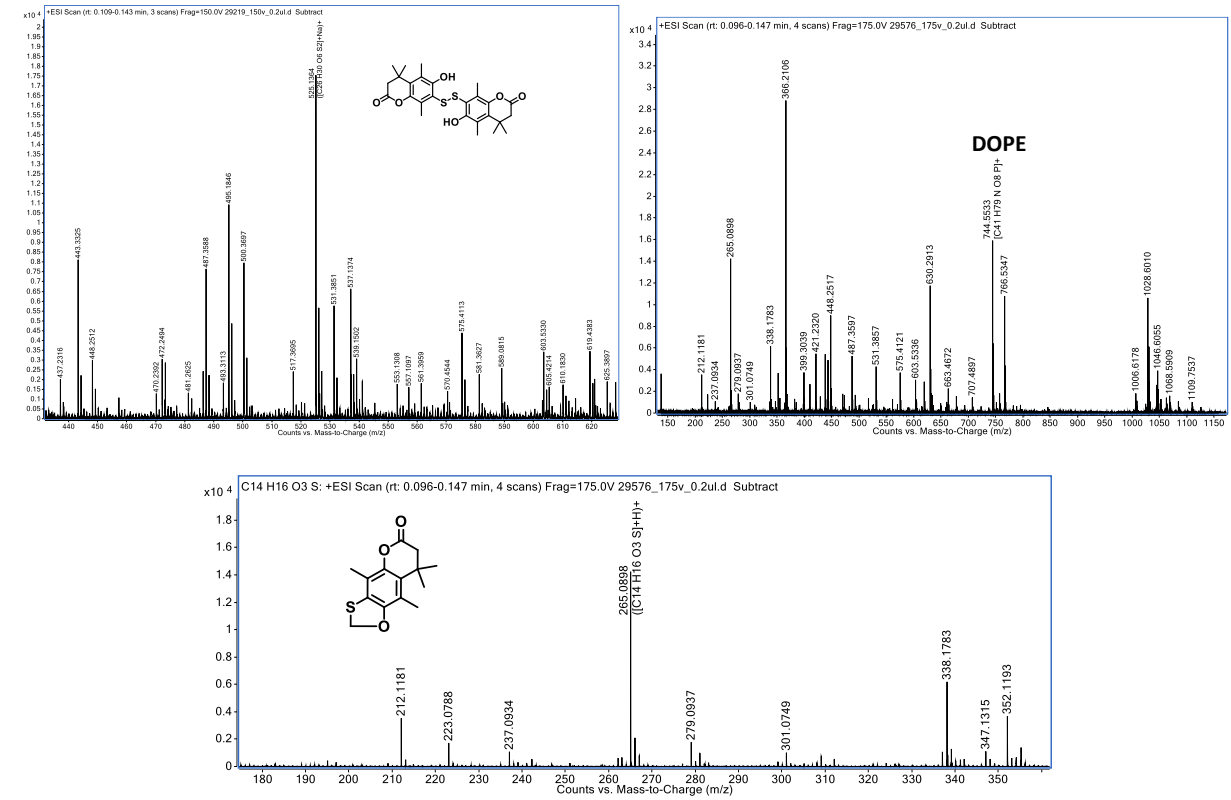

Figure 3.21. HRMS (ESI) of $MeSQ_3DOPE$ LUV_s in water under blue LED irradiation for 2 hours. **A**. Mass calculated for $C_{26}H_{30}O_6S_2$ (compound 5) $[M+Na]^+$ 525.1376, found 525.1364 (1.2 ppm). **B**. Mass calculated for $C_{41}H_{78}NO_8P$ (DOPE) $[M+H]^+$ 744.5538, found 744.5530 (1.43 ppm). **C**. Mass calculated for $C_{14}H_{16}O_3S$ (compound 3) $[M+H]^+$ 265.0893, found 265.0898 (1.81 ppm) .

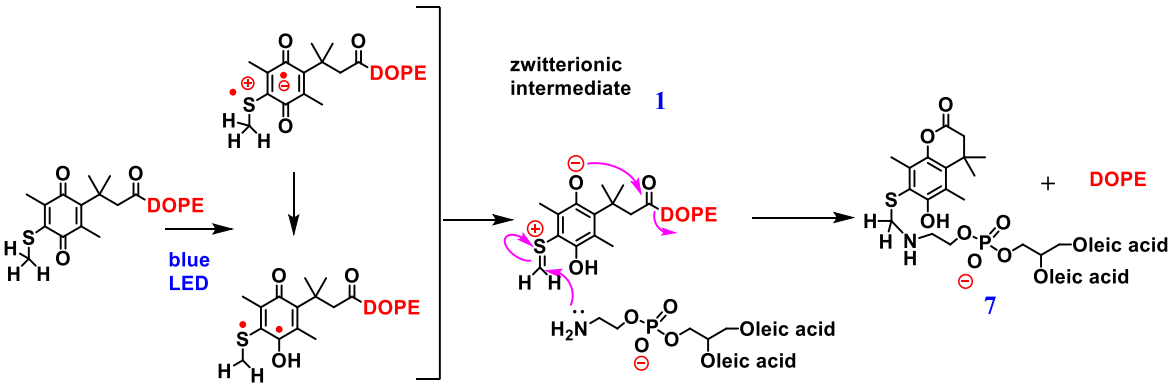

Figure 3.22. Proposal for formation of a new lipid conjugate after $MeSQ_3DOPE$ LUVs are irradiated with the blue LED.

In Figure 3.23 are shown the ^{1}H-NMR spectra of $MeSQ_3DOPE$ in the form of liposomes before and after LED irradiation for 1 hour. The disappearance of the sulfomethyl peak (red star) and the

formation of aldehyle and another peaks (black star) is supportive for the mechanism mentioned in Figure 3.16 and Figure 3.22

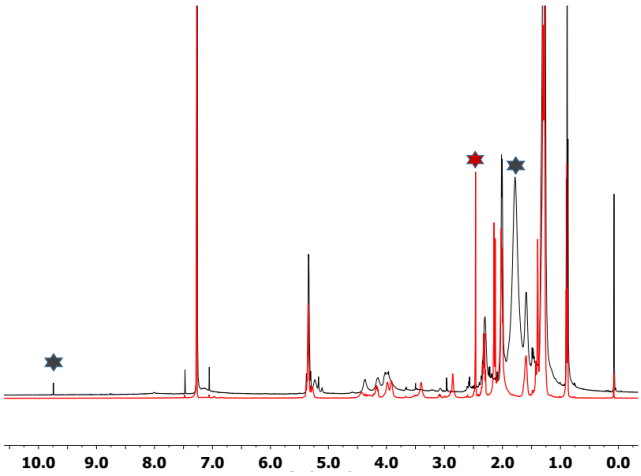

Figure 3.23. ^{1}H-NMR of MeSQ$_3$DOPE LUVs before (red) and after (black) LED irradiation for 1 h at T = 25 °C. LUVs solutions were dried under N_2 gas then the resulting residue was dissolved in $CDCl_3$ containing 1 % (v/v) tetramethylsilane (TMS).

In addition, Nawimanage reported that decaging of several amine-based leaving groups was achieved via quinone methide formation after chemical reduction (SDT) of a hydroxymethyl benzoquinone trigger group (HMBQ).[50] However, when DOPE is the leaving group in the form of in HMBQDOPE LUVs, contents release from HMBQDOPE LUVs was not observed. The author proposed that the highly reactive quinone methide species (compound 8 in Figure 3.24) formed after the reduction is susceptible to nucleophilic attack by the free amine of the recently generated DOPE which is in close proximity, thereby forming a new lamellar-stabilized lipid that inhibits the $L_\alpha \rightarrow H_{II}$ phase transition. Thus, although HMBQDOPE:DOPE 20:80 LUVs have been prepared, their release has not been observed after addition of SDT, as shown in Figure SI3.3 in the supporting information below.

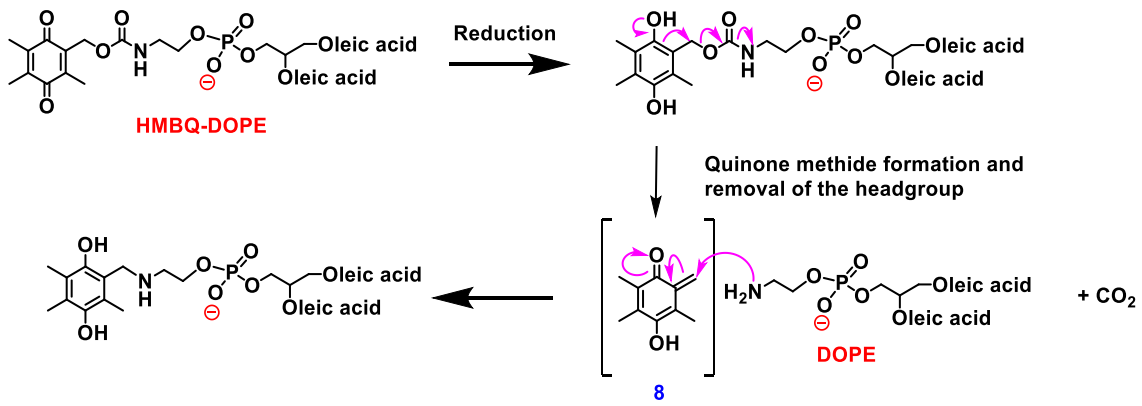

Figure 3.24. Schematic representation of proposed HMBQDOPE liposomes response via quinone methide formation.

The evidence presented herein suggests that blue light from LED can trigger the reduction and cleavage of the $MeSQ_3$ headgroup, but the subsequent formation of a new trigger group-DOPE lipid prevents the lipids in the bilayer from undergoing the $L_\alpha \rightarrow H_{II}$ phase transition, which explains observations from the irradiation/SDT reduction experiment in Figure 3.15. When MeOH (10% v/v) was added to the LUV samples, because of its higher nucleophilicity than water and free amine of DOPE, MeOH preferentially reacts with the intermediate 1, producing DOPE in higher amounts, therefore leading to aggregation of the DOPE-rich vesicles.

3.4. Conclusion

In this chapter, blue light photoresponsive liposomes made from $MeSQ_3$DOPE lipid were prepared with the goal to examine their leakage/fusion as the result of symmetrical cleavage caused by photoreduction via blue LED irradiation. Conventional calcein leakage/fusion assays were not applicable due to photobleaching, which encouraged the employment of new techniques including CE and DOSY. However, this research is still ongoing so as to further validate and optimize CE and DOSY for liposomal leakage quantification. The small amount of data generated here suggests that irradiation by blue LEDs leads to reduction and cleavage of the quinone group from $MeSQ_3$DOPE, but the subsequent reaction of DOPE with the intermediate **1** leads to the formation

of a hydroquinone-caped DOPE lamellar-stabilized lipid, which hinders the $L_{\alpha} \rightarrow H_{II}$ phase transition. Therefore, it is very important to establish a critical proportion of DOPE incorporated in $MeSQ_3$DOPE:DOPE LUVs so that they can maintain the lamellar phase, but in smaller quantities, the conversion of $MeSQ_3$DOPE to DOPE can trigger the collapse of vesicles. In addition, reagents that can compete or block the nucleophilicity of free amine of DOPE, such as a hydrophobic scavenger of zwitterionic intermediate **1** in $MeSQ_3$DOPE LUVs, or a faster-triggered reduction quinone moiety could be utilized to promote the phase transition of $MeSQ_3$DOPE vesicles.

3.5. References

1. Bibi, S., et al., Trigger Release Liposome Systems: Local and Remote Controlled Delivery? *Journal of Microencapsulation* **2012,** *29* (3), 262-276.

2. Wang, Y.; Kohane, D. S., External Triggering and Triggered Targeting Strategies for Drug Delivery. *Nature Reviews Materials* **2017,** *2* (6), 17020.

3. Riaz, M., et al., Surface Functionalization and Targeting Strategies of Liposomes in Solid Tumor Therapy: A Review. *International Journal of Molecular Sciences* **2018,** *19* (1), 195.

4. Puri, A., Phototriggerable Liposomes: Current Research and Future Perspectives. *Pharmaceutics* **2014,** *6* (1), 1-25.

5. Fomina, N., et al., Photochemical Mechanisms of Light-Triggered Release from Nanocarriers. *Advanced Drug Delivery Reviews* **2012,** *64* (11), 1005-1020.

6. Miranda, D.; Lovell, J. F., Mechanisms of Light-Induced Liposome Permeabilization. *Bioengineering & Translational Medicine* **2016,** *1* (3), 267-276.

7. Lajunen, T., et al., Light Activated Liposomes: Functionality and Prospects in Ocular Drug Delivery. *Journal of Controlled Release* **2016,** *244*, 157-166.

8. O'Brien, D. F., et al., Light-Regulated Permeability of Rhodopsin: Egg Phosphatidylcholine Recombinant Membranes. *Proceedings of the National Academy of Sciences* **1977,** *74* (12), 5222-5226.

9. Leung, S. J.; Romanowski, M., Light-Activated Content Release from Liposomes. *Theranostics* **2012,** *2* (10), 1020.

10. Deziel, M.; Girotti, A., Photodynamic Action of Bilirubin on Liposomes and Erythrocyte Membranes. *Journal of Biological Chemistry* **1980,** *255* (17), 8192-8198.

11. Pashkovskaya, A., et al., Light-Triggered Liposomal Release: Membrane Permeabilization by Photodynamic Action. *Langmuir : the ACS Journal of Surfaces and Colloids* **2009,** *26* (8), 5726-5733.

12. Yavlovich, A., et al., Light-Sensitive Lipid-Based Nanoparticles for Drug Delivery: Design Principles and Future Considerations for Biological Applications. *Molecular Membrane Biology* **2010,** *27* (7), 364-381.

13. Shum, P., et al., Phototriggering of Liposomal Drug Delivery Systems. *Advanced Drug Delivery Reviews* **2001,** *53* (3), 273-284.

14. Dolmans, D. E., et al., Photodynamic Therapy for Cancer. *Nature Reviews Cancer* **2003,** *3* (5), 380.

15. An, X., et al., Smart Photothermal-Triggered Bilayer Phase Transition in Aunps–Liposomes to Release Drug. *Langmuir : the ACS Journal of Surfaces and Colloids* **2013,** *29* (4), 1061-1068.

16. Mathiyazhakan, M., et al., A Concise Review of Gold Nanoparticles-Based Photo-Responsive Liposomes for Controlled Drug Delivery. *Nano-micro Letters* **2018,** *10* (1), 10.

17. Paasonen, L., et al., Gold Nanoparticles Enable Selective Light-Induced Contents Release from Liposomes. *Journal of Controlled Release* **2007,** *122* (1), 86-93.

18. Agarwal, A., et al., Remote Triggered Release of Doxorubicin in Tumors by Synergistic Application of Thermosensitive Liposomes and Gold Nanorods. *ACS Nano* **2011,** *5* (6), 4919-4926.

19. Wu, G., et al., Remotely Triggered Liposome Release by near-Infrared Light Absorption Via Hollow Gold Nanoshells. *Journal of the American Chemical Society* **2008,** *130* (26), 8175-8177.

20. Yagai, S., et al., Photocontrollable Self-Assembly. *Chemistry–A European Journal* **2005,** *11* (14), 4054-4063.

21. Bisby, R. H., et al., Fast Laser-Induced Solute Release from Liposomes Sensitized with Photochromic Lipid: Effects of Temperature, Lipid Host, and Sensitizer Concentration. *Biochemical and Biophysical Research Communications* **1999,** *262* (2), 406-410.

22. Bisby, R. H., et al., Active Uptake of Drugs into Photosensitive Liposomes and Rapid Release on Uv Photolysis¶. *Photochemistry and Photobiology* **2000,** *72* (1), 57-61.

23. Kano, K., et al., Photoresponsive Membranes. Regulation of Membrane Properties by Photoreversible Cis–Trans Isomerization of Azobenzenes. *Chemistry Letters* **1980,** *9* (4), 421-424.

24. Cui, Z.-K., et al., Nonphospholipid Fluid Liposomes with Switchable Photocontrolled Release. *Langmuir : the ACS Journal of Surfaces and Colloids* **2014,** *30* (36), 10818-10825.

25. Ohya, Y., et al., Photo-Sensitive Lipid Membrane Perturbation by a Single Chain Lipid Having Terminal Spiropyran Group. *Supramolecular Science* **1998,** *5* (1-2), 21-29.

26. Pidgeon, C.; Hunt, C. A., Light Sensitive Liposomes. *Photochemistry and Photobiology* **1983,** *37* (5), 491-494.

27. Regen, S. L., et al., Polymerized Phosphatidyl Choline Vesicles. Stabilized and Controllable Time-Release Carriers. *Biochemical and Biophysical Research Communications* **1981,** *101* (1), 131-136.

28. Yavlovich, A., et al., A Novel Class of Photo-Triggerable Liposomes Containing Dppc: Dc8, 9pc as Vehicles for Delivery of Doxorubcin to Cells. *Biochimica et Biophysica Acta (BBA)-Biomembranes* **2011,** *1808* (1), 117-126.

29. Yavlovich, A., et al., Design of Liposomes Containing Photopolymerizable Phospholipids for Triggered Release of Contents. *Journal of Thermal Analysis and Calorimetry* **2009,** *98* (1), 97-104.

30. Bondurant, B., et al., Photoinitiated Destabilization of Sterically Stabilized Liposomes. *Biochimica et Biophysica Acta (BBA)-Biomembranes* **2001,** *1511* (1), 113-122.

31. Chandra, B., et al., Formulation of Photocleavable Liposomes and the Mechanism of Their Content Release. *Organic & Biomolecular Chemistry* **2006,** *4* (9), 1730-1740.

32. Pelliccioli, A. P.; Wirz, J., Photoremovable Protecting Groups: Reaction Mechanisms and Applications. *Photochemical & Photobiological Sciences* **2002,** *1* (7), 441-458.

33. Bayer, A. M., et al., Triggered Liposomal Release through a Synthetic Phosphatidylcholine Analogue Bearing a Photocleavable Moiety Embedded within the Sn-2 Acyl Chain. *Chemistry–A European Journal* **2014,** *20* (12), 3350-3357.

34. Zhang, D., et al., Liposomes Formed from Photo-Cleavable Phospholipids: In Situ Formation and Photo-Induced Enhancement in Permeability. *RSC Advances* **2018,** *8* (26), 14669-14675.

35. Zhang, Z.-Y.; Smith, B. D., Synthesis and Characterization of Nvoc-Dope, a Caged Photoactivatable Derivative of Dioleoylphosphatidylethanolamine. *Bioconjugate Chemistry* **1999,** *10* (6), 1150-1152.

36. Chandra, B., et al., Design of Photocleavable Lipids and Their Application in Liposomal "Uncorking". *Chemical Communications* **2005,** (24), 3021-3023.

37. Li, Z., et al., Dithiane-Based Photolabile Amphiphiles: Toward Photolabile Liposomes1, 2. *Langmuir : the ACS Journal of Surfaces and Colloids* **2003,** *19* (16), 6381-6391.

38. Walton, D. P.; Dougherty, D. A., A General Strategy for Visible-Light Decaging Based on the Quinone Trimethyl Lock. *Journal of the American Chemical Society* **2017,** *139* (13), 4655-4658.

39. Sorochkina, A. I., et al., Peptide-Induced Membrane Leakage by Lysine Derivatives of Gramicidin a in Liposomes, Planar Bilayers, and Erythrocytes. *Biochimica et Biophysica Acta (BBA)-Biomembranes* **2013,** *1828* (11), 2428-2435.

40. Shaw, S. K., et al., Non-Covalent Assembly Method That Simultaneously Endows a Liposome Surface with Targeting Ligands, Protective Peg Chains, and Deep-Red Fluorescence Reporter Groups. *Chemistry–A European Journal* **2017,** *23* (51), 12646-12654.

41. Ansar, S. M., et al., Direct Quantification of Unencapsulated Doxorubicin in Liposomal Doxorubicin Formulations Using Capillary Electrophoresis. *International Journal of Pharmaceutics* **2018,** *549* (1-2), 109-114.

42. Ansar, S. M.; Mudalige, T., Direct and Simultaneous Determination of Intra-Liposomal and External Sulfate in Liposomal Doxorubicin Formulations by Capillary Electrophoresis/Inductively Coupled Plasma-Tandem Mass Spectrometry (Ce/Icp-Ms/Ms). *International Journal of Pharmaceutics* **2019,** *561*, 283-288.

43. Taniguchi, M.; Lindsey, J. S., Database of Absorption and Fluorescence Spectra of> 300 Common Compounds for Use in Photochem Cad. *Photochemistry and Photobiology* **2018,** *94* (2), 290-327.

44. Wan, Y., et al., Liposomes from Novel Photolabile Phospholipids: Light-Induced Unloading of Small Molecules as Monitored by Pfg Nmr. *Journal of the American Chemical Society* **2002,** *124* (20), 5610-5611.

45. Orädd, G., et al., Effects of Peptide Hydrophobicity on Its Incorporation in Phospholipid Membranes—an Nmr and Ellipsometry Study. *Biochimica et Biophysica Acta (BBA)-Biomembranes* **2011,** *1808* (1), 244-252.

46. Https://Www.Dojindo.Com/Store/P/623-Calcein.Html (Accessed on 08/26/2019).

47. Regan, C. J., et al., Mechanistic Studies of the Photoinduced Quinone Trimethyl Lock Decaging Process. *Journal of the American Chemical Society* **2017,** *139* (13), 4729-4736.

48. Ingólfsson, H. I.; Andersen, O. S., Alcohol's Effects on Lipid Bilayer Properties. *Biophysical Journal* **2011,** *101* (4), 847-855.

49. Truong, V. X., et al., Visible-Light-Mediated Cleavage of Polymer Chains under Physiological Conditions Via Quinone Photoreduction and Trimethyl Lock. *Chemical Communications* **2017,** *53* (89), 12076-12079.

50. Nawimanage, R. R., Synthesis, Characterization, and Evaluation of Small Molecule-Based Fluorogenic Probes for the Detection of Cellular Thiols. Ph.D Dissertation, Louisiana State University, Baton Rouge, LA, **2015**.

CHAPTER 4
A RATIONAL DESIGN OF MALACHITE GREEN DERIVATIVES FOR MOLECULAR ADSORPTION AND TRANSPORT THROUGH LIPID BILAYER STUDY

4.1. The Importance of the Study

The cell membrane is the boundary where the exchange of contents between the intracellular and extracellular fluids occurs. This membrane-associated movement of biological molecules and ions plays a crucial role to maintain cellular activities and functions, and therefore, containing the information of living cells.[1-3] Mechanisms for molecular transport across membranes can be classified into two categories: active and passive transport. Cells can actively absorb molecules in the direction opposed to the concentration gradient with the help of membrane proteins, which requires regulatory machinery with an input of energy. On the other hand, some molecules can passively enter cells due to their associated concentration gradient, an entropy-driven and nonspecific diffusion process, as in the case of O_2 and CO_2 movement across the membrane.[4-6] Passive transport of molecules and ions across the bilayer membrane can be divided into four consecutive steps: molecular adsorption at the exoplasmic surface (outer surface of the membrane), partitioning the membrane hydrophobic region that has a thickness of about 5–10 nm, diffusion through the membrane to the endoplasmic surface (inner membrane surface), and partitioning/entrance into the cytosol. The adsorption of molecules/ions on membranes is dictated by the adsorption constant that correlates with the affinity of molecule binding to the outer and inner surfaces of the membrane, while the partition coefficient is indicative of the solubility and permeability of adsorbed molecules in the hydrophobic region of the lipid bilayer.[7-9]

Most drugs are transported passively through the membrane.[5, 10-11] Therefore, understanding the mechanism of passive permeation is crucial not only in fundamental biological research but also in medical applications, potentially offering insightful information about drug–

membrane thermodynamics and kinetics. Importantly, of great interest for drug development is a detailed understanding of how structure and properties of drugs and membranes control their interactions and the passive uptake process.[5, 11-12] However, in vivo probing of drug–membrane interactions faces intricacies of the cellular environment, the experimental cost, and complexity, all which limit high-throughput screening capabilities during new drug development. Therefore, in vitro techniques with proper models are significantly important for a rational drug design that has helped in expanding passive-permeation databases.[13]

The cell membrane is composed of a wide variety of lipid species, where their identity and distribution play a role in many events, such as protein organization, membrane fusion, and cellular-signal communication.[14-15] Liposomes—spherical vesicles formed from self-assembly of phospholipids, which have an exterior structure analogous to the cell membrane—have been widely utilized for drug delivery applications.[16-17] The lipid compositions of liposomes are easily tailored by a simple formulation adjustment, which allows them to be the most suitable surface model of the cell membrane in order to investigate interface-related biological processes, especially for molecular interactions at lipid bilayers, such as adsorption and passive transport of compounds through the bilayer.[18-20] On the other hand, elucidation of the comprehensive structure-permeability relationship of drugs is impeded by an overwhelming number of possible drug structures. The chemical structural diversity issue can be simplified by studying chemical analogs, a group of compounds having a similar backbone, but differing from others in respect to a certain component, so as to systematically investigate factors and their significant contributions to passive permeability.

In this chapter, the analogs, *malachite green derivatives* (MGDs), and liposomes composed of different phospholipids, such as DOPG, DOPS, DOPC, Q_3DOPE are produced to investigate

how molecular charge, polarity, size, lipophilicity, and lipid headgroup structures control adsorption and transport processes. In collaboration with the Haber research group at LSU, second harmonic generation (SHG) is used to measure in real-time molecular adsorption and transport through liposomal membranes. In addition, molecular dynamics simulations (MD) provided by the Kumar research group at LSU were used to obtain a detailed estimation of interactions between MGDs and lipid membranes at the molecular level. In Figure 4.1 is presented a general overview of the collaborative study. In this project, I am responsible for the synthesis of MGDs and creation of liposomes. From a measurement science perspective, this chapter focuses on rational synthesis of MGD probes, principles of the measurements, and proof-of-concept data.

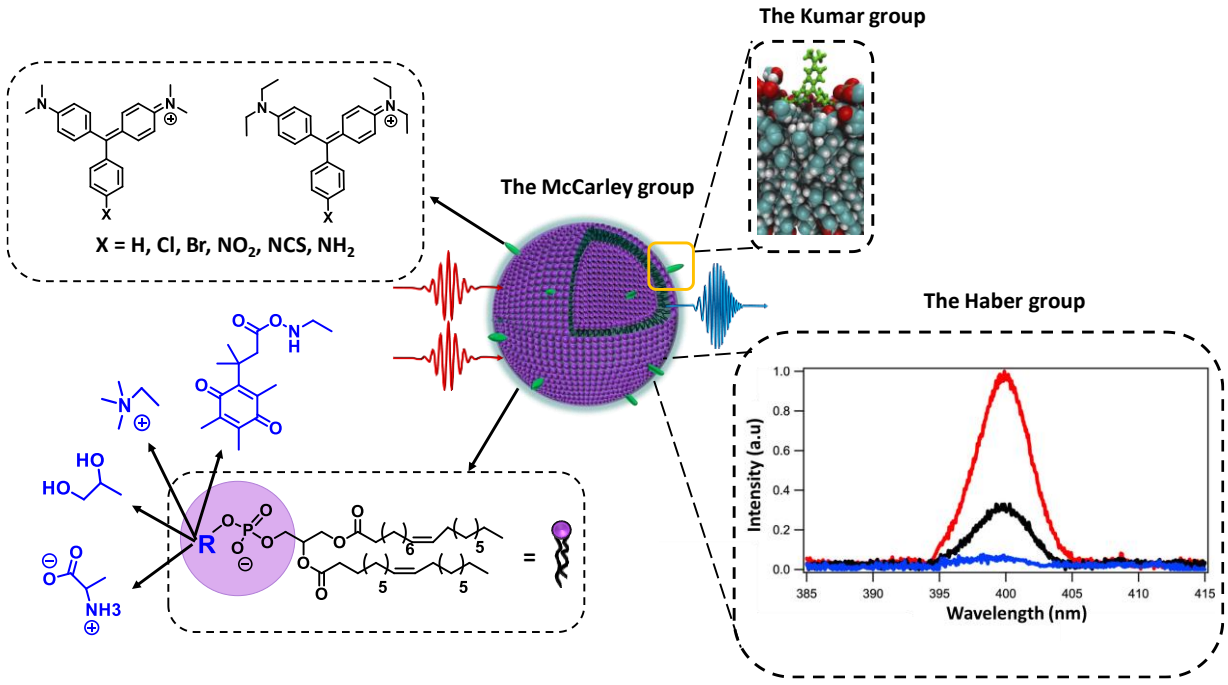

Figure 4.1. Rational design of malachite green derivatives (MGDs) for study of their adsorption and transport at liposomal lipid bilayers by molecular dynamics simulations and second harmonic generation.

4.2. Adsorption and Transport of MGDs Through a Liposomal Bilayer Studied by SHG

4.2.1. Introduction to SHG

The experimental capacity of conventional optical techniques, such as fluorescence, Raman, and infrared spectroscopies, when probing interfacial interactions, provides inadequate information and lack of sensitivity due to the difficulty to resolve the signal from a small number of molecules adsorbed on the surface versus the signal emanating from a much larger population of the same molecules in bulk solution.[21-23] Non-linear optical techniques, such as sum frequency generation (SFG), are able to differentiate the two different origin signals, thanks to the high intensity of light that can be generated from lasers, which makes SFG a versatile technique to interrogate interfacial interactions at the molecular level.

SHG is the most common form of SFG, in which two photons of the incident light with the same frequency (ω) simultaneously interact with a non-linear medium to generate the third photon at the second harmonic frequency (2ω). However, SHG is medium symmetry-dependent, and arises only from media lacking a center of symmetry, such as an anisotropic crystal, or at an interface between two media. In addition to the flat surface of materials, applications of SHG have been extended to a full scope of colloidal surface systems, including polymer particles, nanoparticles, emulsions, and living cells, when the particle size exceeds the critical value of tens of nanometers. Particularly, the non-destructive and label-free nature, and the laser's ultra-fast time scale in SHG are beneficial for monitoring biological systems in an in situ manner.[24-27]

4.2.2. SHG Principles

When light propagates in a medium, the molecules in the medium are polarized and gain an electric dipole moment. A sum of the induced molecular dipoles per unit volume is the electric polarization. This should not be confused with the polarization of the light field, which is related

to the change of its electric field direction. The optical response of the material to an electric field is expressed in terms of the induced polarization P via a Taylor expansion

$$P = \chi^{(1)}E_\omega + \chi^{(2)}E_\omega E_\omega + \chi^{(3)}E_\omega E_\omega E_\omega + \cdots \quad \text{Equation 4.1}$$

where $\chi^{(n)}$is the *n*th order nonlinear susceptibility of the material and describes the local *n*th order optical response of the medium, and is an indicator of how easily the medium is polarized in the electric field vector, E_ω, with frequency, ω, of the incident light. $\chi^{(1)}$ is responsible for the linear polarization, while higher order susceptibilities are responsible for the hyperpolarization. When the electric field is weak, the interaction of light and matter is dominated by the linear process, such as with normal absorption, reflection, and emission in conventional spectroscopy. However, with an intense field generated by a laser beam, for example, higher order nonlinear terms become observable. For instance, $\chi^{(2)}$ describes sum and difference-frequency generation, while $\chi^{(3)}$ describes both two- and three-photon absorption, as well as third harmonic generation and coherent anti-Stokes Raman scattering. The nonlinear polarization contains frequency components which are not present from the fundamental exciting beam, and therefore, it is able to obtain more information of the material.[23, 28-30] In SHG, due to the $\chi^{(2)}$ nonlinearity, the fundamental wave generates a nonlinear polarization wave that oscillates with twice the fundamental frequency. The SHG electric field strength E_{SHG} is proportional to the induced second-order polarization $P_{2\omega}$ by

$$E_{SHG} \propto P_{2\omega} = \chi^{(2)}E_\omega E_\omega \quad \text{Equation 4.2}$$

The macroscopic value of $\chi^{(2)}$ of the medium can be expressed in terms of the microscopic second-order polarizability or the first hyper-polarizability $\beta^{(2)}$ of the molecules in the medium, which is related to a charge oscillation in the molecule depending on the strengths of the interacting fields by

$$\chi^{(2)} = N_s\langle\beta^{(2)}\rangle \quad \text{Equation 4.3}$$

where N_s is the number density of molecules in the medium, and the brackets denote their orientational average. The first hyper-polarizability $\beta^{(2)}$ of the molecules under dipolar approximation can be expressed as

$$\beta^{(2)} \propto \frac{\langle g|\mu|i\rangle\langle i|\mu|f\rangle\langle f|\mu|g\rangle}{\left[(\omega_{gi} - \omega) - \gamma_{ig}\right]\left[(\omega_{gf} - 2\omega) - \gamma_{fg}\right]} \qquad \text{Equation 4.4}$$

where $\langle g|\mu|i\rangle$ represents the transition dipole moment from the g to the i state of the molecule in the material, ω_{gi} is the corresponding frequency of the transition, γ_{ig} is the linewidth associated with the transition, and so on. The physical meaning of Equation 4.4 is that the magnitude of $\beta^{(2)}$, and therefore, $\chi^{(2)}$ and SHG signal intensity, will be greatly enhanced when the fundamental frequency (ω) or/and the second harmonic frequency (2ω) is in resonance with that of the molecular transitions, as demonstrated in Figure 4.2.[31-32]

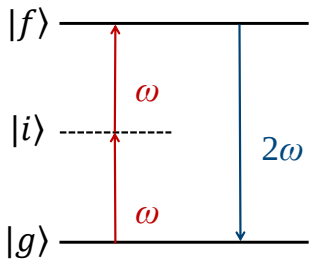

Figure 4.2. The energy diagram in which SHG enhancement occurs when the fundamental frequency ω and/or the SHG frequency 2ω are in resonance with the electronic transitions of the molecules. $|g\rangle$ is the ground state, $|i\rangle$ and $|f\rangle$ are the excited states.

Equation 4.3 shows that not only the molecular energy levels but also the incoherent summation of their nonlinear polarization vectors contribute to the overall SHG response of the medium. This orientational dependence underscores the SHG phase-sensitive property and its need for a noncentrosymmetric region of the medium. For example, when two molecules are within a distance that is much less than the coherence length of the SHG, and they are oppositely oriented, the SHG of those two molecules will be out of phase and add incoherently, thereby diminishing

the net SHG signal. Therefore, in bulk solution, the net SHG from randomly oriented molecules is canceled out for symmetry reasons.[33-35] However, if the molecules are locally adsorbed onto a surface and assemble in a preferential orientation, their individual SHG can constructively interfere to result in a non-zero net SHG signal. As a result, the phase cancellation diminishes at the colloidal interface, where diameters of particles are comparable or larger than the wavelength of the incoming beam, which makes SHG observable.[31, 36-37]

Generally, SHG exploits molecules with a large molecular hyperpolarizability $\beta^{(2)}$ detected in a resonantly enhanced process. Nevertheless, water at a charged interface, such as silica, produces an SHG signal as the result of a mono-molecular water layer oriented directly at the interface and a longer-range induced polarization of the water molecules by the static electric field of the charged surface.[38] Thus, when a surface possesses a charge density, the total observed SHG is expressed by

$$E_{SHG} \propto P_{2\omega} = \sqrt{I_{SHG}} = \chi^{(2)} E_\omega E_\omega + \chi^{(3)} E_\omega E_\omega \Phi_0 \qquad \text{Equation 4.5}$$

where I_{SHG} is the SHG intensity and Φ_0 is the interfacial electrostatic potential arising from its surface charge. The genesis of the $\chi^{(3)}$ susceptibility tensor is the second-order hyperpolarizability of any adsorbed molecules, including water solvent, that are partially aligned by the static electric field generated from the surface charge.[39-40]

Noticeably, incoherent scattering of the second harmonic, named hyper-Rayleigh scattering (HRS), can be observed from the centrosymmetric bulk solution due to the fluctuations in orientation and density of the molecules, which disrupts the phase cancellation discussed previously. While HRS of SHG-active molecules in the bulk solution is linearly proportional to their concentration, the SHG intensity shows a quadratic dependence on the number density of

molecules adsorbed on the nanoparticle surface. This HRS does not have a surface origin and is small compared to the SHG signal from the absorbates on the surface.[41-45]

4.2.3. Malachite Green Derivatives (MGDs)

The amphiphilic nature of malachite green (MG) due to its delocalized positive charge and hydrophobicity from conjugated benzyl rings, in addition to its medium molecular weight (330 g/mol), can represent the soft ion as a drug-like molecule, and is therefore highly relevant to transport of pharmacological agents.[31, 43, 46] MG in solution has a low intensity fluorescence band centered at 460 nm due to the fast nonradiative relaxation, which is related to torsional degrees of freedom of the phenyl rings around the central carbon. The enhanced fluorescent signal is observed when the phenyl rings of MG experience molecular confinement due to specifically binding to proteins or nucleic acids, which makes it widely used for biological molecular labeling.[47-49] Most importantly, MG has a large hyperpolarizability as the result of its strong absorption around 400 nm, which is in resonance with the SHG generated from commonly used 800 nm Ti: sapphire femtosecond lasers. Its large hyperpolarizability and insignificant fluorescence response at 400 nm make MG the most common probe for SHG measurements that use 800 nm fundamental laser beams.[31, 43, 46] Therefore, varying the functional groups and lipophilicity of MG to produce MG analogs, or *malachite green derivatives* (MGDs), not only retains the excellent SHG response of MG but also allows a systematic investigation to study their structure-permeability properties.

4.2.4. Adsorption and Transport Kinetics of MGDs Through a Liposomal Lipid Bilayer Measurement by SHG

In this research, a liposomal lipid bilayer functions as an interface, while MGD dyes are considered as adsorbates. Unlike the case of an interface of solid particles, after MGDs are adsorbed onto the outer surface of the liposomes, they are anticipated to penetrate the hydrophobic

region of the membrane (due to their physicochemical properties), followed by adsorption onto the inner layer of the liposomes. Finally, a portion of the dyes from the inner wall of the membrane diffuse to the interior of the liposomes, because of the driving force of the concentration gradient across the bilayer, as shown in Figure 4.3**.**

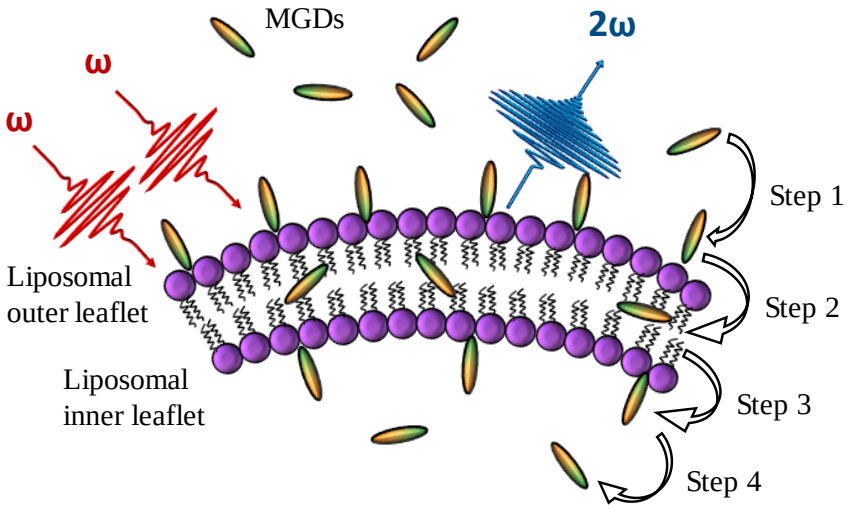

Figure 4.3. Molecular transport dynamics at the liposomal membrane. **Step 1**: Adsorption of dyes at the outer surface of the liposomes. **Step 2**: Penetration of the dyes into the membrane hydrophobic region. **Step 3**: Diffusion through the membrane core to the inner surface. **Step 4**: Partitioning/entrance into the liposomal interior aqueous.

During the adsorption step, MGDs replace water and acquire certain orientations on the outer surface of liposomes, resulting in a rise of SHG signal. When the dyes are translocated to and appear at the inner leaflet of the liposomes, they have orientations opposite to those of the dyes at the outer leaflet. Because they are separated by the bilayer at a thickness of 5–10 nm, which is expected to be much less than the coherence length of the SHG process, the phases of generated SHG fields from each dye are negated, leading to a time-dependent decay in the SHG signal. At equilibrium, the plateau SHG signal will be proportional to the population difference of the dyes between the two surfaces, which results from their total surface area difference, as well as the membrane electric potential due to the positively charged dyes accumulating in the inner bilayer

of the liposomes. Thus, the decay of the SHG intensity in time is attributed to the transport of the dyes from the outer to the inner bilayer.[35, 50-51]

The modified Langmuir adsorption model is used to obtain the adsorption site density and adsorption equilibrium constant in Step 1 of Figure 4.3. The kinetics of adsorption and desorption of dyes (*D*) at the outer membrane surface are described by

$$D + S_o \underset{k_{-1}}{\overset{k_1}{\rightleftharpoons}} DS \qquad \text{Equation 4.6}$$

where *D* is the dyes, S_o and *DS* are empty and filled adsorption sites on the outer liposomal surface, respectively. The kinetics equation that describes the change in the number of adsorbed dyes on the membrane is

$$\frac{dN}{dt} = k_1 \frac{(C - N)}{1}(N_{max} - N) - k_{-1}N \qquad \text{Equation 4.7}$$

where *N* is the concentration of adsorbed dyes at the interface, N_{max} is the maximum concentration of adsorption sites of the membrane surface, and k_1 and k_{-1} are the rate constants for adsorption and desorption of dye. *C* is the total concentration of adsorbed and bulk dye. (*C*−*N*) is the concentration of free dyes in the bulk solution where (*C*−*N*)/1 is its concentration relative to its standard state of 1.0 M, as a reference state, in order to make the equilibrium constant dimensionless. It is important to note that this adsorption model is valid when penetration of the dyes into the membrane occurs at a slower rate compared to the desorption of dyes at the outer membrane surface. When the adsorption and desorption are at equilibrium, their rates are equal (*dN*/*dt* = 0), so then Equation 4.7 becomes

$$k_1 \frac{(C - N)}{1}(N_{max} - N) - k_{-1}N = 0 \qquad \text{Equation 4.8}$$

Dividing both sides of Equation 4.8 by k_{-1} yields

$$K = \frac{k_1}{k_{-1}} = \frac{N}{(C - N)(N_{max} - N)}$$ Equation 4.9

where K is the equilibrium constant of dye adsorption and desorption at the liposomal outer leaflet

Equation 4.9 can be rearranged to obtain a quadratic equation

$$N^2 - \left(C + N_{max} + \frac{1}{K}\right)N + CN_{max} = 0$$ Equation 4.10

Solving for N as an unknown

$$N = \frac{\left(C + N_{max} + \frac{1}{K}\right) - \sqrt{\left(C + N_{max} + \frac{1}{K}\right)^2 - 4CN_{max}}}{2}$$ Equation 4.11

Dividing both sides of Equation 4.11 by N_{max} yields the surface coverage (θ)

$$\theta = \frac{N}{N_{max}} = \frac{(C + N_{max} + \frac{1}{K}) - \sqrt{(C + N_{max} + \frac{1}{K})^2 - 4CN_{max}}}{2N_{max}}$$ Equation 4.12

The total measured SHG intensity I_{SHG} produced at the time the dyes are added to the liposome sample (t = 0 s) is proportional to the relative surface coverage and amount of free dye in the solution:

$$I_{SHG\,(t=0)} = a(\theta)^2 + b + C\alpha$$ Equation 4.13

where a is the SHG intensity at the surface coverage saturation of the dyes, b is the baseline offset, C is the concentration of free dyes in solution, and α is the slope obtained from the plot of I_{SHG} as a function of dye concentration without liposomes, indicating the HRS response from the dye.

Combining Equation 4.12 and Equation 4.13 yields

$$I_{SHG(t=0)} = a\left[\frac{(C + N_{max} + \frac{1}{K}) - \sqrt{(C + N_{max} + \frac{1}{K})^2 - 4CN_{max}}}{2N_{max}})\right]^2 + b + C\alpha$$

Equation 4.14

Thus, by titration of a fixed concentration of liposomes with increasing concentration C of the dyes until the $I_{SHG(t=0)}$ reaches a plateau, a nonlinear least-squares fitting of $I_{SHG(t=0)}$ versus C by the function described in Equation 4.14 allows determination of K and N_{max}. Afterward, adsorption free energy $\Delta G°$ is calculated from the thermodynamic relation:

$$\Delta G° = -RTlnK$$ Equation 4.15

To study the molecular transport of MGDs through the liposome bilayer, the decay of $I_{SHG\ (t)}$ over time at each dye concentration is fitted to single exponential functions given by

$$I_{SHG\ (t)} = a_0 + a_1 e^{-t/\tau}$$ Equation 4.16

where, a_0 and a_1 are proportionality constants, t is the experimental time after MGD addition, and τ is the transport time constant. Notably, when the signal reaches a plateau, all three steps in Figure 4.3 are in equilibrium.

4.3. Experimental

4.3.1. Synthesis of MGDs

In Figure 4.4 is described a general synthesis path for MGDs. Synthesis of B in the first step was carried out by modifying the method given by Wang et alia.[52] To a mixture of A (1.0 mmol) in 5 mL of anhydrous dichloromethane (DCM), anhydrous aluminum chloride (2.0 mmol) was added and stirred for 15 min, followed by the dropwise addition of B (2.2 mmol) at room temperature, during which time the color of the mixture changes from yellow to dark orange and finally becomes green. The resulting mixture was kept stirring overnight, then carefully quenched

with 50 mL of water. A few drops of 1.0 M HCl were added to the mixture until the slurry of aluminum byproduct was dissolved completely. The mixture was extracted with 30 mL of DCM (3 times), followed by washing with 30 mL of brine solution. After the solution was dried over anhydrous Na_2SO_4, the solvent was removed by rotatory evaporation. The solid was then dissolved in a minimum amount of ethyl acetate on a hot plate. Addition of hexane followed by recrystallization results in a bright yellow solid B. Typically, for the nitro-substituted compound B1 ($MGNO_2$-H): yield = 65 %; ^{1}H NMR (400 MHz, $CDCl_3$) δ 8.11 (d, 2H, *J* = 8.82), 7.29 (d, 2H, *J* = 8.44), 6.94 (d, 4H, *J* = 8.65), 6.68 (d, 4H, *J* = 7.55), 5.45 (s, 1H), 2.93 (s, 12H); ^{13}C NMR (126 MHz, $CDCl_3$) δ 153.45, 149.22, 146.17, 130.93, 130.06, 129.83, 123.36, 112.55, 54.90, 40.60; HRMS (ESI) calculated for $C_{23}H_{25}O_2N_3$ $[M+H]^+$ 376.2039, found 376.2039 (0.1 ppm error).

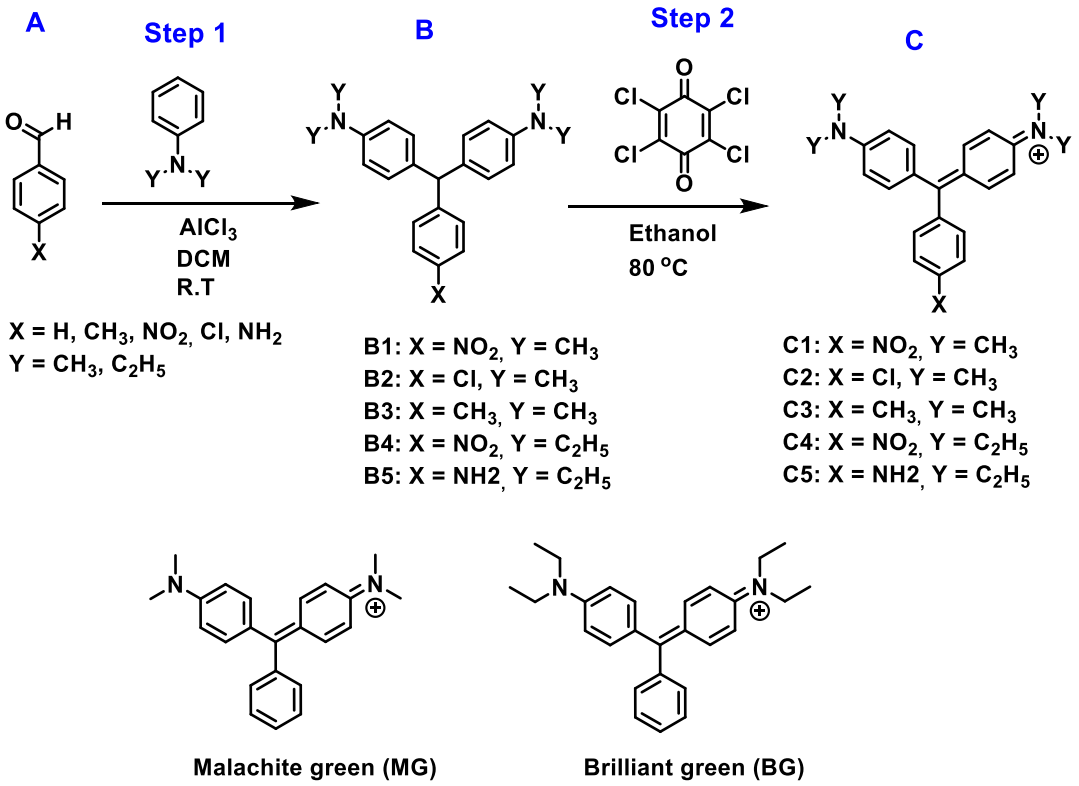

Figure 4.4. The synthesis scheme of malachite green derivatives.

Synthesis of C in the second step is followed as described in the literature.[53] First, B (1.0 mmol) was dissolved in 10 mL of ethanol (EtOH), followed by addition of tetrachloro-1,4-benzoquinone (1.5 mmol). The reaction was stirred at 80 °C and monitored by TLC (SiO_2, MeOH/$CHCl_3$ 1/5 v/v). After completion of the reaction (1−3 hours), the resulting mixture was concentrated under reduced pressure, and the obtained residue was pre-purified by a silica gel column (MeOH/chloroform 1:9 as the mobile phase). The collected green fraction was concentrated under rotatory evaporation and purified by using C18-reversed-phase silica gel flash chromatography with acetonitrile/water 20/80 (v/v) as the mobile phase. The green fractions were dried under flow of N_2 gas to give pure dark blue solid MGDs. Typically, for the nitro-substituted C1 ($MGNO_2^+$): yield = 60 %; ^{1}H NMR (400 MHz, $CDCl_3$) δ 8.13 (d, 2H, *J* = 8.53 Hz), 7.56 (d, 2H, *J* = 8.49 Hz), 7.09 (d, 4H, *J* = 8.48 Hz), 6.66 (d, 4H, *J* = 8.26 Hz), 2.95 (s, 12H); ^{13}C NMR (126 MHz, $CDCl_3$) δ 171.51, 157.14, 149.75, 145.65, 140.44, 134.67, 127.21, 123.48, 114.76, 41.48; HRMS (ESI) calculated for $C_{23}H_{24}O_2N_3^+$ $[M]^+$ 374.1863, found 374.1877 (2.4 ppm error).

4.3.2. $logD$ Calculation

Lipophilicity, or hydrophobicity, is an important physicochemical property to predict in vivo permeability of a possible drug in drug discovery, which is described by the partition coefficient *P* or distribution coefficient *D*. The two coefficients indicate the differential solubility of the compound in two immiscible solvents, typically octan-1-ol (octanol) and water. The partition coefficient, *P*, is the ratio of the concentration of the compound in octanol to its concentration in water, while the distribution coefficient, *D*, is used for the sum of the concentrations of all forms of the compound in each solvent.[54] Thus, the partition coefficient, *P*, is the descriptor of lipophilicity for neutral compounds, or when the compound exists in a single

form, while the distribution coefficient, *D*, can extend to describe an ionizable compound as shown in Equation 4.17

$$log(D_A) = log\frac{\sum[species\ of\ A]_{oct}}{\sum[species\ of\ A]_{water}} \qquad \text{Equation 4.17}$$

A $log(D_A)$ value of 1 means there is a 10:1 ratio of the total concentration of all forms of the compound A in octanol to that of A in water. Hydrophobic drugs with a large $logD$ are mainly distributed to hydrophobic areas, such as lipid bilayers of cells, whereas hydrophilic drugs with small or negative $logD$ are found primarily in aqueous regions such as in the blood serum or extracellular/intracellular spaces. Thus, $logD$ is useful in estimating the distribution of drugs at different locations within the body, and its value should be balanced so that the drug is not only soluble in the aqueous phase but is also soluble in the lipid membrane, thus allowing for its transport across cell membranes.[55-56] Most drugs are weak bases or acids whose acid-base conjugate ratio depends on their pK_a and the pH of the solution, and their charge state can largely affect the permeation process. The majority of drugs cross the lipid membrane in the uncharged form, because there exists a high energy barrier for the charged form to cross the hydrophobic core of a membrane.[57-59] For example, ibuprofen, a nonsteroidal anti-inflammatory drug, with a charge of −1 at pH = 7, is found to localize near the lipid headgroups of membranes. On the other hand, neutral ibuprofen present dominantly at low pH preferentially penetrates deep into membranes. Therefore, $logD$ values reported at a specific pH are used to measure the pH-dependent lipophilicity of the drug. However, experimental determination of $logD$ for every compound is not practical; it may be of interest to calculate $logD$ prior to synthesis of a new drug so as to predict its lipophilicity. In this work, the $logD$ Predictor using ChemAxon method derived from Viswanadhan et al.,[60] was used to calculate the $logD$ of each MGD at pH of 4.0, in which MGDs

are expected to be the most stable. The $logD$ Predictor is a widely accepted and used algorithm that makes use of molecular fragments and their properties to calculate the $logD$ values.[39, 61]

4.3.3. MGD Surface Charge Distribution and Dipole Calculation

The structures of MGDs were built using GaussView 6.0 and optimized using Gaussian 16W, with the following operational parameters—method: ground state, DFT, default spin, B3LYP; basis set: LandL2DZ; charge: +1; spin: singlet; solvation model: CPCM in water.

4.4. Results and Discussion

It is apparent from inspection of Figure 4.5 that addition of a nitro group (-NO_2) to malachite green results in a shift of its λ_{max} for the lowest energy transition from 618 nm to 640 nm, while the other two transitions is essentially unchanged (428 nm vs. 427 nm, and 318 nm vs. 316 nm). Study of molecular electronic energy levels of malachite green has shown that three energy transitions in the absorption spectrum are of the type $n \rightarrow \pi^*$.[62] In addition, the longest wavelength band (~ 600 nm) is characterized by an oscillation of an electron cloud across the molecule between the two auxochromes (two amine groups), while the shorter band (~ 400 nm) corresponds to an oscillation through the phenyl group, accounting for $S_0 \rightarrow S_1$ and $S_0 \rightarrow S_2$ transitions respectively.[63] Thus, the red shift in the first transition of $MGNO_2$ is due to the addition of a resonance effect associated with the nitro group, leading to electron movement among the three auxochromes in $MGNO_2$.

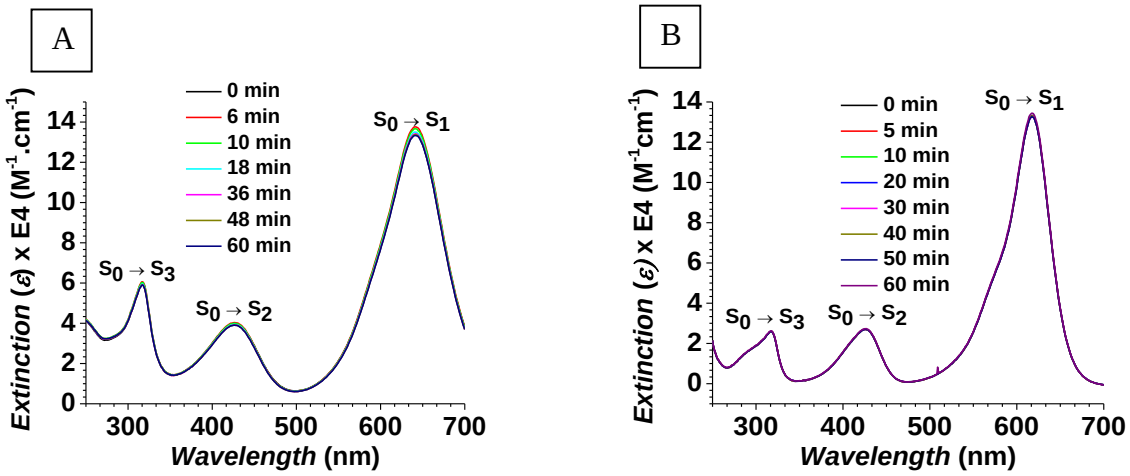

Figure 4.5. Absorption and chemical stability of 5.0×10^{-6} M $MGNO_2$ (A) and MG (B)in 5.0 mM citrate buffer, pH 4.0. $MGNO_2$ has three electronic transitions at λ_{max} of 640 nm, 427 nm, and 316 nm, while those of MG are at 618 nm, 428 nm, and 318 nm.

Previously, our collaborative work with the Haber research group led to the observation that MG is able to be transported through the membranes of 100% DOPG liposomes but not those of 100% DOPC or 100% Q_3DOPE liposomes.[39] In addition, it was found that brilliant green (BG) and methyl green are not transported through DOPG, DOPC or Q_3DOPE membranes. Preliminary data that has been obtained with the Haber group indicate that $MGNO_2$ is transported through membranes of liposomes composed of 100% DOPG and 100% DOPC lipids, but not through those made of 100% Q_3DOPE lipid, which is similar to malachite green isothiocyanate MGITC observed before (data not shown).[64-65]

To explain the different transport behaviors of these similar structure dyes, the different substituted functional groups and their related physical and chemical properties should be highlighted. To that end, I performed computations using Gaussian 16W so as to generate surface charge distribution representations and electric dipole moment values. As seen in Figure 4.6, partial positive charges (blue) are concentrated at the two nitrogen atoms, while the para-position at the substitution position of the function group has less positive charges (red). In addition, the introduction of electron-withdrawing groups (-Cl, $-NO_2$, -NCS) increase the positive charge

density at the two nitrogen atoms and produces a larger electric dipole (blue arrow), as shown in Table 4.1. On the other hand, ethyl substitution at the two nitrogen atoms shields the positive charge of the molecules more pronouncedly compared to the methyl group (less blue), as indicated when compared the same substitution group in BG and MG.

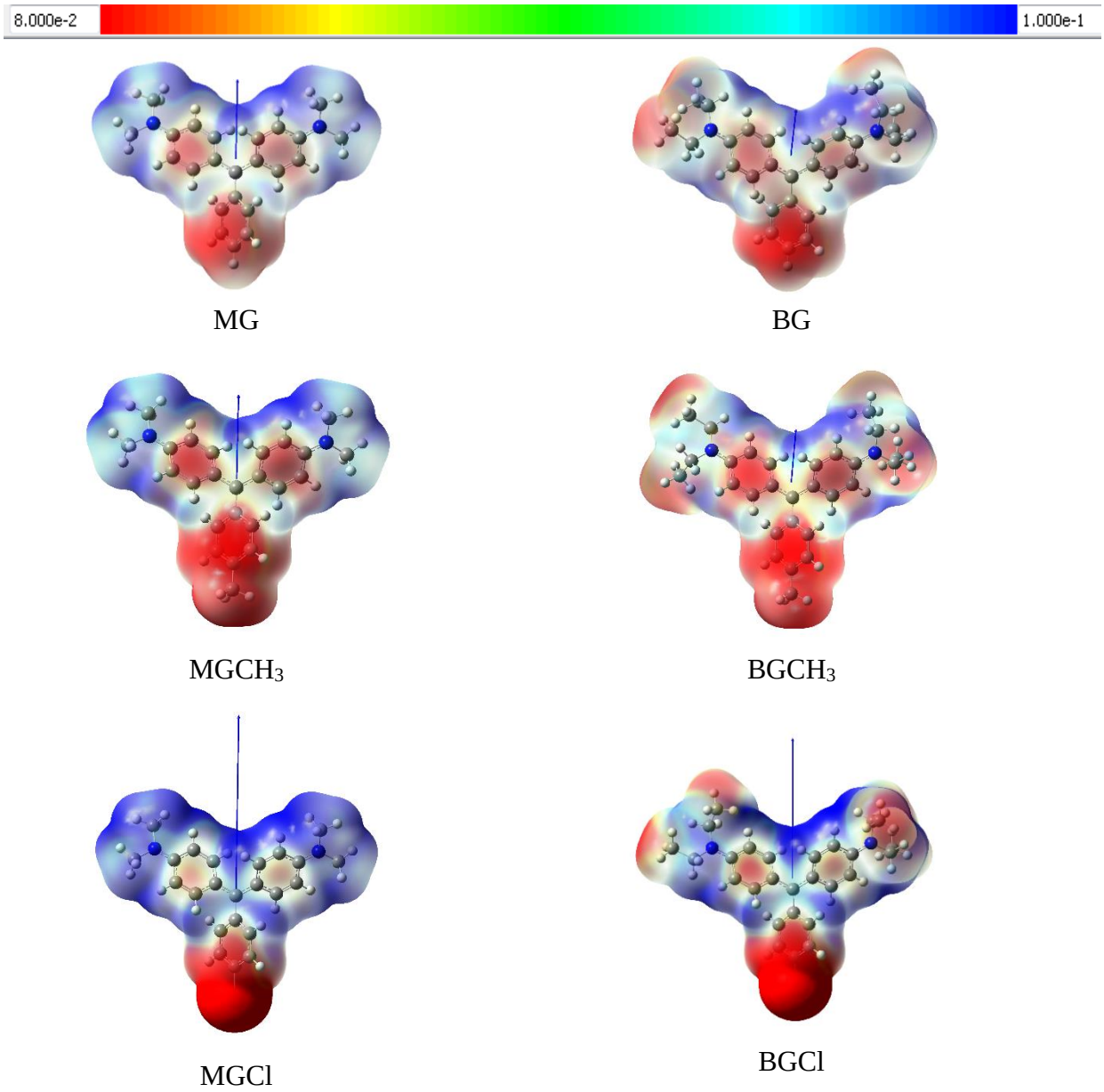

Figure 4.6. Surface charge distribution and electric dipole (blue arrow) representation of MGDs. Blue represents a more negative charge than red. All structures are represented in the same color-electron volt scale.

(figure cont'd.)

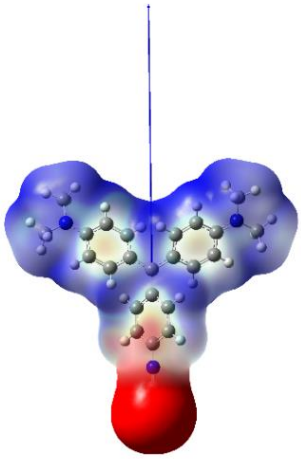

MGITC

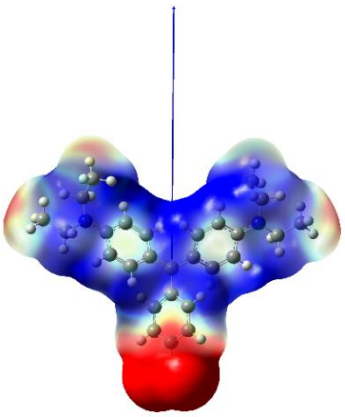

BGITC

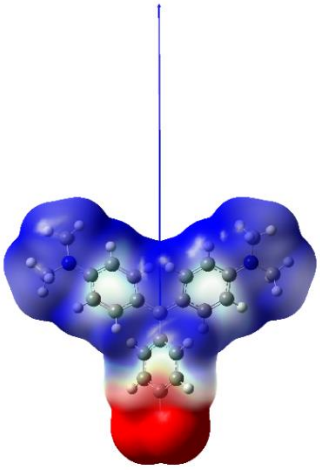

$MGNO_2$

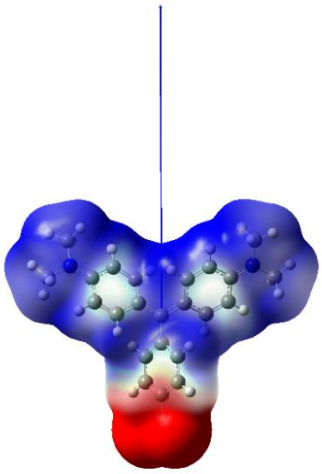

$BGNO_2$

Table 4.1. Calculated $logD$ and dipole values of MGDs at pH 4.0

	$logD$	Dipole (Debye)		$logD$	Dipole (Debye)
MG	0.66	4.67	BG	1.36	2.92
$MGCH_3$	1.18	4.84	$BGCH_3$	1.86	3.25
MGCl	1.22	10.73	BGCl	1.92	8.84
MGITC	1.68	15.76	BGITC	2.38	13.39
$MGNO_2$	0.62	16.96	$BGNO_2$	1.30	14.78

The Gaussian and $logD$ calculations support the experimental observations of MG, MGITC, $MGNO_2$, and BG in DOPG, DOPC and Q_3DOPE liposomes. In the case of the negatively charged liposomal membrane DOPG, charge-charge and dipole-dipole interactions between the

dyes and the membrane are strong and comparable to each other. Thus, dyes with large dipole moments and a significant exposure of positive charge density will adsorb and transport faster in DOPG liposomes, as demonstrated with MG, MGITC, and $MGNO_2$. By contrast, with zwitterionic liposomal membranes made from DOPC, the dipole-dipole interactions are dominant. The general trend observed from SHG studies suggests that MGDs with a large dipole moment will help to transport through DOPC membrane, as observed in MGITC and $MGNO_2$. Interestingly, BG, which is very similar in structure to MG and has spectroscopic properties very close to those of MG, neither adsorbs nor transports on/through either membrane because of its small dipole moment. Additionally, the positive charges in the two nitrogen atoms are shielded in BG, which could lead to much lower electrostatic interactions with the lipid bilayer.

In addition to charge and dipole interactions, the influence of $logD$ should be discussed. The study of some small model guest molecules with a π-moiety indicated that when the octanol-water partition coefficient ($logP_{ow}$) < 1.9, the guest molecules were leaked from the lipid membranes, while most of the guest molecules with ($logP_{ow}$) > 1.9 did not.[66] For example, a dimer of a coumarin derivative ($logP_{ow}$ > 3) was converted to monomers ($logP_{ow}$= 1.78) in the lipid membrane by photoirradiation at 254 nm, and the monomer was released. A few models have been developed to rationale the possible permeation mechanisms, with the two major ones being solubility-diffusion and transient pore formation mechanisms. It was reported that the solubility-diffusion model is reasonable for predicting permeation of small molecules through a thick membrane, with lipid chain lengths of 14–24 carbon atoms, whereas transient pore formation model works well for permeation of a small polar molecule through a thin lipid membrane.[5] In our case, MGITC and $MGNO_2$ are significantly polar, and all liposomes used have a long chain length (18 carbons) with two double bonds, making a wider space compared to other saturated lipids.

Thus, MGITC and $MGNO_2$ may initiate a transport across the membrane by a pore formation before being permeable through the membrane. A reported comparison between DOPC and POPG bilayers proposed that the drugs are prone to concentrate more in DOPC bilayers, while transport through the POPG bilayer appears to be easier.[67]

On the other hand, the influence of $logD$ could lead to another possible explanation for the quick decay in SHG signal. Possibly, MGITC has a rigid orientation when adsorbed on the membrane, while after partitioning into the hydrophobic region, they may adapt free rotation, leading to a decrease in the signal, without transport to the inner surface of the liposomal membrane. If the lipid–water partition coefficient is too big, then the drug is unlikely to leave the membrane and may merely be sequestered within it.[6] In addition, the molecular volume associated permeability of a solute indicates that the membrane barrier possesses polymer characteristics rather than properties of liquid hydrocarbon.[68] Thus, the observation that adsorption and transport of MGDs is not observed in Q_3DOPE liposomal membranes might indicate that a bulky hydrophobic quinone group prevents dyes from adsorbing and penetrating the membrane.

To demonstrate the potential for chemically modified MGDs to still exhibit cell membrane permeability, $MGNO_2$ was tested with human cells. In Figure 4.7 are presented some preliminary SHG measurements, indicating that $MGNO_2$ can cross the cell membrane of H596 lung cancer cells. The adsorption and transport of $MGNO_2$ in real cells show potential applications of the MGDs for cell imaging by SHG microscopy.

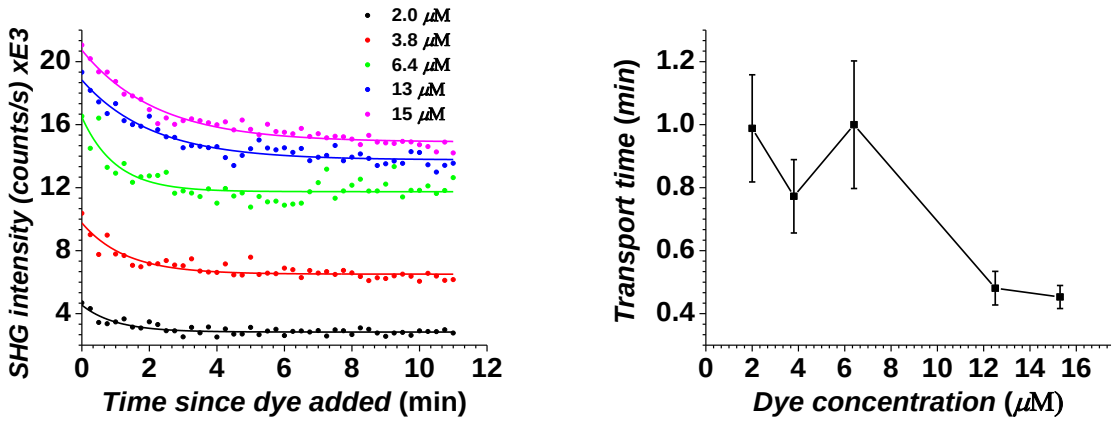

Figure 4.7. Transport of $MGNO_2$ in H596 lung cancer cells. Dead cells are suspended in 5.0×10^{-3} M citrate buffer at pH 4.0 at concentration of 3.2×10^5 cells/ mL.

4.5. Conclusion

Rational design and implementation of MGDs was accomplished with the aid of time-dependent SHG measurements in combination with computational methods. It is proposed that MGDs interact with liposomal membranes via two major mechanisms, charge-charge and dipole-dipole interaction mechanisms, and MGD transport ability is affected by their solubility in the lipid bilayer. A change in charge distribution and electric dipole moment caused by different functional groups allows for control of the adsorption and transport through the membrane. The simulations and experimental measurements of MGD-lipid membrane suggest that the adsorption and transport kinetics are driven by many factors, and a molecular structural design can contribute significantly in drug discovery and cellular imaging.

4.6. References

1. Engelman, D. M., Membranes Are More Mosaic Than Fluid. *Nature* **2005,** *438* (7068), 578.

2. Paula, S., et al., Permeation of Protons, Potassium Ions, and Small Polar Molecules through Phospholipid Bilayers as a Function of Membrane Thickness. *Biophysical Journal* **1996,** *70* (1), 339-348.

3. Sugano, K., et al., Coexistence of Passive and Carrier-Mediated Processes in Drug Transport. *Nature Reviews Drug Discovery* **2010,** *9* (8), 597.

4. Hannesschlaeger, C., et al., Intrinsic Membrane Permeability to Small Molecules. *Chemical Reviews* **2019**.

5. Shinoda, W., Permeability across Lipid Membranes. *Biochimica et Biophysica Acta (BBA)-Biomembranes* **2016,** *1858* (10), 2254-2265.

6. Seddon, A. M., et al., Drug Interactions with Lipid Membranes. *Chemical Society Reviews* **2009,** *38* (9), 2509-2519.

7. Sugano, K., et al., Coexistence of Passive and Carrier-Mediated Processes in Drug Transport. *Nat Rev Drug Discov* **2010,** *9* (8), 597-614.

8. Liu, X., et al., Lipophilicity and Its Relationship with Passive Drug Permeation. *Pharmaceutical Research* **2011,** *28* (5), 962-977.

9. Wolak, D. J.; Thorne, R. G., Diffusion of Macromolecules in the Brain: Implications for Drug Delivery. *Molecular Pharmaceutics* **2013,** *10* (5), 1492-1504.

10. Seydel, J. K.; Wiese, M., *Drug-Membrane Interactions: Analysis, Drug Distribution, Modeling*. John Wiley & Sons: 2009; Vol. 15.

11. Douroumis, D., et al., *Computational Pharmaceutics: Application of Molecular Modeling in Drug Delivery*. John Wiley & Sons: 2015.

12. Bourgaux, C.; Couvreur, P., Interactions of Anticancer Drugs with Biomembranes: What Can We Learn from Model Membranes? *Journal of Controlled Release* **2014,** *190*, 127-138.

13. Menichetti, R., et al., Drug–Membrane Permeability across Chemical Space. *ACS Central Science* **2019**.

14. Harayama, T.; Riezman, H., Understanding the Diversity of Membrane Lipid Composition. *Nature Reviews Molecular Cell Biology* **2018**.

15. Shevchenko, A.; Simons, K., Lipidomics: Coming to Grips with Lipid Diversity. *Nature Reviews Molecular Cell Biology* **2010,** *11* (8), 593.

16. Peetla, C., et al., Biophysical Interactions with Model Lipid Membranes: Applications in Drug Discovery and Drug Delivery. *Molecular Pharmaceutics* **2009,** *6* (5), 1264-1276.

17. Matos, C., et al., Liposomes as a Model for the Biological Membrane: Studies on Daunorubicin Bilayer Interaction. *J. Membrane Biol.* **2012,** *245* (2), 69-75.

18. Chatterjee, S.; Agarwal, S., Liposomes as Membrane Model for Study of Lipid Peroxidation. *Free Radical Biology and Medicine* **1988,** *4* (1), 51-72.

19. Sessa, G.; Weissmann, G., Phospholipid Spherules (Liposomes) as a Model for Biological Membranes. *Journal of Lipid Research* **1968,** *9* (3), 310-318.

20. Ong, S., et al., Immobilized-Artificial-Membrane Chromatography: Measurements of Membrane Partition Coefficient and Predicting Drug Membrane Permeability. *Journal of Chromatography A* **1996,** *728* (1-2), 113-128.

21. Matlack, K., et al., Review of Second Harmonic Generation Measurement Techniques for Material State Determination in Metals. *Journal of Nondestructive Evaluation* **2015,** *34* (1), 273.

22. Shen, Y., Surface Properties Probed by Second-Harmonic and Sum-Frequency Generation. *Nature* **1989,** *337* (6207), 519.

23. Shen, Y., Surfaces Probed by Nonlinear Optics. *Surface Science* **1994,** *299*, 551-562.

24. Butet, J., et al., Optical Second Harmonic Generation in Plasmonic Nanostructures: From Fundamental Principles to Advanced Applications. *ACS Nano* **2015,** *9* (11), 10545-10562.

25. Corn, R. M.; Higgins, D. A., Optical Second Harmonic Generation as a Probe of Surface Chemistry. *Chemical Reviews* **1994,** *94* (1), 107-125.

26. Hicks, J., et al., Studies of Liquid Surfaces by Second Harmonic Generation. *The Journal of Physical Chemistry* **1986,** *90* (4), 560-562.

27. Campagnola, P., Second Harmonic Generation Imaging Microscopy: Applications to Diseases Diagnostics. ACS Publications: 2011.

28. Shen, Y.-R., The Principles of Nonlinear Optics. *New York, Wiley-Interscience, 1984, 575 p.* **1984**.

29. Nalwa, H. S.; Miyata, S., *Nonlinear Optics of Organic Molecules and Polymers*. CRC press: 1996.

30. Zernike, F.; Midwinter, J. E., *Applied Nonlinear Optics*. Courier Corporation: 2006.

31. Zeng, J., A Study of Molecular Adsorption and Transport at Cell Membrane and Biologically Relevant Surfaces by Second Harmonic Generation. Ph.D Dissertation, Univeristy of Pennsylvania, Philadelphia, PA, **2011**.

32. Karam, T. E.; Haber, L. H., Molecular Adsorption and Resonance Coupling at the Colloidal Gold Nanoparticle Interface. *The Journal of Physical Chemistry C* **2013,** *118* (1), 642-649.

33. Heinz, T., et al., Determination of Molecular Orientation of Monolayer Adsorbates by Optical Second-Harmonic Generation. *Physical Review A* **1983,** *28* (3), 1883.

34. Simpson, G. J.; Rowlen, K. L., An Shg Magic Angle: Dependence of Second Harmonic Generation Orientation Measurements on the Width of the Orientation Distribution. *Journal of the American Chemical Society* **1999,** *121* (11), 2635-2636.

35. Zeng, J., et al., Time-Resolved Molecular Transport across Living Cell Membranes. *Biophysical Journal* **2013,** *104* (1), 139-145.

36. Rao, Y., et al., Molecular Orientational Distribution at Interfaces Using Second Harmonic Generation. *The Journal of Physical Chemistry C* **2011,** *115* (23), 11678-11683.

37. Duboisset, J., et al., Generic Model of the Molecular Orientational Distribution Probed by Polarization-Resolved Second-Harmonic Generation. *Physical Review A* **2012,** *85* (4), 043829.

38. Salafsky, J.; Eisenthal, K., Protein Adsorption at Interfaces Detected by Second Harmonic Generation. *The Journal of Physical Chemistry B* **2000,** *104* (32), 7752-7755.

39. Kumal, R. R., et al., Impacts of Salt, Buffer, and Lipid Nature on Molecular Adsorption and Transport in Liposomes as Observed by Second Harmonic Generation. *The Journal of Physical Chemistry C* **2017,** *121* (29), 15851-15860.

40. Gonella, G.; Dai, H.-L., Second Harmonic Light Scattering from the Surface of Colloidal Objects: Theory and Applications. *Langmuir : the ACS Journal of Surfaces and Colloids* **2013,** *30* (10), 2588-2599.

41. Hendrickx, E., et al., Hyper-Rayleigh Scattering in Isotropic Solution. *Accounts of Chemical Research* **1998,** *31* (10), 675-683.

42. Wang, H., et al., Second Harmonic Generation from the Surface of Centrosymmetric Particles in Bulk Solution. *Chemical Physics Letters* **1996,** *259* (1-2), 15-20.

43. Wang, H., et al., Second Harmonic Generation from the Surface of Centrosymmetric Particles in Bulk Solution. *Chemical Physics Letters* **1996,** *259* (1-2), 15-20.

44. Kumal, R. R., Nanoparticle-Based Drug-Delivery Systems Studied by Second Harmonic Generation. **2017**.

45. Di Bella, S., Second-Order Nonlinear Optical Properties of Transition Metal Complexes. *Chemical Society Reviews* **2001,** *30* (6), 355-366.

46. Haber, L. H., et al., Probing the Colloidal Gold Nanoparticle/Aqueous Interface with Second Harmonic Generation. *Chemical Physics Letters* **2011,** *507* (1-3), 11-14.

47. Karam, T. E., et al., Ultrafast and Nonlinear Spectroscopy of Brilliant Green-Based Nanogumbos with Enhanced near-Infrared Emission. *The Journal of Chemical Physics* **2017,** *147* (14), 144701.

48. Yerramilli, V. S.; Kim, K. H., Labeling Rnas in Live Cells Using Malachite Green Aptamer Scaffolds as Fluorescent Probes. *ACS Synthetic Biology* **2018,** *7* (3), 758-766.

49. Naganbabu, M., et al., Multiexcitation Fluorogenic Labeling of Surface, Intracellular, and Total Protein Pools in Living Cells. *Bioconjugate Chemistry* **2016,** *27* (6), 1525-1531.

50. Srivastava, A.; Eisenthal, K. B., Kinetics of Molecular Transport across a Liposome Bilayer. *Chemical Physics Letters* **1998,** *292* (3), 345-351.

51. Liu, Y., et al., Effects of Bilayer Surface Charge Density on Molecular Adsorption and Transport across Liposome Bilayers. *Biophysical Journal* **2001,** *80* (2), 1004-1012.

52. Wang, X., et al., Solvent-Free, Alcl3-Promoted Tandem Friedel–Crafts Reaction of Arenes and Aldehydes. *Journal of Molecular Catalysis A: Chemical* **2006,** *255* (1-2), 31-35.

53. Dong, C.-p., et al., Metal-Free Blue Dye Synthesis: Oxidative Coupling of Benzylamines and N, N-Dimethylanilines to Yield 4, 4′ -Diaminotriarylmethanes in the Presence of Salicylic Acid as a Co-Oxidant. *The Journal of Organic Chemistry* **2017,** *82* (23), 12530-12538.

54. Bhal, S. K., Lipophilicity Descriptors: Understanding When to Use Logp & Logd. *ACD/Labs PhysChem Software Application Notes* **2007**.

55. Wohnsland, F.; Faller, B., High-Throughput Permeability Ph Profile and High-Throughput Alkane/Water Log P with Artificial Membranes. *Journal of Medicinal Chemistry* **2001,** *44* (6), 923-930.

56. Xing, L.; Glen, R. C., Novel Methods for the Prediction of Logp, P K a, and Logd. *Journal of Chemical Information and Computer Sciences* **2002,** *42* (4), 796-805.

57. Manallack, D. T., The P K a Distribution of Drugs: Application to Drug Discovery. *Perspectives in Medicinal Chemistry* **2007,** *1*, 1177391X0700100003.

58. Charifson, P. S.; Walters, W. P., Acidic and Basic Drugs in Medicinal Chemistry: A Perspective. *Journal of Medicinal Chemistry* **2014,** *57* (23), 9701-9717.

59. Boggara, M. B., et al., Structural Association of Nonsteroidal Anti-Inflammatory Drugs with Lipid Membranes. *Journal of the American Chemical Society* **2012,** *134* (48), 19669-19676.

60. Viswanadhan, V. N., et al., Atomic Physicochemical Parameters for Three Dimensional Structure Directed Quantitative Structure-Activity Relationships. 4. Additional Parameters for Hydrophobic and Dispersive Interactions and Their Application for an Automated Superposition of Certain Naturally Occurring Nucleoside Antibiotics. *Journal of Chemical Information and Computer Sciences* **1989,** *29* (3), 163-172.

61. Https://Disco.Chemaxon.Com/Apps/Demos/Logd/ (Accessed 6.13.2019).

62. Mohammad, R. K., et al. In *Study of Molecular Electronic Energy Levels of Malachite Green Dye*, AIP Conference Proceedings, AIP Publishing: 2019; p 030022.

63. Barghouthi, Z.; Amereih, S., Spectrophotometric Determination of Fluoride in Drinking Water Using Aluminium Complexes of Triphenylmethane Dyes. *Water SA* **2012,** *38* (4), 543-548.

64. In Collaboration among the Mccarley Research Group, the Haber Research Group, and the Kumar Research Groupo at Lsu.

65. Hamal, P., et al., Molecular Adsorption and Transport at Liposome Surfaces Studied by Molecular Dynamics Simulations and Second Harmonic Generation Spectroscopy. *The Journal of Physical Chemistry B* **2019**.

66. Goto, Y., et al., Light-Triggered Hydrophilic Drug Release from Liposomes through Removal of a Photolabile Protecting Group. *RSC Advances* **2019,** *9* (1), 166-171.

67. Tejwani, R. W., et al., An Atomic and Molecular View of the Depth Dependence of the Free Energies of Solute Transfer from Water into Lipid Bilayers. *Molecular Pharmaceutics* **2011,** *8* (6), 2204-2215.

68. Walter, A.; Gutknecht, J., Permeability of Small Nonelectrolytes through Lipid Bilayer Membranes. *J. Membrane Biol.* **1986,** *90* (3), 207-217.

CHAPTER 5
CONCLUSIONS AND OUTLOOK

5.1. Summary and Conclusions

Under physiological conditions, zwitterionic DOPE lipids favor existing in the inverted hexagonal phase (H_{II}), due to their small headgroup/lipid ratio. Chemical modification of the headgroup of DOPE with a cleavable quinone group (Q) yields QDOPE lipids, which have increased headgroup size and headgroup charge density, which sustains the formation of the lamellar liquid crystalline phase (L_α) necessary for formation of stable liposomes. When QDOPE liposomes are exposed to a reducing agent of sufficient thermodynamic nature, the quinone headgroup is reduced and subsequently cleaved from QDOPE to produce DOPE at one or both leaflets of the liposome, depending on the membrane permeability of the reagent. Subsequently, interleaflet distribution of DOPE in the liposomal membrane governs the potential for bilayer contact and consequently, the lamellar to hexagonal phase transition ($L_\alpha \rightarrow H_{II}$) that is accompanied by a release of liposomal contents to the surroundings. The goal of my research was to investigate the role of membrane symmetry resulting from asymmetric/symmetric cleavage of the quinone headgroup from the bilayer and the influence of lipid composition in leakage/release and fusion of redox-triggered release of quinone-based liposomes under the action of an internal (enzyme activity, which is simplified in vitro by using sodium dithionite) or external (photoirradiation) stimulus. This study is significant, as it introduces the possibility of a new method for intracellular delivery of therapeutics to cancer cells or their membrane organelles via fusion of liposomes.

In Chapter 2, I was able to demonstrate a system wherein can be formed an asymmetric liposomal membrane resulting from asymmetric reduction and cleavage of the Q_3 quinone headgroup at the outer leaflet of the Q_3PE-based liposomes, while the inner leaflet remained intact. Inclusion of PE lipids (both DOPE and POPE) in Q_3PE-based liposomes leads to a rapid content

release in an off-on switch scenario, with the content release displaying a low concentration dependence. In addition, POPE drastically facilitates the content-mixing fusion when POPE is present in the inner leaflet of liposomes, while the presence of DOPE does not, emphasizing the role of the interleaflet distribution of PEs, which is seemingly related to cell membrane structures and dynamics in biological fusion events.

In Chapter 3, I showed it possible to achieve symmetrical cleavage of a photoresponsive quinone headgroup ($MeSQ_3$), which was synthesized by slight chemical modification of the Q_3 headgroup. This was done by photoinduced reduction of the quinone moiety under blue light. In addition to fluorescence-based techniques, new analytical tools, including diffusion NMR and capillary electrophoresis, were developed to interrogate the leakage/release of the photoresponsive liposomes. Irradiation by blue LEDs led to the reduction and cleavage of the quinone group from $MeSQ_3$DOPE, but it is possible that the subsequent reaction of generated DOPE lipid with the photoreduction intermediate compound resulted in the formation of a hydroquinone-caped DOPE lamellar-stabilized lipid, which hinders the ($L_\alpha \rightarrow H_{II}$) transition. However, high proportions of DOPE incorporated into $MeSQ_3$DOPE LUVs results in a small amount of vesicle aggregation under blue light irradiation of $MeSQ_3$DOPE LUVs.

In Chapter 4, rational design and implementation of SHG probe analogs, malachite green derivatives (MGDs), was demonstrated with the aid of time-dependent SHG measurements in combination with computational methods to investigate how molecular charge, polarity, size, lipophilicity, and lipid headgroup structures control adsorption and transport processes through the liposomal membrane. In collaboration with the Haber research group at LSU, second harmonic generation (SHG) is used to measure real-time molecular adsorption and transport through liposomal membranes. Molecular dynamics simulations (MD) provided by the Kumar research

group at LSU were used to obtain a detailed estimation of interactions between MGDs and lipid membranes at the molecular level. The success of this great collaboration has been demonstrated by a number of published papers and by promising ongoing projects.

5.2. Outlook

5.2.1. Engineering Asymmetrical Liposomes for Leakage/Release and Fusion Studies

In Chapter 2, an asymmetric membrane of Q_3PE-based liposomes was generated by using sodium dithionite as a non-bilayer permeable reagent, which is labeled Approach 1 in Figure 5.1. In Chapter 3, the membrane symmetry of the liposomes was retained by using photoirradiation as the bilayer permeable reagent, which is labeled Approach 2 in Figure 5.1. Approach 2 can also be achieved if appropriate reagents that can cross the membrane are selected. For example, reduction potentials of the quinone headgroup can be tuned so that they are able to reduce by the nonionic and bilayer-permeable reducing agent dithiothreitol (DDT). The redox potential data in Table 5.1 suggests that DDT can potentially reduce and induce the headgroup cleavage of MeOQ_3DOPE. On the other hand, liposomes with asymmetric membranes can be prepared based on a number of reported protocols[1-4], through which, the role of the inner leaflet can be investigated, as labeled Approach 3 in Figure 5.1. The three approaches can provide a comprehensive understanding of membrane symmetry, which dictates liposomal content leakage/release, fusion, and phase transition of Q_3PE-based liposomes, as well as a variety of responsive liposome systems reported so far in literature.

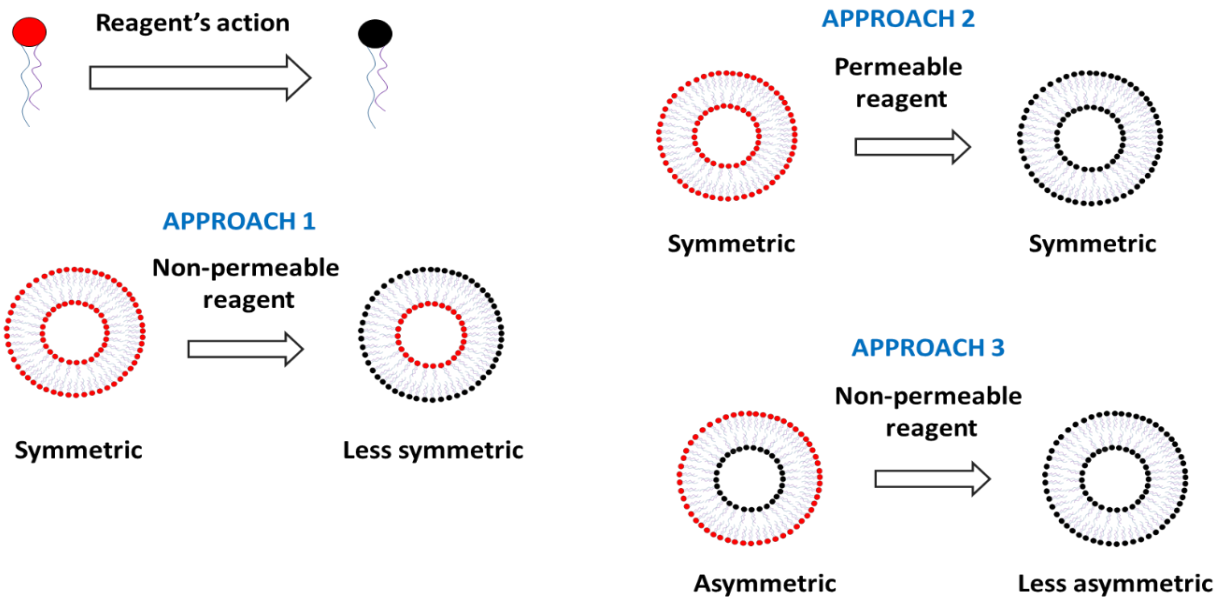

Figure 5.1. Leakage/release and fusion of liposomes related to membrane symmetry can be examined by selecting an appropriate membrane-permeable reagent or engineering liposomes with symmetric/asymmetric membrane at the beginning.

Table 5.1. The standard reduction potential of some quinones and reducing reagents.

Compound		Standard Redox Potential vs SHE (V)
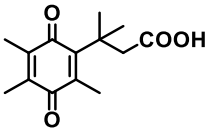	Q_3PA	0.047 (at pH 7)[5]
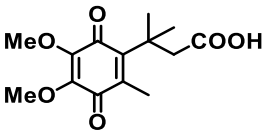	$MeOQ_3PA$	0.128 (at pH 7)[5]
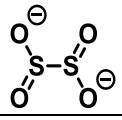	Dithinonite (DT)	−0.66 (at pH 7)[6]
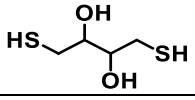	DithioThreitol (DDT)	−0.33 (at pH 7)[7]

5.2.2. Alternative Visible Light Photoresponsive Liposomes

In Chapter 3, after the cleavage of the quinone headgroup of $MeSQ_3DOPE$ liposomes under blue light irradiation occurs, the generated free amine of DOPE lipid is suspected of undergoing an intermolecular chemical reaction with the photoreduction intermediate to form a quinone-

capped lipid, which inhibits the $L_\alpha \rightarrow H_{II}$ phase transition and content release of the $MeSQ_3DOPE$ liposomes. The problem can be overcome by preparing a new photoresponsive lipid, thereby inhibiting the intermolecular chemical reaction under photoirradiation. For example, blue light photoresponsive isoindoline derivatives (substituted lipid **1**) can be synthesized, as shown in Figure 5.2. The initial intramolecular charge transfer excited state would lead to hydrogen/proton transfer, with the intramolecular rearrangement being kinetically favored so as to produce a DOPE leaving group without subsequent chemical reaction of DOPE with intermediates.[8-9]

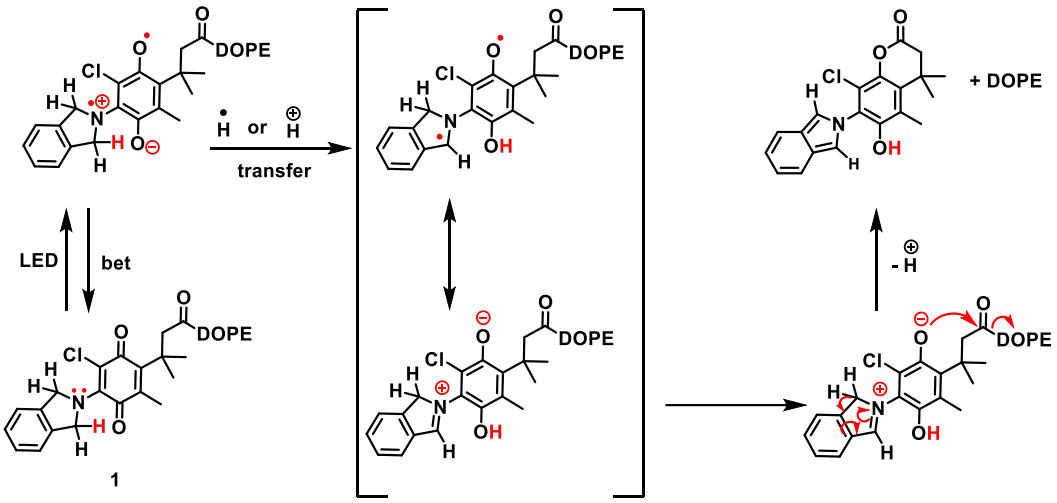

Figure 5.2. Schematic description of the possibility of isoindoline quinone-substituted DOPE lipid to produce DOPE under blue-light irradiation.

5.2.3. New Probes for Liposomal Leakage Quantification by DOSY NMR

Bispyridinium bromide bearing trifluoromethyl groups exhibiting no detectable leakage from liposomes has been demonstrated for liposomal leakage quantification using DOSY.[10] In addition, fluorinated calcein, which is expected to experience minimum leakage when entrapped in liposomes, could be synthesized, and its dual-monitoring probe property might be useful in correlating liposomal leakage quantification by two methods, DOSY, and fluorescence. These two

fluorine-containing probes shown in Figure 5.1 can be synthesized based on reported protocols.[10-11]

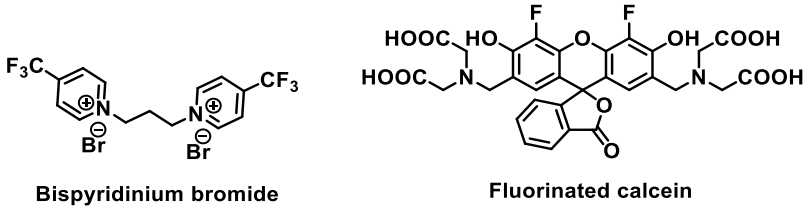

Figure 5.3. Possible fluorine-containing probes for liposomal leakage measurements by DOSY.

5.2.4. Triggered Release of Cell-derived Vesicles (CDVs) for Delivery of Therapeutics

Efficiency and safety of therapeutics delivery will be improved if carriers are made directly from cell materials, known as cell-derived vesicles (CDVs) because these natural vesicles have excellent immune-compatibility as compared to other synthetic carriers.[12] Extracellular vesicles (EVs), including microvesicles and exosomes, are CDVs that are naturally released from cells. These lipid membrane-bound structures, which can be harvested from cell cultures, contain membrane proteins and carry RNA and cytosolic contents. They also play a key role in intercellular communication and material transfer pathways.[13-15]

CDVs of nano-dimensions can also be produced from the plasma cell membrane by subjecting whole cells to chemo-physical processes, including passing cells through extruders or cell-slicing through microchannels.[16-17] In addition, CDVs have been generated in high yields and are easily loaded with a variety of cargos via a technique called nitrogen cavitation.[18] These CDVs are able to deliver many types of cargos, such as therapeutics, and fluorescent labels to the interior of cells both in vitro and in vivo. On the other hand, one-step production of native vesicles by blistering off the plasma membrane while retaining mother cells' surface receptors and cytoplasmic proteins has been demonstrated by incubation of cells with cytochalasin B; this chemical reagent actively destabilizes the cytoskeleton-membrane interactions.[19-20]

Engineering CDVs so that they can load therapeutics or have surface modifications is indispensable for different therapeutics delivery applications.[14, 18] For example, modification of the surface of exosomes has been demonstrated via direct membrane fusion of liposomes and exosomes using a freeze-thaw method.[21] In addition, hybrid EVs created from their fusion with liposomes containing soluble cargoes triggered by polyethylene glycol (PEG) has also been reported.[22] Another example is hybrid exosomes loading plasmids prepared by incubation of exosomes with the mixture of liposomes and plasmids through plasmid-induced exosomes-liposomes.[23] Thus, the fusion-based engineering enables CDVs loaded with potentially any compound associated with synthetic liposomes accompanied by surface modification from liposomes. Additionally, methods for therapeutic post-loading of vesicles after their isolation have also been well reported, including incubation, electroporation, sonication, osmotic shock, and extrusion in the presence of cargo.[13, 24] A combination of complementary features of CDVs and widely available targeted liposomes would result in an advanced new hybrid nanocarrier for therapeutics targeted delivery applications. For example, fusion of exosomes and Q_3DOPE liposomes could produce redox-responsive hybrid exosomes.

5.2.5. Liposomes Incorporating Gold−Silver−Gold—Core−Shell−Shell (GSG—CSS) Nanoparticles

A lot of examples have demonstrated the applicability of controlled release of liposomes resulting from the photothermal effect of gold nanoparticles incorporated into liposomes.[25-29] The Haber research group at LSU has been very successful in the production and application of highly photothermal GSG—CSS nanoparticles, as compared to traditional spherical gold nanoparticles and gold nanorods.[30] These unique nanoparticles with plasmon enhancement and near-infrared light (NIR) absorption is very beneficial for biological applications, such as photothermal cancer treatment and biosensing.[30] Gold nanoparticles have been incorporated within liposomes by

several methods, such as reverse evaporation, thin-film hydration, interdigitation-fusion, lipid vesicle metallization, and chemical bond attachment, which is compatible for any particles that have a gold shell.[25, 31-34] Based on the hydrophobicity of the nanoparticles and the type of liposome formulation technique, the nanoparticles can be located in different parts of liposomes, such as within the lipid bilayer, inside or on the surface of the liposomes, and free in solutions containing liposomes. A systematic study of the interaction of GSG—CSS with the thermally sensitive lipid DPPG and the photothermal release of this hybrid could be investigated.

In addition, acid-responsive fusion of cationic liposomes could be investigated using carboxyl-modified GSG—CSS nanoparticles. Typically, the carboxylic group is deprotonated at neutral pH, creating negatively charged nanoparticles that bound to the surface of cationic liposomes through electrostatic attraction, an event that stabilizes the liposomes. Under acidic conditions, the carboxyl group is protonated, and the subsequent neutral particle stabilizers detach from the liposomes, thereby producing free cationic liposomes that can actively fuse with various biological membranes.[27]

5.2.6. Second Harmonic Imaging Microscopy (SHIM)

SHIM has been established as a viable, label-free, non-invasive imaging technique for biological samples due to its ability to obtain contrasts from repeating asymmetric cellular structures, such as collagen, microtubules, and muscle myosin.[35-37] In addition, SHIM using NIR wavelengths as the incident light offers the ability to construct three-dimensional images of specimens by imaging deeper into thick tissues. SHIM of non-SHG active cellular structures could be obtained by exploiting targeting SHG probes. For example, SHG-active unnatural amino acids have been synthesized for studying protein structures and their conformational changes.[38] Another example is using several noncentrosymmetric nanocrystals, such as titanate (BaTiO3) as a versatile and durable SHG labeling probe for in vivo imaging and immunostaining.[39] Furthermore, time-

resolved SHIM has been used to spatially resolve the adsorption and transport rates of malachite green through lipid membranes of individual living cells.[40] From this context, the MG derivatives from Chapter 4 can be used as potential SHG probes for cell imaging. Interestingly, conjugation of MG derivatives with drugs or subcellular targeting molecules can also be used for tracking the destination of drugs or subcellular visualization by SHIM, respectively. For example, a coumarin−MG conjugate has been synthesized for fluorogenic labeling of surface, intracellular, and total protein pools in living cells.[41]

Likewise, SHG probes can also be used to visualize the uptake and intracellular fate of nanoparticles in cells by SHIM. For example, MGDs can be used with GSG−CSS nanoparticles to determine the destination of nanoparticles after their uptake by cells. Typically, cells can be incubated with nanoparticles, followed by a washing step to remove free nanoparticles. The cells are subsequently incubated with MGDs. The high affinity of MGDs adsorbing on nanoparticle surfaces after being taken up by cells enables the imaging of nanoparticles in the cells. Similarly, MGD−nanoparticles can be chemically conjugated, and their uptake can be determined in the same manner. The stability of the nanoparticles could be useful in tracking cell lineages during embryonic development as they are passed from cell to cell. Thus, not only the "blind" GSG−CSS nanoparticles can be visualized in the cells by SHIM, but they can be potentially used for killing cancer cells due to their excellent photothermal effect.

5.3. References

1. Kreutzberger, A. J., et al., Asymmetric Phosphatidylethanolamine Distribution Controls Fusion Pore Lifetime and Probability. *Biophysical Journal* **2017,** *113* (9), 1912-1915.

2. Pautot, S., et al., Engineering Asymmetric Vesicles. *Proceedings of the National Academy of Sciences* **2003,** *100* (19), 10718-10721.

3. Richmond, D. L., et al., Forming Giant Vesicles with Controlled Membrane Composition, Asymmetry, and Contents. *Proceedings of the National Academy of Sciences* **2011,** *108* (23), 9431-9436.

4. Marquardt, D., et al., Asymmetric Lipid Membranes: Towards More Realistic Model Systems. *Membranes* **2015,** *5* (2), 180-196.

5. Mendoza, M. F., et al., Human Nad (P) H: Quinone Oxidoreductase Type I (Hnqo1) Activation of Quinone Propionic Acid Trigger Groups. *Biochemistry* **2012,** *51* (40), 8014-8026.

6. Mayhew, S. G., The Redox Potential of Dithionite and So− 2 from Equilibrium Reactions with Flavodoxins, Methyl Viologen and Hydrogen Plus Hydrogenase. *European Journal of Biochemistry* **1978,** *85* (2), 535-547.

7. Hermanson, G. T., Fluorescent Probes. *Bioconjugate Techniques (third edition) Chapter* **2013,** *10*, 395-463.

8. Walton, D. P.; Dougherty, D. A., A General Strategy for Visible-Light Decaging Based on the Quinone Trimethyl Lock. *Journal of the American Chemical Society* **2017,** *139* (13), 4655-4658.

9. Chen, Y.; Steinmetz, M. G., Photoactivation of Amino-Substituted 1, 4-Benzoquinones for Release of Carboxylate and Phenolate Leaving Groups Using Visible Light. *The Journal of Organic Chemistry* **2006,** *71* (16), 6053-6060.

10. Li, Z., et al., Dithiane-Based Photolabile Amphiphiles: Toward Photolabile Liposomes1, 2. *Langmuir : the ACS Journal of Surfaces and Colloids* **2003,** *19* (16), 6381-6391.

11. Sun, W.-C., et al., Synthesis of Fluorinated Fluoresceins. *The Journal of Organic Chemistry* **1997,** *62* (19), 6469-6475.

12. Li, Y.-J., et al., Autologous Cancer Cell-Derived Extracellular Vesicles as Drug-Delivery Systems: A Systematic Review of Preclinical and Clinical Findings and Translational Implications. *Nanomedicine* **2019,** *14* (4), 493-509.

13. van der Meel, R., et al., Extracellular Vesicles as Drug Delivery Systems: Lessons from the Liposome Field. *Journal of Controlled Release* **2014,** *195*, 72-85.

14. Li, X., et al., Challenges and Opportunities in Exosome Research—Perspectives from Biology, Engineering, and Cancer Therapy. *APL Bioengineering* **2019,** *3* (1), 011503.

15. Fuhrmann, G., et al., Cell-Derived Vesicles for Drug Therapy and Diagnostics: Opportunities and Challenges. *Nano Today* **2015,** *10* (3), 397-409.

16. Antimisiaris, S., et al., Exosomes and Exosome-Inspired Vesicles for Targeted Drug Delivery. *Pharmaceutics* **2018,** *10* (4), 218.

17. García-Manrique, P., et al., Therapeutic Biomaterials Based on Extracellular Vesicles: Classification of Bio-Engineering and Mimetic Preparation Routes. *Journal of Extracellular Vesicles* **2018,** *7* (1), 1422676.

18. Bunggulawa, E. J., et al., Recent Advancements in the Use of Exosomes as Drug Delivery Systems. *Journal of Nanobiotechnology* **2018,** *16* (1), 81.

19. Pick, H., et al., Investigating Cellular Signaling Reactions in Single Attoliter Vesicles. *Journal of the American Chemical Society* **2005,** *127* (9), 2908-2912.

20. Eyer, K., et al., Cell-Free Microfluidic Determination of P-Glycoprotein Interactions with Substrates and Inhibitors. *Pharmaceutical Research* **2014,** *31* (12), 3415-3425.

21. Sato, Y. T., et al., Engineering Hybrid Exosomes by Membrane Fusion with Liposomes. *Scientific Reports* **2016,** *6*, 21933.

22. Piffoux, M., et al., Modification of Extracellular Vesicles by Fusion with Liposomes for the Design of Personalized Biogenic Drug Delivery Systems. *ACS Nano* **2018,** *12* (7), 6830-6842.

23. Lin, Y., et al., Exosome–Liposome Hybrid Nanoparticles Deliver Crispr/Cas9 System in Mscs. *Advanced Science* **2018,** *5* (4).

24. Johnsen, K. B., et al., A Comprehensive Overview of Exosomes as Drug Delivery Vehicles—Endogenous Nanocarriers for Targeted Cancer Therapy. *Biochimica et Biophysica Acta (BBA)-Reviews on Cancer* **2014,** *1846* (1), 75-87.

25. Mathiyazhakan, M., et al., A Concise Review of Gold Nanoparticles-Based Photo-Responsive Liposomes for Controlled Drug Delivery. *Nano-micro Letters* **2018,** *10* (1), 10.

26. Paasonen, L., et al., Gold Nanoparticles Enable Selective Light-Induced Contents Release from Liposomes. *Journal of Controlled Release* **2007,** *122* (1), 86-93.

27. Pornpattananangkul, D., et al., Stimuli-Responsive Liposome Fusion Mediated by Gold Nanoparticles. *ACS Aano* **2010,** *4* (4), 1935-1942.

28. Rengan, A. K., et al., In Vivo Analysis of Biodegradable Liposome Gold Nanoparticles as Efficient Agents for Photothermal Therapy of Cancer. *Nano Letters* **2015,** *15* (2), 842-848.

29. Wu, G., et al., Remotely Triggered Liposome Release by near-Infrared Light Absorption Via Hollow Gold Nanoshells. *Journal of the American Chemical Society* **2008,** *130* (26), 8175-8177.

30. Karam, T. E., et al., Enhanced Photothermal Effects and Excited-State Dynamics of Plasmonic Size-Controlled Gold–Silver–Gold Core–Shell–Shell Nanoparticles. *The Journal of Physical Chemistry C* **2015,** *119* (32), 18573-18580.

31. Al-Jamal, W. T.; Kostarelos, K., Liposome–Nanoparticle Hybrids for Multimodal Diagnostic and Therapeutic Applications. **2007**.

32. Al-Jamal, W. T., et al., Functionalized-Quantum-Dot–Liposome Hybrids as Multimodal Nanoparticles for Cancer. *Small* **2008,** *4* (9), 1406-1415.

33. Preiss, M. R.; Bothun, G. D., Stimuli-Responsive Liposome-Nanoparticle Assemblies. *Expert Opinion on Drug Delivery* **2011,** *8* (8), 1025-1040.

34. Bonnaud, C., et al., Insertion of Nanoparticle Clusters into Vesicle Bilayers. *ACS Nano* **2014,** *8* (4), 3451-3460.

35. Campagnola, P., Second Harmonic Generation Imaging Microscopy: Applications to Diseases Diagnostics. ACS Publications: 2011.

36. Campagnola, P. J.; Dong, C. Y., Second Harmonic Generation Microscopy: Principles and Applications to Disease Diagnosis. *Laser & Photonics Reviews* **2011,** *5* (1), 13-26.

37. Cohen, B. E., Biological Imaging: Beyond Fluorescence. *Nature* **2010,** *467* (7314), 407.

38. Salafsky, J. S.; Cohen, B., A Second-Harmonic-Active Unnatural Amino Acid as a Structural Probe of Biomolecules on Surfaces. *The Journal of Physical Chemistry B* **2008,** *112* (47), 15103-15107.

39. Pantazis, P., et al., Second Harmonic Generating (Shg) Nanoprobes for in Vivo Imaging. *Proceedings of the National Academy of Sciences* **2010,** *107* (33), 14535-14540.

40. Sharifian Gh, M., et al., Spatially Resolved Membrane Transport in a Single Cell Imaged by Second Harmonic Light Scattering. *Biochemistry* **2019,** *58* (14), 1841-1844.

41. Naganbabu, M., et al., Multiexcitation Fluorogenic Labeling of Surface, Intracellular, and Total Protein Pools in Living Cells. *Bioconjugate Chemistry* **2016,** *27* (6), 1525-1531.

APPENDIX A. SUPPORTING INFORMATION FOR CHAPTER 2

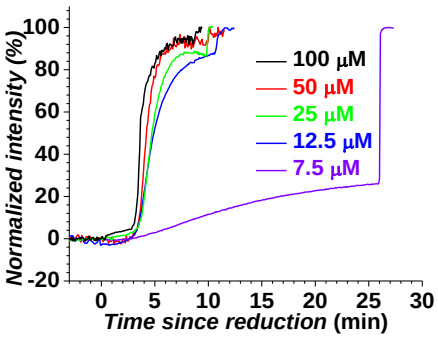

Figure SI2.1. Q_3DOPE:DOPE 20:80 LUVs concentration dependence. Conditions: 0.040 M calcein encapsulated in LUVs with 0.10 M KCl and 1.0×10^{-4} M EDTA buffered with 0.050 M phosphate, pH = 7.4; T = 37 °C; lipid concentration = 1.0×10^{-4} M.

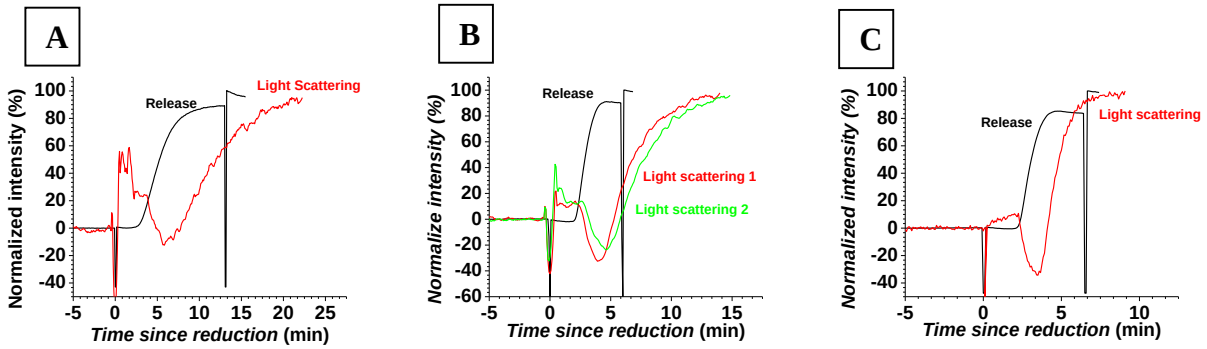

Figure SI2.2. Content release and light scattering from Q_3DOPE:POPE 20:80 LUVs at various lipid concentrations. **A**. 50 μM, **B**. 100 μM, **C**. 500 μM. Conditions: 0.040 M calcein encapsulated in LUVs with 0.10 M KCl and 1.0×10^{-4} M EDTA buffered with 0.050 M phosphate, pH = 7.4; T = 41 °C.

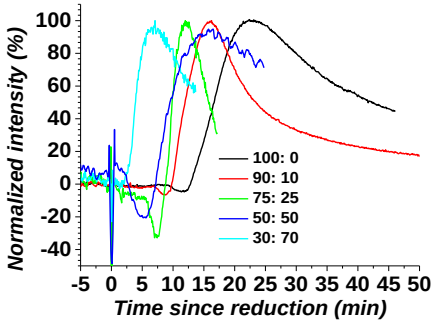

Figure SI2.3. Light scattering of Q_3DOPE:DOPE LUVs at various DOPE portions. Conditions: 0.040 M calcein encapsulated in LUVs with 0.10 M KCl and 1.0 × 10^{-4} M EDTA buffered with 0.050 M phosphate, pH = 7.4; T = 37 °C; lipid concentration = 1.0 × 10^{-4} M.

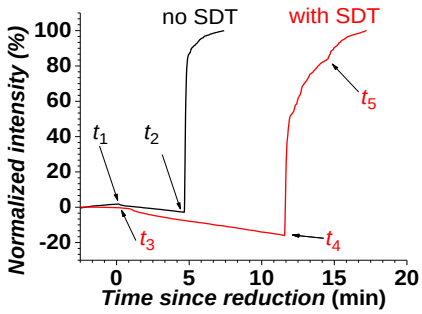

Figure SI2.4. Content release of Q_3POPE LUVs at 70 °C with (red curve) and without SDT (black curve). **t_1**: cuvette containing LUVs was taken out from the fluorometer and incubated in a 70 °C water bath for 15 mins before it was placed back in the fluorometer; **t_2**: triton 0.1% (final v/v) was added to lysed LUVs; **t_3**: SDT was added to the cuvette containing LUVs at 37 °C in the fluorometer; **t_4**: the cuvette was taken out from the fluorometer and incubated in 70 °C water bath for 5 mins before it was placed back in the fluorometer; **t_5**: triton 0.1% (final v/v) was added to lysed LUVs. Conditions: 0.05 M phosphate, 0.1 M KCl, EDTA 1.0 × 10^{-4} M, pH 7.4. Note: the cuvette was incubated in 70 °C water bath instead of directly increasing temperature of the cuvette holder of the fluorometer by Peltier temperature controller to avoid bubling in the cuvette during the fluorescence measurement.

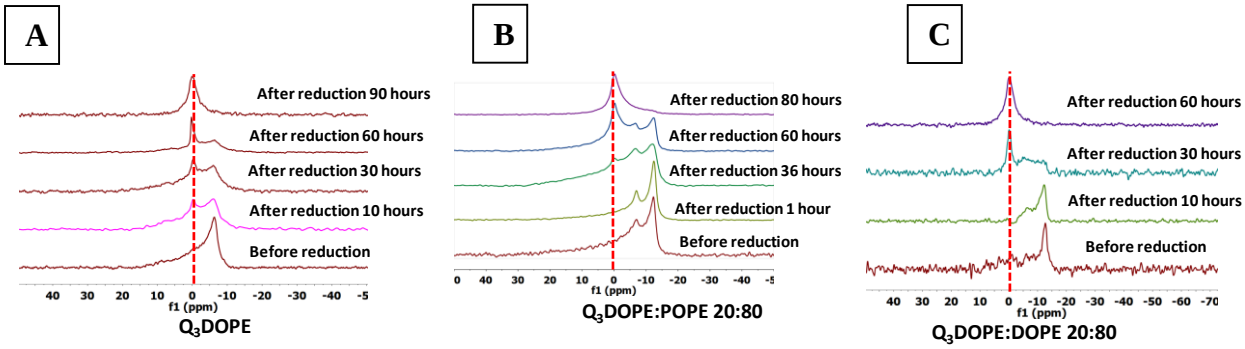

Figure SI2.5. ^{31}P NMR of Q_3DOPE-based GUVs in solution containing 0.2 M sucrose, 10 % (v/v) D_2O. Graph B is reproduced from Winter.[33]

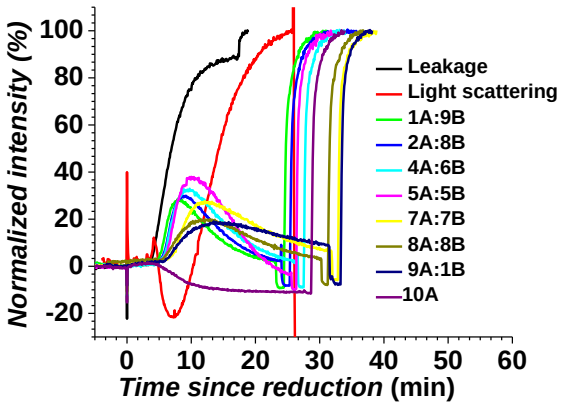

Figure SI2.6. Q_3DOPE:POPE 20:80 LUVs fusion with different vesicles ratios.

APPENDIX B. SUPPORTING INFORMATION FOR CHAPTER 3

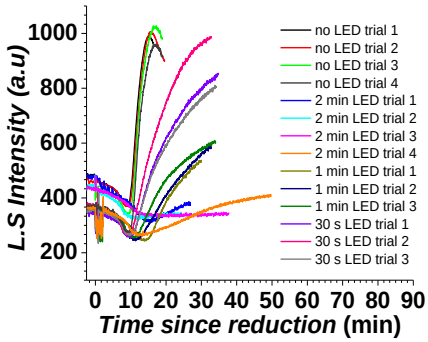

Figure SI3.1. $MeSQ_3DOPE$ LUVs irradiated under blue LED at different time periods before added SDT. Conditions: PBS buffer at 25 °C, lipid concentration = 1.0×10^{-4} M.

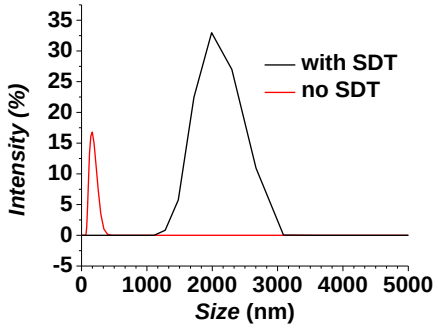

Figure SI3.2. DLS measurement of $MeSQ_3DOPE$:DOPE 20:80 LUVs with and without SDT in PBS buffer.

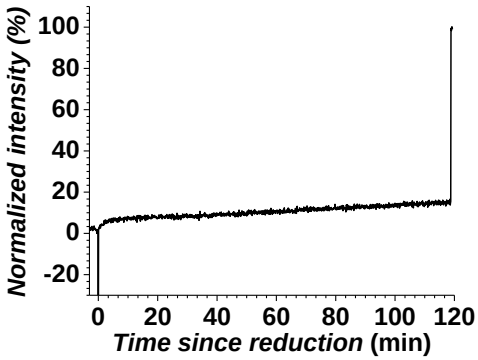

Figure SI3.3. Content release of HMBQDOPE:DOPE 20:80 LUVs with SDT. Conditions: 0.040 M calcein encapsulated in LUVs with 0.10 M KCl and 1.0×10^{-4} M EDTA buffered with 0.050 M phosphate, pH = 7.4, lipid concentration = 1.0×10^{-4} M.

APPENDIX C. ^{1}H NMR AND MS OF QPE-RELATED COMPOUNDS

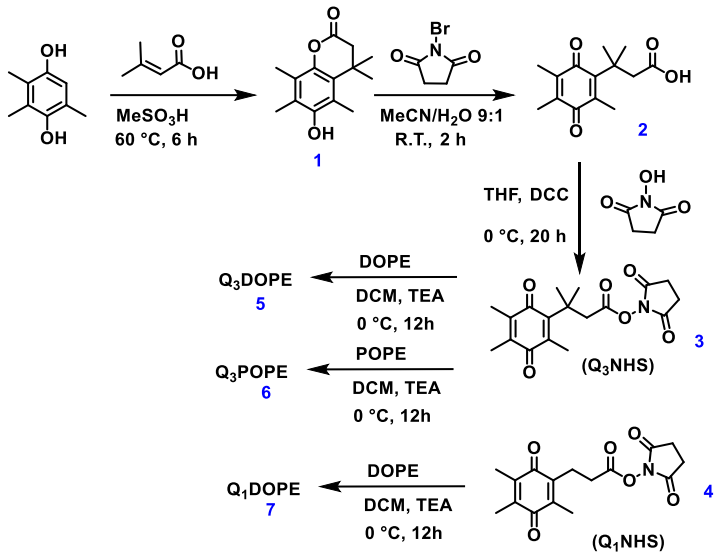

C.1. ^{1}H NMR of Q_3lactone (Compound 1)

1H NMR (400 MHz, $CDCl_3$) δ 4.54 (s, 1H), 2.55 (s, 2H), 2.36 (s, 3H), 2.23 (s, 3H), 2.19 (s, 3H), 1.46 (s, 6H).

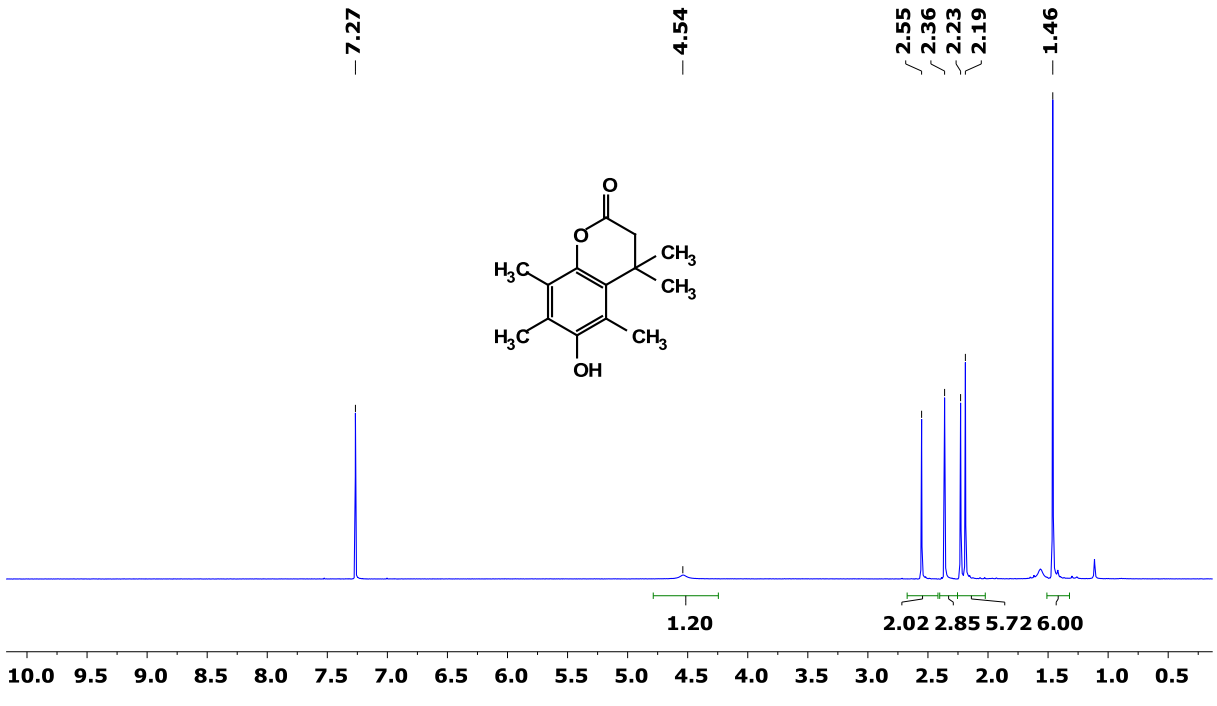

C.2. ^{1}H NMR of Q_3acid (Compound 2)

1H NMR (400 MHz, $CDCl_3$) δ 3.04 (s, 2H), 2.16 (s, 3H), 1.96 (s, 6H), 1.45 (s, 6H).

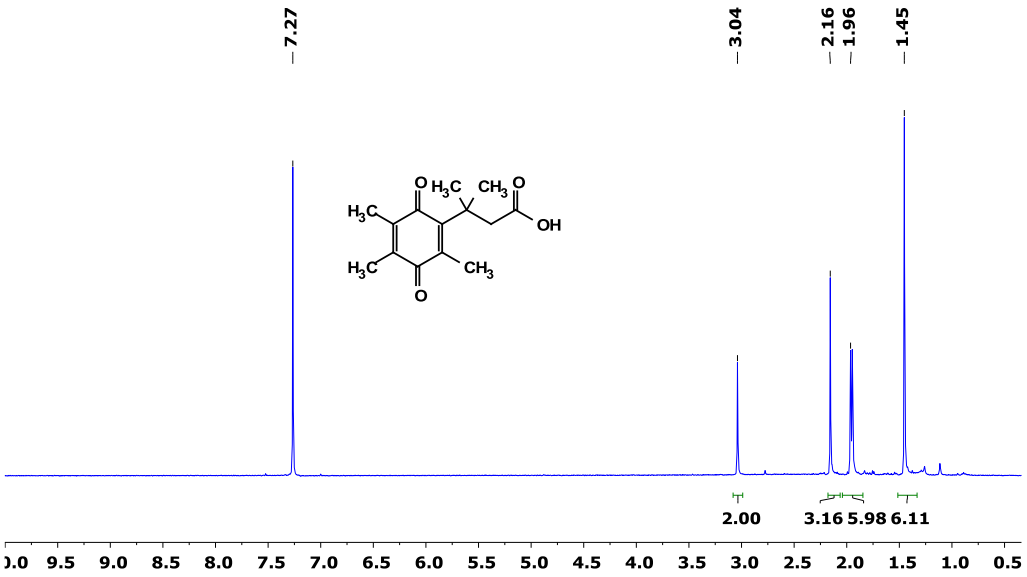

C.3. ^{1}H NMR of Q_3NHS (Compound 3)

1H NMR (400 MHz, $CDCl_3$) δ 3.28 (s, 2H), 2.78 (s, 4H), 2.16 (s, 3H), 1.95 (s, 6H), 1.52 (s, 6H).

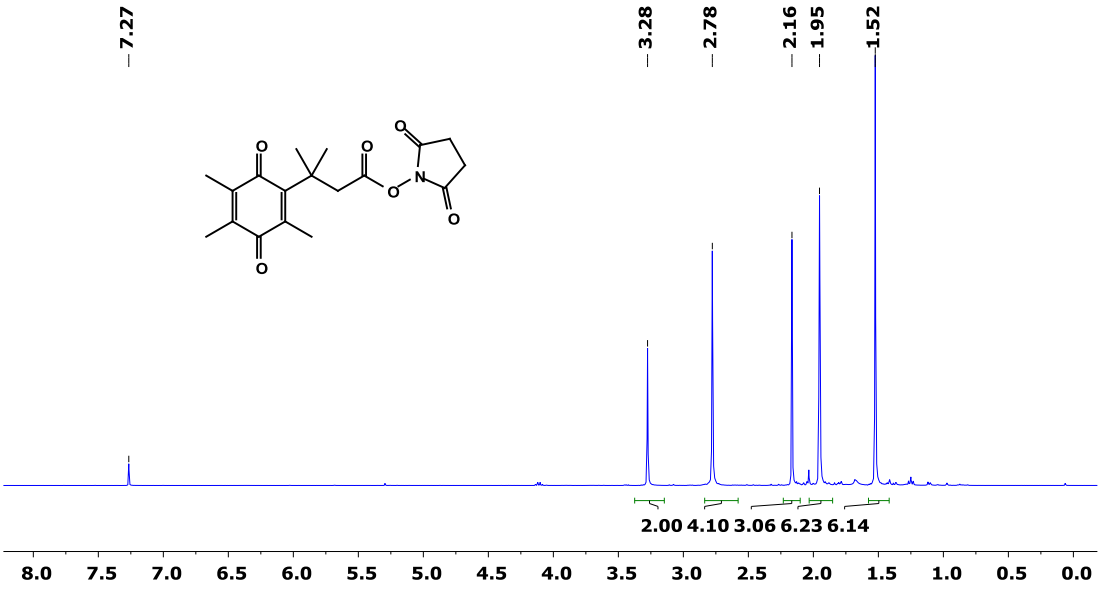

C.4. ^{1}H NMR of Q_1NHS (Compound 4)

1H NMR (400 MHz, $CDCl_3$) δ 2.91 (m, 2H), 2.80 (m, 6H), 2.07 (s, 3H), 2.02 (s, 6H).

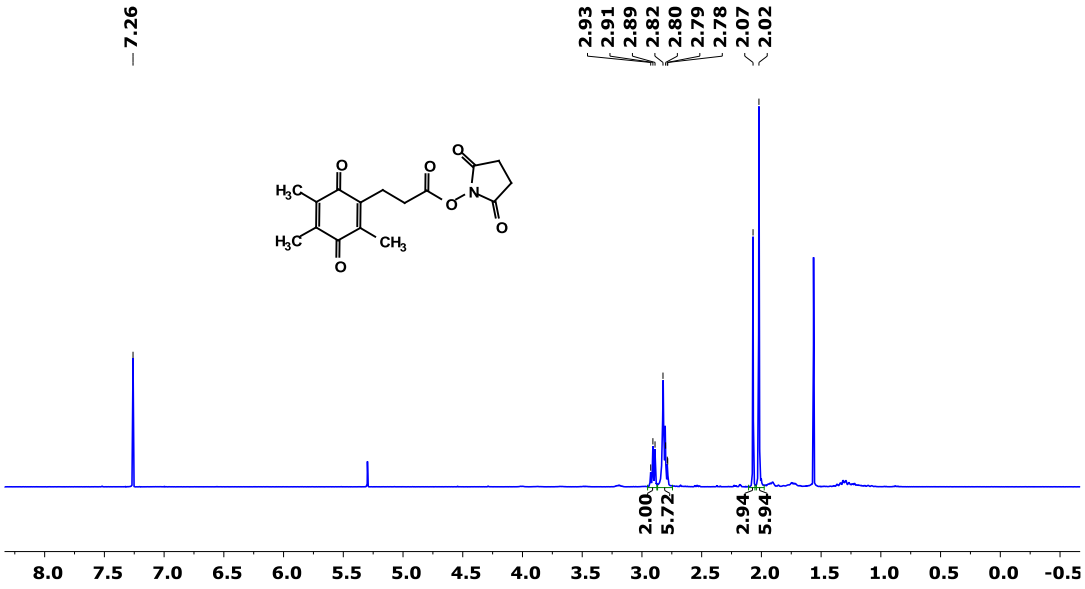

C.5. ^{1}H NMR and MS of Q_3DOPE (Compound 5)

1H NMR (400 MHz, $CDCl_3$) δ 5.34 (m, 5H), 4.43 (m, 1H), 4.18 (m, 1H), 3.94 (m, 2H), 3.85 (m, 2H), 3.37 (m, 2H), 2.85 (s, 2H), 2.30 (m, 4H), 2.10 (s, 3H), 2.01-1.94 (m 14H), 1.57 (m 4H), 1.38 (s, 6H) 1.26 (m, 40H), 0.88 (t, 6H).

HRMS (ESI) calculated for $C_{55}H_{94}O_{11}NP$ $[M-H]^-$ 974.6492, found 974.6481 (1.02 ppm).

HRMS (ESI) calculated for $C_{55}H_{94}O_{11}NP$ $[M+H]^+$ 976.6637, found 976.6638 (0.12 ppm).

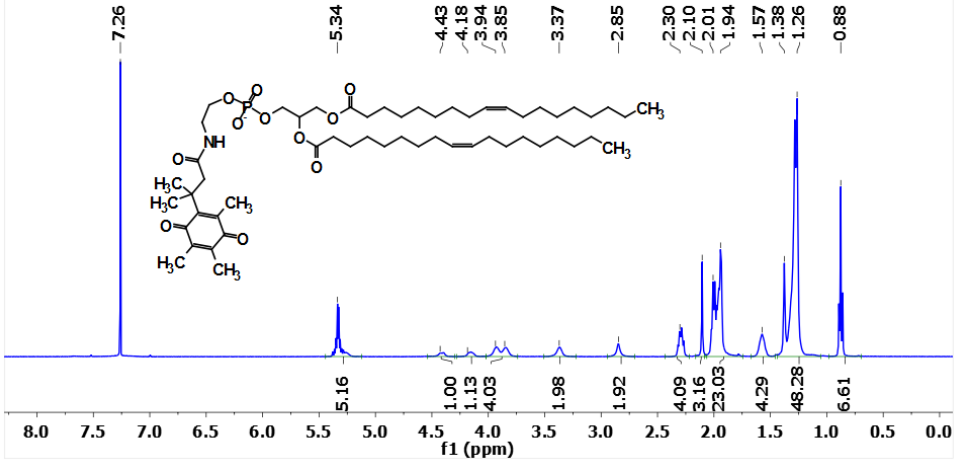

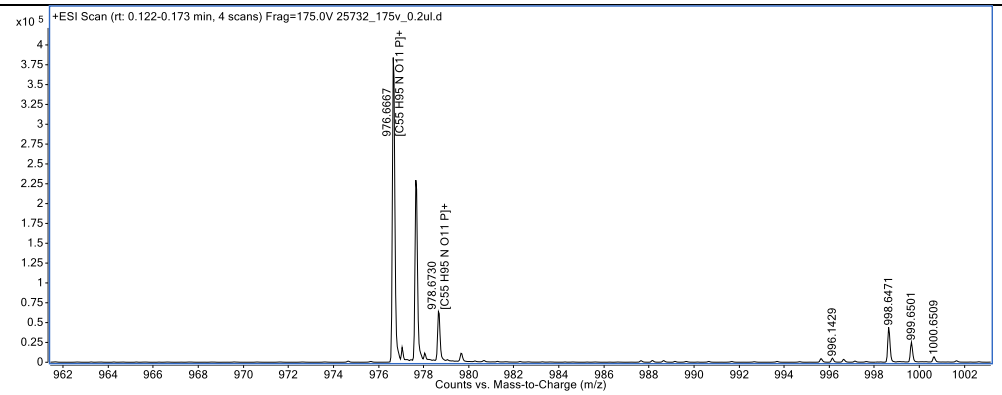

C.6. ^{1}H NMR and MS of Q$_3$POPE (Compound 6)

1H NMR (400 MHz, $CDCl_3$) δ 7.46 (bs, 1H), 5.34 (m, 2H) 5.24 (m, 1H), 4.41 (m, 1H), 4.18 (m, 1H), 3.96 (m, 4H) 3.37 (m, 2H), 3.08 (m, 4H), 2.83 (s, 2H), 2.30 (m, 4H), 2.10-1.93 (m, 15H) 1.58 (m, 4H), 1.39 (s, 6H), 1.25 (m, 34) 0.87 (t, 6H).

HRMS (ESI) calculated for $C_{53}H_{92}O_{11}NP$ [M-H]- 948.6335, found 948.6314 (1.85 ppm).

HRMS (ESI) calculated for $C_{53}H_{92}O_{11}NP$ [M+H]+ 950.6481, found 976.6468 (1.43 ppm).

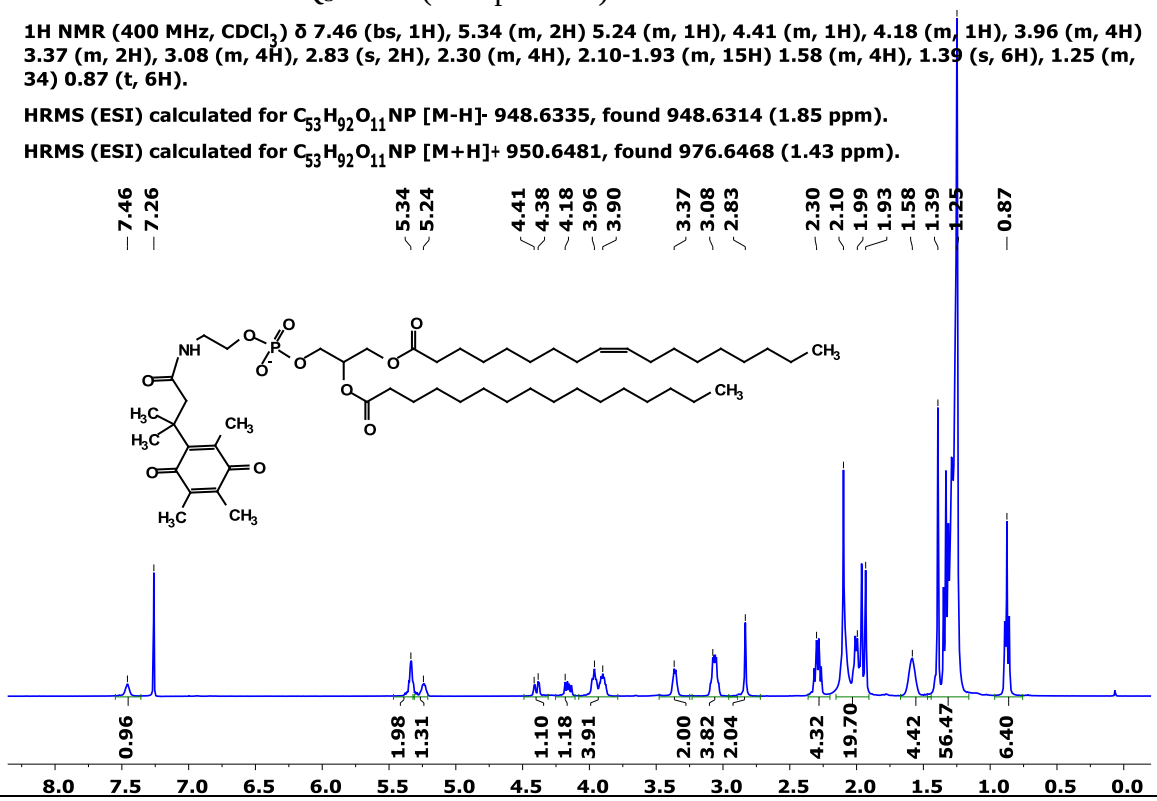

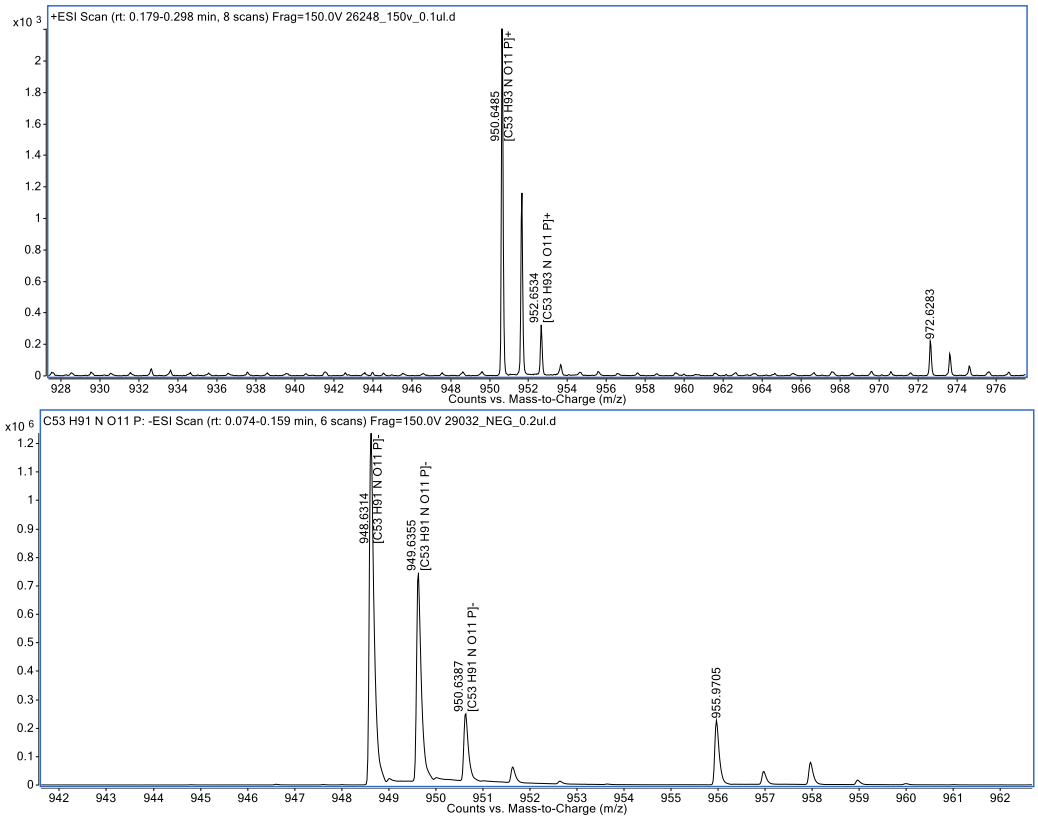

C.7. ^{1}H NMR and MS of Q_1DOPE (Compound 7)

1H NMR (500 MHz, $CDCl_3$) δ 5.33 (m, 4H), 5.21 (m, 1H), 4.37 (m, 1H), 4.12 (m, 1H), 3.95 (m 4H), 3.47 (m 2H), 2.76 (t, 2H), 2.33 (t, 2H), 2.25 (m, 4H), 1.98 (m, 17H), 1.54 (m, 4H), 1.26 (m, 40H), 0.87 (t, 6H).

HRMS (ESI) calculated for $C_{53}H_{90}O_{11}NP$ [M-H]- 946.6179, found 946.6166 (0.81 ppm).

HRMS (ESI) calculated for $C_{53}H_{90}O_{11}NP$ [M+H]+ 948.6324, found 948.6330 (1.06 ppm).

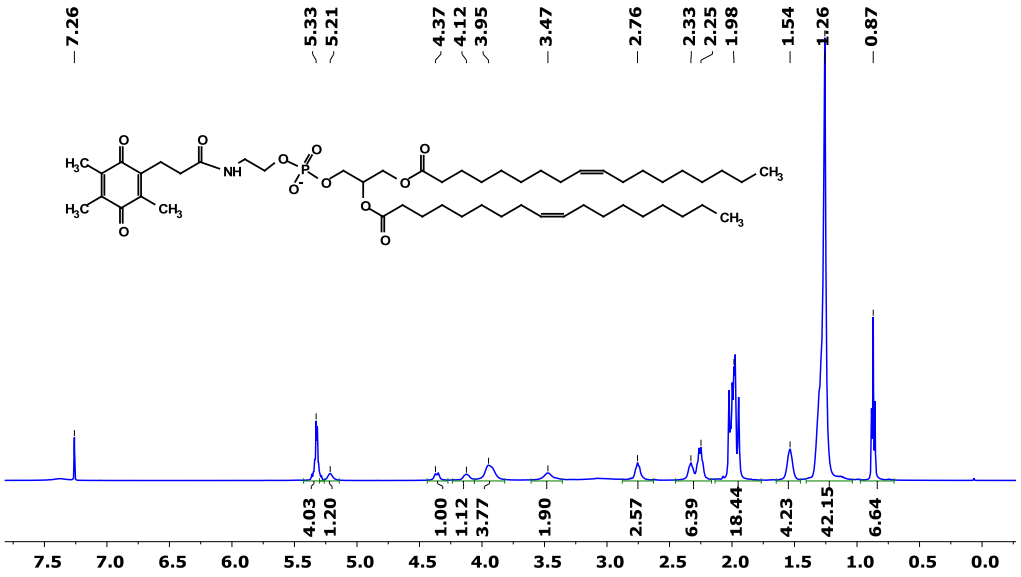

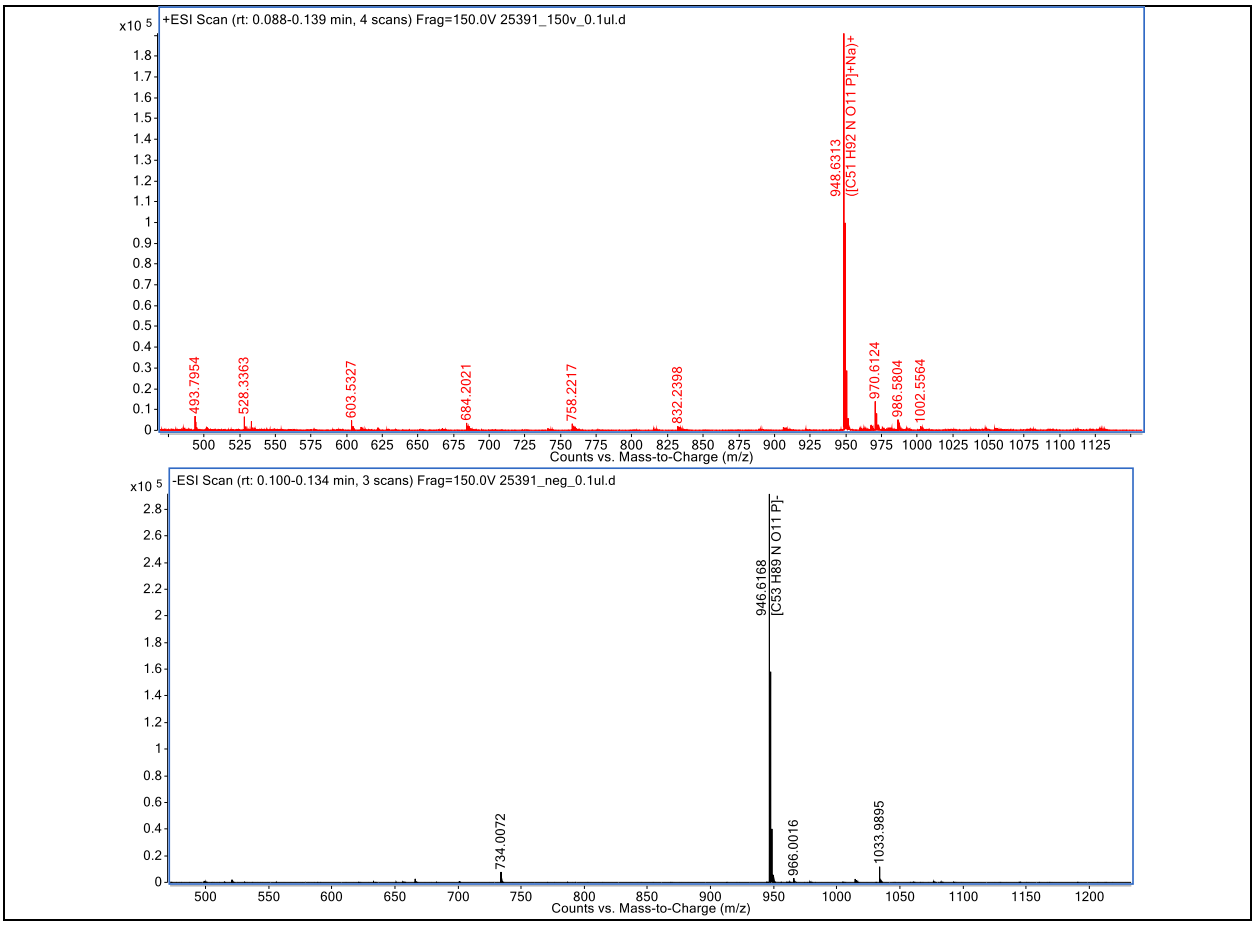
+ESI Scan (rt: 0.088-0.139 min, 4 scans) Frag=150.0V 25391_150v_0.1ul.d
x10 5
948.6313
([C51 H92 N O11 P]+Na)+
493.7954
528.3363
603.5327
684.2021
758.2217
832.2398
970.6124
986.5804
1002.5564
Counts vs. Mass-to-Charge (m/z)
-ESI Scan (rt: 0.100-0.134 min, 3 scans) Frag=150.0V 25391_neg_0.1ul.d
x10 5
946.6168
[C53 H89 N O11 P]-
734.0072
966.0016
1033.9895
Counts vs. Mass-to-Charge (m/z)

APPENDIX D. ^{1}H NMR AND MS OF MeSQ$_3$DOPE-RELATED COMPOUNDS

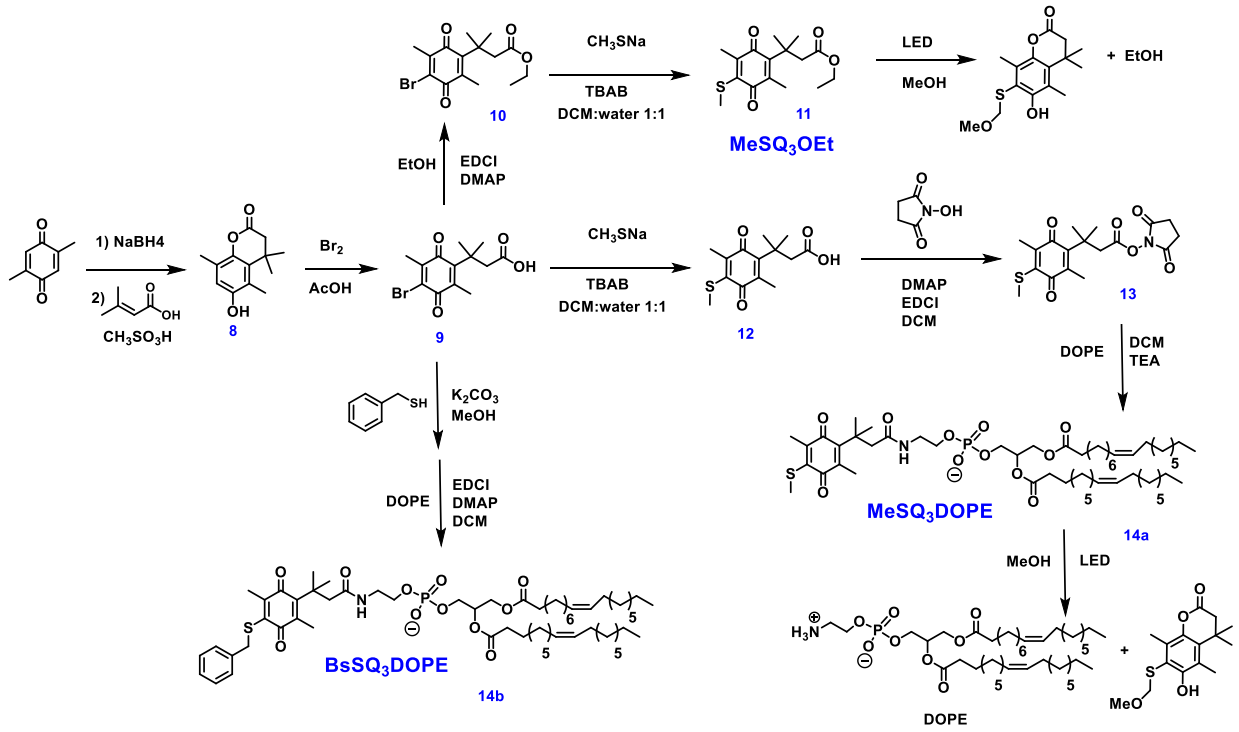

D.1. ^{1}H NMR and MS of lactone (Compound 8)

1H NMR (400 MHz, $CDCl_3$) δ 6.57 (s, 1H), 2.57 (s, 2H), 2.34 (s, 3H), 2.23 (s, 3H), 1.48 (s, 6H)

HRMS (ESI) calculated 221.1172 for $C_{13}H_{16}O_3$ [M+H]+, found 221.1175, (0.66 ppm)

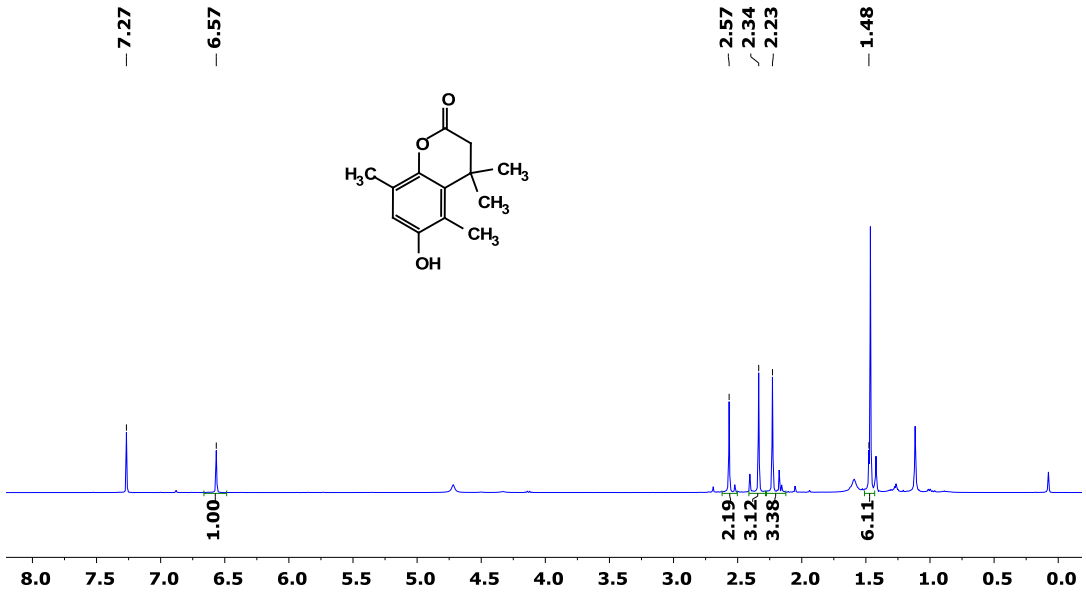

D.2. ^{1}H NMR and MS of bromoacid (Compound 9)

1H NMR (500 MHz, $CDCl_3$) δ 3.02 (s, 2H), 2.21 (s, 3H), 2.14 (s, 3H), 1.45 (s, 6H)

HRMS (ESI) calculated 315.0226 for $C_{13}H_{15}BrO_4$ [M+H]+, found 315.0219 (2.47 ppm)

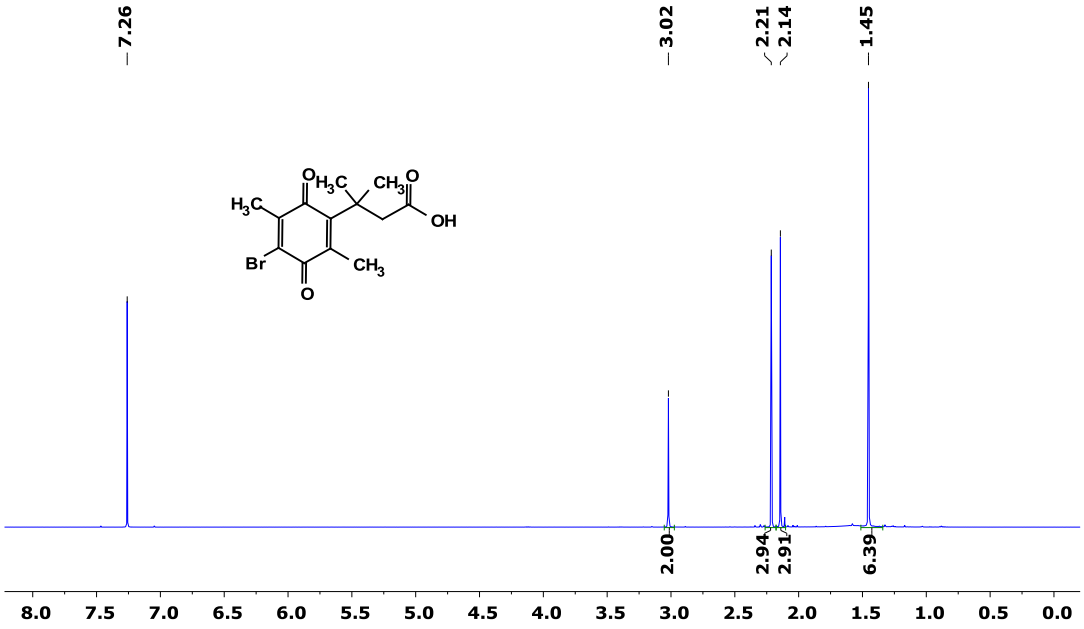

D.3. ^{1}H NMR and MS of bromoester (Compound 10)

1H NMR (400 MHz, Chloroformd) δ 4.03 (q, J = 7.1 Hz, 2H), 2.92 (s, 2H), 2.18 (s, 3H), 2.15 (s, 3H), 1.41 (s, 6H), 1.19 (t, J = 7.1 Hz, 3H).

HRMS (ESI) calculated for $C_{15}H_{20}BrO_4$ [M+H]+ 343.0539 (100%), found 343.0546 (2.04 ppm)

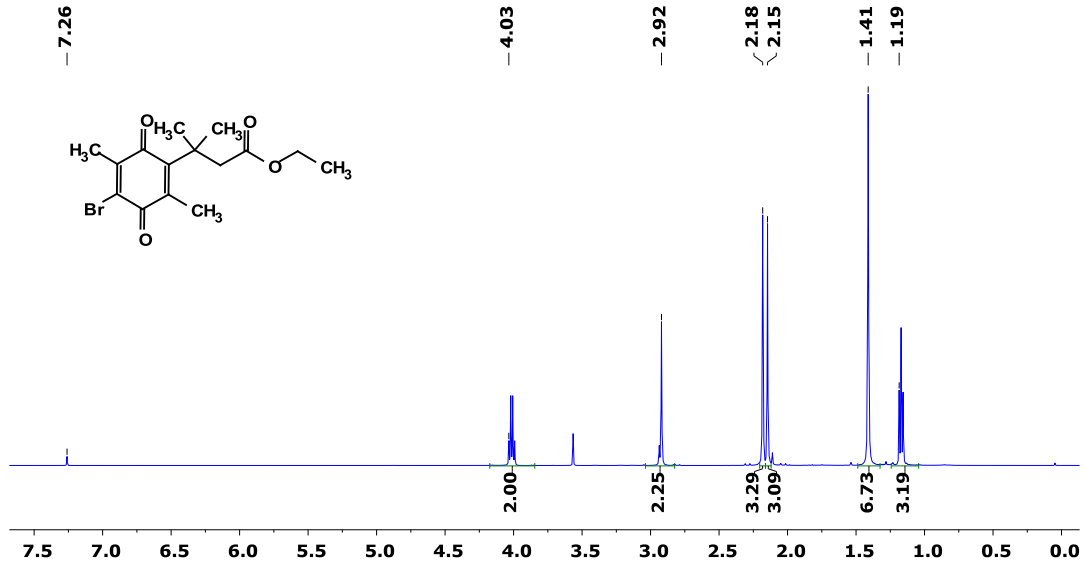

D.4. ^{1}H NMR and MS of MeSQ$_3$OEt (Compound 11)

1H NMR (400 MHz, $CDCl_3$) δ 4.04 (q, J = 7.1 Hz, 2H), 2.95 (s, 2H), 2.47 (s, 2H), 2.16 (s, 3H), 2.13 (s, 2H), 1.42 (s, 6H), 1.19 (t, J = 7.1 Hz, 2H).

HRMS (ESI) calculated for $C_{16}H_{23}O_4S$ [M+H]+ 311.1312, found 311.1314 (0.67 ppm).

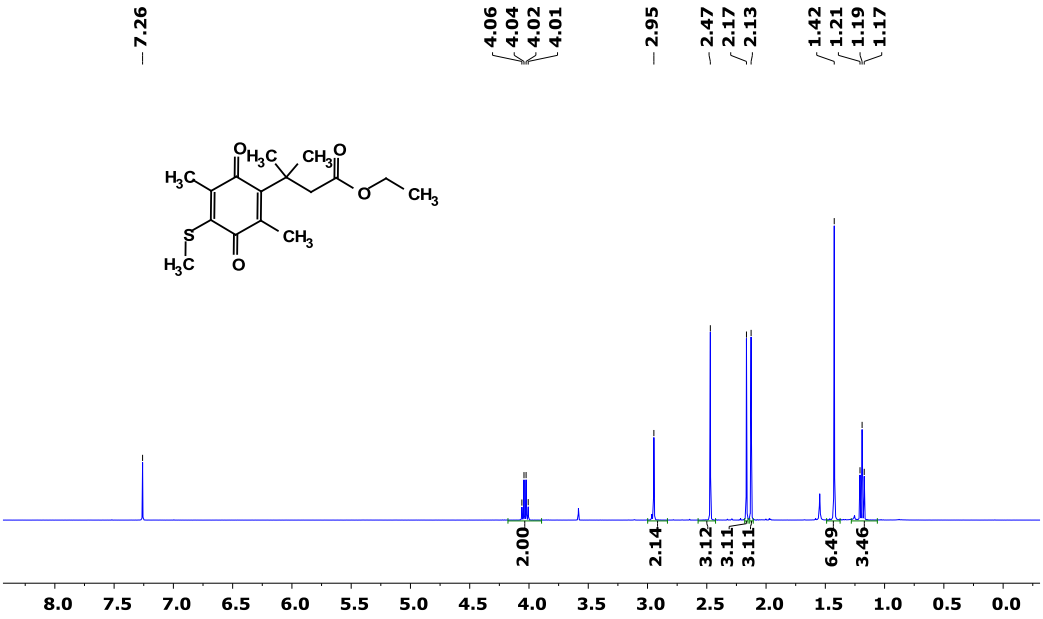

D.5. ^{1}H NMR and MS of MeSQ$_3$NHS (Compound 13)

1H NMR (500 MHz, $CDCl_3$) δ 3.25 (s, 2H), 2.79 (s, 4H), 2.46 (s, 3H), 2.19 (s, 3H), 2.11 (s, 3H), 1.52 (s, 6H).

HRMS (ESI) calculated for $C_{18}H_{21}NO_6S$ [M+Na]+ 402.0982, found 402.0972 (1.13 ppm).

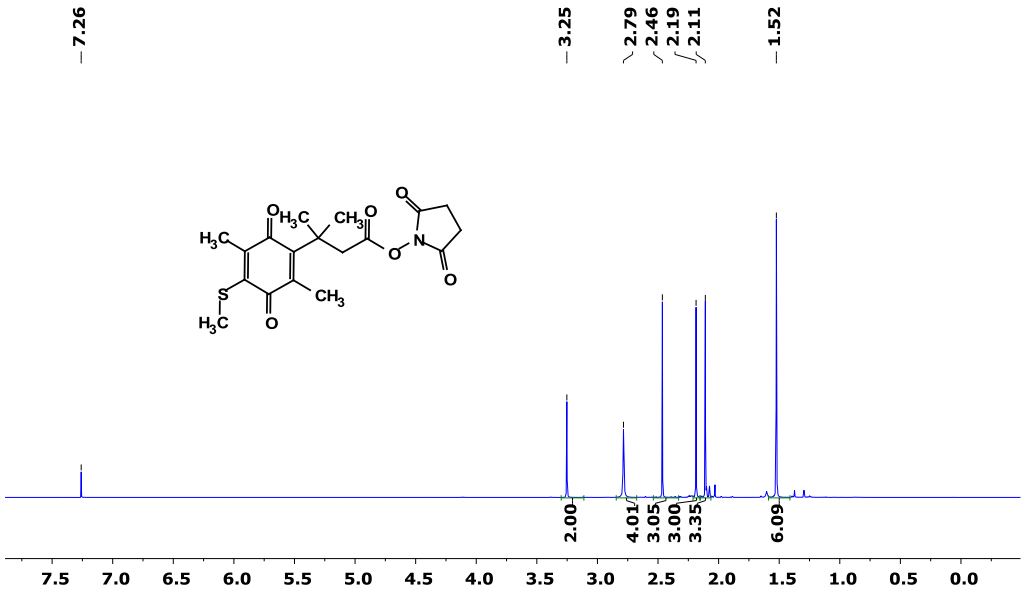

D.6. ^{1}H NMR and MS of MeSQ$_3$DOPE (Compound 14a)

1H NMR (400 MHz, $CDCl_3$) δ 5.34 (m, 5H), 4.45 (m, 1H) 4.16 (m, 1H), 3.95 (m, 2H), 3.87 (m, 2H), 3.48 (s,1H), 3.38 (m,2H), 2.84 (s, 2H), 2.45 (s,3H), 2.31 (m, 4H), 2.11-1.99 (m, 17H), 1.58 (m, 4H), 1.38-1.26 (m, 46H), 1.26 (m, 40H), 0.88 (t, 6H).

HRMS (ESI) calculated for $C_{55}H_{93}NO_{11}PS$ [M-H]⁻ 1006.6212, found 1006.6218 (0.13 ppm).

HRMS (ESI) calculated for $C_{55}H_{94}NO_{11}PS$ [M+H]+ 1008.6358, found 1006.6382 (1.8 ppm).

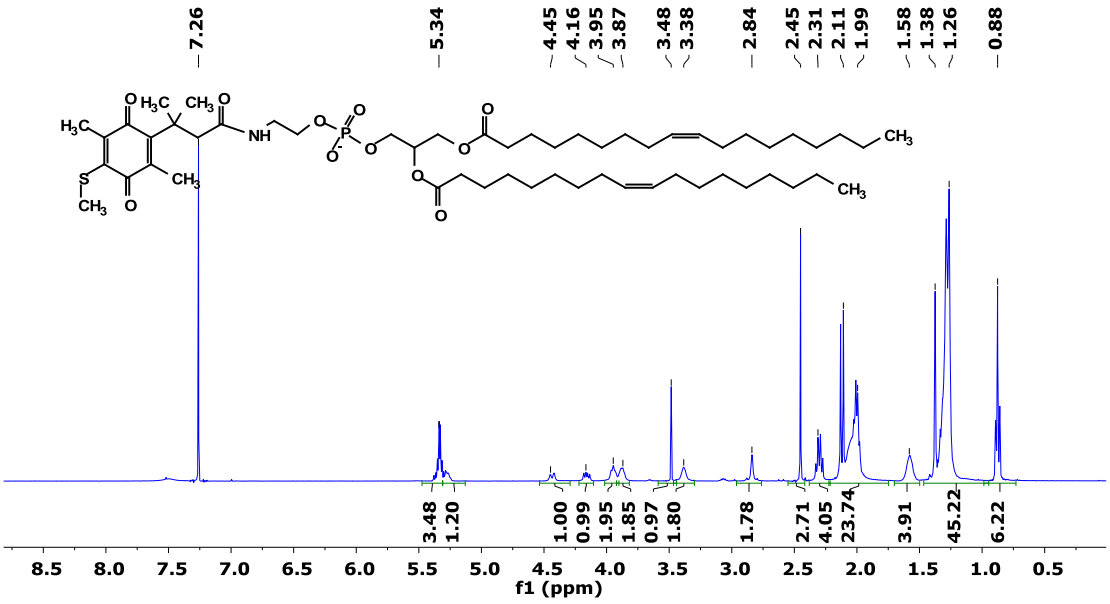

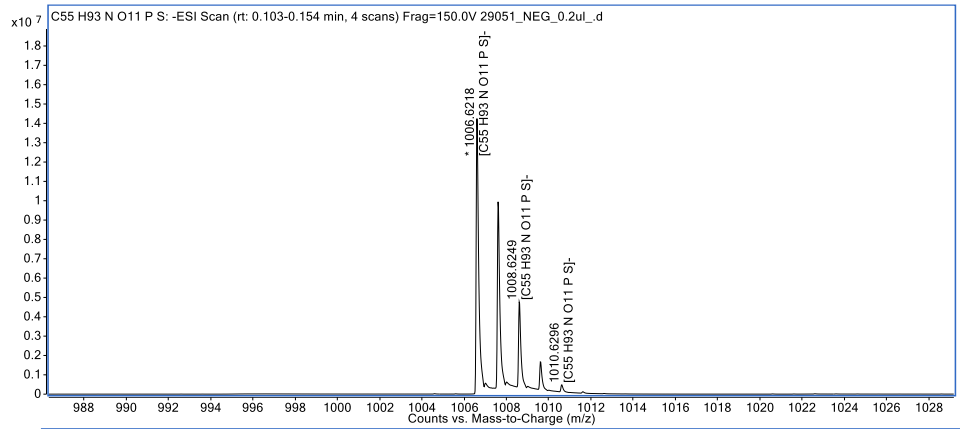

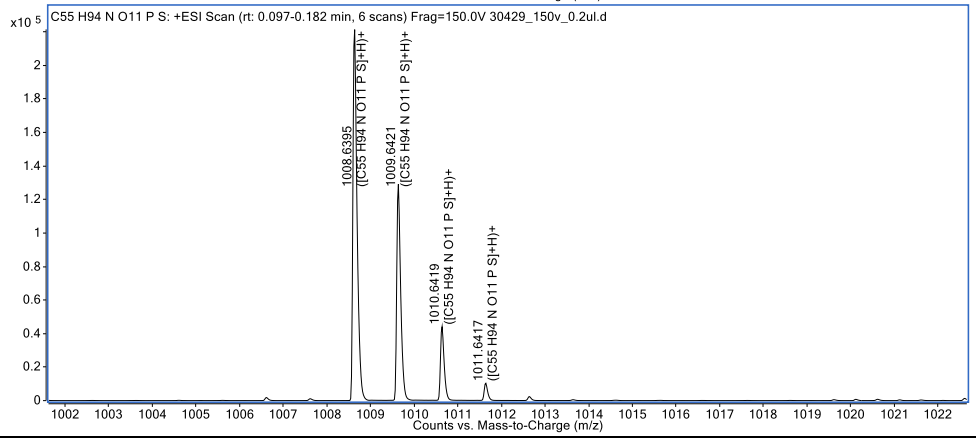

D.7. MS of $BnSQ_3DOPE$ (Compound 14b)

HRMS (ESI) calculated for $C_{61}H_{98}O_{11}NPS$ $[M-H]^-$ 1082.6598, found 1082.6523 (0.99 ppm), $[M+H]^+$ 1084.6671, found 1084.6667 (0.12 ppm)

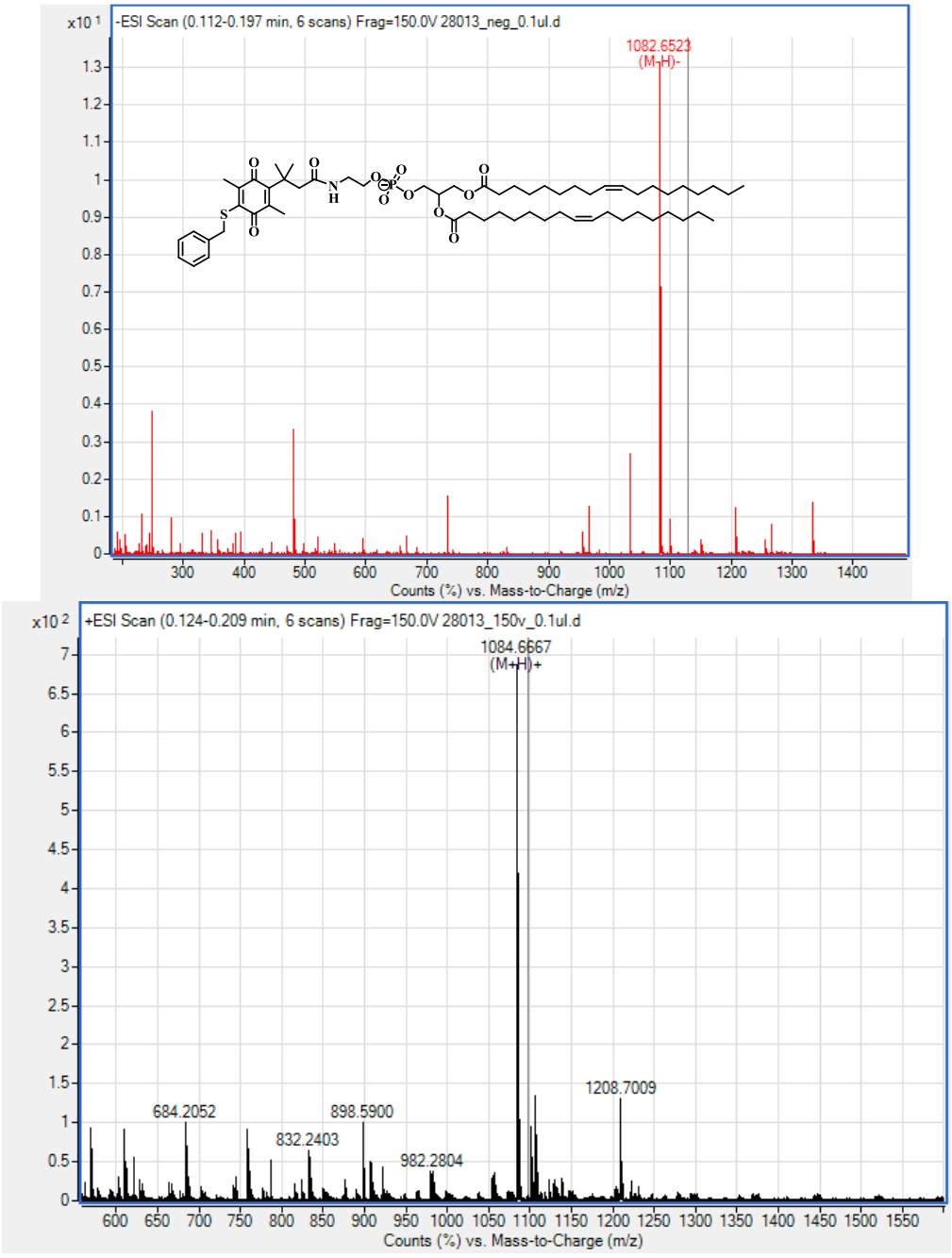

APPENDIX E. ^{1}H NMR AND MS OF HMBQDOPE-RELATED COMPOUNDS

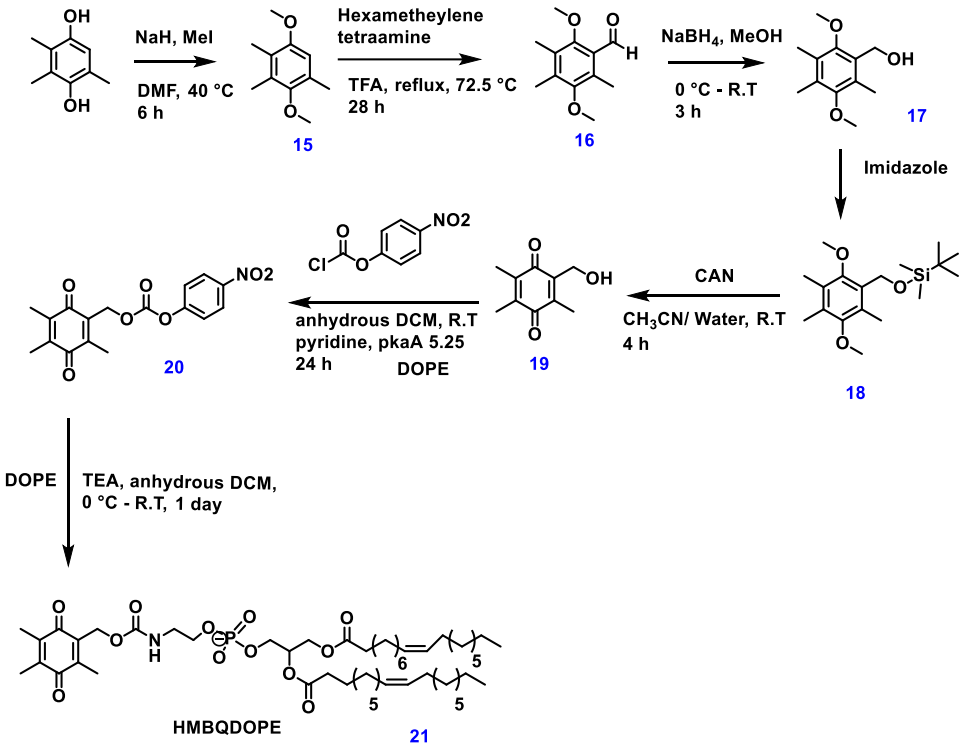

E.1. ^{1}H NMR of Dimethoxy trimethyl benzene (Compound 15)

1H NMR (400 MHz, CDCl3) δ 6.54 (s, 1H), 3.79 (s, 3H), 3.66 (s, 3H), 2.29 (s, 3H), 2.21 (s, 3H), 2.12 (s, 3H).

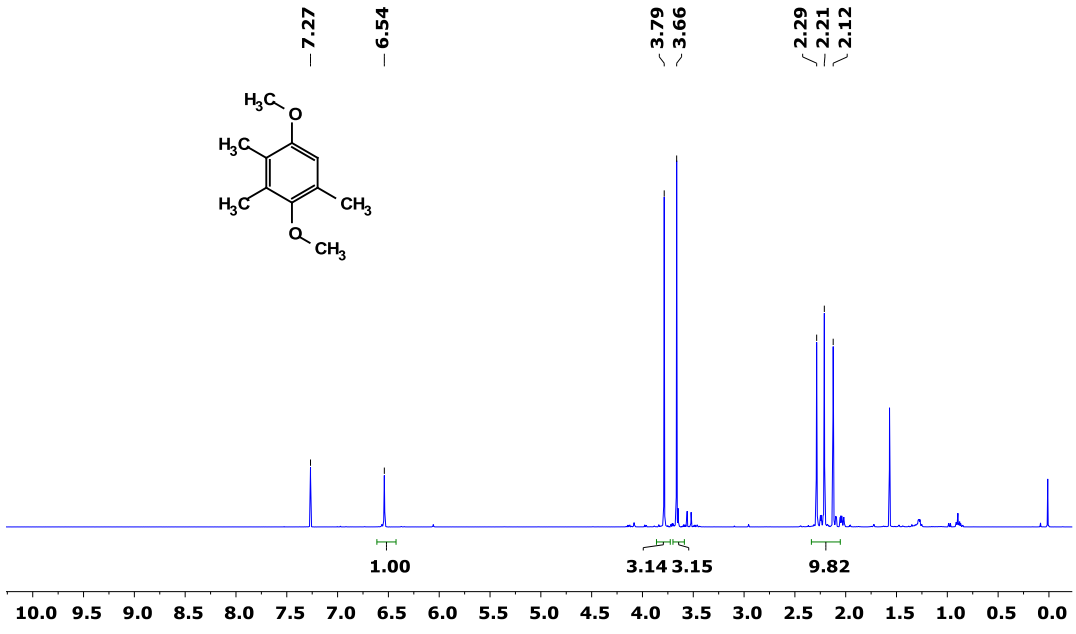

E.2. ^{1}H NMR of dimethoxy trimethyl benzaldehyde (Compound 16)

1H NMR (400 MHz, CDCl3) δ 10.49 (s), 7.26 (s), 3.78 (s), 3.66 (s), 2.50 (s), 2.27 (s), 2.21 (s).

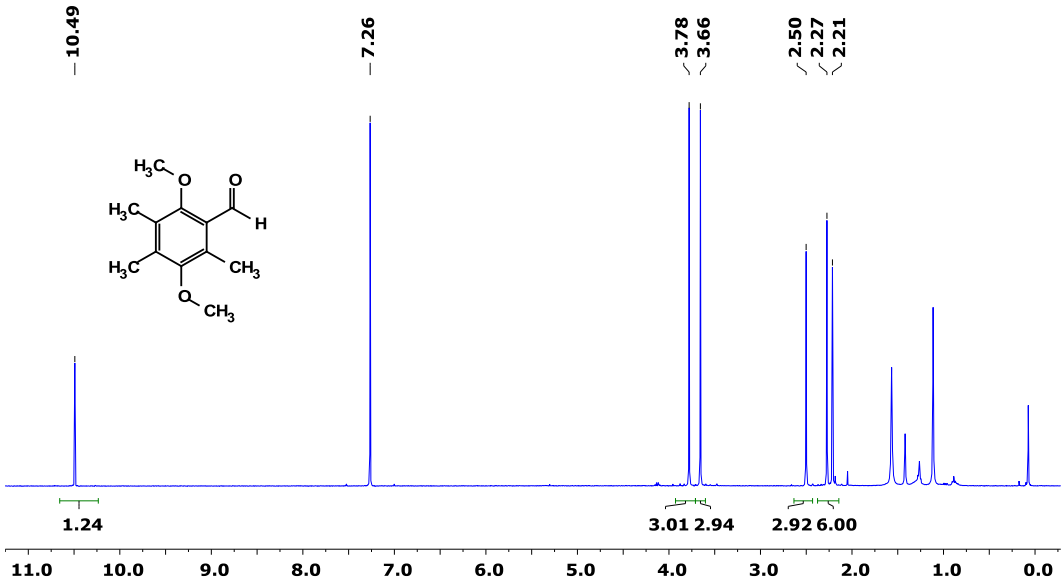

E.3. ^{1}H NMR of dimethoxy trimethyl benzyl alcohol (Compound 17)

1H NMR (400 MHz, CDCl3) δ 7.26, 4.74 (s), 3.74 (s), 3.66 (s), 2.32 (s), 2.21 (s), 1.78 (s).

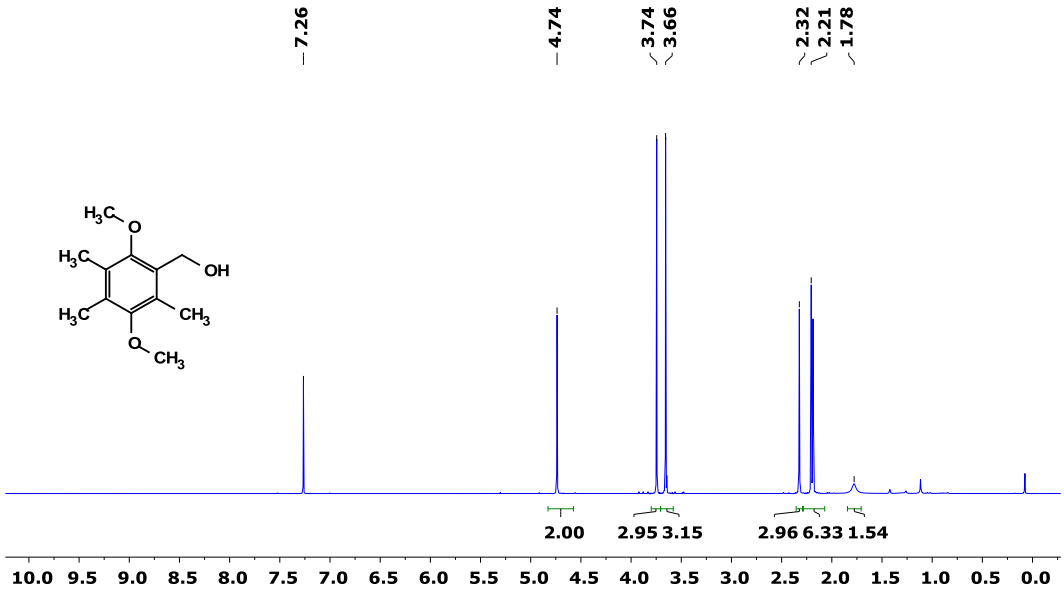

E.4. ^{1}H NMR of dimethoxy trimethylsilyl ether (Compound 18)

1H NMR (400 MHz, CDCl3) δ 4.74 (s), 3.74 (s), 3.67 (s), 2.33 (s), 2.21 (s), 2.20 (s), 0.94 (s), 0.15 (s).

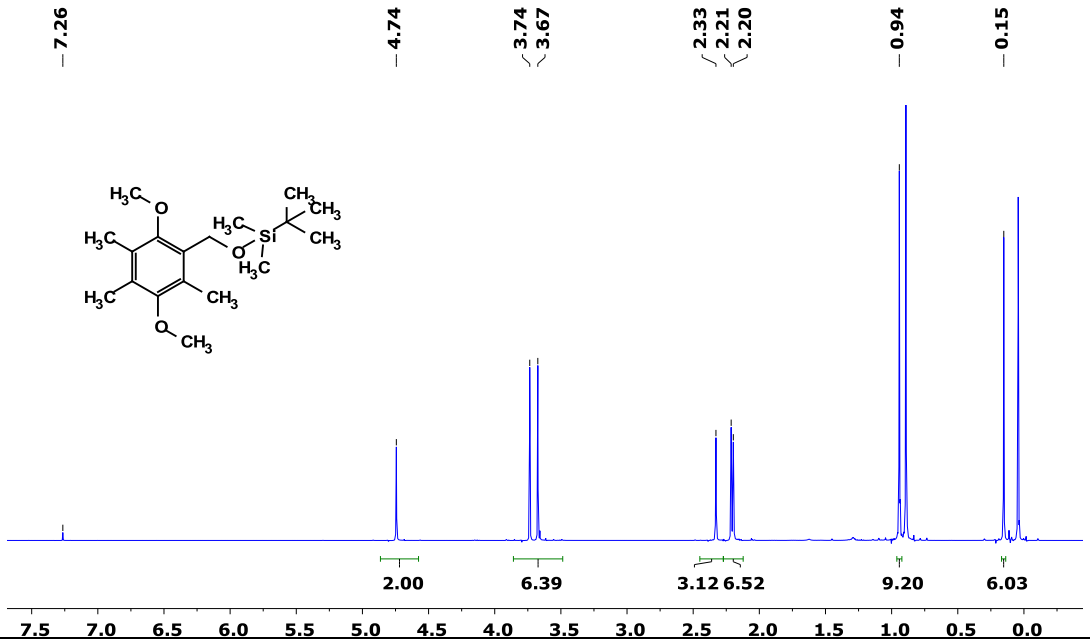

E.5. ^{1}H NMR of hydroxymethyl trimethyl benzoquinone (Compound 19)

1H NMR (400 MHz, CDCl3) δ 4.56 (s), 2.10 (s), 2.04 (s), 2.03 (s).

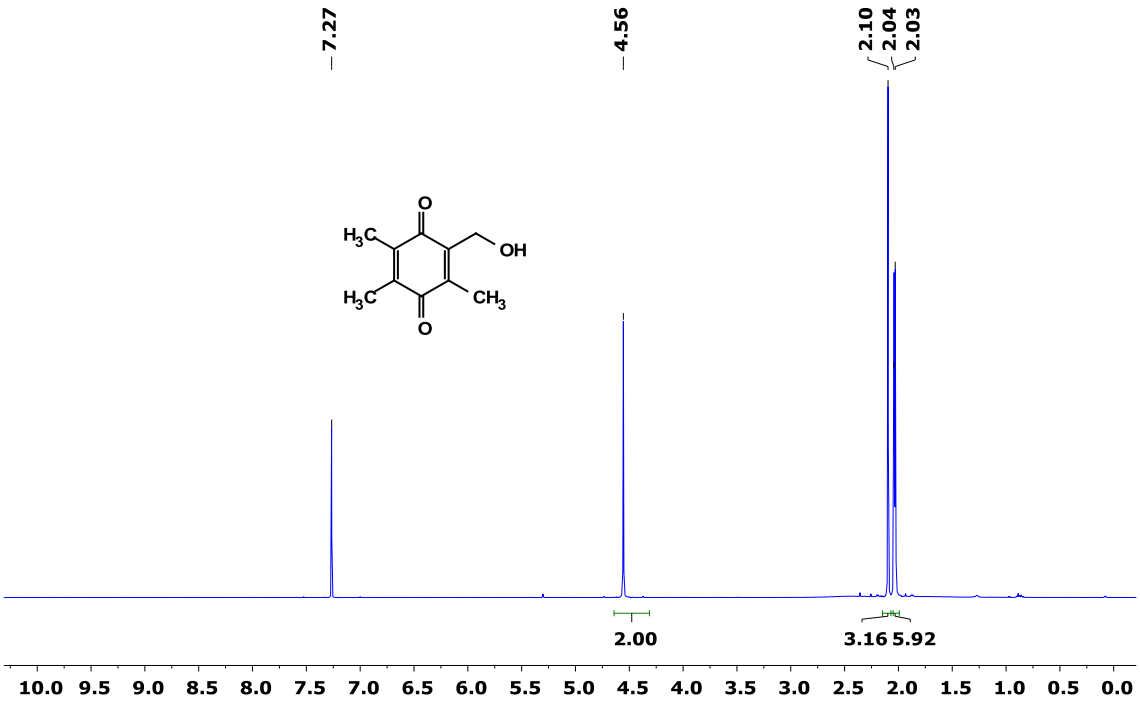

E.6. ^{1}H NMR of MS of nitrophenyl quinone carbonate (Compound 20)

1H NMR (400 MHz, CDCl3) δ 8.28 (d, J = 9.20), 7.40 (d, J = 9.20), 5.26 (s), 2.21 (s), 2.08 (s).

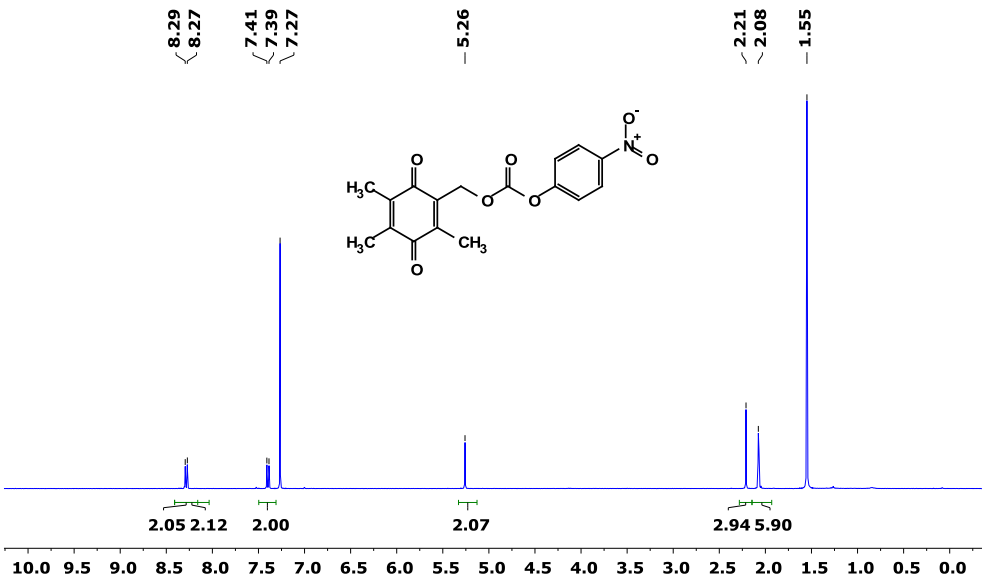

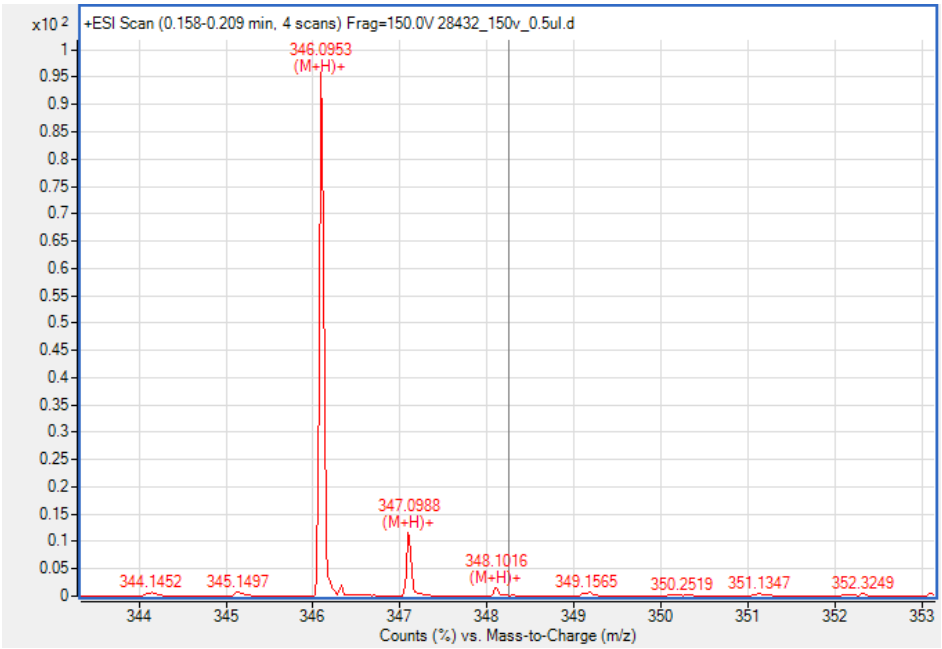

E.7. ^{1}H NMR of and MS of HMBQDOPE (Compound 21)

1H NMR (500 MHz, $CDCl_3$) δ 5.33 (m, 5H), 4.73 (m, 2H), 4.36 (m, 2H), 4.05-3.96 (b, 6H), 2.28 (m 3H), 2.00 (m 14H), 1.57 (m 4H), 1.26 (m 32H), 0.89 (s, 6H).

HRMS (ESI) calculated for $C_{52}H_{88}O_{12}NP$ [M-H]- 948.5971, found 948.5974 (0.16 ppm).

HRMS (ESI) calculated for $C_{52}H_{88}O_{12}NP$ [M+Na]+ 972.5936, found 972.5917 (2.83 ppm).

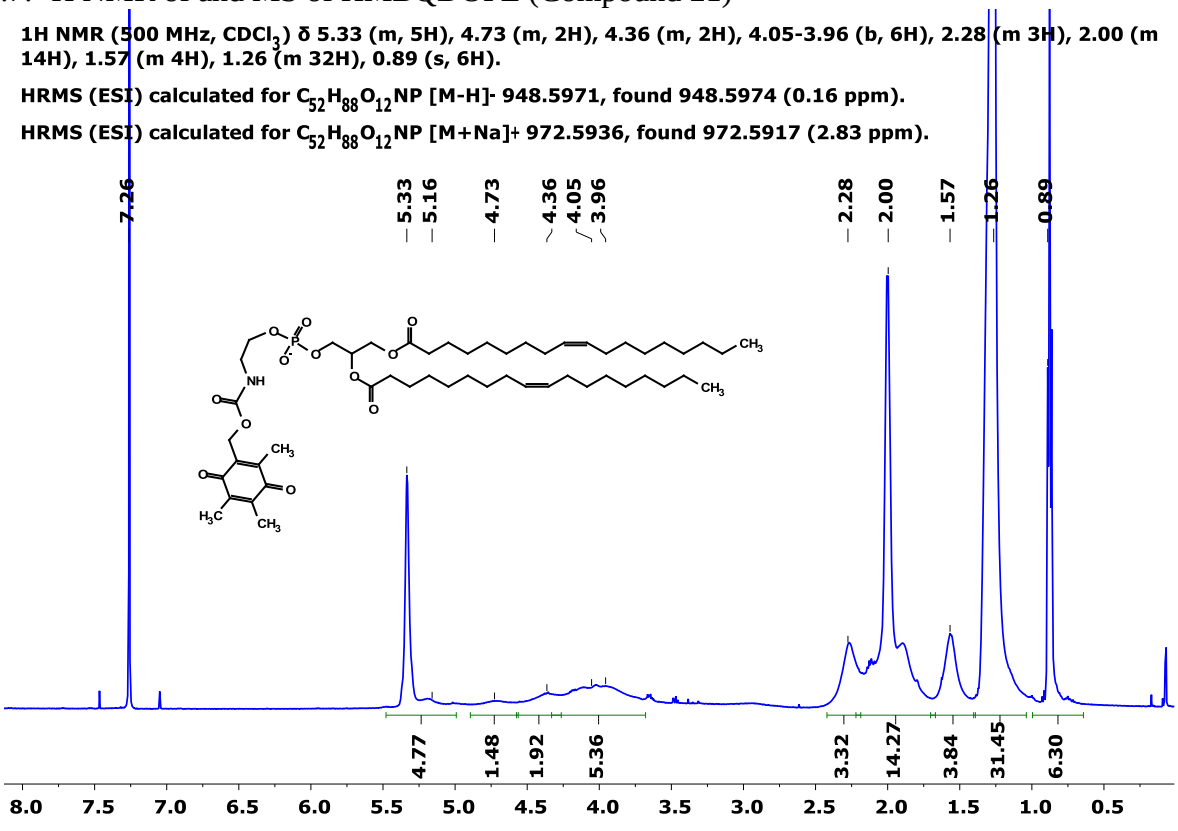

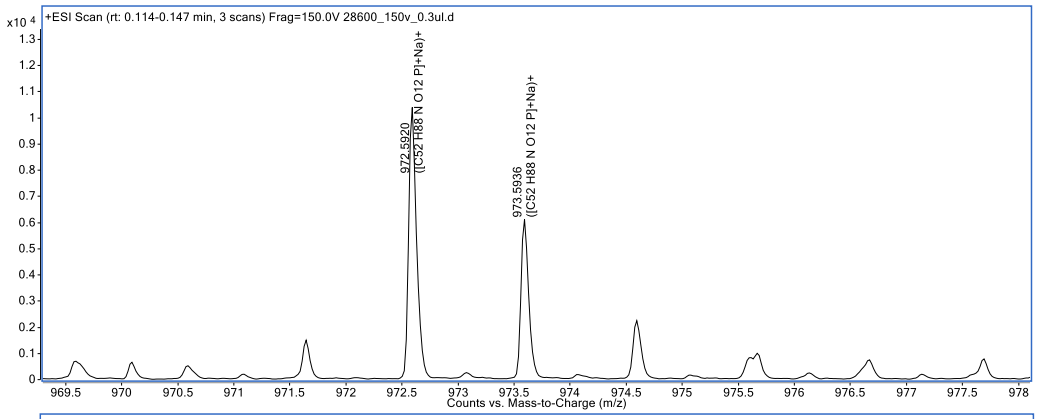

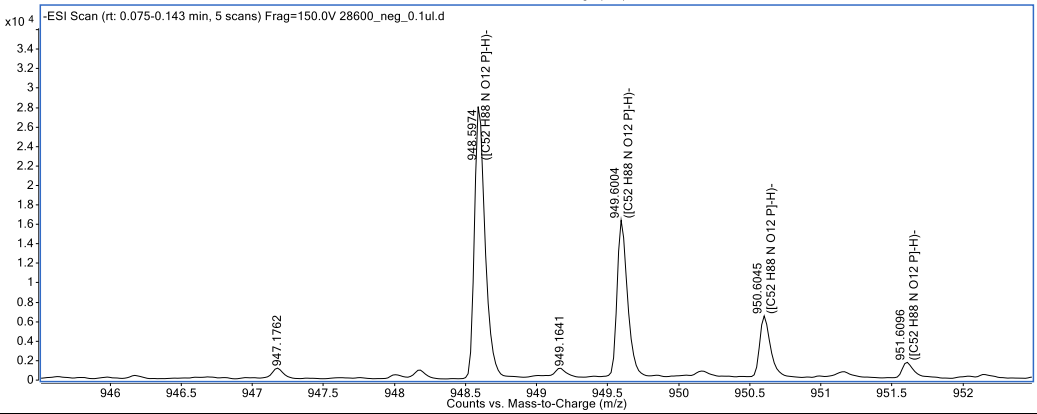

E.8. ^{1}H NMR of and MS of NitroDOPE (Byproduct of the step producing Compound 21)

1H NMR (500 MHz, $CDCl_3$) δ 8.16 (d, 2H, J = 8.65), 7.29 (d, 2H, J = 20.51 Hz) 5.33 (m, 5H), 4.38 (m 1H, 4.12), 3.97, 3.46, 2.23, 2.00, 1.53, 1.26, 0.87.

HRMS (ESI) calculated for $C_{48}H_{81}O_{12}N_2P$ [M-H]· 907.5353, found 907.5454 (0.16 ppm).

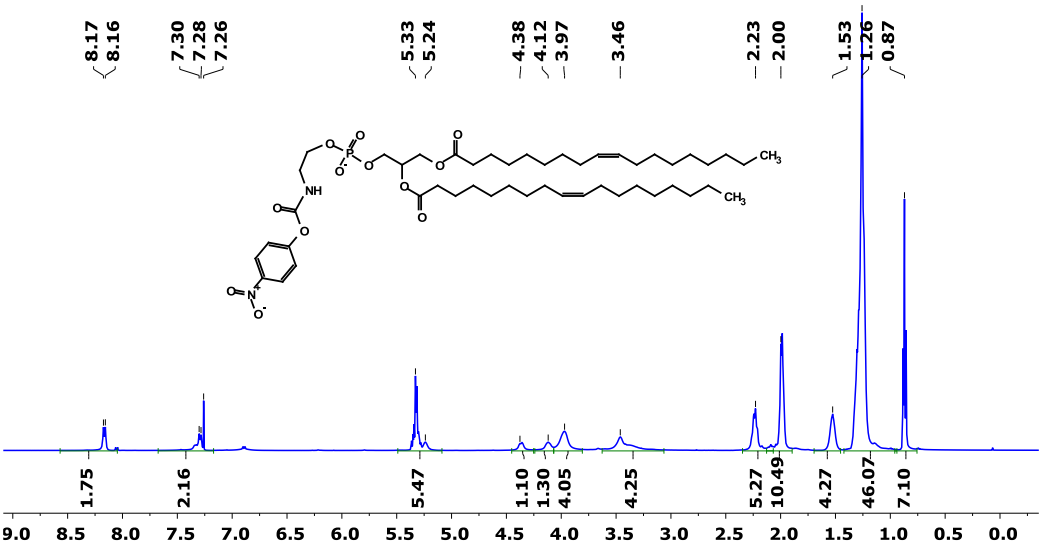

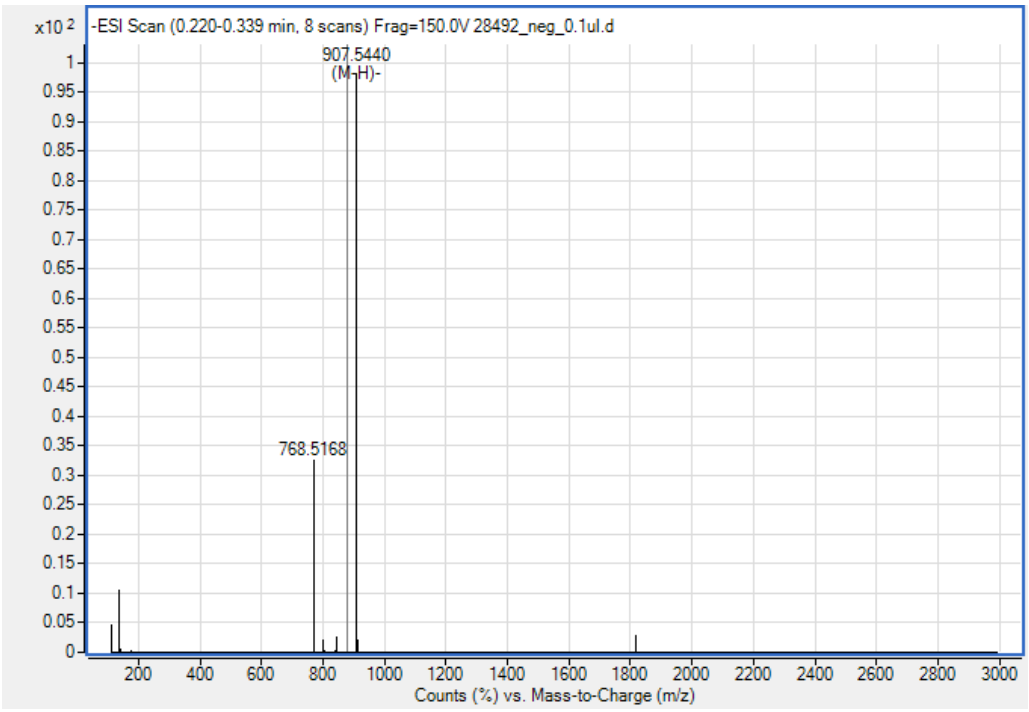

APPENDIX F. ^{1}H NMR, ^{13}C NMR, AND MS OF MALACHITE GREEN DERIVATIES

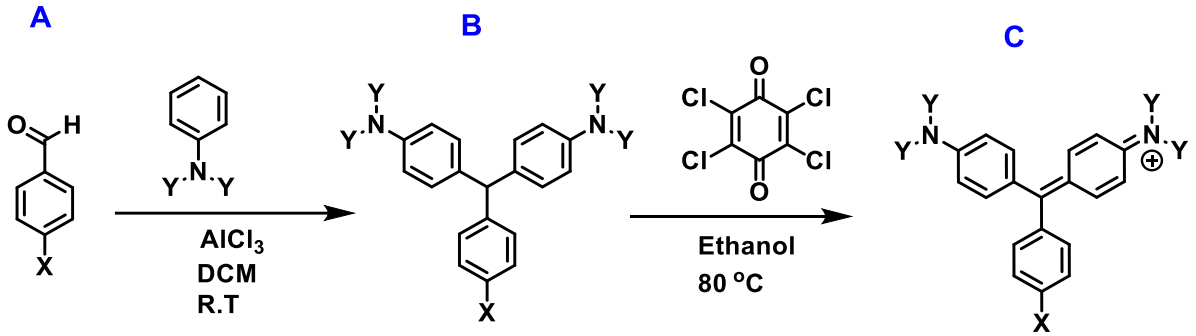

X = H, CH_3, NO_2, Cl, NH_2
Y = CH_3, C_2H_5

B1: X = NO_2, Y = CH_3
B2: X = Cl, Y = CH_3
B3: X = CH_3, Y = CH_3
B4: X = NO_2, Y = C_2H_5
B5: X = NH2, Y = C_2H_5

C1: X = NO_2, Y = CH_3
C2: X = Cl, Y = CH_3
C3: X = CH_3, Y = CH_3
C4: X = NO_2, Y = C_2H_5
C5: X = NH2, Y = C_2H_5

F.1. ^{1}H NMR, ^{13}C NMR, and MS of $MGNO_2$-H (Compound B1)

1H NMR (400 MHz, $CDCl_3$) δ 8.11 (d, 2H, J = 8.82), 7.29 (d, 2H, J = 8.44), 6.94 (d, 4H, J = 8.65), 6.68 (d, 4H, J = 7.55), 5.45 (s, 1H), 2.93 (s, 12H).

HRMS (ESI) calculated for $C_{23}H_{25}O_2N_3$ [M+H]+ 376.2039, found 376.2039 (0.1 ppm).

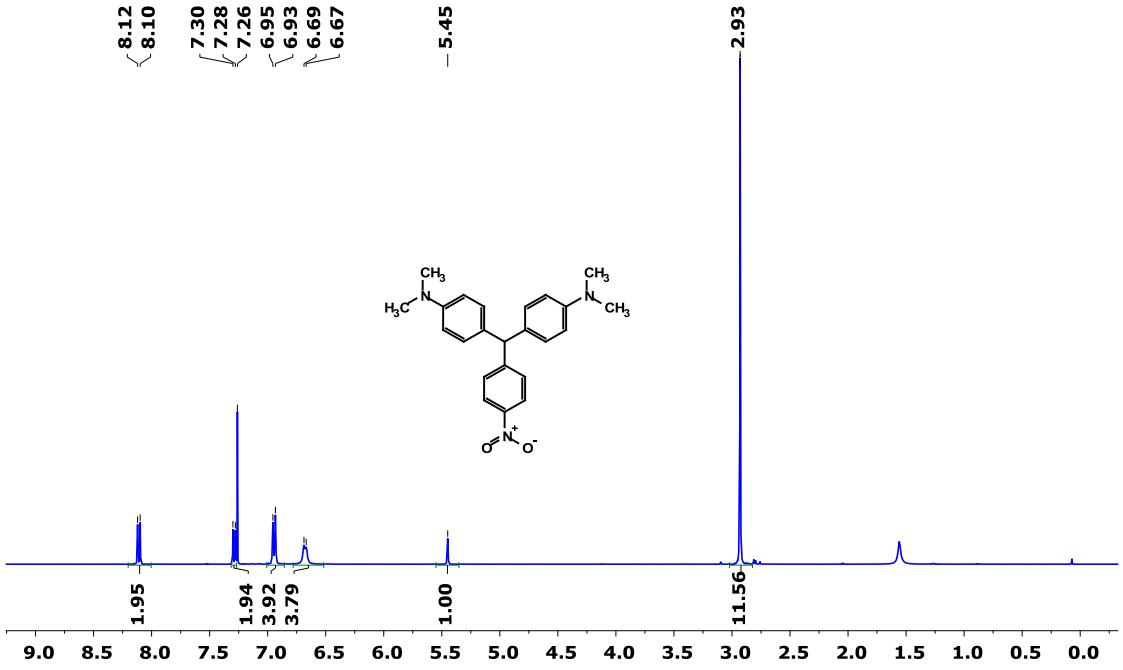

13C NMR (126 MHz, $CDCl_3$) δ 153.45, 149.22, 146.17, 130.93, 130.06, 129.83, 123.36, 112.55, 54.90, 40.60.

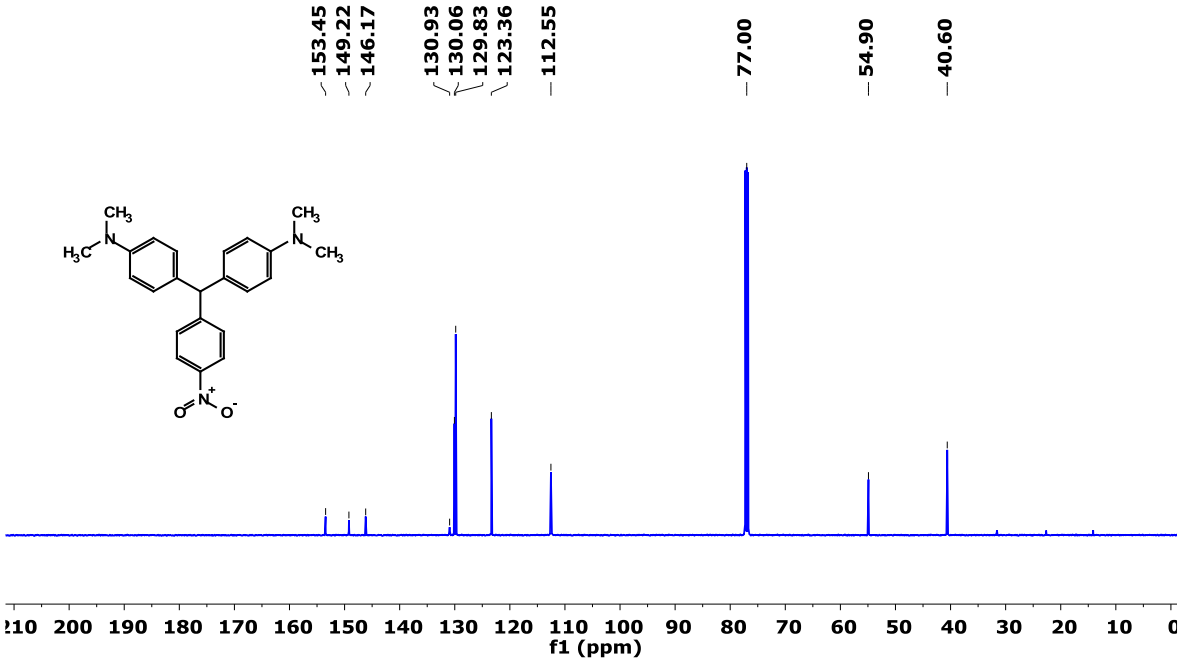

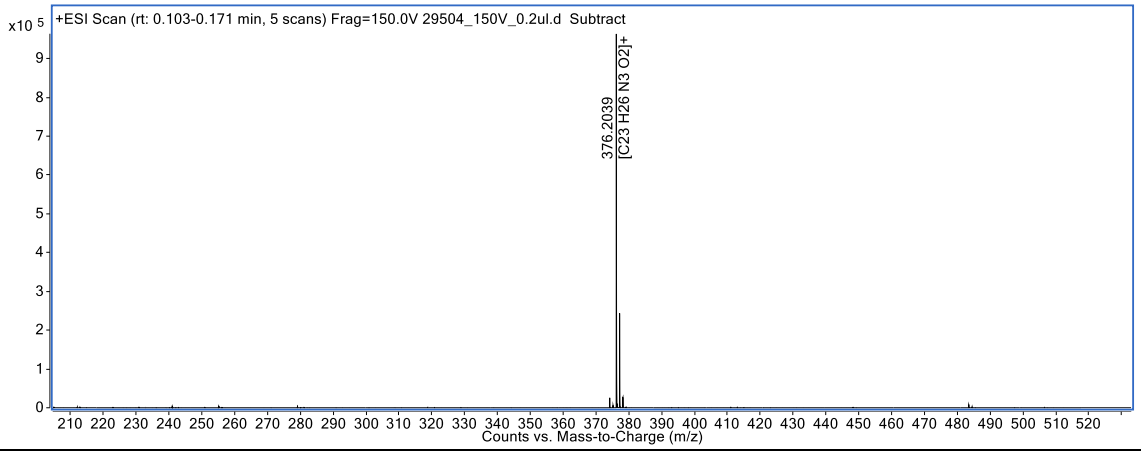

F.2. ^{1}H NMR, ^{13}C NMR, and MS of $MGNO_2$-OH (Hydration product of compound B1)

1H NMR (500 MHz, $CDCl_3$) δ 8.13 (d, 2H, J = 8.94 Hz), 7.56 (D, 2H, J = 8.94 Hz), 7.08 (d, 4H, J = 8.93 Hz), 6.66 (d, 4H, J = 8.91 Hz), 2.95 (s, 12 H).

HRMS (ESI) calculated for $C_{23}H_{25}O_3N_3$ $[M+H]^+$ 392.1969, found 392.1989 (2.1 ppm).

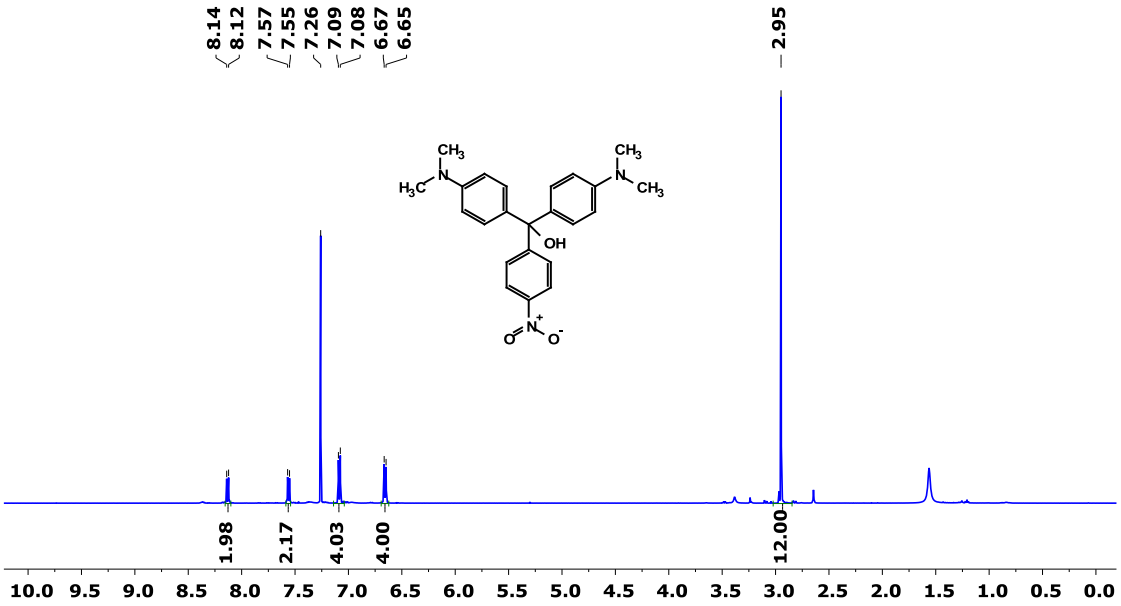

13C NMR (126 MHz, CDCl3) δ 155.20, 149.76, 146.56, 133.95, 128.69, 122.86, 111.76, 96.11, 81.28, 40.42.

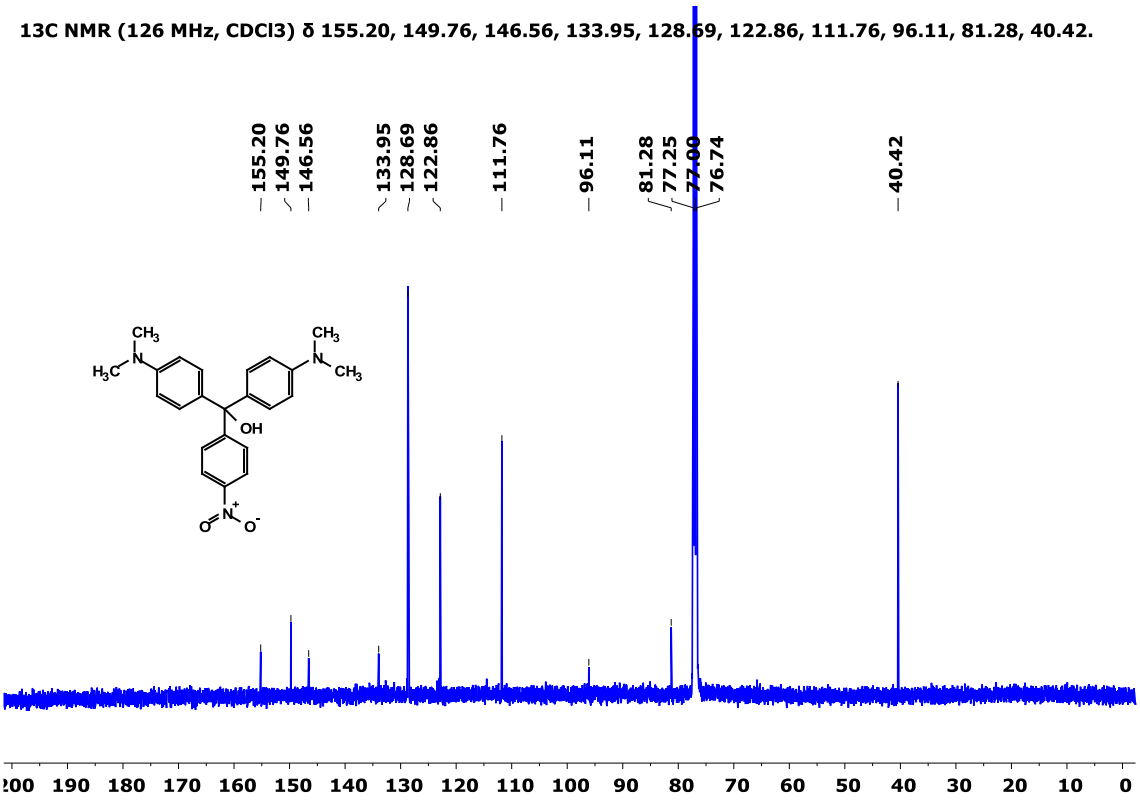

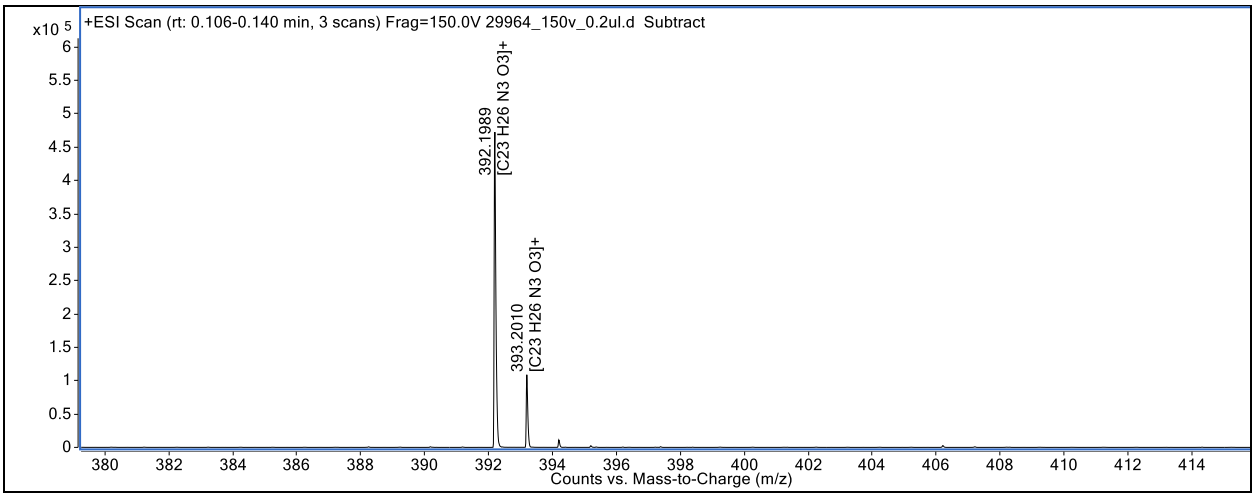

F.3. ^{1}H NMR, ^{13}C NMR, and MS of $MGNO_2^+$ (Compound C1)

1H NMR (400 MHz, $CDCl_3$) δ 8.13 (d, 2H, J = 8.53 Hz), 7.56 (d, 2H, J = 8.49 Hz), 7.09 (d, 4H, J = 8.48 Hz), 6.66 (d, 4H, J =8.26 Hz), 2.95 (s, 12H).

HRMS (ESI) calculated for $C_{23}H_{24}O_2N_3^+$ [M]+ 374.1863, found 374.1877 (2.4 ppm).

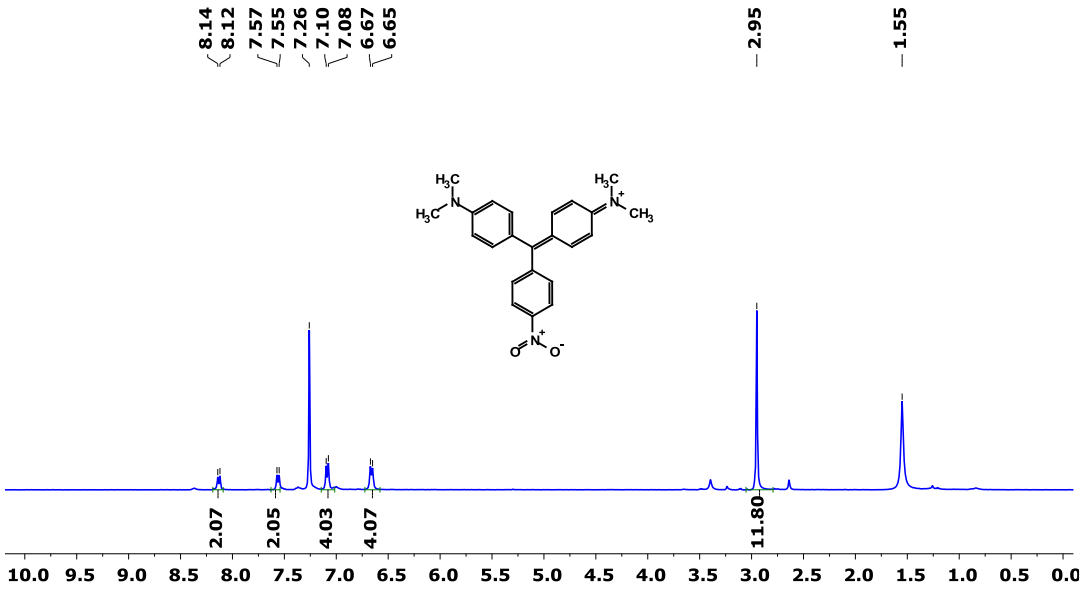

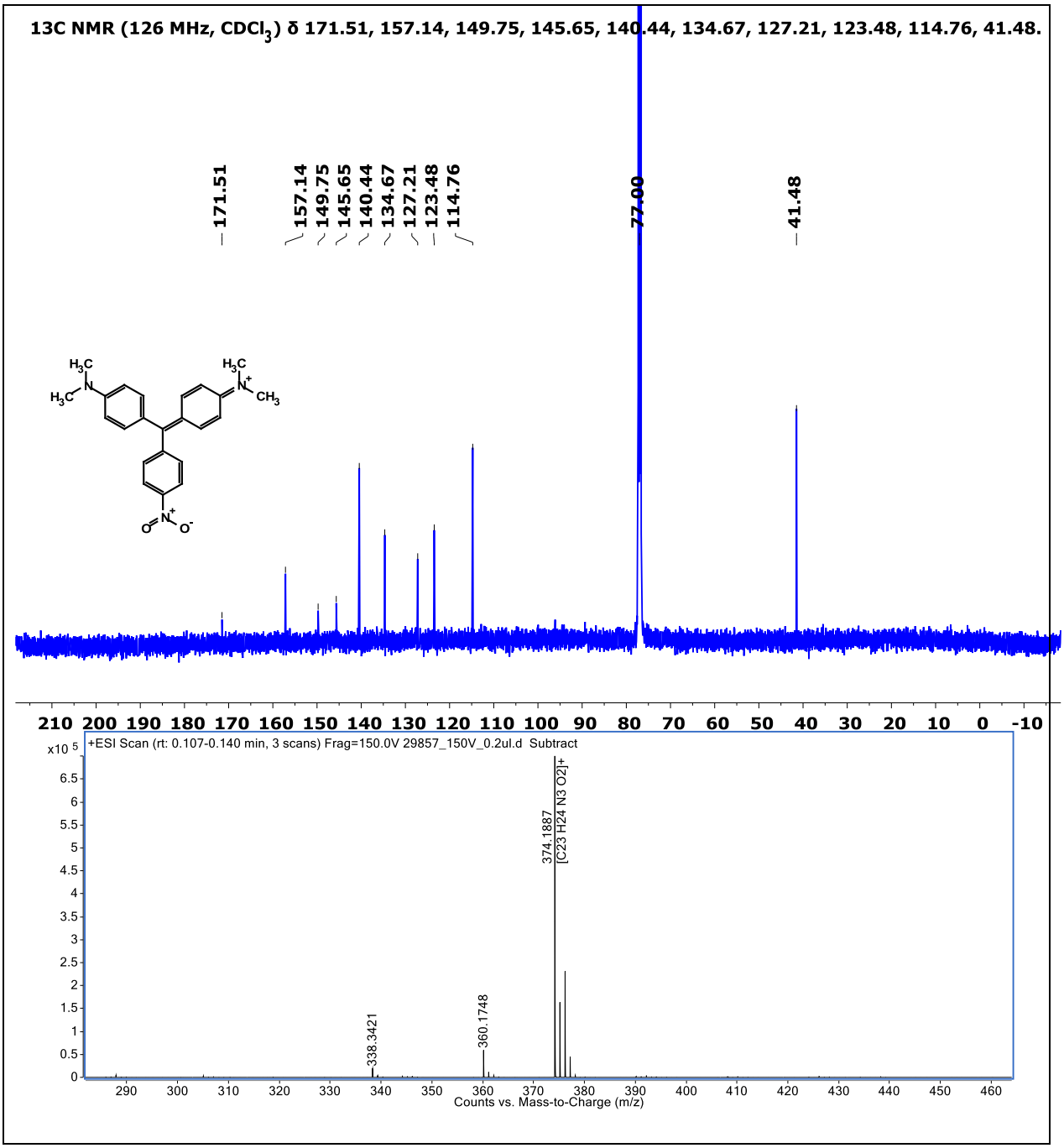
13C NMR (126 MHz, CDCl3) δ 171.51, 157.14, 149.75, 145.65, 140.44, 134.67, 127.21, 123.48, 114.76, 41.48.
171.51
157.14
149.75
145.65
140.44
134.67
127.21
123.48
114.76
77.00
41.48
210 200 190 180 170 160 150 140 130 120 110 100 90 80 70 60 50 40 30 20 10 0 -10
x10 5
+ESI Scan (rt: 0.107-0.140 min, 3 scans) Frag=150.0V 29857_150V_0.2ul.d Subtract
374.1887
[C23 H24 N3 O2]+
360.1748
338.3421
Counts vs. Mass-to-Charge (m/z)

F.4. ^{1}H NMR of and MS of MGCH3-H (Compound B3)

1H NMR (400 MHz, $CDCl_3$) δ 7.08 (d, 2H, J = 27.24 Hz), 7.08 (d, 2H, J =10.99 Hz), 7.03 (d, 2H, J = 8.66 Hz), 6.71 (d, 4H, J =8.77 Hz), 5.38 (s, 1H), 2.94 (s, 12H), 2.35 (s, 3H).

HRMS (ESI) calculated for $C_{24}H_{28}N_2$ [M+H]+ 345.2325, found 345.2319 (0.7 ppm).

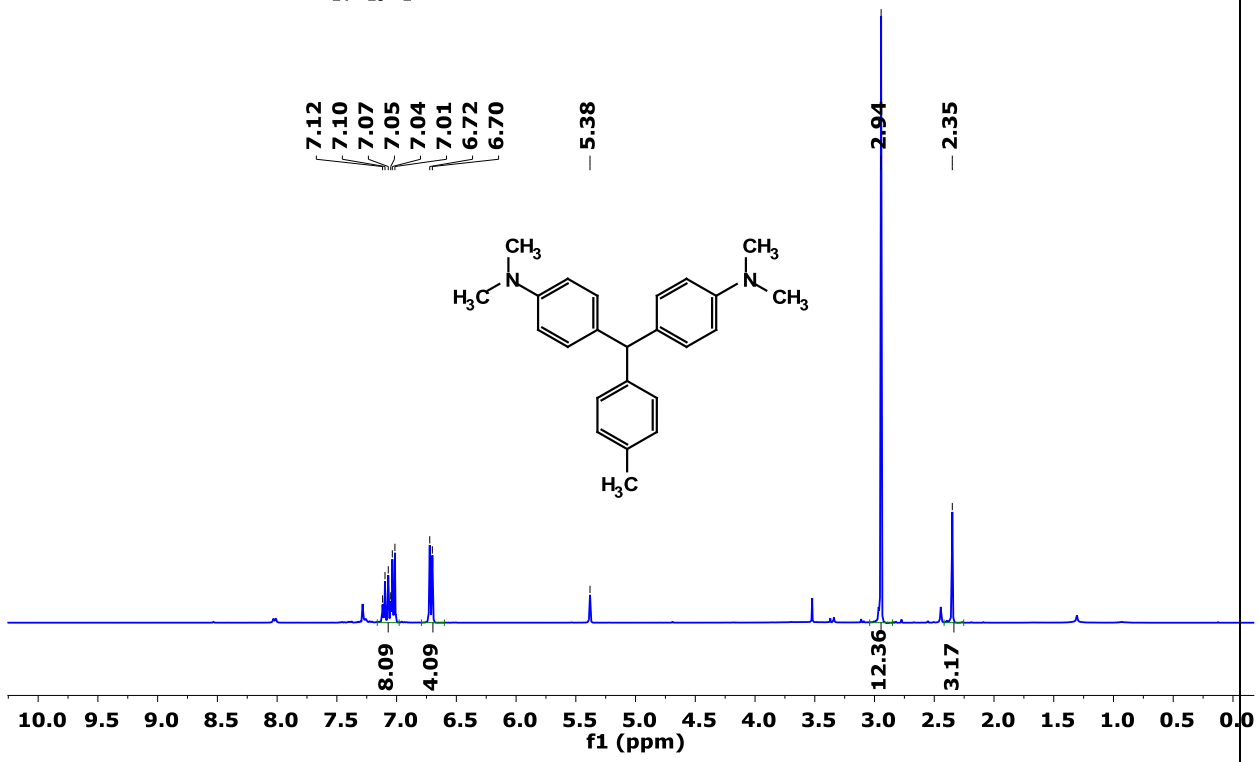

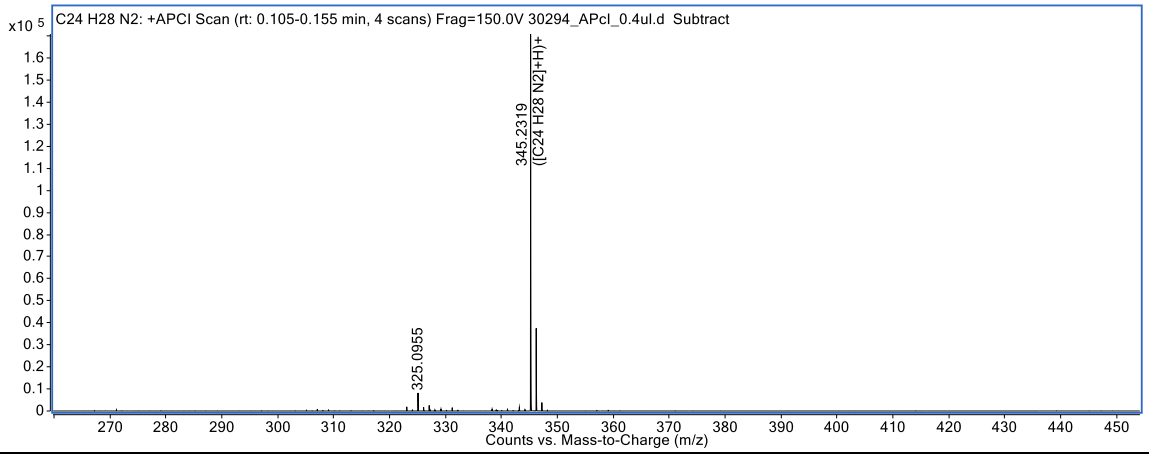

F.5. MS of $MGCl^+$ (Compound C2)

HRMS (ESI) calculated for $C_{23}H_{24}N_2Cl^+$ [M]+ 363.1623, found 363.1623 (0.1 ppm).

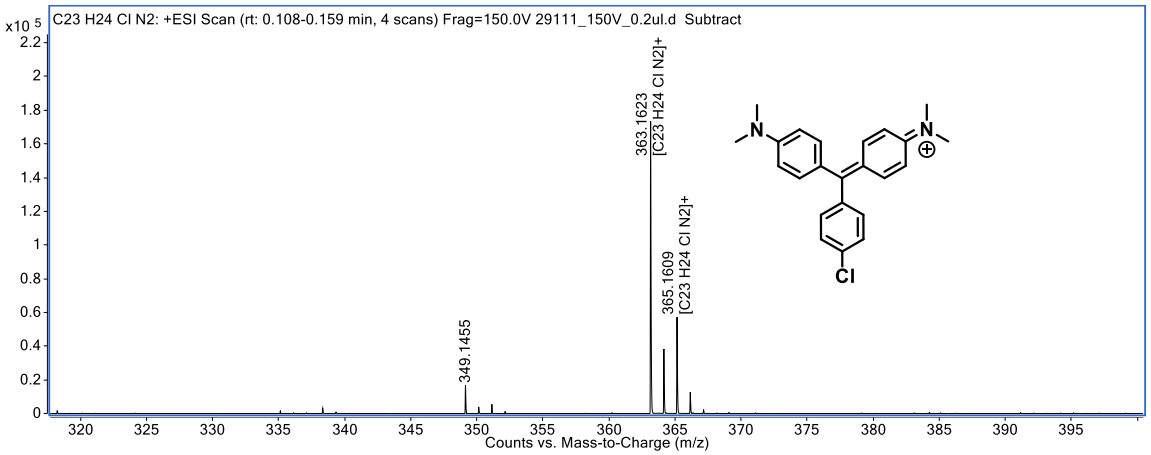

F.6. ^1H NMR of and MS of BGNO2-H (Compound B4)

1H NMR (400 MHz, $CDCl_3$) δ 8.22 (d, 2H, J = 8.74 Hz)), 7.44 (d, 2H, J = 8.70 Hz), 7.07 (d, 4H, J = 8.74 Hz), 6.75 (d, 4H, J = 11.99 Hz), 5.53 (s, 1H), 3.45 (q, 8H), 1.28 (t, 12H, J = 7.04).

HRMS (ESI) calculated for $C_{27}H_{33}O_3N_2$ [M+H]+ 432.2646, found 4322643 (0.3 ppm).

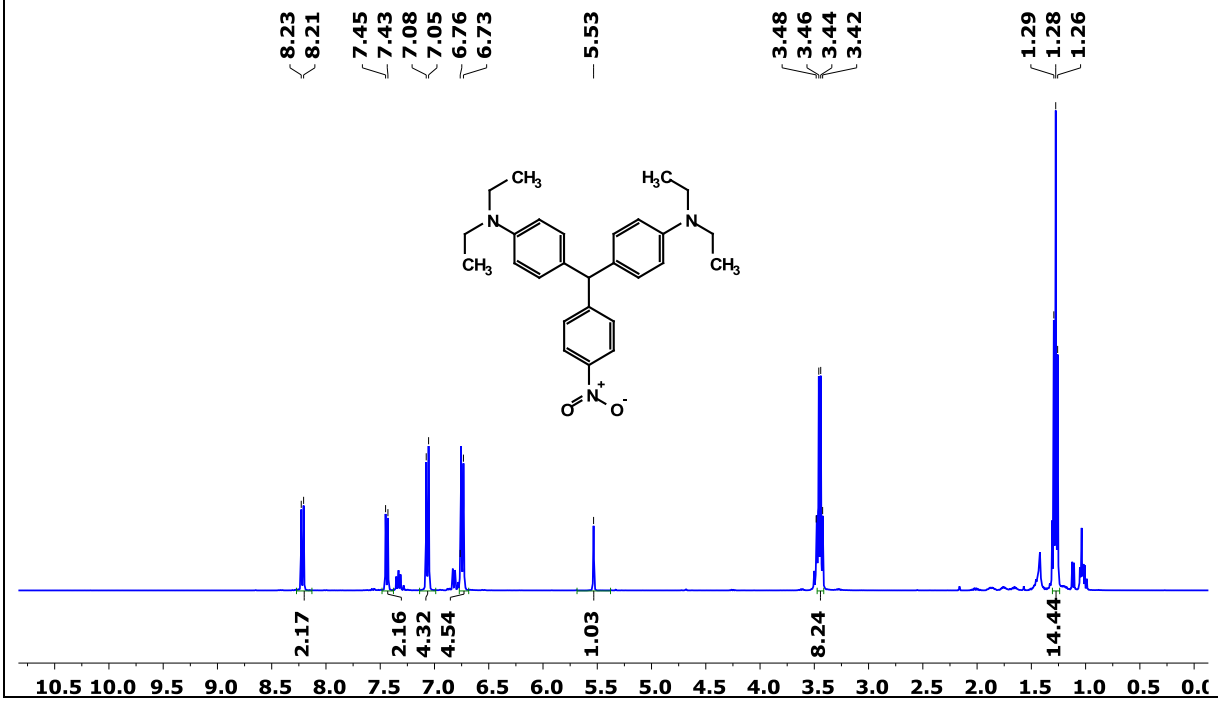

F.7. MS of $BGNO2^+$ (Compound C4)
HRMS (ESI) calculated for $C_{27}H_{32}N_3O_2^+$ $[M]^+$ 430.2489, found 430.2515 (2.6 ppm).

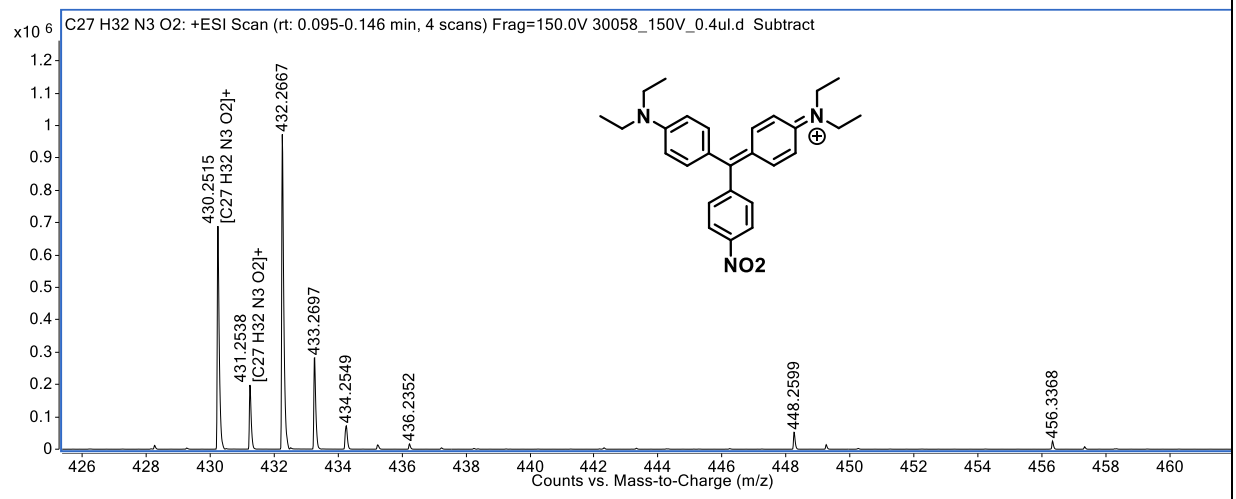

F.8. MS of $BGNH_2^+$ (Compound C5), and $BGNH_2$-H (Compound B5)
HRMS (ESI) calculated for ($BGNH_2$-H) $C_{27}H_{35}N_3$ $[M+H]^+$ 402.2904, found 400.2913 (0.9 ppm), for ($BGNH_2^{+)}$ $C_{27}H_{34}N_3^+$ $[M]^+$ 400.2747, found 400.2764 (1.6 ppm).

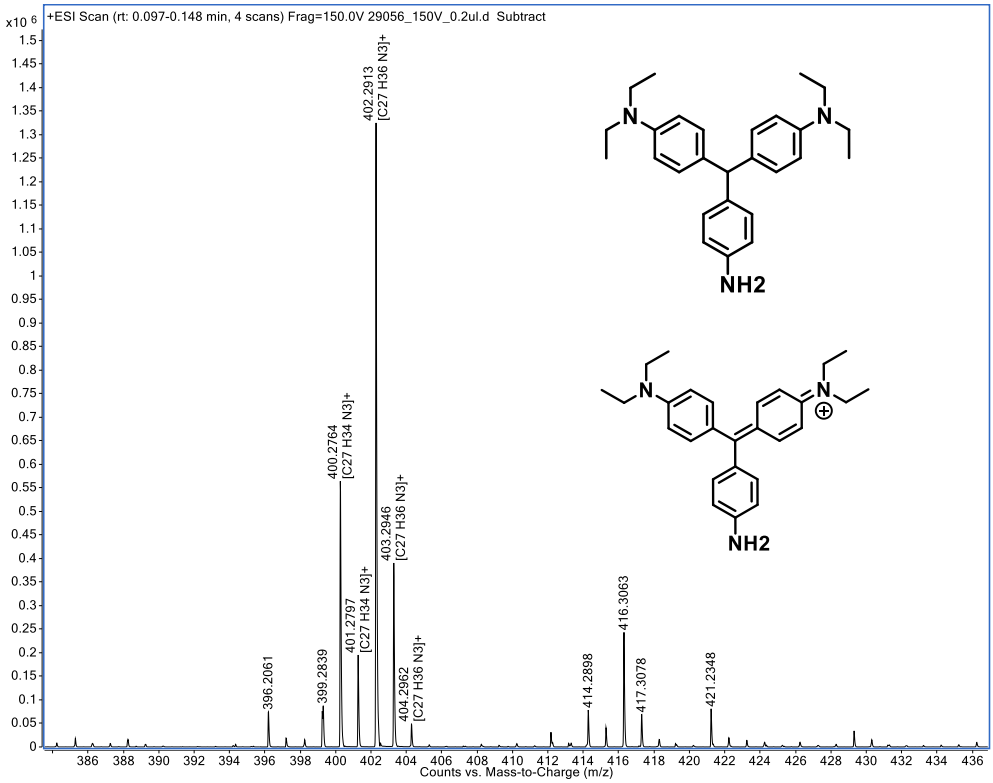

APPENDIX G. LIPID CONCENTRATION ASSAYS

G.1. Calibration curve of total organic phosphorous quantification by Steward assay

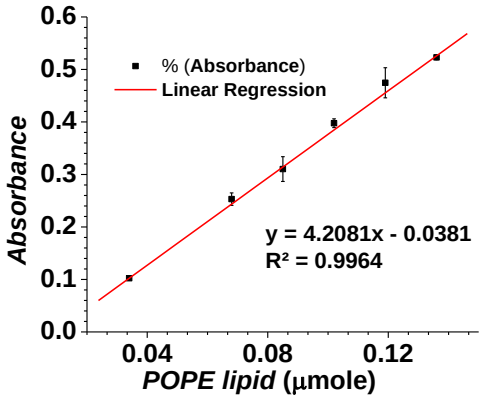

G.2. Calibration curve of total phosphorous quantification by Barlette assay

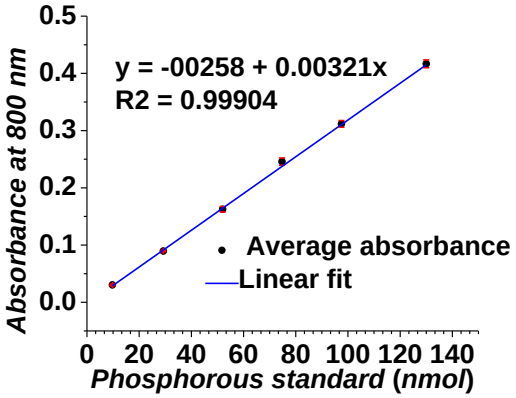

LIST OF REFERENCES

Abidian, M. R., et al., Conducting-Polymer Nanotubes for Controlled Drug Release. *Advanced Materials* **2006,** *18* (4), 405-409.

Aeffner, S., et al., Energetics of Stalk Intermediates in Membrane Fusion Are Controlled by Lipid Composition. *Proceedings of the National Academy of Sciences* **2012,** *109* (25), E1609-E1618.

Agarwal, A., et al., Remote Triggered Release of Doxorubicin in Tumors by Synergistic Application of Thermosensitive Liposomes and Gold Nanorods. *ACS Nano* **2011,** *5* (6), 4919-4926.

Ahmed, F., et al., Shrinkage of a Rapidly Growing Tumor by Drug-Loaded Polymersomes: Ph-Triggered Release through Copolymer Degradation. *Molecular Pharmaceutics* **2006,** *3* (3), 340-350.

Airley, R., *Cancer Chemotherapy: Basic Science to the Clinic*. John Wiley & Sons: 2009.

Akbarzadeh, A., et al., Liposome: Classification, Preparation, and Applications. *Nanoscale Research Letters* **2013,** *8* (1), 102.

Alavi, M., et al., Application of Various Types of Liposomes in Drug Delivery Systems. *Advanced Pharmaceutical bBulletin* **2017,** *7* (1), 3.

Al-Jamal, W. T., et al., Functionalized-Quantum-Dot–Liposome Hybrids as Multimodal Nanoparticles for Cancer. *Small* **2008,** *4* (9), 1406-1415.

Al-Jamal, W. T.; Kostarelos, K., Liposome–Nanoparticle Hybrids for Multimodal Diagnostic and Therapeutic Applications. **2007**.

An, X., et al., Photoinduced Drug Release from Thermosensitive Aunps-Liposome Using a Aunps-Switch. *Chemical Communications* **2010,** *46* (38), 7202-7204.

An, X., et al., Smart Photothermal-Triggered Bilayer Phase Transition in Aunps–Liposomes to Release Drug. *Langmuir : the ACS Journal of Surfaces and Colloids* **2013,** *29* (4), 1061-1068.

Andresen, T. L., et al., Enzymatic Release of Antitumor Ether Lipids by Specific Phospholipase A2 Activation of Liposome-Forming Prodrugs. *Journal of Medicinal Chemistry* **2004,** *47* (7), 1694-1703.

Andresen, T. L., et al., Enzyme-Triggered Nanomedicine: Drug Release Strategies in Cancer Therapy (Invited Review). *Molecular Membrane Biology* **2010,** *27* (7), 353-363.

Ansar, S. M., et al., Direct Quantification of Unencapsulated Doxorubicin in Liposomal Doxorubicin Formulations Using Capillary Electrophoresis. *International Journal of Pharmaceutics* **2018,** *549* (1-2), 109-114.

Ansar, S. M.; Mudalige, T., Direct and Simultaneous Determination of Intra-Liposomal and External Sulfate in Liposomal Doxorubicin Formulations by Capillary Electrophoresis/Inductively Coupled Plasma-Tandem Mass Spectrometry (Ce/Icp-Ms/Ms). *International Journal of Pharmaceutics* **2019,** *561*, 283-288.

Anselmo, A. C.; Mitragotri, S., Nanoparticles in the Clinic. *Bioengineering & Translational Medicine* **2016,** *1* (1), 10-29.

Antimisiaris, S., et al., Exosomes and Exosome-Inspired Vesicles for Targeted Drug Delivery. *Pharmaceutics* **2018,** *10* (4), 218.

Antonny, B., et al., From Zero to Six Double Bonds: Phospholipid Unsaturation and Organelle Function. *Trends in Cell Biology* **2015,** *25* (7), 427-436.

Au, J. L., et al., Delivery of Cancer Therapeutics to Extracellular and Intracellular Targets: Determinants, Barriers, Challenges and Opportunities. *Adv Drug Deliv Rev* **2016,** *97*, 280-301.

Aubry, L., et al., Kinetics of Endosomal Ph Evolution in Dictyostelium Discoideum Amoebae. Study by Fluorescence Spectroscopy. *Journal of cell science* **1993,** *105* (3), 861-866.

Auguste, D. T., et al., Triggered Release of Sirna from Poly (Ethylene Glycol)-Protected, Ph-Dependent Liposomes. *Journal of Controlled Release* **2008,** *130* (3), 266-274.

Azagarsamy, M. A., et al., Enzyme-Triggered Disassembly of Dendrimer-Based Amphiphilic Nanocontainers. *Journal of the American Chemical Society* **2009,** *131* (40), 14184-14185.

Azevedo, C., et al., Strategies for the Enhanced Intracellular Delivery of Nanomaterials. *Drug Discovery Today* **2018,** *23* (5), 944-959.

Bader, R. A.; Wardwell, P. R., Polysialic Acid: Overcoming the Hurdles of Drug Delivery. *Therapeutic Delivery* **2014,** *5* (3), 235-237.

Bae, Y., et al., Design of Environment-Sensitive Supramolecular Assemblies for Intracellular Drug Delivery: Polymeric Micelles That Are Responsive to Intracellular Ph Change. *Angewandte Chemie International Edition* **2003,** *42* (38), 4640-4643.

Balasubramanian, S. K., et al., Biodistribution of Gold Nanoparticles and Gene Expression Changes in the Liver and Spleen after Intravenous Administration in Rats. *Biomaterials* **2010,** *31* (8), 2034-2042.

Barenholz, Y. C., Doxil®—the First Fda-Approved Nano-Drug: Lessons Learned. *Journal of Controlled Release* **2012,** *160* (2), 117-134.

Barghouthi, Z.; Amereih, S., Spectrophotometric Determination of Fluoride in Drinking Water Using Aluminium Complexes of Triphenylmethane Dyes. *Water SA* **2012,** *38* (4), 543-548.

Bayer, A. M., et al., Triggered Liposomal Release through a Synthetic Phosphatidylcholine Analogue Bearing a Photocleavable Moiety Embedded within the Sn-2 Acyl Chain. *Chemistry–A European Journal* **2014,** *20* (12), 3350-3357.

Bazak, R., et al., Cancer Active Targeting by Nanoparticles: A Comprehensive Review of Literature. *Journal of Cancer Research and Clinical Oncology* **2015,** *141* (5), 769-784.

Bentz, J.; Ellens, H., Membrane Fusion: Kinetics and Mechanisms. *Colloids and Surfaces* **1987,** *30* (1), 65-112.

Besterman, J. M.; Low, R. B., Endocytosis: A Review of Mechanisms and Plasma Membrane Dynamics. *Biochemical Journal* **1983,** *210* (1), 1.

Bhal, S. K., Lipophilicity Descriptors: Understanding When to Use Logp & Logd. *ACD/Labs PhysChem Software Application Notes* **2007**.

Bibi, S., et al., Trigger Release Liposome Systems: Local and Remote Controlled Delivery? *Journal of Microencapsulation* **2012,** *29* (3), 262-276.

Bisby, R. H., et al., Active Uptake of Drugs into Photosensitive Liposomes and Rapid Release on Uv Photolysis¶. *Photochemistry and Photobiology* **2000,** *72* (1), 57-61.

Bisby, R. H., et al., Fast Laser-Induced Solute Release from Liposomes Sensitized with Photochromic Lipid: Effects of Temperature, Lipid Host, and Sensitizer Concentration. *Biochemical and Biophysical Research Communications* **1999,** *262* (2), 406-410.

Boggara, M. B., et al., Structural Association of Nonsteroidal Anti-Inflammatory Drugs with Lipid Membranes. *Journal of the American Chemical Society* **2012,** *134* (48), 19669-19676.

Bondurant, B., et al., Photoinitiated Destabilization of Sterically Stabilized Liposomes. *Biochimica et Biophysica Acta (BBA)-Biomembranes* **2001,** *1511* (1), 113-122.

Bonnaud, C., et al., Insertion of Nanoparticle Clusters into Vesicle Bilayers. *ACS Nano* **2014,** *8* (4), 3451-3460.

Bourgaux, C.; Couvreur, P., Interactions of Anticancer Drugs with Biomembranes: What Can We Learn from Model Membranes? *Journal of Controlled Release* **2014,** *190*, 127-138.

Bozzuto, G.; Molinari, A., Liposomes as Nanomedical Devices. *International Journal of Nanomedicine* **2015,** *10*, 975.

Brannon-Peppas, L.; Blanchette, J. O., Nanoparticle and Targeted Systems for Cancer Therapy. *Advanced Drug Delivery Reviews* **2012,** *64*, 206-212.

Bray, F., et al., Global Cancer Statistics 2018: Globocan Estimates of Incidence and Mortality Worldwide for 36 Cancers in 185 Countries. *CA: a Cancer Journal for Clinicians* **2018,** *68* (6), 394-424.

Brocca, P., et al., Shape Fluctuations of Large Unilamellar Lipid Vesicles Observed by Laser Light Scattering: Influence of the Small-Scale Structure. *Langmuir : the ACS Journal of Surfaces and Colloids* **2004,** *20* (6), 2141-2148.

Brock, R., The Uptake of Arginine-Rich Cell-Penetrating Peptides: Putting the Puzzle Together. *Bioconjugate Chemistry* **2014,** *25* (5), 863-868.

Bulbake, U., et al., Liposomal Formulations in Clinical Use: An Updated Review. *Pharmaceutics* **2017,** *9* (2), 12.

Bunggulawa, E. J., et al., Recent Advancements in the Use of Exosomes as Drug Delivery Systems. *Journal of Nanobiotechnology* **2018,** *16* (1), 81.

Burgoyne, R. D.; Morgan, A., Membrane Trafficking: Three Steps to Fusion. *Current Biology* **2007,** *17* (7), R255-R258.

Butet, J., et al., Optical Second Harmonic Generation in Plasmonic Nanostructures: From Fundamental Principles to Advanced Applications. *ACS Nano* **2015,** *9* (11), 10545-10562.

Caffrey, M., et al., A Database of Lipid-Phase Transition Temperatures and Enthalpy Changes. *Journal of Chemical Information and Computer Sciences* **1991,** *31* (2), 275-284.

Campagnola, P. J.; Dong, C. Y., Second Harmonic Generation Microscopy: Principles and Applications to Disease Diagnosis. *Laser & Photonics Reviews* **2011,** *5* (1), 13-26.

Casal, H. L.; Mantsch, H. H., Polymorphic Phase Behaviour of Phospholipid Membranes Studied by Infrared Spectroscopy. *Biochimica et Biophysica Acta (BBA)-Reviews on Biomembranes* **1984,** *779* (4), 381-401.

Chandra, B., et al., Design of Photocleavable Lipids and Their Application in Liposomal "Uncorking". *Chemical Communications* **2005,** (24), 3021-3023.

Chandra, B., et al., Formulation of Photocleavable Liposomes and the Mechanism of Their Content Release. *Organic & Biomolecular Chemistry* **2006,** *4* (9), 1730-1740.

Charifson, P. S.; Walters, W. P., Acidic and Basic Drugs in Medicinal Chemistry: A Perspective. *Journal of Medicinal Chemistry* **2014,** *57* (23), 9701-9717.

Chatterjee, S.; Agarwal, S., Liposomes as Membrane Model for Study of Lipid Peroxidation. *Free Radical Biology and Medicine* **1988,** *4* (1), 51-72.

Chen, Y.; Steinmetz, M. G., Photoactivation of Amino-Substituted 1, 4-Benzoquinones for Release of Carboxylate and Phenolate Leaving Groups Using Visible Light. *The Journal of Organic Chemistry* **2006,** *71* (16), 6053-6060.

Chou, L. Y., et al., Strategies for the Intracellular Delivery of Nanoparticles. *Chemical Society Reviews* **2011,** *40* (1), 233-245.

Chu, C.-J., et al., Efficiency of Cytoplasmic Delivery by Ph-Sensitive Liposomes to Cells in Culture. *Pharmaceutical Research* **1990,** *7* (8), 824-834.

Cohen, B. E., Biological Imaging: Beyond Fluorescence. *Nature* **2010,** *467* (7314), 407.

Cooke, I. R.; Deserno, M., Coupling between Lipid Shape and Membrane Curvature. *Biophysical Journal* **2006,** *91* (2), 487-495.

Corn, R. M.; Higgins, D. A., Optical Second Harmonic Generation as a Probe of Surface Chemistry. *Chemical Reviews* **1994,** *94* (1), 107-125.

Cortajarena, A. L., et al., Engineering Iron Oxide Nanoparticles for Clinical Settings. *Nanobiomedicine* **2014,** *1* (Godište 2014), 1-2.

Cossart, P.; Helenius, A., Endocytosis of Viruses and Bacteria. *Cold Spring Harbor Perspectives in Biology* **2014,** *6* (8), a016972.

Cui, Z.-K., et al., Nonphospholipid Fluid Liposomes with Switchable Photocontrolled Release. *Langmuir : the ACS Journal of Surfaces and Colloids* **2014,** *30* (36), 10818-10825.

Cullis, P. R., et al., Lipid Polymorphism and the Roles of Lipids in Membranes. *Chemistry and Physics of Lipids* **1986,** *40* (2-4), 127-144.

Cullis, P.; De Kruijff, B., The Polymorphic Phase Behaviour of Phosphatidylethanolamines of Natural and Synthetic Origin. A 31p Nmr Study. *Biochimica et Biophysica Acta (BBA)-Biomembranes* **1978,** *513* (1), 31-42.

Daleke, D. L., Phospholipid Flippases. *Journal of Biological Chemistry* **2007,** *282* (2), 821-825.

Dang, C. V., Links between Metabolism and Cancer. *Genes & Development* **2012,** *26* (9), 877-890.

Daraee, H., et al., Application of Liposomes in Medicine and Drug Delivery. *Artificial Cells, Nanomedicine, and Biotechnology* **2016,** *44* (1), 381-391.

Davis, M. E., The First Targeted Delivery of Sirna in Humans Via a Self-Assembling, Cyclodextrin Polymer-Based Nanoparticle: From Concept to Clinic. *Molecular Pharmaceutics* **2009,** *6* (3), 659-668.

Deeba, F., et al., Phospholipid Diversity: Correlation with Membrane–Membrane Fusion Events. *Biochimica et Biophysica Acta (BBA)-Biomembranes* **2005,** *1669* (2), 170-181.

Derfus, A. M., et al., Remotely Triggered Release from Magnetic Nanoparticles. *Advanced Materials* **2007,** *19* (22), 3932-3936.

Devaux, P. F., Static and Dynamic Lipid Asymmetry in Cell Membranes. *Biochemistry* **1991,** *30* (5), 1163-1173.

Devaux, P. F.; Morris, R., Transmembrane Asymmetry and Lateral Domains in Biological Membranes. *Traffic* **2004,** *5* (4), 241-246.

Deziel, M.; Girotti, A., Photodynamic Action of Bilirubin on Liposomes and Erythrocyte Membranes. *Journal of Biological Chemistry* **1980,** *255* (17), 8192-8198.

Di Bella, S., Second-Order Nonlinear Optical Properties of Transition Metal Complexes. *Chemical Society Reviews* **2001,** *30* (6), 355-366.

Dolmans, D. E., et al., Photodynamic Therapy for Cancer. *Nature Reviews Cancer* **2003,** *3* (5), 380.

Dong, C.-p., et al., Metal-Free Blue Dye Synthesis: Oxidative Coupling of Benzylamines and N, N-Dimethylanilines to Yield 4, 4′ -Diaminotriarylmethanes in the Presence of Salicylic Acid as a Co-Oxidant. *The Journal of Organic Chemistry* **2017,** *82* (23), 12530-12538.

Douroumis, D., et al., *Computational Pharmaceutics: Application of Molecular Modeling in Drug Delivery*. John Wiley & Sons: 2015.

Drummond, D. C., et al., Current Status of Ph-Sensitive Liposomes in Drug Delivery. *Progress in Lipid Research* **2000,** *39* (5), 409-460.

Du, J., et al., Stimuli-Responsive Nanoparticles for Targeting the Tumor Microenvironment. *Journal of Controlled Release* **2015,** *219*, 205-214.

Du, J.-Z., et al., Tailor-Made Dual Ph-Sensitive Polymer–Doxorubicin Nanoparticles for Efficient Anticancer Drug Delivery. *Journal of the American Chemical Society* **2011,** *133* (44), 17560-17563.

Duboisset, J., et al., Generic Model of the Molecular Orientational Distribution Probed by Polarization-Resolved Second-Harmonic Generation. *Physical Review A* **2012,** *85* (4), 043829.

Duncan, R.; Gaspar, R., Nanomedicine (S) under the Microscope. *Molecular Pharmaceutics* **2011,** *8* (6), 2101-2141.

Dunn, G. P., et al., Cancer Immunoediting: From Immunosurveillance to Tumor Escape. *Nature Immunology* **2002,** *3* (11), 991.

Durell, S. R., et al., What Studies of Fusion Peptides Tell Us About Viral Envelope Glycoprotein-Mediated Membrane Fusion. *Molecular Membrane Biology* **1997,** *14* (3), 97-112.

Duronio, R. J.; Xiong, Y., Signaling Pathways That Control Cell Proliferation. *Cold Spring Harbor Perspectives in Biology* **2013,** *5* (3), a008904.

Ellens, H., et al., Fusion of Phosphatidylethanolamine-Containing Liposomes and Mechanism of L. Alpha.-Hii Phase Transition. *Biochemistry* **1986,** *25* (14), 4141-4147.

El-Sayed, I. H., et al., Surface Plasmon Resonance Scattering and Absorption of Anti-Egfr Antibody Conjugated Gold Nanoparticles in Cancer Diagnostics: Applications in Oral Cancer. *Nano Letters* **2005,** *5* (5), 829-834.

Engelman, D. M., Membranes Are More Mosaic Than Fluid. *Nature* **2005,** *438* (7068), 578.

Eyer, K., et al., Cell-Free Microfluidic Determination of P-Glycoprotein Interactions with Substrates and Inhibitors. *Pharmaceutical Research* **2014,** *31* (12), 3415-3425.

Fadeel, B.; Xue, D., The Ins and Outs of Phospholipid Asymmetry in the Plasma Membrane: Roles in Health and Disease. *Critical Reviews in Biochemistry and Molecular Biology* **2009,** *44* (5), 264-277.

Farhood, H., et al., The Role of Dioleoyl Phosphatidylethanolamine in Cationic Liposome Mediated Gene Transfer. *Biochimica et Biophysica Acta (BBA)-Biomembranes* **1995,** *1235* (2), 289-295.

Fattal, E., et al., "Smart" Delivery of Antisense Oligonucleotides by Anionic Ph-Sensitive Liposomes. *Advanced Drug Delivery Reviews* **2004,** *56* (7), 931-946.

Feller, S. E., Molecular Dynamics Simulations of Lipid Bilayers. *Current Opinion in Colloid & Interface Science* **2000,** *5* (3-4), 217-223.

Fenton, W. S., et al., Essential Fatty Acids, Lipid Membrane Abnormalities, and the Diagnosis and Treatment of Schizophrenia. *Biological Psychiatry* **2000,** *47* (1), 8-21.

Fiedler, E. C.; Hemann, M. T., Aiding and Abetting: How the Tumor Microenvironment Protects Cancer from Chemotherapy. *Annual Review of Cancer Biology* **2019**.

Finger, F. P.; White, J. G., Fusion and Fission: Membrane Trafficking in Animal Cytokinesis. *Cell* **2002,** *108* (6), 727-730.

Fomina, N., et al., Photochemical Mechanisms of Light-Triggered Release from Nanocarriers. *Advanced Drug Delivery Reviews* **2012,** *64* (11), 1005-1020.

Forster, J. C., et al., A Review of the Development of Tumor Vasculature and Its Effects on the Tumor Microenvironment. *Hypoxia* **2017,** *5*, 21.

Fouad, Y. A.; Aanei, C., Revisiting the Hallmarks of Cancer. *American Journal of Cancer Research* **2017,** *7* (5), 1016.

Frolov, V. A., et al., Lipid Polymorphisms and Membrane Shape. *Cold Spring Harbor Perspectives in Biology* **2011,** *3* (11), a004747.

Fuhrmann, G., et al., Cell-Derived Vesicles for Drug Therapy and Diagnostics: Opportunities and Challenges. *Nano Today* **2015,** *10* (3), 397-409.

Fulda, S., Tumor Resistance to Apoptosis. *International Journal of Cancer* **2009,** *124* (3), 511-515.

Gabizon, A.; Papahadjopoulos, D., Liposome Formulations with Prolonged Circulation Time in Blood and Enhanced Uptake by Tumors. *Proceedings of the National Academy of Sciences* **1988,** *85* (18), 6949-6953.

Gadella, B.; Harrison, R., The Capacitating Agent Bicarbonate Induces Protein Kinase a-Dependent Changes in Phospholipid Transbilayer Behavior in the Sperm Plasma Membrane. *Development* **2000,** *127* (11), 2407-2420.

Ganta, S., et al., A Review of Stimuli-Responsive Nanocarriers for Drug and Gene Delivery. *Journal of Controlled Release* **2008,** *126* (3), 187-204.

Gao, X., et al., Lectin-Conjugated Peg–Pla Nanoparticles: Preparation and Brain Delivery after Intranasal Administration. *Biomaterials* **2006,** *27* (18), 3482-3490.

García-Manrique, P., et al., Therapeutic Biomaterials Based on Extracellular Vesicles: Classification of Bio-Engineering and Mimetic Preparation Routes. *Journal of Extracellular Vesicles* **2018,** *7* (1), 1422676.

Ge, J., et al., Drug Release from Electric-Field-Responsive Nanoparticles. *ACS nano* **2011,** *6* (1), 227-233.

Gilleron, J., et al., Image-Based Analysis of Lipid Nanoparticle–Mediated Sirna Delivery, Intracellular Trafficking and Endosomal Escape. *Nature Biotechnology* **2013,** *31* (7), 638.

Giraudo, C. G., et al., Snares Can Promote Complete Fusion and Hemifusion as Alternative Outcomes. *The Journal of Cell Biology* **2005,** *170* (2), 249-260.

Gomez-Hens, A.; Fernandez-Romero, J., Analytical Methods for the Control of Liposomal Delivery Systems. *TrAC Trends in Analytical Chemistry* **2006,** *25* (2), 167-178.

Gonella, G.; Dai, H.-L., Second Harmonic Light Scattering from the Surface of Colloidal Objects: Theory and Applications. *Langmuir : the ACS Journal of Surfaces and Colloids* **2013,** *30* (10), 2588-2599.

Goto, Y., et al., Light-Triggered Hydrophilic Drug Release from Liposomes through Removal of a Photolabile Protecting Group. *RSC Advances* **2019,** *9* (1), 166-171.

Gouaux, E.; MacKinnon, R., Principles of Selective Ion Transport in Channels and Pumps. *science* **2005,** *310* (5753), 1461-1465.

Guan, X., Cancer Metastases: Challenges and Opportunities. *Acta Pharmaceutica Sinica B* **2015,** *5* (5), 402-418.

Günes, C.; Rudolph, K. L., The Role of Telomeres in Stem Cells and Cancer. *Cell* **2013,** *152* (3), 390-393.

Guo, X., et al., Mechanism of Ph-Triggered Collapse of Phosphatidylethanolamine Liposomes Stabilized by an Ortho Ester Polyethyleneglycol Lipid. *Biophysical Journal* **2003,** *84* (3), 1784-1795.

Haber, L. H., et al., Probing the Colloidal Gold Nanoparticle/Aqueous Interface with Second Harmonic Generation. *Chemical Physics Letters* **2011,** *507* (1-3), 11-14.

Hamal, P., et al., Molecular Adsorption and Transport at Liposome Surfaces Studied by Molecular Dynamics Simulations and Second Harmonic Generation Spectroscopy. *The Journal of Physical Chemistry B* **2019**.

Hanahan, D.; Weinberg, R. A., Hallmarks of Cancer: The Next Generation. *Cell* **2011,** *144* (5), 646-674.

Hanahan, D.; Weinberg, R. A., The Hallmarks of Cancer. *Cell* **2000,** *100* (1), 57-70.

Hannesschlaeger, C., et al., Intrinsic Membrane Permeability to Small Molecules. *Chemical Reviews* **2019**.

Harayama, T.; Riezman, H., Understanding the Diversity of Membrane Lipid Composition. *Nature reviews Molecular cell biology* **2018**.

Harayama, T.; Riezman, H., Understanding the Diversity of Membrane Lipid Composition. *Nature Reviews Molecular Cell Biology* **2018**.

Harlos, K.; Eibl, H., Hexagonal Phases in Phospholipids with Saturated Chains: Phosphatidylethanolamines and Phosphatidic Acids. *Biochemistry* **1981,** *20* (10), 2888-2892.

Harrison, S. C., Viral Membrane Fusion. *Nature Structural & Molecular Biology* **2008,** *15* (7), 690.

Heinz, T., et al., Determination of Molecular Orientation of Monolayer Adsorbates by Optical Second-Harmonic Generation. *Physical Review A* **1983,** *28* (3), 1883.

Helenius, A., et al., Endosomes. *Trends in Biochemical Sciences* **1983,** *8* (7), 245-250.

Hendrickx, E., et al., Hyper-Rayleigh Scattering in Isotropic Solution. *Accounts of Chemical Research* **1998,** *31* (10), 675-683.

Hermanson, G. T., Fluorescent Probes. *Bioconjugate Techniques (third edition) Chapter* **2013,** *10*, 395-463.

Hernot, S.; Klibanov, A. L., Microbubbles in Ultrasound-Triggered Drug and Gene Delivery. *Advanced Drug Delivery Reviews* **2008,** *60* (10), 1153-1166.

Hicks, A. M., et al., Unique Molecular Signatures of Glycerophospholipid Species in Different Rat Tissues Analyzed by Tandem Mass Spectrometry. *Biochimica et Biophysica Acta (BBA)-Molecular and Cell Biology of Lipids* **2006,** *1761* (9), 1022-1029.

Hicks, J., et al., Studies of Liquid Surfaces by Second Harmonic Generation. *The Journal of Physical Chemistry* **1986,** *90* (4), 560-562.

Hillen, F.; Griffioen, A. W., Tumour Vascularization: Sprouting Angiogenesis and Beyond. *Cancer and Metastasis Reviews* **2007,** *26* (3-4), 489-502.

Hills Jr, R. D.; McGlinchey, N., Model Parameters for Simulation of Physiological Lipids. *Journal of Computational Chemistry* **2016,** *37* (12), 1112-1118.

Hofheinz, R.-D., et al., Liposomal Encapsulated Anti-Cancer Drugs. *Anti-cancer Drugs* **2005,** *16* (7), 691-707.

Holthuis, J. C.; Menon, A. K., Lipid Landscapes and Pipelines in Membrane Homeostasis. *Nature* **2014,** *510* (7503), 48.

Hossen, S., et al., Smart Nanocarrier-Based Drug Delivery Systems for Cancer Therapy and Toxicity Studies: A Review. *J Adv Res* **2019,** *15*, 1-18.

Https://Disco.Chemaxon.Com/Apps/Demos/Logd/ (Accessed 6.13.2019).

Https://Ucsd-Ceng-176.Fandom.Com/Wiki/Liposome_Nanoparticles (Access 07.02.2019).

Https://Www.Dojindo.Com/Store/P/623-Calcein.Html (Accessed on 08/26/2019).

Https://Www.Who.Int/News-Room/Fact-Sheets/Detail/Cancer (Accessed 5/1/2019).

Hu, Q., et al., Enzyme-Responsive Nanomaterials for Controlled Drug Delivery. *Nanoscale* **2014,** *6* (21), 12273-12286.

Hunter, K. W., et al., Mechanisms of Metastasis. *Breast Cancer Research* **2008,** *10* (1), S2.

In Collaboration among the Mccarley Research Group, the Haber Research Group, and the Kumar Research Groupo at Lsu.

Ingólfsson, H. I., et al., Lipid Organization of the Plasma Membrane. *Journal of the American Chemical Society* **2014,** *136* (41), 14554-14559.

Ingólfsson, H. I.; Andersen, O. S., Alcohol's Effects on Lipid Bilayer Properties. *Biophysical Journal* **2011,** *101* (4), 847-855.

Israelachvili, J.; Wennerström, H., Role of Hydration and Water Structure in Biological and Colloidal Interactions. *Nature* **1996,** *379* (6562), 219.

Iversen, T.-G., et al., Endocytosis and Intracellular Transport of Nanoparticles: Present Knowledge and Need for Future Studies. *Nano Today* **2011,** *6* (2), 176-185.

Jahn, R., et al., Membrane Fusion. *Cell* **2003,** *112* (4), 519-533.

Jahn, R.; Grubmüller, H., Membrane Fusion. *Current Opinion in Cell Biology* **2002,** *14* (4), 488-495.

Jahn, R.; Scheller, R. H., Snares—Engines for Membrane Fusion. *Nature Reviews Molecular Cell Biology* **2006,** *7* (9), 631.

Johnsen, K. B., et al., A Comprehensive Overview of Exosomes as Drug Delivery Vehicles—Endogenous Nanocarriers for Targeted Cancer Therapy. *Biochimica et Biophysica Acta (BBA)-Reviews on Cancer* **2014,** *1846* (1), 75-87.

Kano, K., et al., Photoresponsive Membranes. Regulation of Membrane Properties by Photoreversible Cis–Trans Isomerization of Azobenzenes. *Chemistry Letters* **1980,** *9* (4), 421-424.

Kao, Y.; Juliano, R. L., Interactions of Liposomes with the Reticuloendothelial System Effects of Reticuloendothelial Blockade on the Clearance of Large Unilamellar Vesicles. *Biochimica et Biophysica Acta (BBA)-General Subjects* **1981,** *677* (3-4), 453-461.

Karagiannis, E. D., et al., Rational Design of a Biomimetic Cell Penetrating Peptide Library. *ACS nano* **2013,** *7* (10), 8616-8626.

Karam, T. E., et al., Enhanced Photothermal Effects and Excited-State Dynamics of Plasmonic Size-Controlled Gold–Silver–Gold Core–Shell–Shell Nanoparticles. *The Journal of Physical Chemistry C* **2015,** *119* (32), 18573-18580.

Karam, T. E., et al., Ultrafast and Nonlinear Spectroscopy of Brilliant Green-Based Nanogumbos with Enhanced near-Infrared Emission. *The Journal of Chemical Physics* **2017,** *147* (14), 144701.

Karam, T. E.; Haber, L. H., Molecular Adsorption and Resonance Coupling at the Colloidal Gold Nanoparticle Interface. *The Journal of Physical Chemistry C* **2013,** *118* (1), 642-649.

Kasson, P. M.; Pande, V. S., Control of Membrane Fusion Mechanism by Lipid Composition: Predictions from Ensemble Molecular Dynamics. *PLoS Computational Biology* **2007,** *3* (11), e220.

Kendall, D. A.; MacDonald, R. C., A Fluorescence Assay to Monitor Vesicle Fusion and Lysis. *Journal of Biological Chemistry* **1982,** *257* (23), 13892-13895.

Kiessling, V., et al., Domain Coupling in Asymmetric Lipid Bilayers. *Biochimica et Biophysica Acta (BBA)-Biomembranes* **2009,** *1788* (1), 64-71.

Kim, H. J., et al., Ultrasound-Triggered Smart Drug Release from a Poly (Dimethylsiloxane)–Mesoporous Silica Composite. *Advanced Materials* **2006,** *18* (23), 3083-3088.

Kim, Y. J., et al., A Smart Hyperthermia Nanofiber with Switchable Drug Release for Inducing Cancer Apoptosis. *Advanced Functional Materials* **2013,** *23* (46), 5753-5761.

Kinnunen, P. K., On the Mechanism of the Lamellar→ Hexagonal H H Phase Transition and the Biological Significance of the H H Propensity. *Handbook of Nonmedical Applications of Liposomes. Vol* **1996,** *1*, 153-171.

Kinnunen, P. K., On the Molecular-Level Mechanisms of Peripheral Protein-Membrane Interactions Induced by Lipids Forming Inverted Non-Lamellar Phases. *Chemistry and Physics of Lipids* **1996,** *81* (2), 151-166.

Koynova, R.; Caffrey, M., Phases and Phase Transitions of the Hydrated Phosphatidylethanolamines. *Chemistry and Physics of Lipids* **1994,** *69* (1), 1-34.

Kozlov, M. M.; Markin, V. S., [Possible Mechanism of Membrane Fusion]. *Biofizika* **1983,** *28* (2), 242-7.

Kreutzberger, A. J., et al., Asymmetric Phosphatidylethanolamine Distribution Controls Fusion Pore Lifetime and Probability. *Biophysical Journal* **2017,** *113* (9), 1912-1915.

Kreutzberger, A. J., et al., Asymmetric Phosphatidylethanolamine Distribution Controls Fusion Pore Lifetime and Probability. *Biophysical Journal* **2017,** *113* (9), 1912-1915.

Kuai, R., et al., Efficient Delivery of Payload into Tumor Cells in a Controlled Manner by Tat and Thiolytic Cleavable Peg Co-Modified Liposomes. *Molecular Pharmaceutics* **2010,** *7* (5), 1816-1826.

Kučerka, N., et al., Structural Significance of Lipid Diversity as Studied by Small Angle Neutron and X-Ray Scattering. *Membranes* **2015,** *5* (3), 454-472.

Kuhn, P., et al., A Microfluidic Device for the Delivery of Enzymes into Cells by Liposome Fusion. *Engineering in Life Sciences* **2018,** *18* (2), 149-156.

Kumal, R. R., et al., Impacts of Salt, Buffer, and Lipid Nature on Molecular Adsorption and Transport in Liposomes as Observed by Second Harmonic Generation. *The Journal of Physical Chemistry C* **2017,** *121* (29), 15851-15860.

Kunisawa, J., et al., Pharmacotherapy by Intracellular Delivery of Drugs Using Fusogenic Liposomes: Application to Vaccine Development. *Advanced Drug Delivery Reviews* **2001,** *52* (3), 177-186.

Kunisawa, J., et al., Pharmacotherapy by Intracellular Delivery of Drugs Using Fusogenic Liposomes: Application to Vaccine Development. *Advanced Drug Delivery Reviews* **2001,** *52* (3), 177-186.

Kuzmin, P. I., et al., A Quantitative Model for Membrane Fusion Based on Low-Energy Intermediates. *Proceedings of the National Academy of Sciences* **2001,** *98* (13), 7235-7240.

Lajunen, T., et al., Light Activated Liposomes: Functionality and Prospects in Ocular Drug Delivery. *Journal of Controlled Release* **2016,** *244*, 157-166.

Lake, R. A.; Robinson, B. W., Immunotherapy and Chemotherapy—a Practical Partnership. *Nature Reviews Cancer* **2005,** *5* (5), 397.

Lammers, T., et al., Drug Targeting to Tumors: Principles, Pitfalls and (Pre-) Clinical Progress. *Journal of Controlled Release* **2012,** *161* (2), 175-187.

Laouini, A., et al., Preparation, Characterization and Applications of Liposomes: State of the Art. *Journal of Colloid Science and Biotechnology* **2012,** *1* (2), 147-168.

LaVan, D. A., et al., Moving Smaller in Drug Discovery and Delivery. *Nature Reviews Drug Discovery* **2002,** *1* (1), 77.

Leung, S. J.; Romanowski, M., Light-Activated Content Release from Liposomes. *Theranostics* **2012,** *2* (10), 1020.

Li, H.-J., et al., Stimuli-Responsive Clustered Nanoparticles for Improved Tumor Penetration and Therapeutic Efficacy. *Proceedings of the National Academy of Sciences* **2016,** *113* (15), 4164-4169.

Li, J., et al., A Review on Phospholipids and Their Main Applications in Drug Delivery Systems. *Asian Journal of Pharmaceutical Sciences* **2015,** *10* (2), 81-98.

Li, L.; Hui, S., The Effect of Lipid Molecular Packing Stress on Cationic Liposome-Induced Rabbit Erythrocyte Fusion. *Biochimica et Biophysica Acta (BBA)-Biomembranes* **1997,** *1323* (1), 105-116.

Li, X., et al., Challenges and Opportunities in Exosome Research—Perspectives from Biology, Engineering, and Cancer Therapy. *APL Bioengineering* **2019,** *3* (1), 011503.

Li, Y., et al., Delivery of Nanomedicines to Extracellular and Intracellular Compartments of a Solid Tumor. *Advanced Drug Delivery Reviews* **2012,** *64* (1), 29-39.

Li, Y.-J., et al., Autologous Cancer Cell-Derived Extracellular Vesicles as Drug-Delivery Systems: A Systematic Review of Preclinical and Clinical Findings and Translational Implications. *Nanomedicine* **2019,** *14* (4), 493-509.

Li, Z., et al., Dithiane-Based Photolabile Amphiphiles: Toward Photolabile Liposomes1, 2. *Langmuir : the ACS Journal of Surfaces and Colloids* **2003,** *19* (16), 6381-6391.

Li, Z., et al., The Ratio of Phosphatidylcholine to Phosphatidylethanolamine Influences Membrane Integrity and Steatohepatitis. *Cell Metabolism* **2006,** *3* (5), 321-331.

Lin, Y., et al., Exosome–Liposome Hybrid Nanoparticles Deliver Crispr/Cas9 System in Mscs. *Advanced Science* **2018,** *5* (4).

Lipinski, C. A., Drug-Like Properties and the Causes of Poor Solubility and Poor Permeability. *Journal of Pharmacological and Toxicological Methods* **2000,** *44* (1), 235-249.

Lis, L., et al., Interactions between Neutral Phospholipid Bilayer Membranes. *Biophysical Journal* **1982,** *37* (3), 657.

Little, A., et al., A Double-Blind, Placebo Controlled Trial of High-Dose Lecithin in Alzheimer's Disease. *Journal of Neurology, Neurosurgery & Psychiatry* **1985,** *48* (8), 736-742.

Liu, H.; Webster, T. J., Nanomedicine for Implants: A Review of Studies and Necessary Experimental Tools. *Biomaterials* **2007,** *28* (2), 354-369.

Liu, X., et al., Lipophilicity and Its Relationship with Passive Drug Permeation. *Pharmaceutical Research* **2011,** *28* (5), 962-977.

Liu, Y., et al., Effects of Bilayer Surface Charge Density on Molecular Adsorption and Transport across Liposome Bilayers. *Biophysical Journal* **2001,** *80* (2), 1004-1012.

Liu, Y., et al., Folic Acid Conjugated Nanoparticles of Mixed Lipid Monolayer Shell and Biodegradable Polymer Core for Targeted Delivery of Docetaxel. *Biomaterials* **2010,** *31* (2), 330-338.

Loew, M., et al., Lipid Nature and Their Influence on Opening of Redox-Active Liposomes. *Langmuir : the ACS Journal of Surfaces and Colloids* **2013,** *29* (22), 6615-6623.

Luzio, J. P., et al., Lysosomes: Fusion and Function. *Nature Reviews Molecular Cell Biology* **2007,** *8* (8), 622.

Ma, N., et al., Dual Redox Responsive Assemblies Formed from Diselenide Block Copolymers. *Journal of the American Chemical Society* **2009,** *132* (2), 442-443.

Ma, X., et al., Functional Silica Nanoparticles for Redox-Triggered Drug/Ssdna Co-Delivery. *Advanced Healthcare Materials* **2012,** *1* (6), 690-697.

Maeda, H., et al., A Retrospective 30 Years after Discovery of the Enhanced Permeability and Retention Effect of Solid Tumors: Next-Generation Chemotherapeutics and Photodynamic Therapy—Problems, Solutions, and Prospects. *Microcirculation* **2016,** *23* (3), 173-182.

Maeda, H., et al., The Epr Effect for Macromolecular Drug Delivery to Solid Tumors: Improvement of Tumor Uptake, Lowering of Systemic Toxicity, and Distinct Tumor Imaging in Vivo. *Advanced Drug Delivery Reviews* **2013,** *65* (1), 71-79.

Manallack, D. T., The P K a Distribution of Drugs: Application to Drug Discovery. *Perspectives in Medicinal Chemistry* **2007,** *1*, 1177391X0700100003.

Mannock, D. A., et al., An Analysis of the Relationship between Fatty Acid Composition and the Lamellar Gel to Liquid-Crystalline and the Lamellar to Inverted Nonlamellar Phase Transition Temperatures of Phosphatidylethanolamines and Diacyl-A-D-Glucosyl Glycerols. *European Biophysics Journal* **2001,** *30* (7), 537-554.

Manocha, B.; Margaritis, A., Controlled Release of Doxorubicin from Doxorubicin/Γ-Polyglutamic Acid Ionic Complex. *Journal of Nanomaterials* **2010,** *2010*, 12.

Marquardt, D., et al., Asymmetric Lipid Membranes: Towards More Realistic Model Systems. *Membranes* **2015,** *5* (2), 180-196.

Marsden, H. R., et al., Model Systems for Membrane Fusion. *Chemical Society Reviews* **2011,** *40* (3), 1572-1585.

Marsh, D., Lateral Pressure Profile, Spontaneous Curvature Frustration, and the Incorporation and Conformation of Proteins in Membranes. *Biophysical Journal* **2007,** *93* (11), 3884-3899.

Marsh, D., Water Adsorption Isotherms and Hydration Forces for Lysolipids and Diacyl Phospholipids. *Biophysical Journal* **1989,** *55* (6), 1093-1100.

Marshall, C. J., Tumor Suppressor Genes. *Cell* **1991,** *64* (2), 313-326.

Martin Loew, R. M., unpublished results.

Mathiyazhakan, M., et al., A Concise Review of Gold Nanoparticles-Based Photo-Responsive Liposomes for Controlled Drug Delivery. *Nano-micro Letters* **2018,** *10* (1), 10.

Mathiyazhakan, M., et al., A Concise Review of Gold Nanoparticles-Based Photo-Responsive Liposomes for Controlled Drug Delivery. *Nano-micro Letters* **2018,** *10* (1), 10.

Matlack, K., et al., Review of Second Harmonic Generation Measurement Techniques for Material State Determination in Metals. *Journal of Nondestructive Evaluation* **2015,** *34* (1), 273.

Matos, C., et al., Liposomes as a Model for the Biological Membrane: Studies on Daunorubicin Bilayer Interaction. *J. Membrane Biol.* **2012,** *245* (2), 69-75.

Matsuzaki, K., et al., Optical Characterization of Liposomes by Right Angle Light Scattering and Turbidity Measurement. *Biochimica et Biophysica Acta (BBA)-Biomembranes* **2000,** *1467* (1), 219-226.

May, J. P.; Li, S.-D., Hyperthermia-Induced Drug Targeting. *Expert Opinion on Drug Delivery* **2013,** *10* (4), 511-527.

Mayer, L. D., et al., Vesicles of Variable Sizes Produced by a Rapid Extrusion Procedure. *Biochimica et Biophysica Acta* **1986,** *858* (1), 161-8.

Mayhew, S. G., The Redox Potential of Dithionite and So− 2 from Equilibrium Reactions with Flavodoxins, Methyl Viologen and Hydrogen Plus Hydrogenase. *European Journal of Biochemistry* **1978,** *85* (2), 535-547.

McCarley, R. L., et al., Release Rates of Liposomal Contents Are Controlled by Kosmotropes and Chaotropes. *Langmuir : the ACS Journal of Surfaces and Colloids* **2013,** *29* (46), 13991-13995.

McCarley, R. L., Redox-Responsive Delivery Systems. *Annual Review of Analytical Chemistry* **2012,** *5*, 391-411.21. Loew, M., et al., Lipid Nature and Their Influence on Opening of Redox-Active Liposomes. *Langmuir : the ACS Journal of Surfaces and Colloids* **2013,** *29* (22), 6615-23.

McMahon, H. T.; Boucrot, E., Membrane Curvature at a Glance. *J Cell Sci* **2015,** *128* (6), 1065-1070.

Mendoza, M. F., et al., Human Nad (P) H: Quinone Oxidoreductase Type I (Hnqo1) Activation of Quinone Propionic Acid Trigger Groups. *Biochemistry* **2012,** *51* (40), 8014-8026.

Menichetti, R., et al., Drug–Membrane Permeability across Chemical Space. *ACS Central Science* **2019**.

Merisko-Liversidge, E. M.; Liversidge, G. G., Drug Nanoparticles: Formulating Poorly Water-Soluble Compounds. *Toxicologic Pathology* **2008,** *36* (1), 43-48.

Miller, C. R., et al., Visible Light-Induced Destabilization of Endocytosed Liposomes. *FEBS Letters* **2000,** *467* (1), 52-56.

Milton, H. J., et al., Pegylation: A Novel Process for Modifying Pharmacokinetics. *Clin Pharmacokinet* **2001,** *40* (7), 539-551.

Min, Y., et al., Clinical Translation of Nanomedicine. *Chemical Reviews* **2015,** *115* (19), 11147-11190.

Miranda, D.; Lovell, J. F., Mechanisms of Light-Induced Liposome Permeabilization. *Bioengineering & Translational Medicine* **2016,** *1* (3), 267-276.

Mohammad, R. K., et al. In *Study of Molecular Electronic Energy Levels of Malachite Green Dye*, AIP Conference Proceedings, AIP Publishing: 2019; p 030022.

Mondal Roy, S.; Sarkar, M., Membrane Fusion Induced by Small Molecules and Ions. *Journal of Lipids* **2011,** *2011*.

Mout, R., et al., Surface Functionalization of Nanoparticles for Nanomedicine. *Chemical Society Reviews* **2012,** *41* (7), 2539-2544.

Muhammad, F., et al., Ph-Triggered Controlled Drug Release from Mesoporous Silica Nanoparticles Via Intracelluar Dissolution of Zno Nanolids. *Journal of the American Chemical Society* **2011,** *133* (23), 8778-8781.

Muñoz-Úbeda, M., et al., Gene Vectors Based on Doepc/Dope Mixed Cationic Liposomes: A Physicochemical Study. *Soft Matter* **2011,** *7* (13), 5991-6004.

Murata, N.; Los, D. A., Membrane Fluidity and Temperature Perception. *Plant physiology* **1997,** *115* (3), 875.

Murthy, N., et al., A Macromolecular Delivery Vehicle for Protein-Based Vaccines: Acid-Degradable Protein-Loaded Microgels. *Proceedings of the National Academy of Sciences* **2003,** *100* (9), 4995-5000.

Naganbabu, M., et al., Multiexcitation Fluorogenic Labeling of Surface, Intracellular, and Total Protein Pools in Living Cells. *Bioconjugate Chemistry* **2016,** *27* (6), 1525-1531.

Nalwa, H. S.; Miyata, S., *Nonlinear Optics of Organic Molecules and Polymers*. CRC press: **1996**.

Narvekar, M., et al., Nanocarrier for Poorly Water-Soluble Anticancer Drugs—Barriers of Translation and Solutions. *Aaps Pharmscitech* **2014,** *15* (4), 822-833.

Nawimanage, R. R., Synthesis, Characterization, and Evaluation of Small Molecule-Based Fluorogenic Probes for the Detection of Cellular Thiols. Ph.D Dissertation, Louisiana State University, Baton Rouge, LA, **2015**.

Ng, K. K., et al., Lipoprotein-Inspired Nanoparticles for Cancer Theranostics. *Accounts of Chemical Research* **2011,** *44* (10), 1105-1113.

Nigam, S., et al., Development of Citrate-Stabilized Fe3o4 Nanoparticles: Conjugation and Release of Doxorubicin for Therapeutic Applications. *Journal of Magnetism and Magnetic Materials* **2011,** *323* (2), 237-243.

Nogueira, E., et al., Design of Liposomal Formulations for Cell Targeting. *Colloids and Surfaces B: Biointerfaces* **2015,** *136*, 514-526.

Obaid, G., et al., Cancer Targeting with Biomolecules: A Comparative Study of Photodynamic Therapy Efficacy Using Antibody or Lectin Conjugated Phthalocyanine-Peg Gold Nanoparticles. *Photochemical & Photobiological Sciences* **2015,** *14* (4), 737-747.

O'Brien, D. F., et al., Light-Regulated Permeability of Rhodopsin: Egg Phosphatidylcholine Recombinant Membranes. *Proceedings of the National Academy of Sciences* **1977,** *74* (12), 5222-5226.

Ohya, Y., et al., Photo-Sensitive Lipid Membrane Perturbation by a Single Chain Lipid Having Terminal Spiropyran Group. *Supramolecular Science* **1998,** *5* (1-2), 21-29.

Ong, S., et al., Immobilized-Artificial-Membrane Chromatography: Measurements of Membrane Partition Coefficient and Predicting Drug Membrane Permeability. *Journal of Chromatography A* **1996,** *728* (1-2), 113-128.

Ong, W., et al., Redox-Triggered Contents Release from Liposomes. *Journal of the American Chemical Society* **2008,** *130* (44), 14739-14744.

Orädd, G., et al., Effects of Peptide Hydrophobicity on Its Incorporation in Phospholipid Membranes—an Nmr and Ellipsometry Study. *Biochimica et Biophysica Acta (BBA)-Biomembranes* **2011,** *1808* (1), 244-252.

Orsi, M.; Essex, J. W., Physical Properties of Mixed Bilayers Containing Lamellar and Nonlamellar Lipids: Insights from Coarse-Grain Molecular Dynamics Simulations. *Faraday Discussions* **2013,** *161*, 249-272.

Otsuka, H., et al., Pegylated Nanoparticles for Biological and Pharmaceutical Applications. *Advanced Drug Delivery Reviews* **2012,** *64*, 246-255.

Ouyang, L., et al., Programmed Cell Death Pathways in Cancer: A Review of Apoptosis, Autophagy and Programmed Necrosis. *Cell Proliferation* **2012,** *45* (6), 487-498.

Paasonen, L., et al., Gold Nanoparticles Enable Selective Light-Induced Contents Release from Liposomes. *Journal of Controlled Release* **2007,** *122* (1), 86-93.

Pan, L., et al., Nuclear-Targeted Drug Delivery of Tat Peptide-Conjugated Monodisperse Mesoporous Silica Nanoparticles. *Journal of the American Chemical Society* **2012,** *134* (13), 5722-5725.

Pantazis, P., et al., Second Harmonic Generating (Shg) Nanoprobes for in Vivo Imaging. *Proceedings of the National Academy of Sciences* **2010,** *107* (33), 14535-14540.

Panyam, J., et al., Rapid Endo-Lysosomal Escape of Poly (Dl-Lactide-Co-Glycolide) Nanoparticles: Implications for Drug and Gene Delivery. *The FASEB journal* **2002,** *16* (10), 1217-1226.

Parente, R. A.; Lentz, B. R., Fusion and Phase Separation Monitored by Lifetime Changes of a Fluorescent Phospholipid Probe. *Biochemistry* **1986,** *25* (5), 1021-1026.

Park, M.-R., et al., Dual Ionic Interaction System Based on Polyelectrolyte Complex and Ionic, Injectable, and Thermosensitive Hydrogel for Sustained Release of Human Growth Hormone. *Biomaterials* **2013,** *34* (4), 1327-1336.

Pashkovskaya, A., et al., Light-Triggered Liposomal Release: Membrane Permeabilization by Photodynamic Action. *Langmuir : the ACS Journal of Surfaces and Colloids* **2009,** *26* (8), 5726-5733.

Paula, S., et al., Permeation of Protons, Potassium Ions, and Small Polar Molecules through Phospholipid Bilayers as a Function of Membrane Thickness. *Biophysical Journal* **1996,** *70* (1), 339-348.

Pautot, S., et al., Engineering Asymmetric Vesicles. *Proceedings of the National Academy of Sciences* **2003,** *100* (19), 10718-10721.

Pavlova, N. N.; Thompson, C. B., The Emerging Hallmarks of Cancer Metabolism. *Cell Metabolism* **2016,** *23* (1), 27-47.

Peetla, C., et al., Biophysical Interactions with Model Lipid Membranes: Applications in Drug Discovery and Drug Delivery. *Molecular Pharmaceutics* **2009,** *6* (5), 1264-1276.

Pelliccioli, A. P.; Wirz, J., Photoremovable Protecting Groups: Reaction Mechanisms and Applications. *Photochemical & Photobiological Sciences* **2002,** *1* (7), 441-458.

Peracchia, M., et al., Stealth® Pegylated Polycyanoacrylate Nanoparticles for Intravenous Administration and Splenic Targeting. *Journal of Controlled Release* **1999,** *60* (1), 121-128.

Pick, H., et al., Investigating Cellular Signaling Reactions in Single Attoliter Vesicles. *Journal of the American Chemical Society* **2005,** *127* (9), 2908-2912.

Pidgeon, C.; Hunt, C. A., Light Sensitive Liposomes. *Photochemistry and Photobiology* **1983,** *37* (5), 491-494.

Piffoux, M., et al., Modification of Extracellular Vesicles by Fusion with Liposomes for the Design of Personalized Biogenic Drug Delivery Systems. *ACS Nano* **2018,** *12* (7), 6830-6842.

Pinot, M., et al., Polyunsaturated Phospholipids Facilitate Membrane Deformation and Fission by Endocytic Proteins. *Science* **2014,** *345* (6197), 693-697.

Piper, R. C.; Luzio, J. P., Late Endosomes: Sorting and Partitioning in Multivesicular Bodies. *Traffic* **2001,** *2* (9), 612-621.

Pornpattananangkul, D., et al., Stimuli-Responsive Liposome Fusion Mediated by Gold Nanoparticles. *ACS Aano* **2010,** *4* (4), 1935-1942.

Post, J., et al., Phosphatidylethanolamine and Sarcolemmal Damage During Ischemia or Metabolic Inhibition of Heart Myocytes. *American Journal of Physiology-Heart and Circulatory Physiology* **1995,** *268* (2), H773-H780.

Preiss, M. R.; Bothun, G. D., Stimuli-Responsive Liposome-Nanoparticle Assemblies. *Expert Opinion on Drug Delivery* **2011,** *8* (8), 1025-1040.

Primakoff, P.; Myles, D. G., Penetration, Adhesion, and Fusion in Mammalian Sperm-Egg Interaction. *Science* **2002,** *296* (5576), 2183-2185.

Puri, A., Phototriggerable Liposomes: Current Research and Future Perspectives. *Pharmaceutics* **2014,** *6* (1), 1-25.

Raff, M., et al., Molecular Biology of the Cell 4th Edition. National Center for Biotechnology InformationÕs Bookshelf: 2002.

Rand, R.; Parsegian, V., Hydration Forces between Phospholipid Bilayers. *Biochimica et Biophysica Acta (BBA)-Reviews on Biomembranes* **1989,** *988* (3), 351-376.

Rao, Y., et al., Molecular Orientational Distribution at Interfaces Using Second Harmonic Generation. *The Journal of Physical Chemistry C* **2011,** *115* (23), 11678-11683.

Regan, C. J., et al., Mechanistic Studies of the Photoinduced Quinone Trimethyl Lock Decaging Process. *Journal of the American Chemical Society* **2017,** *139* (13), 4729-4736.

Regen, S. L., et al., Polymerized Phosphatidyl Choline Vesicles. Stabilized and Controllable Time-Release Carriers. *Biochemical and Biophysical Research Communications* **1981,** *101* (1), 131-136.

Rengan, A. K., et al., In Vivo Analysis of Biodegradable Liposome Gold Nanoparticles as Efficient Agents for Photothermal Therapy of Cancer. *Nano Letters* **2015,** *15* (2), 842-848.

Riaz, M., et al., Surface Functionalization and Targeting Strategies of Liposomes in Solid Tumor Therapy: A Review. *International Journal of Molecular Sciences* **2018,** *19* (1), 195.

Ribas, A., Adaptive Immune Resistance: How Cancer Protects from Immune Attack. *Cancer Discovery* **2015,** *5* (9), 915-919.

Richmond, D. L., et al., Forming Giant Vesicles with Controlled Membrane Composition, Asymmetry, and Contents. *Proceedings of the National Academy of Sciences* **2011,** *108* (23), 9431-9436.

Riggi, N., et al., Cancer Metastasis: A Reappraisal of Its Underlying Mechanisms and Their Relevance to Treatment. *Annual Review of Pathology: Mechanisms of Disease* **2018,** *13*, 117-140.

Ruan, G., et al., Imaging and Tracking of Tat Peptide-Conjugated Quantum Dots in Living Cells: New Insights into Nanoparticle Uptake, Intracellular Transport, and Vesicle Shedding. *Journal of the American Chemical Society* **2007,** *129* (47), 14759-14766.

Sabella, S., et al., A General Mechanism for Intracellular Toxicity of Metal-Containing Nanoparticles. *Nanoscale* **2014,** *6* (12), 7052-7061.

Sahoo, S. K.; Labhasetwar, V., Enhanced Antiproliferative Activity of Transferrin-Conjugated Paclitaxel-Loaded Nanoparticles Is Mediated Via Sustained Intracellular Drug Retention. *Molecular Pharmaceutics* **2005,** *2* (5), 373-383.

Salafsky, J. S.; Cohen, B., A Second-Harmonic-Active Unnatural Amino Acid as a Structural Probe of Biomolecules on Surfaces. *The Journal of Physical Chemistry B* **2008,** *112* (47), 15103-15107.

Salafsky, J.; Eisenthal, K., Protein Adsorption at Interfaces Detected by Second Harmonic Generation. *The Journal of Physical Chemistry B* **2000,** *104* (32), 7752-7755.

Sanhai, W. R., et al., Seven Challenges for Nanomedicine. *Nature Nanotechnology* **2008,** *3* (5), 242.

Satarkar, N. S.; Hilt, J. Z., Magnetic Hydrogel Nanocomposites for Remote Controlled Pulsatile Drug Release. *Journal of Controlled Release* **2008,** *130* (3), 246-251.

Sato, Y. T., et al., Engineering Hybrid Exosomes by Membrane Fusion with Liposomes. *Scientific Reports* **2016,** *6*, 21933.

Seaman, M.; Luzio, J., Lysosomes and Other Late Compartments of the Endocytic Pathway. *Endocytosis (Marsh, M., ed.)* **2001**, 111-148.

Seddon, A. M., et al., Drug Interactions with Lipid Membranes. *Chemical Society Reviews* **2009,** *38* (9), 2509-2519.

Seddon, J. M., Structure of the Inverted Hexagonal (Hii) Phase, and Non-Lamellar Phase Transitions of Lipids. *Biochimica et Biophysica Acta (BBA)-Reviews on Biomembranes* **1990,** *1031* (1), 1-69.

Seelig, A.; Seelig, J., Dynamic Structure of Fatty Acyl Chains in a Phospholipid Bilayer Measured by Deuterium Magnetic Resonance. *Biochemistry* **1974,** *13* (23), 4839-4845.

Seidi, F., et al., Saccharides, Oligosaccharides, and Polysaccharides Nanoparticles for Biomedical Applications. *Journal of Controlled Release* **2018**.

Sercombe, L., et al., Advances and Challenges of Liposome Assisted Drug Delivery. *Frontiers in Pharmacology* **2015,** *6*, 286.

Sessa, G.; Weissmann, G., Phospholipid Spherules (Liposomes) as a Model for Biological Membranes. *Journal of Lipid Research* **1968,** *9* (3), 310-318.

Seydel, J. K.; Wiese, M., *Drug-Membrane Interactions: Analysis, Drug Distribution, Modeling*. John Wiley & Sons: 2009; Vol. 15.

Sezgin, E., et al., The Mystery of Membrane Organization: Composition, Regulation and Roles of Lipid Rafts. *Nature reviews Molecular Cell Biology* **2017,** *18* (6), 361.

Shahriari, M., et al., Enzyme Responsive Drug Delivery Systems in Cancer Treatment. *Journal of Controlled Release* **2019**.

Sharei, A., et al., A Vector-Free Microfluidic Platform for Intracellular Delivery. *Proceedings of the National Academy of Sciences* **2013,** *110* (6), 2082-2087.

Sharifian Gh, M., et al., Spatially Resolved Membrane Transport in a Single Cell Imaged by Second Harmonic Light Scattering. *Biochemistry* **2019,** *58* (14), 1841-1844.

Sharma, P., et al., Primary, Adaptive, and Acquired Resistance to Cancer Immunotherapy. *Cell* **2017,** *168* (4), 707-723.

Shaw, S. K., et al., Non-Covalent Assembly Method That Simultaneously Endows a Liposome Surface with Targeting Ligands, Protective Peg Chains, and Deep-Red Fluorescence Reporter Groups. *Chemistry–A European Journal* **2017,** *23* (51), 12646-12654.

Shen, Y., Surface Properties Probed by Second-Harmonic and Sum-Frequency Generation. *Nature* **1989,** *337* (6207), 519.

Shen, Y., Surfaces Probed by Nonlinear Optics. *Surface Science* **1994,** *299*, 551-562.

Shen, Y.-R., The Principles of Nonlinear Optics. *New York, Wiley-Interscience, 1984, 575 p.* **1984**.

Sherr, C. J., Principles of Tumor Suppression. *Cell* **2004,** *116* (2), 235-246.

Shevchenko, A.; Simons, K., Lipidomics: Coming to Grips with Lipid Diversity. *Nature Reviews Molecular Cell Biology* **2010,** *11* (8), 593.

Shinoda, W., Permeability across Lipid Membranes. *Biochimica et Biophysica Acta (BBA)-Biomembranes* **2016,** *1858* (10), 2254-2265.

Shum, P., et al., Phototriggering of Liposomal Drug Delivery Systems. *Advanced Drug Delivery Reviews* **2001,** *53* (3), 273-284.

Silvius, J. R., Thermotropic Phase Transitions of Pure Lipids in Model Membranes and Their Modifications by Membrane Proteins. *Lipid-protein Interactions* **1982,** *2*, 239-281.

Simpson, G. J.; Rowlen, K. L., An Shg Magic Angle: Dependence of Second Harmonic Generation Orientation Measurements on the Width of the Orientation Distribution. *Journal of the American Chemical Society* **1999,** *121* (11), 2635-2636.

Singer, S. J.; Nicolson, G. L., The Fluid Mosaic Model of the Structure of Cell Membranes. *Science* **1972,** *175* (4023), 720-731.

Söderberg, M., et al., Fatty Acid Composition of Brain Phospholipids in Aging and in Alzheimer's Disease. *Lipids* **1991,** *26* (6), 421.

Sorochkina, A. I., et al., Peptide-Induced Membrane Leakage by Lysine Derivatives of Gramicidin a in Liposomes, Planar Bilayers, and Erythrocytes. *Biochimica et Biophysica Acta (BBA)-Biomembranes* **2013,** *1828* (11), 2428-2435.

Srivastava, A.; Eisenthal, K. B., Kinetics of Molecular Transport across a Liposome Bilayer. *Chemical Physics Letters* **1998,** *292* (3), 345-351.

Stella, B., et al., Design of Folic Acid-Conjugated Nanoparticles for Drug Targeting. *Journal of Pharmaceutical Sciences* **2000,** *89* (11), 1452-1464.

Stevens, M. J., et al., Insights into the Molecular Mechanism of Membrane Fusion from Simulation: Evidence for the Association of Splayed Tails. *Physical Review Letters* **2003,** *91* (18), 188102.

Stewart, J. C., Colorimetric Determination of Phospholipids with Ammonium Ferrothiocyanate. *Analytical Biochemistry* **1980,** *104* (1), 10-4.

Stewart, M. P., et al., In Vitro and Ex Vivo Strategies for Intracellular Delivery. *Nature* **2016,** *538* (7624), 183.

Stillwell, W.; Wassall, S. R., Docosahexaenoic Acid: Membrane Properties of a Unique Fatty Acid. *Chemistry and Physics of Lipids* **2003,** *126* (1), 1-27.

Strandberg, E., et al., Lipid Shape Is a Key Factor for Membrane Interactions of Amphipathic Helical Peptides. *Biochimica et Biophysica Acta (BBA)-Biomembranes* **2012,** *1818* (7), 1764-1776.

Sud, M., et al., Lmsd: Lipid Maps Structure Database. *Nucleic acids research* **2006,** *35* (suppl_1), D527-D532.

Sugano, K., et al., Coexistence of Passive and Carrier-Mediated Processes in Drug Transport. *Nat Rev Drug Discov* **2010,** *9* (8), 597-614.

Sun, W.-C., et al., Synthesis of Fluorinated Fluoresceins. *The Journal of Organic Chemistry* **1997,** *62* (19), 6469-6475.

Sun, Y., Tumor Microenvironment and Cancer Therapy Resistance. *Cancer Letters* **2016,** *380* (1), 205-215.

Ta, T.; Porter, T. M., Thermosensitive Liposomes for Localized Delivery and Triggered Release of Chemotherapy. *Journal of Controlled Release* **2013,** *169* (1-2), 112-125.

Taniguchi, M.; Lindsey, J. S., Database of Absorption and Fluorescence Spectra of> 300 Common Compounds for Use in Photochem Cad. *Photochemistry and Photobiology* **2018,** *94* (2), 290-327.

Tejwani, R. W., et al., An Atomic and Molecular View of the Depth Dependence of the Free Energies of Solute Transfer from Water into Lipid Bilayers. *Molecular Pharmaceutics* **2011,** *8* (6), 2204-2215.

Tilcock, C., et al., Influence of Cholesterol on the Structural Preferences of Dioleoylphosphatidylethanolamine-Dioleoylphosphatidylcholine Systems: A Phosphorus-31 and Deuterium Nuclear Magnetic Resonance Study. *Biochemistry* **1982,** *21* (19), 4596-4601.

Torchilin, V. P., et al., Tat Peptide on the Surface of Liposomes Affords Their Efficient Intracellular Delivery Even at Low Temperature and in the Presence of Metabolic Inhibitors. *Proceedings of the National Academy of Sciences* **2001,** *98* (15), 8786-8791.

Torchilin, V. P., Recent Advances with Liposomes as Pharmaceutical Carriers. *Nature Reviews Drug Discovery* **2005,** *4* (2), 145.

Torchilin, V. P., Recent Approaches to Intracellular Delivery of Drugs and DNA and Organelle Targeting. *Annu. Rev. Biomed. Eng.* **2006,** *8*, 343-375.

Toy, R., et al., Shaping Cancer Nanomedicine: The Effect of Particle Shape on the in Vivo Journey of Nanoparticles. *Nanomedicine* **2014,** *9* (1), 121-134.

Tran, S., et al., Cancer Nanomedicine: A Review of Recent Success in Drug Delivery. *Clin Transl Med* **2017,** *6* (1), 44.

Truong, V. X., et al., Visible-Light-Mediated Cleavage of Polymer Chains under Physiological Conditions Via Quinone Photoreduction and Trimethyl Lock. *Chemical Communications* **2017,** *53* (89), 12076-12079.

Van der Meel, R., et al., Extracellular Vesicles as Drug Delivery Systems: Lessons from the Liposome Field. *Journal of Controlled Release* **2014,** *195*, 72-85.

Van Meer, G., et al., Membrane Lipids: Where They Are and How They Behave. *Nature Reviews Molecular Cell Biology* **2008,** *9* (2), 112.

Vanni, S., et al., A Sub-Nanometre View of How Membrane Curvature and Composition Modulate Lipid Packing and Protein Recruitment. *Nature Communications* **2014,** *5*, 4916.
Varkouhi, A. K., et al., Endosomal Escape Pathways for Delivery of Biologicals. *Journal of Controlled Release* **2011,** *151* (3), 220-228.

Varkouhi, A. K., et al., Endosomal Escape Pathways for Delivery of Biologicals. *Journal of Controlled Release* **2011,** *151* (3), 220-228.

Veatch, S. L.; Keller, S. L., Seeing Spots: Complex Phase Behavior in Simple Membranes. *Biochimica et Biophysica Acta (BBA)-Molecular Cell Research* **2005,** *1746* (3), 172-185.

Venable, R. M., et al., Mechanical Properties of Lipid Bilayers from Molecular Dynamics Simulation. *Chemistry and Physics of Lipids* **2015,** *192*, 60-74.

Verkleij, A., et al. In *Non-Bilayer Structures in Membrane Fusion*, Ciba Foundation Symposium, 1984; pp 45-59.

Viswanadhan, V. N., et al., Atomic Physicochemical Parameters for Three Dimensional Structure Directed Quantitative Structure-Activity Relationships. 4. Additional Parameters for Hydrophobic and Dispersive Interactions and Their Application for an Automated Superposition of Certain Naturally Occurring Nucleoside Antibiotics. *Journal of Chemical Information and Computer Sciences* **1989,** *29* (3), 163-172.

Vivero-Escoto, J. L., et al., Photoinduced Intracellular Controlled Release Drug Delivery in Human Cells by Gold-Capped Mesoporous Silica Nanosphere. *Journal of the American Chemical Society* **2009,** *131* (10), 3462-3463.

Voskuhl, J.; Ravoo, B. J., Molecular Recognition of Bilayer Vesicles. *Chemical Society Reviews* **2009,** *38* (2), 495-505.

Walter, A.; Gutknecht, J., Permeability of Small Nonelectrolytes through Lipid Bilayer Membranes. *J. Membrane Biol.* **1986,** *90* (3), 207-217.
Walton, D. P.; Dougherty, D. A., A General Strategy for Visible-Light Decaging Based on the Quinone Trimethyl Lock. *Journal of the American Chemical Society* **2017,** *139* (13), 4655-4658.

Walton, D. P.; Dougherty, D. A., A General Strategy for Visible-Light Decaging Based on the Quinone Trimethyl Lock. *Journal of the American Chemical Society* **2017,** *139* (13), 4655-4658.

Wan, Y., et al., Liposomes from Novel Photolabile Phospholipids: Light-Induced Unloading of Small Molecules as Monitored by Pfg Nmr. *Journal of the American Chemical Society* **2002,** *124* (20), 5610-5611.

Wang, H., et al., Overcoming Ovarian Cancer Drug Resistance with a Cold Responsive Nanomaterial. *ACS Central Science* **2018,** *4* (5), 567-581.

Wang, H., et al., Second Harmonic Generation from the Surface of Centrosymmetric Particles in Bulk Solution. *Chemical Physics Letters* **1996,** *259* (1-2), 15-20.

Wang, M.; Thanou, M., Targeting Nanoparticles to Cancer. *Pharmacological Research* **2010,** *62* (2), 90-99.

Wang, X., et al., Solvent-Free, Alcl3-Promoted Tandem Friedel–Crafts Reaction of Arenes and Aldehydes. *Journal of Molecular Catalysis A: Chemical* **2006,** *255* (1-2), 31-35.

Wang, Y., et al., Nanomedicine: Swarming Towards the Target. *Nature Materials* **2011,** *10* (7), 482.

Wang, Y.; Kohane, D. S., External Triggering and Triggered Targeting Strategies for Drug Delivery. *Nature Reviews Materials* **2017,** *2* (6), 17020.

Weissig, V., et al., Nanopharmaceuticals (Part 1): Products on the Market. *International Journal of Nanomedicine* **2014,** *9*, 4357.

White, G. F., et al., Physical Properties of Liposomes and Proteoliposomes Prepared from Escherichia Coli Polar Lipids. *Biochimica et Biophysica Acta (BBA)-Biomembranes* **2000,** *1468* (1), 175-186.

Wicki, A., et al., Nanomedicine in Cancer Therapy: Challenges, Opportunities, and Clinical Applications. *Journal of Controlled Release* **2015,** *200*, 138-157.

Wickner, W.; Schekman, R., Membrane Fusion. *Nature structural & Molecular Biology* **2008,** *15* (7), 658.

Winter, J. E., On the Development of Analytical Methodologies to Interrogate the Lipid Dynamics and Phase Transition Resulting from the Reduction of Stimuli-Responsive Vesicles. Ph.D Dissertation, Louisiana State University, Baton Rouge, LA, 2015.

Witsch, E., et al., Roles for Growth Factors in Cancer Progression. *Physiology* **2010,** *25* (2), 85-101.

Witz, I. P., Tumor–Microenvironment Interactions: Dangerous Liaisons. *Advances in Cancer Research* **2008,** *100*, 203-229.

Wohnsland, F.; Faller, B., High-Throughput Permeability Ph Profile and High-Throughput Alkane/Water Log P with Artificial Membranes. *Journal of Medicinal Chemistry* **2001,** *44* (6), 923-930.

Wolak, D. J.; Thorne, R. G., Diffusion of Macromolecules in the Brain: Implications for Drug Delivery. *Molecular Pharmaceutics* **2013,** *10* (5), 1492-1504.

Wu, G., et al., Remotely Triggered Liposome Release by near-Infrared Light Absorption Via Hollow Gold Nanoshells. *Journal of the American Chemical Society* **2008,** *130* (26), 8175-8177.

Wu, L.-G., et al., Exocytosis and Endocytosis: Modes, Functions, and Coupling Mechanisms. *Annual Review of Physiology* **2014,** *76*, 301-331.

Xing, L.; Glen, R. C., Novel Methods for the Prediction of Logp, P K a, and Logd. *Journal of Chemical Information and Computer Sciences* **2002,** *42* (4), 796-805.

Yagai, S., et al., Photocontrollable Self-Assembly. *Chemistry–A European Journal* **2005,** *11* (14), 4054-4063.

Yang, J., et al., Drug Delivery Via Cell Membrane Fusion Using Lipopeptide Modified Liposomes. *Acs Central Science* **2016,** *2* (9), 621-630.

Yang, L., et al., Single Chain Epidermal Growth Factor Receptor Antibody Conjugated Nanoparticles for in Vivo Tumor Targeting and Imaging. *Small* **2009,** *5* (2), 235-243.

Yavlovich, A., et al., A Novel Class of Photo-Triggerable Liposomes Containing Dppc: Dc8, 9pc as Vehicles for Delivery of Doxorubcin to Cells. *Biochimica et Biophysica Acta (BBA)-Biomembranes* **2011,** *1808* (1), 117-126.

Yavlovich, A., et al., Design of Liposomes Containing Photopolymerizable Phospholipids for Triggered Release of Contents. *Journal of Thermal Analysis and Calorimetry* **2009,** *98* (1), 97-104.

Yavlovich, A., et al., Light-Sensitive Lipid-Based Nanoparticles for Drug Delivery: Design Principles and Future Considerations for Biological Applications. *Molecular Membrane Biology* **2010,** *27* (7), 364-381.

Yeagle, P. L., *The Structure of Biological Membranes*. CRC press: **2011.**

Yerramilli, V. S.; Kim, K. H., Labeling Rnas in Live Cells Using Malachite Green Aptamer Scaffolds as Fluorescent Probes. *ACS Synthetic Biology* **2018,** *7* (3), 758-766.

Yesylevskyy, S. O., et al., The Influence of Curvature on the Properties of the Plasma Membrane. Insights from Atomistic Molecular Dynamics Simulations. *Scientific Reports* **2017,** *7* (1), 16078.

Yoo, J.-W., et al., Factors That Control the Circulation Time of Nanoparticles in Blood: Challenges, Solutions and Future Prospects. *Current Pharmaceutical Design* **2010,** *16* (21), 2298-2307.

Zalipsky, S., et al., New Detachable Poly (Ethylene Glycol) Conjugates: Cysteine-Cleavable Lipopolymers Regenerating Natural Phospholipid, Diacyl Phosphatidylethanolamine. *Bioconjugate Chemistry* **1999,** *10* (5), 703-707.

Zeng, J., A Study of Molecular Adsorption and Transport at Cell Membrane and Biologically Relevant Surfaces by Second Harmonic Generation. Ph.D Dissertation, Univeristy of Pennsylvania, Philadelphia, PA, **2011**.

Zeng, J., et al., Time-Resolved Molecular Transport across Living Cell Membranes. *Biophysical Journal* **2013,** *104* (1), 139-145.

Zernike, F.; Midwinter, J. E., *Applied Nonlinear Optics*. Courier Corporation: 2006.

Zhang, D., et al., Liposomes Formed from Photo-Cleavable Phospholipids: In Situ Formation and Photo-Induced Enhancement in Permeability. *RSC Advances* **2018,** *8* (26), 14669-14675.

Zhang, L., et al., Nanoparticles in Medicine: Therapeutic Applications and Developments. *Clinical Pharmacology & Therapeutics* **2008,** *83* (5), 761-769.

Zhang, T., et al., Application of Sialic Acid/Polysialic Acid in the Drug Delivery Systems. *Asian Journal of Pharmaceutical Sciences* **2014,** *9* (2), 75-81.

Zhang, Z.-Y.; Smith, B. D., Synthesis and Characterization of Nvoc-Dope, a Caged Photoactivatable Derivative of Dioleoylphosphatidylethanolamine. *Bioconjugate Chemistry* **1999,** *10* (6), 1150-1152.

Zhao, B., et al., Studies on the Photosensitized Reduction of Resorufin and Implications for the Detection of Oxidative Stress with Amplex Red. *Free Radical Biology and Medicine* **2011,** *51* (1), 153-159.

Zheng, G., et al., Rerouting Lipoprotein Nanoparticles to Selected Alternate Receptors for the Targeted Delivery of Cancer Diagnostic and Therapeutic Agents. *Proceedings of the National Academy of Sciences* **2005,** *102* (49), 17757-17762.

Zinser, E., et al., Phospholipid Synthesis and Lipid Composition of Subcellular Membranes in the Unicellular Eukaryote Saccharomyces Cerevisiae. *Journal of Bacteriology* **1991,** *173* (6), 2026-2034.

Zope, H. R., et al., In Vitro and in Vivo Supramolecular Modification of Biomembranes Using a Lipidated Coiled-Coil Motif. *Angewandte Chemie International Edition* **2013,** *52* (52), 14247-14251.

VITA

Huy Huu Nguyen was born and raised in Haiphong, Vietnam. In August 2008, he moved to the capital city and entered Hanoi University of Science, an integral part of Vietnam National University. He received his Bachelor of Science (B.S., cum laude) degree in Honors Program of Chemistry in 2013.

He joined the research group of Prof. Robin L. McCarley in January 2015 where he carried out his doctoral research work on development of drug delivery by triggered release of liposomes. He plans to receive his Doctor of Philosophy degree (Ph.D.) in the Spring 2020 commencement ceremony.